The stability of orbits of putative Earth-mass planets or satellites of giant planets within known exoplanetary systems.

Thesis

THE STABILITY OF ORBITS OF PUTATIVE EARTH-MASS PLANETS OR SATELLITES OF GIANT PLANETS WITHIN KNOWN EXOPLANETARY SYSTEMS

A Ph.D. Thesis by
David R. Underwood, M. Math. (Hons.),
Physics & Astronomy Department,
Open University,
Milton Keynes, UK.
10th October, 2006

Principal Supervisor:
Professor Barrie W. Jones

Second Supervisor:
Dr Carole Haswell

DATE OF SUBMISSION: 29 AUGUST 2006
DATE OF AWARD: 4 MAY 2007

ProQuest LLC.
789 East Eisenhower Parkway
P.O. Box 1346
Ann Arbor, MI 48106 – 1346

Abstract

The movement of the habitable zone of 55 stars from 0.5 to 1.5 Solar masses and 0.75% to 5% metallicity were modelled over their main sequence lifetimes. 156 stars known to have planetary systems had their mass and metallicity matched to their nearest model, giving approximate habitable zones, which were compared with their giant planet(s)'s orbital range and gravitational reach. Habitable zones lying outside a giant's gravitational reach for one billion years (two billion years after star birth) could host an Earth-mass planet in a stable confined orbit long enough for life to develop. Low eccentricity giant orbits confined to the habitable zone could also host Earth-mass satellites. Results show 85 of 156 exosystems could house a habitable Earth-mass body over the last billion years, 113 could do so for at least a billion years at sometime during their main sequence lifetimes, excluding the heavy bombardment period.

An orbital integrator computer program modelled orbits of Earth-mass planets in the habitable zones of τ^1 Gruis, HD 196050, HD 52265, 55 Cancri, and Earth-mass giant planet satellites in HD 23079 and HD 28185. The integrator's predictions for satellite orbits were shown to comply with restricted three-body problem theory. 'Earths' were 'launched' at different distances from the star or planet and their orbital parameters monitored with time until the program concluded after either one billion years, 100 million years, or a cataclysmic event. Orbits lasting the full run time are assumed to remain stable for the star's main sequence lifetime. Results reveal the possibility of habitable Earth-mass *planets* around HD 52265, 55 Cancri, and *satellites* around the giants of HD 23079 and HD 28185. The τ^1 Gruis system cannot host a habitable 'Earth' whereas HD 196050 could, provided the planet's semimajor axis was at the inner 20% of the habitable zone width.

Acknowledgements

Thanks go, first and foremost, to my supervisor Professor Barrie W. Jones of the Department of Physics and Astronomy, Open University, Milton Keynes, UK, for enabling me to pursue this thesis and for his invaluable guidance, assistance, advice and contributions over the course of its duration. Thanks also go to John Chambers of the Carnegie Institution, Washington D.C. for his contribution towards creating the Mercury Orbital Integrator and making it publicly available for its use in the greatest part of this thesis, plus his advice on how best to proceed with satellite integrations. Doctor Nick Sleep, a former student of Professor Jones has helped considerably with studies in determining the extent of giant planet gravitational reach when in eccentric orbits, plus creating a short program to decrease the considerable size of the stellar evolution data by a factor of ten. Thanks go to Doctor Ulrich Kolb of the Open University and Doctor Sean Ryan of the University of Hertfordshire for their help with background information regarding stellar evolution and to Doctor John Barker, a former student of Dr. Kolb, whose assistance and guidance with the use of the stellar evolution program was essential. Finally I would like to thank my partner, Anne Pigott, without whose hard work in virtually single-handedly running our new business over the fourth year of this Ph.D., this thesis would not have been completed.

Contents

Figures

1. Introduction

1.1 Goal

The search for carbon based extraterrestrial life outside of our Solar System has always assumed the existence of Earth-mass planets in stable orbits confined within the habitable zones of exoplanetary systems. The goal here is to continue to authenticate the possibility of this assumption by examining orbits of putative Earth-mass planets within the exosystems τ^1 Gruis, HD 196050, HD 52265, 55 Cancri, and of Earth-mass satellites of the giant planets orbiting HD 23079 and HD 28185. The Mercury Orbital Integrator computer program was used to simulate the motion of terrestrial planets within known exosystems using Mixed Variable Symplectic or Hybrid Integrators and the motion of giant planet satellites using a RADAU Integrator (Chambers & Migliorini, 1997). Planets or satellites, which are small compared to the star and giant planet(s), are launched with almost circular orbits at a range of distances from the central body, which in the case of Earth-sized planets, are at suitable distances for them to sustain life. Orbital instabilities are caused by the gravitational perturbations due to the proximity of other large bodies. This results in a possible Earth-sized body's close encounter with a large body, collision with a large body or an ejection from the system. The ranges of motion of a giant planet(s) and its gravitational influence in a system have been mapped onto the habitable zone, which has been determined over the star's main sequence lifetime using a stellar evolution-modelling program (Mazzitelli, 1989). This reveals regions of potentially stable orbits, for both terrestrial planets, and satellites of giant planets confined to the habitable zone. If putative Earth-mass bodies can exist in stable orbits within these regions of exoplanetary systems, they may be capable of sustaining life. The possibility of their existence will then have been confirmed and the goal reached.

1.2 Background

Planets or satellites of giant planets, which are confined to the habitable zone in stable orbits for the last 1Gyr (10^9 years) or 100Myr (10^8 years), around stars at least 2Gyr old, are good candidates for supporting any possible detectable life. The habitable zone (HZ) is defined as the distance from a star where liquid water, which is necessary for life, can exist on the surface of a planet. A stable orbit is an orbit with only small variations in semimajor axis and eccentricity over 1Gyr or 100Myr. If stable for these times, it is considered to be stable for the main sequence lifetime of the star. An orbit confined to the habitable zone is an orbit with a semimajor axis between the habitable zone limits. These planets must be sufficiently large, from $0.1M_{\oplus}$ (Earth Mass) to $8M_{\oplus}$ (Leger et al., 2003), to sustain an atmosphere dense enough to allow liquid water. Planets larger than $8M_{\oplus}$ will retain too much hydrogen during accretion and their content may resemble that of the "ice giants", Uranus and Neptune. The first extrasolar planet was discovered in 1995 (Mayor & Queloz, 1995) and had a surprisingly close orbit to its star, 51 Pegasi. Eleven years on (10^{th} October, 2006), there are now 206 known giant planets, of the order of Jupiter's or Neptune's mass, in 178 main sequence star systems. The large majority of planets discovered so far are giants because their signatures on the motion of their parent star are much greater than that of any possible terrestrial sized planet. Since giant planets exist in extrasolar systems then perhaps other smaller planets, similar to Earth, exist with them. There could also be Earth-mass satellites of giant planets orbiting in habitable zones.

The early Earth suffered massive impacts in its first 700 million years through the period of heavy bombardment within the Solar System. Many of these impacts could possibly have evaporated the oceans and the planet may have been sterilised many times by these events. First detected signs of life on Earth, which may date back to shortly after this time, and possible fossil records 300 million years after this from Warrawoona, Australia,

indicate organisms capable of photosynthesis and able to build mineral mounds (Ward & Brownlee (2000)). This implies a period in the order of one billion years, from the birth of the planet, for primitive life to get started and to evolve. In other planetary systems the heavy bombardment period may last for different lengths of time depending on factors such as the stellar mass, disc density and the positions of giant planets. If life could exist elsewhere it may take longer to reach such stages and longer still for life to change significantly the contents of a planet's atmosphere.

If carbon-based life as on Earth is to be discovered on a terrestrial planet in an extrasolar system it must leave atmospheric signatures, which will most likely be identified by spectroscopy. On Earth, these atmospheric changes began to occur from 2Gyr after the Earth's origin or approximately 1Gyr after the period of heavy bombardment ceased. Since this is the only model available, it is assumed that this would be similar in other exoplanetary systems with life. Looking for signatures of even the simplest forms of extraterrestrial life, such as the presence of ozone in the atmosphere, assumes that life elsewhere would follow similar evolutionary trends. If such life had reached this stage, the planet it inhabited would be rocky, be of similar order to Earth's mass and would have had an orbit with a semimajor axis within the limits of the habitable zone (i.e. confined) for at least 2Gyr from its birth. The stars, which have a main sequence lifetime of at least this duration, are of $1.5M_{\odot}$ (solar masses) and less.

The detection of Earth-mass extrasolar planets is, at the moment, beyond present technology. Satellite missions in the next few years, however, such as CoRoT (2006) and Kepler (2008) may facilitate this search. The detection of Earth-like planets in the infrared with the Darwin project, using extra-large space telescopes of 70m to 100m equivalent apertures, may be up to 12 years in the future (Lagrange, 2003 and Ollivier, 2003). With such instruments it would be possible to detect life signatures in the atmosphere of an Earth-sized planet at up to 10 parsecs.

1.3 Previous Research

Any exosolar terrestrial planet searches will be pursued in the exoplanetary systems known at the time. These searches will very likely concentrate on systems where the gravitational influence of any giant planet(s) would allow the existence of terrestrial bodies confined within the habitable zone for at least the past 1Gyr. The use of the Mercury Orbital Integrator computer program to identify these targets is part of ongoing work at the Open University, UK, to which the work within this thesis is a major contributor (Jones et al., 2006, Jones et al., 2005). Exoplanet systems already investigated are ρ Coronae Borealis, Gliese 876, υ Andromedae (Jones et al., 2001), 47 Ursae Majoris (Jones & Sleep, 2002) and ε Eridani (Jones & Sleep, 2003). The ρ Coronae Borealis and ε Eridani systems have one giant planet each, 47 Ursae Majoris and Gliese 876 have two each and υ Andromedae has three. Each of these systems was discovered by Doppler shifting of the star's spectral lines as it moves towards and away from Earth as a reaction to the giant planets orbital motion. The shortfall of this technique is that the inclinations of planets' orbits, relative to the plane of the sky, are unattainable. This introduces the concept of minimum mass, included in the previous research, and is the mass a planet would have if it orbited directly in an observer's line of sight. For a planet of minimum mass, m, actual mass, M_p, orbiting at angle, i_0 (see Figure 1.1):

$$M_p = m/\sin i_0 \qquad 1.1.$$

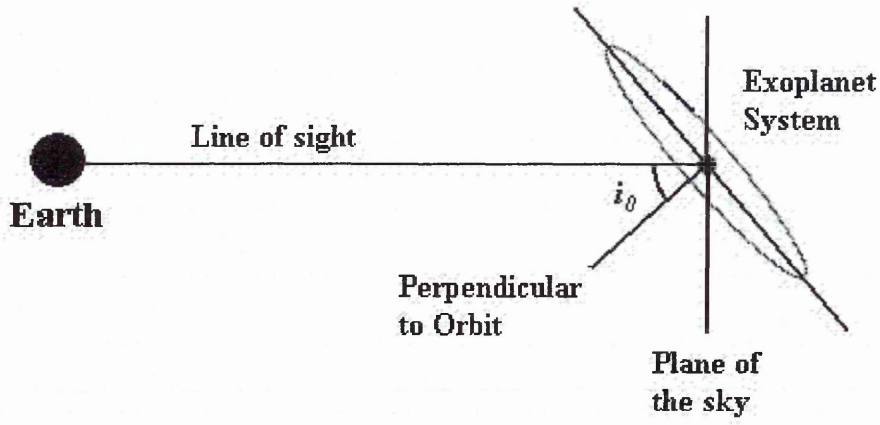

Figure 1.1 Geometrical arrangement for an exoplanet with an inclined orbit.

The ρ Coronae Borealis system investigated by Jones et al., 2001, has a high probability of having a terrestrial planet in an orbit confined to the habitable zone. The giant planet is a "Warm Jupiter" (see chapter 2, section 4), i.e in an orbit closer to the star than the inner boundary of the habitable zone but not a "Hot Jupiter". It has an orbit close enough to the star to have little or no gravitational effect on the habitable zone, even when the mass of the giant is assumed to be 8 times its minimum mass, since from equation (1.1), $M_p \geq m$. The short orbital period of the giant, however, required a much shorter time step for the accurate operation of the orbital integrator, then set to $^1/_{12}$th or less of the orbital period of the innermost planet. This requires much more computer time for a normal run of 10^9 years, so the time of integrations was reduced to 10^8 years. As there was little effect by the giant on one terrestrial planet in this system, most runs involved two terrestrial planets. It was found that the giant did not destabilise either of these orbits when they were near the inner edge of the habitable zone at 0.723AU (astronomical units), even when the launching semimajor axes were only 0.047AU apart. This effect was not as great near the outer edge at 1.4AU, where the semimajor axes needed to be 0.2AU apart for stability.

There is a high probability of a habitable planet in the habitable zone of 47 Ursae Majoris, (Jones & Sleep, 2002) but only near its inner edge since the gravitational influence of the inner giant extends across a large fraction of the outer regions of the habitable zone. Stable terrestrial planet orbits were found to a semimajor axis of 1.3AU for minimum mass giants, however as the giant planets' masses were increased, their influence stretched further into the habitable zone until the only stable orbits at 4 times minimum mass were interior to the HZ.

Of the remaining three systems, ε Eridani is a very young star, estimated to be only 500 Myr old (Greaves et al., 1998), so even if a terrestrial planet could have a stable orbit within its habitable zone, it would be too young for life to have left any atmospheric spectroscopic signature (Jones & Sleep, 2003). There is a circumstellar disc, which implies orbital inclinations, i_0, of 46°, which when incorporated into the mass of the giant, allows Earth-Moon orbits confined to the HZ only to 0.44AU from the star, right on the very inner edge of the habitable zone. The outer two of the three giant planets in υ Andromedae and both giants in Gliese 876 were found to affect orbits of any putative Earth across the entire habitable zone in both systems (Jones et al., 2001). There is little chance of habitable terrestrial planets being found in any of these three systems.

Research by other groups has not pursued integrations over long periods approaching hundreds of millions or billions of years. An extensive study by Menou & Tabachnik, 2003 investigated all of the 85 then known extrasolar planetary systems to evaluate the stabilities of Earth-mass planets within the habitable zones of the stars. Their runs, using a

second order Mixed Variable Symplectic Integrator, were over one million years using zero age main sequence (ZAMS) habitable zones, eliminating the need to know stellar ages. Their constraints for life were more stringent in that the planet must not cross the HZ boundary at any time during its orbit, compared to the criterion used here where the planet's semimajor axis must lie in the HZ. They concluded that one third of systems could contain habitable Earth-like planets. Asghari et al., 2004 examined the possibility of the existence of stable terrestrial planets in five systems, Gliese 777A, HD 72659, Gliese 614, 47 Ursae Majoris and HD 4208. For each system, a grid of 80 eccentricities for the giant and 160 semimajor axes for the terrestrial planet was examined over one million years each. A Lie series integration method was used with a variable time step showing that Gliese 777A could support stable orbits over nearly all of the HZ, and that no stable orbits were possible for Gliese 614. The remainder can support terrestrial planets which "survive for a sufficiently long time", although how this can be determined from one million year integrations is open to debate.

Noble et al., 2002 performed integrations over only hundreds or thousands of years when investigating possible stable terrestrial planet orbits confined to the HZ in 51 Pegasi, 47 Ursae Majoris and HD 210277. Their time step was only 10^{-7} year, claiming the advantage over mixed variable symplectic integrations being that their fourth order Runga-Kutta integration technique could handle close encounters. They had clearly overlooked the Hybrid integrator in John Chamber's Mercury program. They found stable orbits were possible in 47 UMa towards the inner HZ boundary, none were possible in HD 210277 but all the HZ could house stable terrestrial planet orbits in 51 Pegasi, provided they survived the inward migration of the giant. This survival during migration was examined by Fogg & Nelson, 2005, whose investigations suggested that terrestrial planets can be formed from reaccretion after migration. Mandell & Sigurdsson, 2003 used the Mercury Orbital Hybrid Integrator and integrated for up to two million years during a giant planet's inward migration through four terrestrial planets with the same orbits as the inner solar system. They found fewer terrestrial planet ejections occurred when inward giant planet migration was faster, leaving 40% of terrestrial bodies in the HZ after a 0.5Myr migration, dropping to 15% after a 2Myr migration.

Other work has examined the stability in binary systems where David et al., 2003, performed ~40,000 numerical experiments limited to 10Myr in determining that 50% of binaries allow terrestrial planets to remain in stable orbits over the age of the solar system. Holman & Wiegert, 1999, performed numerical integrations over a period of 10^4 binary revolutions in systems where binary eccentricities and mass ratios were varied. They derived a relationship for a critical planetary semimajor axis, within which orbits are stable, and the orbited star's mass fraction of the system, the binary's semimajor axis and its eccentricity.

1.4 The OU Group's Rapid Results Method

It is very time consuming to apply orbital integration to investigate a particular exoplanetary system in detail, to determine whether long term survival of a terrestrial planet in the habitable zone is possible. Therefore, the OU group has developed a rapid method of evaluating the extent to which a habitable zone could harbour a terrestrial planet. This method was first published by Jones et al. in 2005, but had been in use by the OU group for a few years before this publication appeared. The rapid method relies on multipliers n of the Hill radius of a giant planet (chapter 4 section 1). These give the distances from a giant planet within which the survival of a terrestrial planet is very unlikely – the gravity of the giant will eject it within these distances.

The rapid method does not provide the fine detail provided by orbital integration. For example, it does not pick out the effects of orbital resonances within otherwise stable distances from a giant, but detailed studies of a few systems have established that this usually makes little difference to the overall evaluation of habitability.

This rapid method has been applied to systems as the habitable zone (HZ) moves during the star's main sequence lifetime. Underwood et al., 2003 has obtained this movement using a stellar evolution model (Chapter 3). Figure 1.2 shows the outcome for the Solar System. The values of n depend on the eccentricity of the orbits of Jupiter and Saturn, and on whether we are considering the region interior or exterior to the giant – see chapter 4, section 4. Studies of a growing number of exoplanetary systems, using the rapid method, can be found in Underwood et al, 2003, Jones et al. 2005, and Jones et al. 2006.

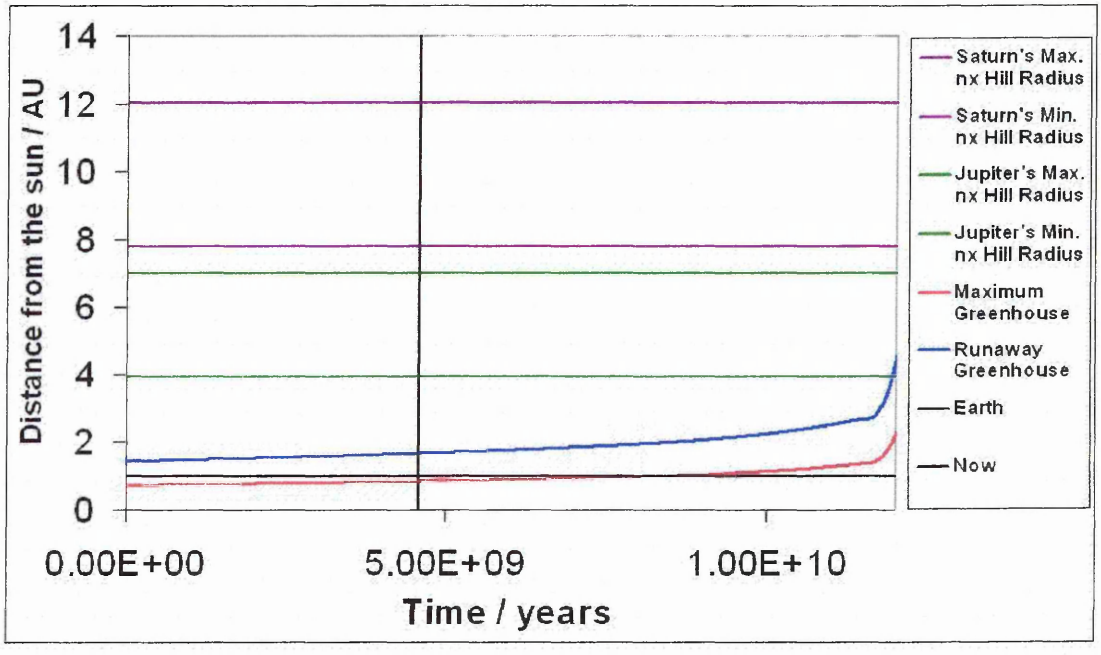

Figure 1.2 Variation of the Sun's HZ with Jupiter and Saturn's gravitational limits.

A putative terrestrial planet, or a satellite of a giant planet, may exist in an orbit where it spends all of the star's main sequence lifetime within the habitable zone. If so, it would be in the continuously habitable zone (CHZ) and would be a very good candidate in searching for signs of possible extraterrestrial life. A planet may only exist within the habitable zone for part of a star's main sequence lifetime, possibly due to changes in the planet's orbit caused by other bodies in the system or the outward migration of the star's habitable zone during its main sequence lifetime. If this period were over billions of years, the system would still be a good candidate for life to exist. A planet existing for only a short time or no time at all within the habitable zone would be a poor candidate for life.

Depending on the configuration of the habitable zone and position of the giant planet(s), a "score" may be attributed to the known exoplanetary systems, where "yes" = 10, "no" = 0, and figures from 1 to 9 represent 10 times the fraction of the HZ which could house a habitable Earth (see table 3.20, chapter 3, section 8). It is hoped that this information will ameliorate the search for extraterrestrial planets and the signatures of extraterrestrial life by allowing search efforts to be concentrated on the most likely candidates.

2. Overview of Extrasolar Planets

2.1 What is a Planet?

The upper mass limit definition of a planet adopted by the International Astronomical Union is, "An object that is in orbit about a star and that is smaller than the ~13M_J (Jupiter masses) limit for deuterium fusion to occur," (Lissauer, 2002). The current lower mass limit is still under debate and was hoped to be resolved at an International Astronomical Union meeting in September, 2006. A current guided definition for low mass planets is of an object in orbit around a star that has sufficient mass to self-gravitate itself into a sphere and that has swept its orbit clear of debris. If pulsar planets are not included, the first detected extrasolar planet orbiting 51 Pegasi was found in 1995 by observing Doppler shifting of spectral lines using spectroscopy (Mayor & Queloz, 1995). As at 10th October, 2006, 206 planets are known to exist in 178 exoplanetary systems, discovered either by stellar radial velocity changes or by the planet transiting the star. Ten of these planets transit their host star and Gliese 876 has been confirmed astrometrically (Benedict et al, 2002).

2.2 Categorising Habitable Exoplanetary Systems

The habitable zone around any star is the distance an Earth-mass planet orbits from a star where liquid water can exist on its surface, provided it has a dense enough atmosphere. For a full definition see chapter 3, section 1. The limit of gravitational influence of a giant planet can be expressed in terms of multiples of its Hill radius, the distance from the planet where its gravitational attraction and that of the star balance in the rotating frame of the giant's orbit (see chapter 4, section 1 for a full definition and also Appendices 1 and 3). The multiples depend on the giant's orbital eccentricity and whether an Earth-mass planet is in an inferior or superior orbit (Sleep, 2005).

For an Earth-mass planet to support life, it must have a stable orbit around its star and have its semimajor axis confined to the habitable zone. If a system's habitable zone is totally or partially clear from any gravitational influence from the giant planet, then the star in question could be a candidate for having a possible Earth-type planet with life. In cases where the giant planet's orbital semimajor axis resides within the habitable zone, then this is a good candidate for a habitable Earth-mass satellite. Different general categories for the known systems, where giant planet orbits are overlaid with the habitable zone over a star's main sequence lifetime, are shown in Figures 1.2 and 2.1 to 2.4. These examples include three of the nine systems investigated by orbital integration so far to show the diversity of these systems.

Category 1 – The entire Habitable Zone lies interior to the gravitational influence of the giant planet. The first profile in Figure 1.2 is for Jupiter's and Saturn's gravitational reaches within our Solar System and shows that Jupiter's inner gravitational reach extends to 3.9AU from the Sun, which confirms that it is too far away to severely perturb Earth's orbit so as to make it unstable. It also shows that 3.5Gyr from now; Earth's semimajor axis will no longer be confined to the habitable zone shown.

Category 2 - Part of the Habitable Zone lies inside or outside the gravitational influence of the giant planet. Figure 2.1 shows the configuration for 47 Ursae Majoris, where the gravitational influence of 47 UMa b, the inner of the two giant planets in this example, encroaches onto a **part** of the present habitable zone, in this case the outer region. A terrestrial planet may have existed near to the inner edge of the habitable zone in a confined orbit since the star's inception and would also be regarded as a good candidate for housing extraterrestrial life. This category would also include inner giants with

gravitational influences that also partially encroach into the inner regions of the habitable zone, allowing possible life bearing planets to exist near to its outer edge.

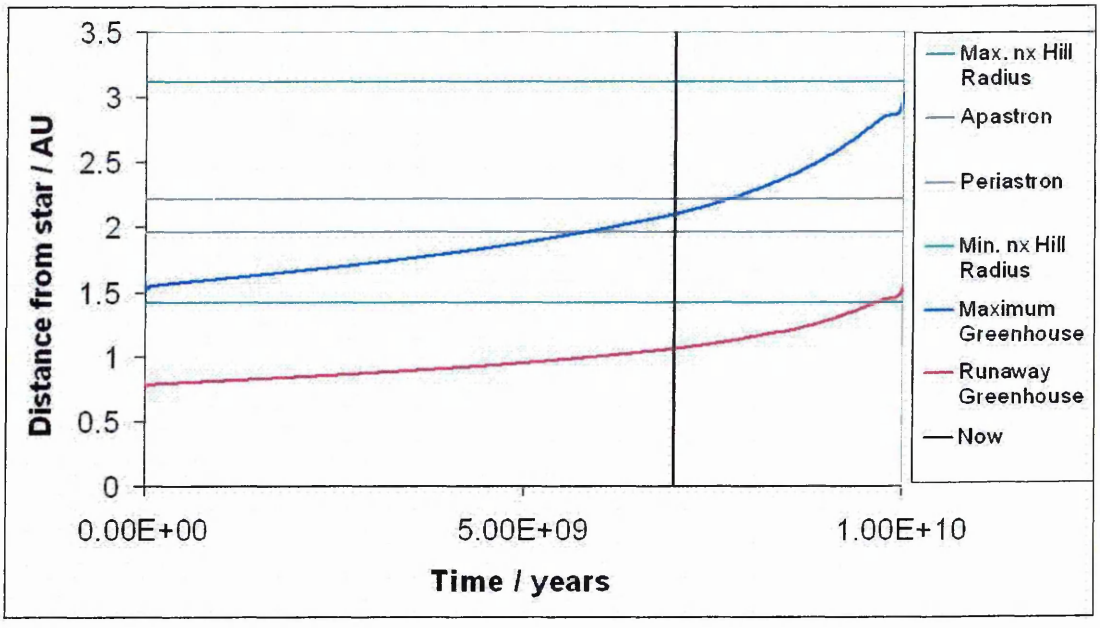

Figure 2.1 Variation of 47 Ursae Majoris's HZ with 47 UMa b's gravitational limits. The max. and min. *n* x Hill radius refers to the extremes of gravitational reach of the giant on an Earth-Mass planet (chapter 4, section 4). Maximum Greenhouse and Runaway Greenhouse refer to the Habitable Zone limits (chapter 3, section 1).

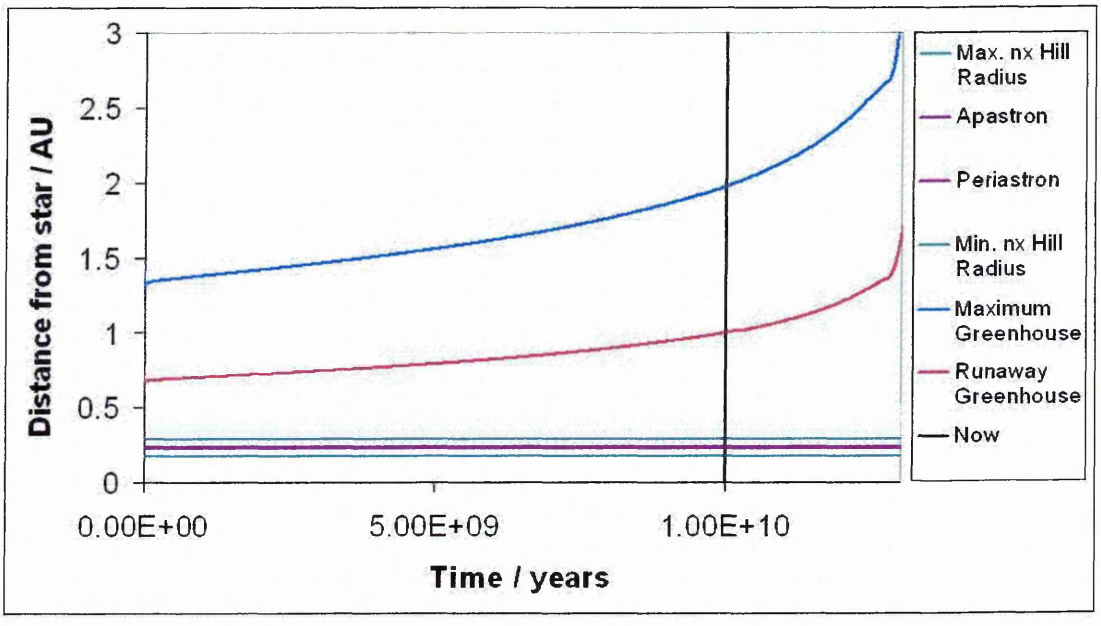

Figure 2.2 Variation of ρ Coronae Borealis' HZ with ρ CrB b's gravitational limits.

Category 3 – All of the Habitable Zone lies outside the gravitational influence of the giant planet. There are also many good candidates in exosystems where the giant is in an orbit interior to the habitable zone, such as ρ Coronae Borealis, shown in Figure 2.2, where the habitable zone is clear from any gravitational interference from the giant. The concern with these systems is whether the inward migration of their giant planet could have disrupted the orbits of any terrestrial planets already formed, or subsequently formed, in their habitable zone. Initial findings by Fogg & Nelson, 2005 suggest that terrestrial planets can be formed from reaccretion after migration. Mandell & Sigurdsson, 2003 suggest that terrestrial planet orbits already present are disrupted during migration, of

which a significant fraction survives, which increases as the speed of the giant's migration rate increases through the habitable zone.

Category 4 – All of the Habitable Zone lies within the gravitational reach of the giant planet. Figure 2.3 shows the configuration for the habitable zone and the giant's orbital extremes and gravitational reach for 16 Cygni B. This is an example of a system where a giant planet's orbit and gravitational influence completely engulf the habitable zone and where there would be no chance of a habitable planet existing at any time. The giant planet also has a very eccentric orbit ruling out the possibility of any habitable satellites around the giant.

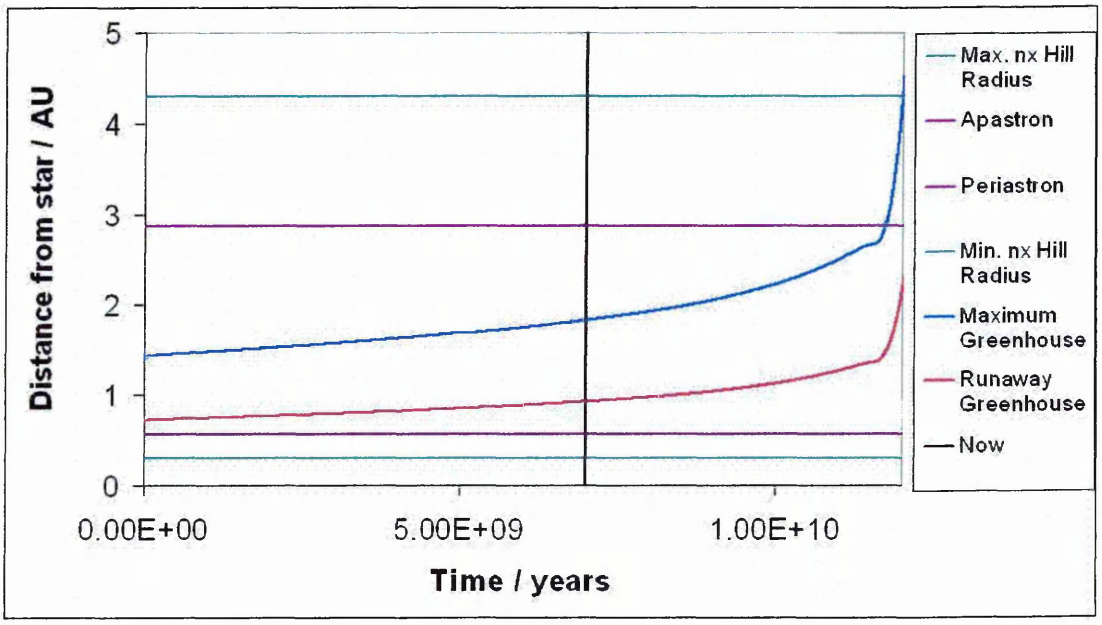

Figure 2.3 Variation of 16 Cygni B's HZ with 16 Cygni B b's gravitational limits.

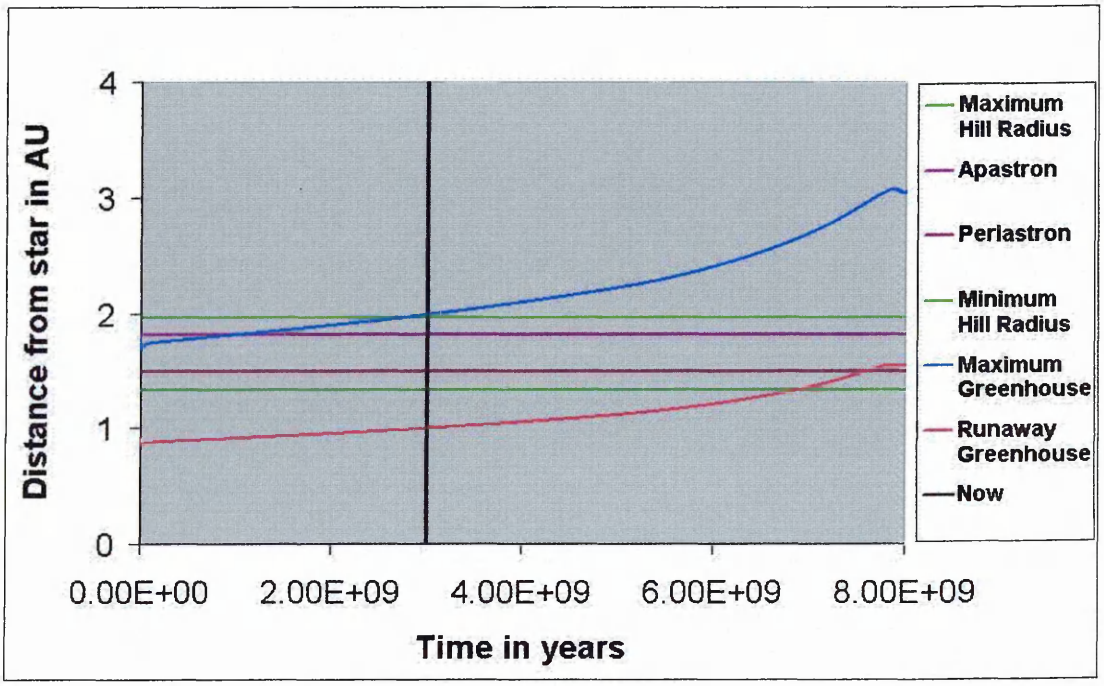

Figure 2.4 Variation of HD 23079's HZ with HD 23079 b's Hill radius.

Category 5 – A habitable satellite could exist in orbit around the giant planet. The system shown in Figure 2.4, HD 23079, shows the giant planet sitting in the middle of the habitable zone with only a slightly eccentric orbit. This is an excellent candidate for the possibility of a habitable Earth-sized satellite orbiting the giant. The Hill radius is shown in this diagram as opposed to gravitational reach. This is because satellites must remain bound to the giant and hence within the Hill radius for their orbits to remain stable.

2.3 Discovery Methods

2.3.1. Radial Velocities

The discovery of exoplanets, by radial velocity measurements of the primary star is likely to remain the primary method in the short term. The star and the planet orbit their centre of mass, so the star will also exhibit an orbital motion, much smaller than the planet's motion. The star's orbit is revealed by Doppler shifting of its spectral lines as it moves towards and away from Earth. Spectral information on the star gives its approximate age and mass. From the regular sinusoidal movement of these lines, the orbital period of the planet is determined; hence the planet's orbital semimajor axis and minimum mass are obtained. For a planet with orbital period, P, around a star of mass, M_*, then from Newton's Gravitational Law, the orbital semimajor axis, a, is given by:

$$a = \left(\frac{GM_* P^2}{4\pi^2} \right)^{1/3} \qquad 2.1,$$

where G is the universal gravitational constant. For a stellar radial velocity of amplitude, v_{rA}, caused by a planet of minimum mass, m, (Jones, 2003):

$$m = v_{rA} \left(\frac{PM_*^2}{2\pi G} \right)^{1/3} \qquad 2.2$$

The orbital eccentricity, e, may be found from variations in the rate of change of spectral line movement over several orbits. Circular orbits will give a perfect sine wave, whereas any departures will increase with increasing orbital eccentricity. The star 51 Pegasi's spectral lines were observed by the fibre-fed Echelle Spectrograph ELODIE of the Haute-Provence Observatory in France. The radial velocity amplitude was found to be 56 metres per second, easily detectable with the instrument, which has an accuracy of about 13 metres per second. Subsequent calculations revealed the planet to have a minimum mass of $0.46 M_J$, orbiting in 4.22 days (Mayor & Queloz, 1995). The downside to this technique is that Doppler shifting of spectral lines alone does not reveal the plane of the orbit. This may be inferred from other information such as shapes of dust rings around the central stars of exoplanetary systems. If such a ring is assumed to be circular, then a value for i_0 may be estimated from its apparent ellipticity, as is so for ε Eridani (Greaves et al., 1998), ρ Coronae Borealis and HD 210277 (Trilling et al., 2000).

2.3.2 Transits

A sure method of finding the planet's true mass is when v_{rA} is known and the orbit lies nearly edge-on, i.e. $i_0 \approx 90^{\circ}$. The planet then transits the star, as with ten of the discovered exoplanets. Surveys of nearby star clusters, such as EXPLORE and STEPSS, and all sky surveys such as PASS, hope to reveal more extra-solar planets in this way (Mallen-Ornelas et al., 2002, Burke et al., 2002 and Konacki et al., 2003 respectively), whereas the Optical Gravitational Microlensing Experiment, OGLE, has already uncovered 59 transiting candidates (Konacki et al., 2003). Figure 2.5 shows the geometry for transiting planets and for a planet of radius, R_p, orbiting a star of radius, R_*, in an orbit of radius, a, inclined at

angle, i_0, with respect to the plane of the sky, perpendicular to the line of sight to Earth, then:

$$\cos i_0 = \left(\frac{R_* + R_P}{a}\right) \Leftrightarrow i_0 = \cos^{-1}\left(\frac{R_* + R_P}{a}\right) \qquad 2.3,$$

where i_0 is measured in radians and $0 \le i_0 \le \pi/2$. The probability, p, of transits occurring for a randomly orientated orbit is $p = ((\pi/2) - i_0)/(\pi/2) = 1 - (2i_0/\pi)$, hence:

$$p = 1 - \left(\frac{2}{\pi}\right)\cos^{-1}\left(\frac{R_* + R_p}{a}\right) \qquad 2.4.$$

This probability, p, is the same for any angle, ϕ, rotated around the line "to Earth" out of the plane of the page. So for example, if Jupiter, of radius $\approx 0.1R_\odot$ (solar radii), orbited the Sun at $10R_\odot$ the probability it would transit the Sun as seen from anywhere outside the Solar System, would be ≈ 0.07. This is a scenario similar to known "Hot Jupiter" planets and clearly this probability will increase for larger R_p, larger R_* and smaller a. The probability estimate from the example is in good agreement with current estimates that 10% of such planets do transit their star (Charbonneau et al, 2000).

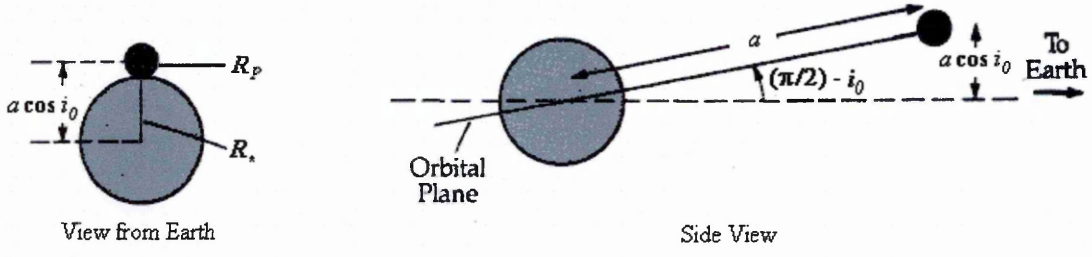

Figure 2.5 Geometry for a transiting planet

The transit of the planet causes a drop in radiation received from the star. For Jupiter transiting the Sun, this would be ~1%, which is of the order of the 1.2% observed for OGLE-TR-56 (Konacki et al., 2003) and 1.6% for HD 209458 (Charbonneau et al, 2000). The time between successive transits gives the orbital period and from the stellar spectral information inferring the star's mass, the planetary semimajor axis is determined from equation (2.1). The shape of the star's radiation curve as the planet crosses the stellar disc gives the planetary radius and the transiting position, so the exact orbital inclination with respect to the plane of the sky is deduced leading to a better value of the planet's true mass. The drawbacks of this technique are that, statistically, less than 10% of all Hot Jupiter giant planets in exosystems may transit their star and a much smaller percentage of giant planets with larger orbits. Also, Earth-type transiting bodies would cause an approximate stellar radiation drop of only 0.01% or less, which is currently undetectable. The big plus, however, is that the atmospheric content may be found for a giant planet, from spectral line differences between the star and planet, as it transits, and the star alone. Information on the lower atmosphere of HD 209458 b has already been determined (Charbonneau et al, 2002 and Vidal-Madjar et al., 2003).

2.3.3. Astrometry

A third technique for detecting extrasolar planets is to track the proper motion of a star, known as astrometry. This has been used to verify the parameters of Gliese 876, with the mass of Gliese 876b now being established as $1.89 \pm 0.34\ M_J$ (Benedict et al., 2002). Positional astronomy is the oldest branch of astronomy and is the measurement of precise movements of objects on the celestial sphere and, therefore, includes the science of tracking the proper motions of stars across the sky with time. Any regular movements, within a star's direction of motion, may be detected revealing the presence of any unseen bodies causing the effects. Information from the motion of a star, with a known mass, will reveal the planet's orbital period, its semimajor axis, eccentricity and its actual mass. This method can, however, be only applied to stars with detectable effects of planetary

companions on their proper motions, which restricts its use to relatively nearby objects. For a star at distance, d, with an angular orbital excursion in radians, β, then, for $M_* >> M_p$,

$$M_* \beta d = M_p a \qquad 2.5.$$

Substituting for a from equation (2.1) to obtain an expression for the planet mass, M_p, in terms of its period, P, gives:

$$M_p = \beta d \left(\frac{4\pi^2 M_*^2}{GP^2} \right)^{1/3} \qquad 2.6.$$

Any eccentricity in the planet's orbit can be determined from its position-time curve.

The ESA mission GAIA will make high-precision astrometric measurements and will contribute to a database of stars within 25pc, complementing radial velocity surveys of nearby F, G and K type stars (Sozzetti et al., 2003). The Space Interferometry Mission (SIM) will also be making precise astrometric measurements of nearby stars, of which simulated observations estimate planets may be detected to $3M_\oplus$ (Ford & Tremaine, 2003).

2.3.4 Direct Detection by Observation

The most obvious technique to be considered to detect extrasolar planets would be direct imaging. The biggest difficulty to overcome here is one of contrast, illustrated by the appearance of our Solar System from α Centauri, the nearest star, at 1.3pc. In visible light the Sun would have a visual magnitude of 0.4 and Jupiter would be 4 arcsec distant with a visual magnitude of 22, whilst the Earth would be 0.77 arcsec distant with a visual magnitude of 28 (Illingworth, 1985). The Sun is, hence, about 10^9 times brighter than Jupiter in visible light, however the difference is less marked in the infrared where it is only 10^5 times brighter due to the planet emitting in this spectral region. Using current technology, the glare from the star would make it extremely difficult to observe any surrounding planets, by optical, photographic or electronic processes. Projects under development, to circumvent this problem are based on coronagraphy, nulling interferometry and fixed delay interferometry. Coronagraphy occults the central object and can reduce scattered light by up to 10^4 (Kitchin, 1998), nulling removes the central object by destructive interference for example by using a phase mask coronagraph (Guyon & Roddier, 2002), and fixed delay interferometry measures the stellar fringe phase shifts (Ge, 2002). A ground based search of selected young stars, using adaptive optics and an "unsharped masking" technique, with the twin Keck 10 metre telescopes on Mauna Kea, Hawaii, is already under way (Kaisler et al., 2003). This should find planets of 1-10M_J within 100AU of young (t < 60Myr) nearby (d < 60pc) stars. Presently, four planet candidates have been found using direct imaging although two may be Brown Dwarfs. The space based project Darwin should find many candidates within the next fifteen to twenty years.

2.3.5 Gravitational Microlensing

A fifth method of finding extra-solar planets is by gravitational microlensing. Two stars need to be in close alignment, with the nearer one having the orbiting exoplanet. When the relative proper motions take the nearer star close to the background star, it distorts the image of the distant star as its light becomes bent around it (Figure 2.6, Carroll & Ostlie, 1996), causing it first to brighten then dim as it moves away, giving a bell shaped light profile. Any planet of the nearby star will similarly affect the background star-light, only the planet's Einstein ring will be much smaller than the star's. The Einstein ring is the image of the background star when there is exact alignment between the observer, the lensing star, and the background star. The angular radius of the ring is given by (Gaudi, 2000)

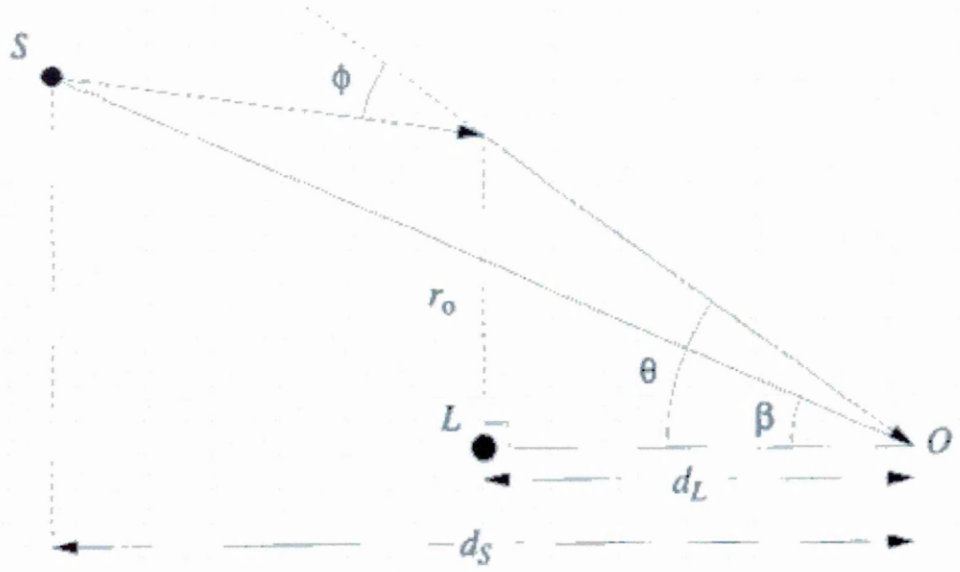

Figure 2.6 The geometry for a gravitational microlens. Light from the source, *S*, passes within a distance r_o of a microlensing point mass at *L* on its way to an observer at *O*. The angles involved are actually just a fraction of a degree, with r_o very small compared to d_L.

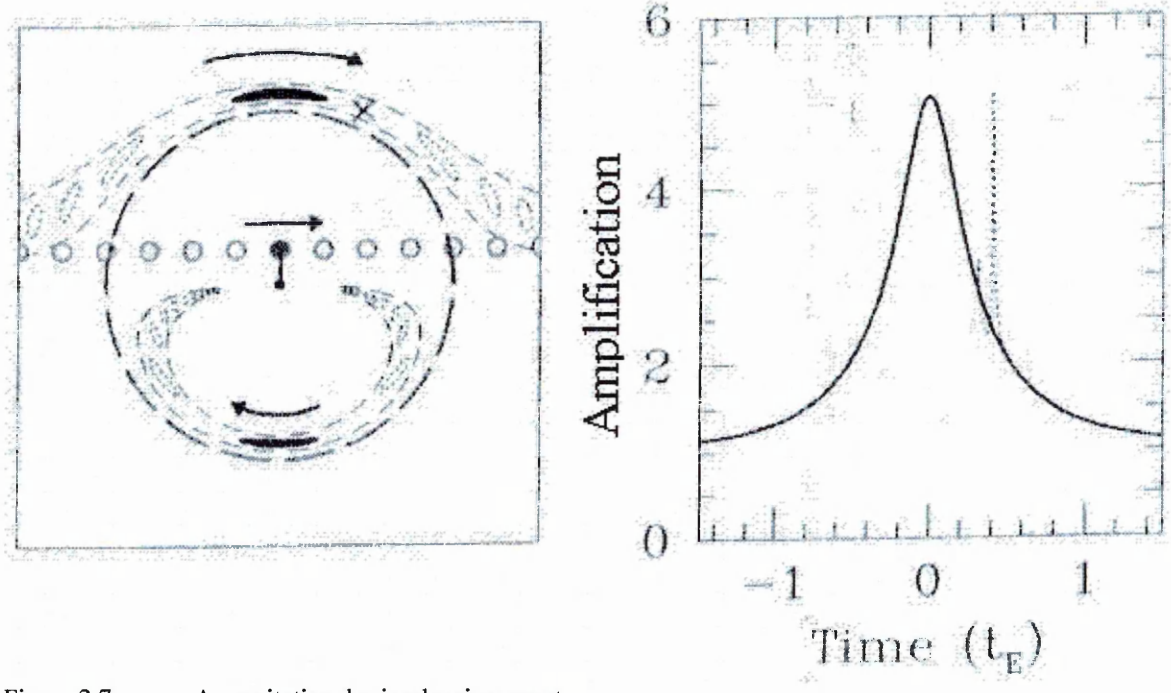

Figure 2.7 A gravitational microlensing event

Left: The dashed circle is the Einstein ring. The black dot at its centre is the foreground microlensing star with a planet at X. The open circles denote the true path of the background star, filled in at its closest angular approach. The images of the background star are shown by the "lozenges". At closest approach these are filled in black, otherwise they have dotted outlines.

Right: The solid line is the observed light curve with no planet at X; the dotted line is the difference to the curve made by the planet.

$$\theta_E = \left(\frac{4GM(d_s - d_l)}{c^2 d_s d_l} \right)^{1/2} \qquad 2.7.$$

Here, θ_E is the Einstein Ring radius, *G* is the universal gravitational constant, *M* is the mass of the lens, d_s is the source distance, d_l is the lens distance and *c* is the speed of light. If the alignment is not exact, then the image of the background star is not a ring. In Figure 2.7 (left) the actual path of the background star is shown by the open circles. At the distance of closest (angular) approach the background star is imaged as the two black arcs. Suppose

that the lensing star has a planet at X (Figure 2.7 (left)). As the background star moves to the right its upper image will move to the right as shown by the dotted "lozenges". Clearly this upper image will sweep over X.

Figure 2.7 (right) shows the light curve that would be measured for this event. The smooth curve is the brightness of the background star, where the amplification A of its unlensed brightness is given by (Gaudi, 2000),

$$A = \frac{x^2 + 2}{x(x^2 + 4)^{1/2}} \qquad 2.8,$$

where x is minimum angular separation between the stars as a fraction of θ_E.

The effect of the planet is to place a narrow spike in the light curve, as shown in Figure 2.7 (right). The duration of the spike is much less than the duration of the whole event, but the spike will generally be clear.

Results from the MACHO project (Alcock, 2000), suggest two light curves from stellar sources in the galactic bulge, which are consistent with 0.05 $M_\odot$ companions. Presently four microlensing candidates have been announced (Schneider, 2006), through the OGLE project. Investigations have shown that a space based gravitational microlensing survey for terrestrial solar planets is feasible in the near future using a 1-2 metre space telescope with a 2 degree field of view (Bennett & Rhie, 2002). The shortcomings of gravitational microlensing are that they are one off events. The planet "spike" on the bell shaped light curve can still give information regarding the planet's mass and a projected value can be obtained of its orbital semimajor axis.

2.4 The Planets Discovered – So Far

Ignoring planets around pulsars (Wolszczan & Frail, 1992), the discovery methods used so far have uncovered giant planets, of the order of Jupiter's and Neptune's masses, mostly in short period orbits around stars within 60pc of Earth (Lissauer, 2002). The short periods are easily detected from the sinusoidal motions of velocity curves derived from the regular Doppler shift of spectral lines of the accompanying star. The planets are giants, as these have the largest effect on the star's movement, which are most easily detected for nearby stars. So far, the longest orbit has a period of more than 12 years (55 Cancri d, announced 20/12/2002 by Marcy et al., 2002), the smallest mass planet is 7 $M_\oplus$. (Gliese 876 d, announced 22/08/2005 by Rivera et al., 2005). The only stars further than 60pc are those discovered by the transiting technique. As individual stars are observed over longer times, then orbits with longer periods and hence larger semimajor axes will become apparent. Also, with long term observations of light curves it will be possible to discern the tiny alterations made to the curves by Earth-mass planets. After a few tens of years of observations there will certainly be more exoplanetary systems resembling the Solar System, of which perhaps a not inconsiderable number may be good candidates for Earth-type planets with life. There may also be many planetary systems found around binary systems, such as γ Cephei, which make up approximately half of the population of all stars.

Of the currently known systems around main sequence stars, 108 of the 210 planets could be classified as "Warm Jupiters". These are defined in this thesis as having orbits of low eccentricity and orbital periods of less than 300 days. This orbital period approximately defines the inner limit of the habitable zone of stars with masses comparable to that of the Sun. Note the contrast with definitions for "Hot Jupiters", giant planets close to a star with orbits of less than 16 days (Weldrake et al., 2005) or 14 days (Basri, 2004) or at 0.05AU or less (Shkolnik et al., 2006). Of these 108 planets, 73 have periods of less than 50 days and

52 have periods of less than 10 days. There are 30 giants with periods of between 300 and 600 days, in or near the habitable zone. An orbital period of 600 days approximates the outer limit of the habitable zone of a star. Of these 30 giants, 12 have orbital eccentricities less than 0.2 and would be very good candidates for habitable satellites of giant planets. The remaining 72 planets orbit beyond the habitable zone and would be more like the familiar gas giants of our Solar System. The known exoplanets have a wide variety of eccentric orbits, from almost circular ones to $e = 0.927$ for HD 80606 (Naef et al., 2001).

3. Stellar Evolution and Habitable Zones

3.1 Defining the Habitable Zone and Continuously Habitable Zone

The smallest exoplanet around a main-sequence star that has been discovered so far orbits Gliese 876 and has a minimum mass of approximately 7 times that of Earth (Rivera et al., 2005). Bodies of Earth's mass are too small to be currently detected but they may well exist alongside known giant planets either as planets in their own right or as satellites of the giants. Some of these Earth-mass bodies may exist with liquid water on their surfaces, the necessity for habitability. Indeed, a first definition of the Habitable Zone is, "**the distance from a star where a body resembling the Earth, in a stable orbit and with sufficient mass, can support liquid water on its surface long enough for life to evolve and survive.**" For this to be so; the pressures and temperatures, depicted in figure 3.1, are required for liquid water to exist on a planet's surface.

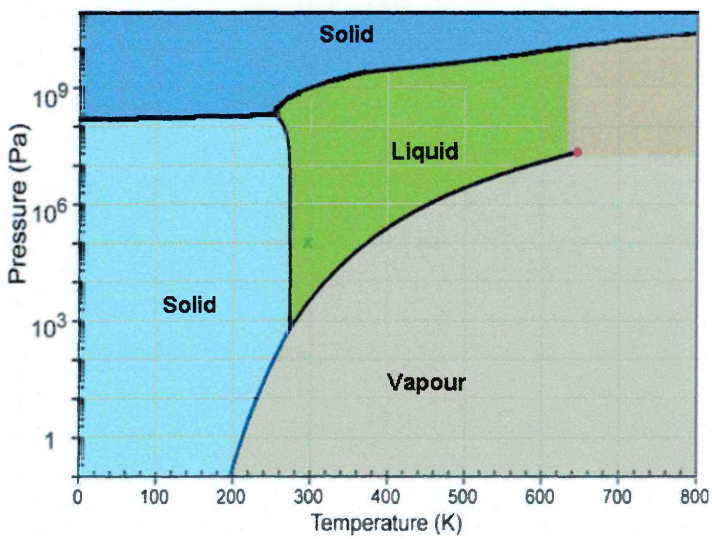

Figure 3.1 Phase diagram for water (Chaplin, 2004)

Figure 3.1 shows the phase diagram for water over a range of temperatures and pressures revealing the temperature and pressure boundary for liquid water. The phases of water are distinct and the only unexplained boundary is between the two solid phases. This is where ice becomes denser above 200MPa due to a pressure induced change in its crystal structure. The green cross is at 1 Earth-atmosphere and 298K, the red circle is the critical point of water at 647K and 22.1MPa.

The diagram shows that a body with liquid water must have sufficient mass to support an atmosphere that exerts a surface pressure greater than that of the triple point of pure water, i.e. 612Pa or ~0.006 Earth atmospheres (Young and Freedman, 2000). Water on any size of planet, as is the case on Earth, is very unlikely to be pure. Living creatures in water are themselves a contamination and require more than pure water to survive. Dissolved solutes from land or the ocean-bed will depress water's freezing point in terms of both temperature and pressure. When water freezes, the solutes in the remaining liquid become more concentrated, and through this process of sequestration, it is easily possible to retain liquid water down to 255K. So a planet could harbour liquid water with high solute levels provided, at the very minimum, it was large enough to sustain an atmosphere of a few hundred Pascals and a temperature of 255K over much of its orbit. Mars has an atmospheric pressure of about 560Pa (Jones, 2004), just below the pressure required for pure water to be liquid but possible for water with high solute levels to be liquid. It is also too cold, with temperatures ranging from 273K during an equatorial summer to 150K

during a polar winter (Beatty et al., 1999), but a Mars sized body closer to a star in an exosystem would be warmer, releasing more of its volatiles into the atmosphere. This may increase the amount of atmosphere sufficiently to give surface pressures great enough to support liquid water. The minimum mass for a habitable planet could thus be taken as 0.1 Earth-masses, i.e. around the size of Mars.

At the other extremes, vast pressures turn water to ice at any temperature where life could exist. This occurs at about 1GPa at 300K and 200MPa at the lowest temperature of pure liquid water at ~250K. These pressures are equivalent to a depth of approximately 100km of water at 300K and 20km at 250K (30km and 6km of solid silicates respectively). Although Earth's oceans are "only" 11km at their deepest, they may be far deeper on putative exo-Earths and such oceans could exist on slightly more massive Earth-sized bodies which have retained the right combination of volatiles. Such planets with masses of 6 Earths have been modelled (Leger et al., 2003) and if they formed inside the ice-line of a primordial system, the distance from a star beyond which ice could condense, they would be like a large Earth. Planets of the same mass but formed beyond the ice-line would resemble a small Uranus or Neptune, which have an abundance of hydrogen and helium in their outer layers rendering them uninhabitable. Therefore there is no reason to have 6 Earth masses as the upper limit – this could be 10 Earth masses or even greater. This is heavier than the 7 Earth-mass smallest exoplanet discovered so far, however this discovery was aided by it orbiting very close to its star. Its effect on the radial motion of its star is enhanced by its proximity, as discussed in chapter 2. A similar sized planet in the habitable zone would be much more distant and would have a much smaller effect on the radial motion of its star, making its detection far more difficult.

Pure liquid water can exist up to its critical point temperature of 647K from pressures of 22.1MPa up to 11GPa. Hence a planet could also sustain liquid water as long as its orbit maintained a periastron distance that did not elevate its temperature above 647K. Its mass would also need to be less great to produce atmospheric surface pressures greater than about 11GPa. Life is restricted at higher temperatures by where carbon compounds start to break down, at 435K (Jones, 2004). As the temperature of water approaches its critical point at 647K, water acts more like a hydrophobic solvent, with a lower affinity for electrolytes and a greater liking for non-polar molecules caused by its much lower dielectric constant and poor hydrogen bonding (Chaplin, 2004).

These boundaries for liquid water seem extreme when comparing them with the conditions for life on Earth's surface. There are life forms which can survive under such extreme conditions, however. Barophiles, or pressure lovers, have been found at the bottom of Earth's deepest oceans and in the crust, implying that living organisms are quite capable of equilibrating themselves with whatever pressure range they must endure. So pressure limits for life may only be constrained by the pressure boundaries for water depicted in Figure 3.1. If this is so then the habitability of a planet is less dependent on the mass related density of its atmosphere and/or its amount of volatiles. This implies that the most important determining factor for habitability is temperature. Psychrophiles, or cold lovers, have been found to survive down at 255K, provided the water is liquid and hence containing a high level of solutes. At the other end of the scale, extreme heat lovers, hyperthermophiles, have been found to survive at temperatures approaching 400K. It may even be possible that life could exist over an approximate temperature range from 245K to 435K (Jones, 2004).

So the freezing and critical temperatures of pure water are not solely regarded as defining habitable temperature ranges. The lower boundary seems more clearly defined by the freezing properties of water, but is affected by the freezing point depression effects of solutes. The upper boundary is more likely to be defined by the fate of liquid water at elevated temperatures on a planet's surface, not its critical temperature. On warm planets, water may be lost through dissociation due to reactions with UV radiation in a wet upper atmosphere leading to hydrogen loss. More violently, oceans may boil away due to the rapid onset of a Venusian type greenhouse effect. Hence the definition of the Habitable Zone requires some qualification and is investigated by looking at atmospheric models.

Kasting et al., 1993 introduced three definitions for each of the inner and outer boundaries of the Habitable Zone and they are as follows:

At the inner edges, in order of decreasing stellar flux:

1. **Recent Venus.** Assuming Venus formed with water, the conditions on Venus when water could have last flowed, approximately 1Gyr ago (Solomon and Head, 1991).
2. **Runaway Greenhouse Effect.** For cloud cover equal to that of Earth; a runaway greenhouse effect where temperatures at the surface of a planet reach the critical point of water (647K).
3. **Water Loss.** For cloud cover equal to that of Earth; an atmosphere with a wet stratosphere, where water is lost in the upper atmosphere by dissociation and subsequent hydrogen loss.

At the outer edges, in order of decreasing stellar flux:

4. **First Carbon Dioxide Condensation.** For a surface temperature of 273K, the distance at which carbon dioxide clouds first form.
5. **Maximum Greenhouse Effect.** The maximum distance at which a surface temperature of 273K can be maintained by a cloud free carbon dioxide atmosphere.
6. **Early Mars.** The conditions on Mars at the beginning of the solar main sequence lifetime, when free standing bodies of water are believed to have existed.

Conditions 2 to 5 are used to calculate the distance of a planet from its star deduced from the stellar flux at the top of its atmosphere capable of causing these scenarios. Conditions 1 and 6 are based on what is believed to have been the situations for Venus and Mars in the solar system's past, the solar fluxes being derived from the distances of Venus and Mars from the Sun and the solar luminosity **at the time.**

The term "at the time" is highlighted because the Sun's luminosity is not constant. All main sequence stars, including the Sun, burn hydrogen to helium during their main sequence lifetimes. The main sequence stage of any star is when it is most stable and is the only time long enough for life to evolve on any of its planets. As hydrogen burns in the stellar core, helium levels slowly increase causing the core temperature and pressure to increase. These higher temperatures are transferred to the outer layers of the star resulting in it becoming more luminous and voluminous over its main sequence lifetime. Initially as it slowly grows larger, its effective temperature will increase due to the core temperature increase. Later in the main sequence, as it grows larger more rapidly, its effective temperature will hit a maximum and then decrease before it starts to enter its red giant

phase. Figure 3.2 shows how the Sun's luminosity, radius and effective temperature change over its main sequence lifetime.

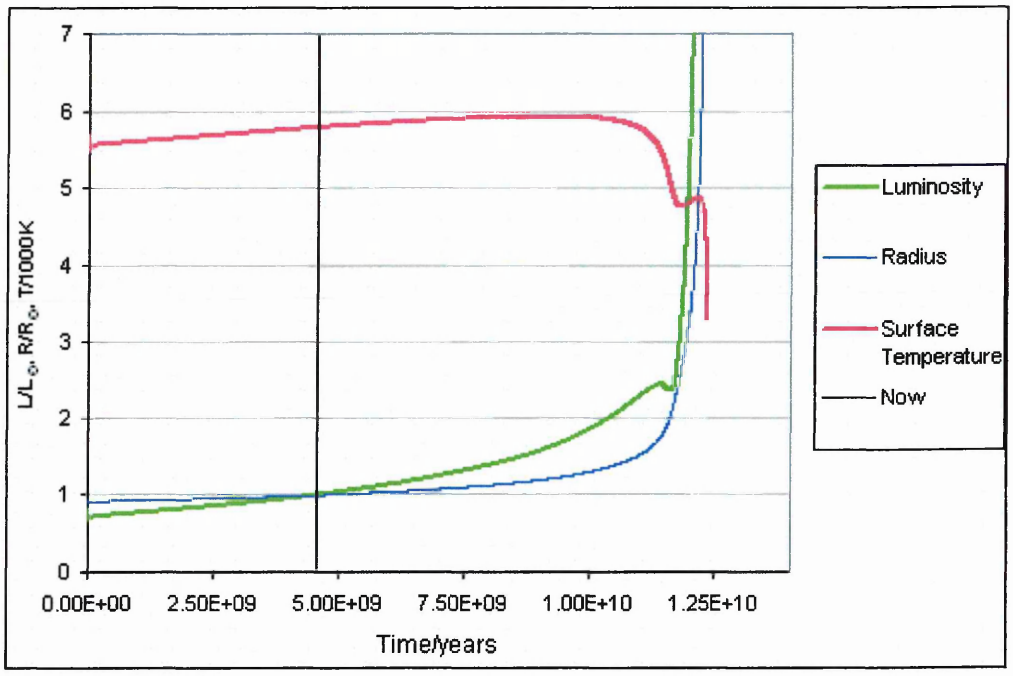

Figure 3.2 Change in the Sun's luminosity, radius and surface temperature over the course of its main sequence lifetime.

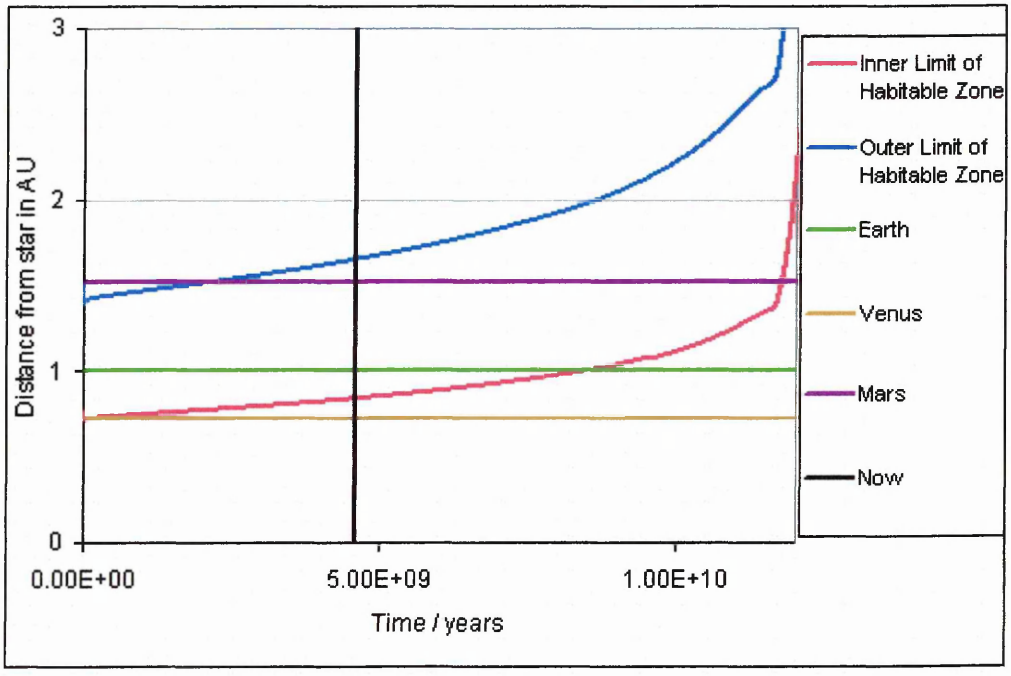

Figure 3.3 Movement of the Sun's Habitable Zone during its main sequence lifetime.

The consequence of this is that the habitable zone moves away from the star, shown in Figure 3.3 for the Sun, where a runaway greenhouse effect (Kasting scenario 2) gives the inner boundary and a maximum greenhouse effect (Kasting scenario 5) gives the outer boundary. So a planet that was originally within and near to the inner edge of the HZ may find itself on the sunward side of this region as the star ages. Provided this happened after life had changed the atmospheric composition of the planet, i.e. 2Gyr from the system's formation, the planet would be regarded as detectably habitable. This timescale is based on our Solar System; however the density of a primordial dust ring around a star, itself dependent on a star's metal content, will determine the length of the heavy bombardment time. Stars heavier in metals will have a dust ring also heavier in metals that will not be

evaporated so readily by the young stellar radiation as in a low metal star. The 2Gyr consists of approximately 1Gyr of heavy bombardment, characteristic of early stellar system evolution, plus a further 1Gyr for life to have a significant enough time to alter the planet's atmosphere. The consequences for life there, however, would be grim as it would inevitably be destroyed within a few 100Myr as the star aged. Indeed this will be the fate of the Earth within the next 1.2Gyr to 5Gyr, depending on the inner HZ boundary criterion, and could be well before the Sun reaches the end of its main sequence stage. Alternatively, a planet that was originally beyond the outer edge of the HZ may end up within it, as has already happened to Mars. A planet in this situation may slowly thaw, enabling any life to commence, be it later than if the planet were initially within the habitable zone. As long as there were to be 1Gyr before the onset of the star's red giant phase, such a planet would still be deemed as habitable, with sufficient time for life to alter the planet's atmosphere. There may be some planets which are in orbits fortunate enough to remain within the HZ for the entire main sequence lifetime of the star. These planets will reside in the **"Continuously Habitable Zone"** (CHZ) bounded by the distances from the star of the inner edge of the HZ at the end of its main sequence lifetime and the outer edge of the HZ at the beginning of the star's main sequence lifetime, otherwise known as zero age main sequence (ZAMS).

3.2 Determining Distances of Habitable Zones

As discussed in chapter 1, life on Earth took about 2Gyr from its origin to have an observable effect on the atmosphere. If this length of time is regarded as a requirement for the minimum lifetime of a star, then habitable zones need only be determined for stars with main sequence lifetimes longer than this, i.e. those which are less than $1.5M_{\odot}$ and thus of stellar type F and later (Kasting et al., 1993). A second reason for this upper limit is that hotter stars emit more radiation which is weighted towards ultraviolet wavelengths, too much of which destroys cellular life on a planet's surface. The crumb of comfort in this case is that subsurface life would be unaffected and such intense radiation may serve to create a thicker ozone layer on such a habitable planet. There is no real lower limit to a star's mass other than the minimum of $0.08M_{\odot}$ that defines a star (D'Antona and Mazzitelli, 1985), the mass required for hydrogen burning to take place in its core. A problem with low-mass M-type stars is that they exhibit flare activity, which may regularly sterilise planets within their normally habitable zones (Segura et al., 2006). Each flare may create a temporary habitable zone beyond the tidal lock distance, but for too short a time for life to gain any foothold. The variation in distances of such zones would also depend on flare intensity, which may not be consistent. So a lower limit is now introduced whereby a planet within the habitable zone would be far enough from the star to be relatively safe from such events. This is taken to be the distance where the habitable zone is beyond the tidal locking zone. Within a star's tidal locking distance, one side of a planet faces the star at all times, and the HZ lies inside this distance for stars less than about $0.5M_{\odot}$. This is depicted in figure 3.4 along with the increasing distance of the habitable zone as stellar mass increases. Tidal locking may not prevent planets being habitable, though, as atmospheric circulation may serve to reduce any thermal extremities on such a body. Also if an Earth-mass satellite is in synchronous rotation with a giant planet within this region, there will still be periods of day and night. Outside this tidal lock radius, planets may freely rotate about their own axis.

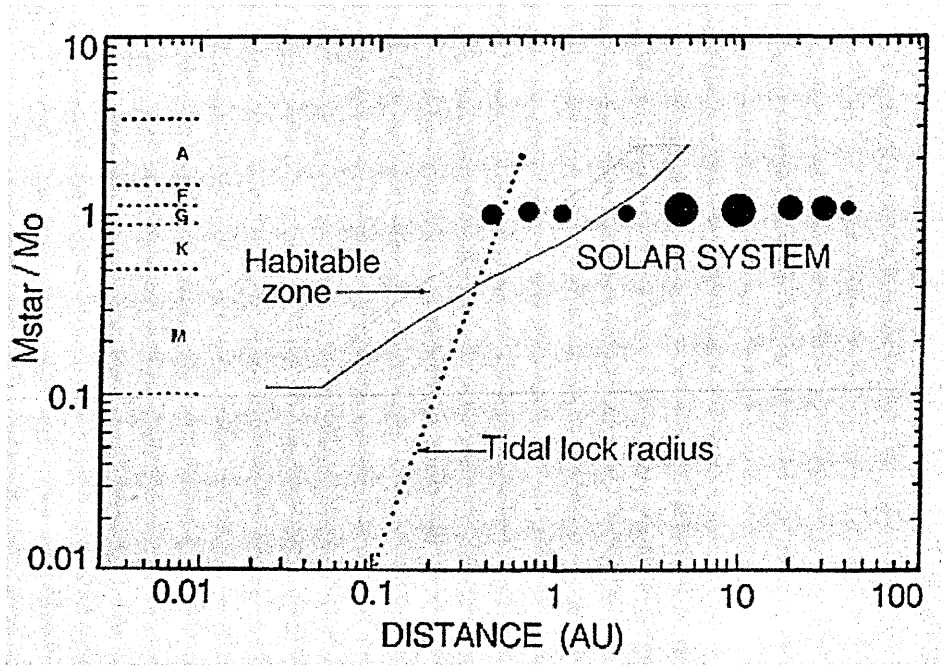

Figure 3.4 Habitable Zone at zero age main sequence and Tidal Lock Radius for different stellar masses.

It is not only the masses of stars which determine habitability of their systems. Stars must also contain sufficient metals for rocky Earth-type planets to have formed within the stellar accretion disk. The stars with known exoplanetary systems, most of which are within 60 parsecs of Earth, are generally higher in metals than the Sun, which is relatively metal rich compared to the general population over the same volume of space (Butler et al., 2000). The lowest mass fraction metallicity of a star known to have exoplanets is 0.008 compared to a little less than 0.02 for the Sun (Zeilik and Gregory, 1998 and Carroll and Ostlie, 1996), the most metal rich stars with planetary systems contain up to 0.06 mass fraction of metals. Although lower metallicity stars may have gas giant planets, the metal content at which rocky terrestrial planets may form is uncertain. However it is quite possible that Earth-like planets may form around stars with mass fraction metal contents, Z, as low as 0.008. Higher levels of metals within a star may enhance its chances of having its own planetary system; they also slow down the nuclear processes within a star. For two stars of the same mass, the one with the higher metallicity will be slightly less luminous and its time on the main sequence will be longer. This effect is minor compared to getting the same changes by decreasing stellar mass.

For stellar mass boundaries set by habitable zones being beyond the tidal locking distance of a star and a minimum main sequence lifetime of 2Gyr, HZs need be determined for main sequence stars between $0.5M_{\odot}$ and $1.5M_{\odot}$, i.e. F, G, K and early M type stars, with metallicity mass fractions from 0.008 to 0.06. Of these stars, the more luminous will clearly have their habitable zones at greater distances. A lesser effect on the HZ distance, however, is a stars effective temperature. According to Wien's displacement law, a black body of absolute temperature, T, has a peak intensity wavelength, λ_{max}, over its emission profile of intensity versus wavelength, where,

$$T\lambda_{max} = 2.90 \times 10^{-3}\text{Km} \qquad 3.1$$

This shows that a cooler star, with a lower effective temperature, will have a black body emission profile that will be weighted towards longer wavelengths of the electromagnetic spectrum. Secondly, according to the Stefan-Boltzmann law, for total emissive power, E, stellar radius, R and Stefan's constant, σ, then

$$E = 4\pi R^2 \sigma T^4 \qquad 3.2$$

So a body with a lower effective temperature will need to have a larger surface area in order to have the same total emissive power as a hotter body. For stars of the same luminosity with equidistant planets, the greenhouse effect is greatest around the star emitting the greatest amount of infrared radiation. Planets with volatiles such as water and carbon dioxide will retain such molecules in its atmosphere if they become too warm and oceans evaporate. These molecules absorb infrared radiation heating a planet above the expected temperature for its distance from a star as if in a greenhouse. Thus for two stars of equal luminosity, the one which is cooler and hence larger will emit a greater proportion of its radiation at infrared wavelengths and will effectively increase the distance of the habitable zone from that star. Figure 3.2 shows how the Sun's radius, luminosity and effective temperature profile changes over its main sequence lifetime, and is typical of main sequence stars. The early luminosity and effective temperature increase will cause the habitable zone to move out slightly less than if the temperature had remained the same. However during later main-sequence stages, when the star's luminosity increases but effective temperature decreases as it approaches its red giant phase, the outward movement of the habitable zone will be accelerated.

Table 3.1 Critical Solar Fluxes for Different Stellar Types.

Stellar Type	**M0**	**G2**	**F0**
T_{eff} / K	3700	5700	7200
Habitable Zone Limit		***S****	
Recent Venus**	1.60	1.76	2.00
Runaway Greenhouse	1.05	1.41	1.90
Water Loss	1.00	1.10	1.25
1st CO_2 Condensation	0.46	0.53	0.61
Maximum Greenhouse	0.27	0.36	0.46
Early Mars***	0.24	0.32	0.41

* Values relative to the present mean solar flux at the top of Earth's atmosphere (1370Wm^{-2}).

** Recent Venus fluxes, for M0 and F0 stars, are derived from the product of their critical water loss fluxes and the same flux ratio of recent Venus over water loss for the G2 star.

*** Early Mars fluxes, for M0 and F0 stars, are derived from the product of their maximum greenhouse fluxes and the same flux ratio of early Mars over maximum greenhouse for the G2 star.

The six habitable zone boundaries, mentioned in section 3.1, are obtained from known critical stellar fluxes (power per square metre), S, at the top of planetary atmospheres. These are determined from one-dimensional radiative-convective atmospheric models by Kasting (1993), where the cloud cover for the interior boundaries is fixed at terrestrial levels. These critical fluxes are determined for a standard Earth-mass planet ($1M_{\oplus}$) and represent approximate average values obtained also for planets of $0.1M_{\oplus}$ to $10M_{\oplus}$. The habitable zone for a more massive planet will be closer to the star than for a smaller planet, since larger bodies, with higher surface gravities, are able to retain their volatiles more effectively so their "Water Loss" and "Runaway Greenhouse Effect" will occur at higher temperatures. The heavier atmosphere of a larger planet would also induce "1st CO_2 Condensation" at higher temperatures, although the "Maximum Greenhouse" scenario will occur at approximately equal fluxes for all planetary masses since a surface temperature of 273K is required in each case. This implies that the habitable zone of a more massive planet would be wider than for a smaller planet. Table 3.1 gives the values of the critical fluxes for an Earth-mass planet, which are dependent on effective stellar temperature as discussed in the previous section, giving three values for each habitable zone boundary. From each of these six sets of three values, the critical stellar fluxes can be determined for

effective temperatures, T_{eff}, between the extremes of 3700K and 7200K, by means of curve-fitting.

For each of the six curves, S is dependent on T_{eff}, hence $S = f(T_{eff})$, which will be quadratic in nature as the degree of a best fit curve is always one less than its number of coordinates. The six equations below were calculated using Maple V Release 5 software (November 27th, 1997), by Waterloo Maple Inc. The statistical fit value, r^2, is 1 for all six equations and with S in terms of $S_{\oplus}$, the flux at the top of the Earth's atmosphere of 1370Wm^{-2} (Zeilik and Gregory, 1998), and T_{eff} in Kelvin, they are,

Recent Venus:	$S = 2.286\times10^{-8}\,T_{eff}^2 - 1.349\times10^{-4}\,T_{eff} + 1.786$	3.3
Runaway Greenhouse:	$S = 4.190\times10^{-8}\,T_{eff}^2 - 2.139\times10^{-4}\,T_{eff} + 1.268$	3.4
Water Loss:	$S = 1.429\times10^{-8}\,T_{eff}^2 - 8.429\times10^{-5}\,T_{eff} + 1.116$	3.5
1st CO_2 Condensation:	$S = 5.238\times10^{-9}\,T_{eff}^2 - 1.424\times10^{-5}\,T_{eff} + 0.4410$	3.6
Maximum Greenhouse:	$S = 6.190\times10^{-9}\,T_{eff}^2 - 1.319\times10^{-5}\,T_{eff} + 0.2341$	3.7
Early Mars:	$S = 5.714\times10^{-9}\,T_{eff}^2 - 1.371\times10^{-5}\,T_{eff} + 0.2125$	3.8

Now for a star of luminosity, L, and flux, S, then $S \propto L$, and at distance, d, $S \propto \frac{1}{d^2}$. The semimajor axis, a, of the Earth's orbit around the Sun is $1.495978707 \times 10^{11}$m (Murray and Dermott, 1999), defined as the astronomical unit. Hence for L measured in terms of solar luminosity $L_{\odot}$, S in terms of the solar constant, $S_{\oplus}$, and d in astronomical units, then,

$$S = \frac{L}{d^2} \qquad 3.9$$

The distance of any particular habitable zone boundary can now be determined by,

$$d = \sqrt{\frac{L}{S}} \qquad 3.10.$$

3.3 Modelling Stars – Previous Work

Figure 3.2 shows the changes of the sun's luminosity, effective temperature and radius over the course of its main sequence lifetime, and Figure 3.3 shows the outward movement of the solar habitable zone caused by these changes over this period. Programs that calculate these stellar parameters have often been used in studies predicting the past climates on Earth, and the fate of life on Earth in the future. Solar models of Newman and Rood (1977), Gough (1981) and Gilliland (1989) have predicted that the Sun's luminosity was approximately $0.7L_{\odot}$ when it first formed and will be almost $3L_{\odot}$ at the end of its main sequence lifetime in 7Gyr. Models of Sackmann et al. (1993) agree with the Sun's initial luminosity but predict a final main sequence luminosity of $2.2L_{\odot}$ in 6.5Gyr time.

Stellar models have also been applied previously to stars other than the Sun. Montalban et al. (2000) have investigated models of low-mass population II stars in order to improve agreement with data from metal rich globular clusters. Girardi et al. (2000) have used stellar evolution models to follow the evolution of star clusters and galaxies by means of population synthesis. The first person to combine stellar evolution models with habitable zones was Hart (1979), where he investigated continuously habitable zones around main sequence stars. He also included planetary atmospheric evolution in his models, concluding that CHZs became thinner for stars less massive than the Sun and disappeared for stars of spectral type K0 and later. Subsequent work by Kasting et al. (1993) also included atmospheric modelling in their studies, which was used to determine habitable

zone boundaries around stars dependent on different atmospheric scenarios. They used stellar models from Iben (1967) and Gough (1981) to determine the changes in stellar parameters for stars from $0.5M_{\odot}$ to $1.5M_{\odot}$ at intervals of $0.25M_{\odot}$. This work is the basis of the determination of habitable zones in this investigation although a more updated stellar evolution code, developed by Mazzitelli (1989), is used to model the stars.

Kasting's work, however, only incorporated terrestrial levels of cloud into their simulated atmospheres. Forget and Pierrehumbert (1997) used models to show that the surface of early Mars could have been warmed by carbon dioxide ice clouds reflecting outgoing infrared radiation back to the surface. This may also explain how the early Earth was not significantly cooler, if at all, than it is now despite the Sun being less luminous. Mischna et al. (2000), suggest that the presence of carbon dioxide clouds in an atmosphere could extend the outer edge of the solar system's habitable zone from 1.8AU, predicted by Kasting's cloudless models, to 2.4AU. More recent work of Williams and Pollard (2002), with other models, suggests that the runaway greenhouse effect, scenario 2 of the atmospheric models listed in section 1 of this chapter, would occur only somewhat closer to the star. They also suggest that planets on highly eccentric orbits with semimajor axes within the habitable zone would be susceptible to large climatic variations. However their long-term climate stability depends on average stellar fluxes over one complete orbit and not the time spent within the HZ. This would allow planets to approach its star to much closer distances at periastron than that which may cause a runaway greenhouse effect on planets in more circular orbits. Williams and Kasting (1997) investigated the effect on climate of changing the Earth's axial tilt up to 90°. They found that planets with small continents would not suffer as greatly as planets with large land masses and those planets further out in the HZ would also be less affected, due to an accumulation of carbon dioxide, which enhances atmospheric heat transportation. They conclude that an Earth with a high axial tilt would remain habitable at a slightly further distance than one with its present inclination.

The only other known current investigation of a similar nature to this chapter's study is that of Turnbull and Tarter (2003), which concentrates its efforts towards the Search for Extraterrestrial Intelligence (SETI). They use a stellar evolution program called TYCHO (Young et al., 2001) to model habitable zones, also based on atmospheric models of Kasting. Since they are looking for communicating intelligence, they restrict their potentially habitable candidates to single **and multiple** stars known to be at least 3Gyr old in their pursuit to create a "Catalogue of Habitable Stellar Systems" or "HabCat". As they are not considering the future, the outward movement of the HZ, due to stellar luminosity increase over a star's main sequence lifetime, is effectively bypassed. Turnbull and Tarter regard a communicating intelligence also capable of moving to more temperate planets, further out in a system, when their original planet becomes uninhabitable. They use their elimination techniques to select 17,163 suitable "HabCat" stars from the 118,218 stars in the Hipparcos Catalogue. Included in these 17,163 stars are those with the then known 55 giant planet systems. Using the criterion that a giant planet cannot approach within 3 Hill radii ($3R_{H}$) of an HZ boundary, introduced in chapter 1, they eliminate 34 of these candidates, including those with possible satellites due to high radiation from the giant. Hence their final list of habitable stars is reduced to 17,129.

3.4 The Computer Program

The data used to draw the curves in figure 3.2 and calculate the habitable zone curves in figure 3.3 are determined using Mazzitelli's stellar evolution computer program, which can run on any computer using a Linux or Unix operating system. The program was written in the Fortran language and models the main sequence evolution of stars, from their initial

nuclear burning of hydrogen to helium in the stellar core at zero-age main sequence (ZAMS), up to the onset of their red-giant phase when the core hydrogen supply is depleted. This program was recommended by Kolb (2003) and it has been extensively tried and tested in the evolutionary study of single and binary stars (Barker and Kolb, 2003, Kolb et al., 2000, Stehle et al., 1994, Kolb and Ritter, 1992).

During a simulation, all relevant output information regarding the variations in stellar luminosity and effective temperature with age is stored in an output file, both of which are necessary for determining habitable zone distances. The time step between each calculation on the model's main sequence is determined by the user. When a stellar model is in its infancy and at the end of its time on the main sequence, however, processes within the star occur more rapidly and the program will set its own time-step to allow for these rapid changes.

The output from each simulation can be imported to most spreadsheet programs for editing, calculation, plotting and analysis. For this study, the spreadsheet program used was Microsoft ® Excel 2002 SP3. The output of stellar age is in years, luminosity is in terms of $\log_{10}(L/L_{\odot})$, effective temperature is given as $\log_{10}(T_{eff}/K)$ and stellar radius is in terms of solar radii. The critical fluxes of habitable zone boundaries are then determined for each stellar age using equations 3.3 to 3.8, from which the distances of these boundaries can be found from equation 3.10.

3.5 The First Stellar Matrix

3.5.1 Calibrating the Matrix using the Sun

Before using the program to simulate any stars, the stellar evolution model had to be calibrated using the present day Sun as the standard. The maximum time interval between each successive modelling step was one million years for all but a few cases, which will be mentioned when encountered. Also no mass loss was allowed for in any stellar model as this is only a few hundredths of one percent for any star of mass $1.5M_{\odot}$ or less, over its main sequence lifetime (Beatty et al., 1999). The first solar model had a helium mass fraction of 0.27 and metals mass fraction of 0.02 (Beatty et al., 1999). The use of metals mass fraction in this thesis is as required by the stellar evolution program, rather than [Fe/H] values normally quoted in the astronomical literature. The carbon, nitrogen and oxygen mass fractions of the metals were 0.1308, 0.043 and 0.39 respectively (from the Mazzitelli program's "reading.f" help file). Values of mixing length, α, are presently indeterminable (Young et al., 2001), this term has no units as it is the ratio of the distance a rising gas bubble travels, before equilibrating with its surroundings, to the pressure scale height ($p/\rho g$, where p is pressure, ρ is density and g is acceleration due to gravity). An initial suggested value for α was set at 1.4 (Kolb, 2003). The initial solar mass ($M/M_{\odot}$), luminosity ($L/L_{\odot}$), effective temperature (T_{eff}/K), core pressure (p/Pa) and core temperature (T/K) were taken from the "starters.rk" file within the program with values of 1, -0.13, 3.7400, 17.17000 and 7.1400 respectively, where all values are logarithmic except the solar mass. From these starting parameters, the sun reached its present day luminosity after 4.560Gyr, from its initial luminosity at zero-age main sequence (ZAMS) of $0.74L_{\odot}$ ($10^{-0.13}L_{\odot}$). However the solar radius was slightly too large at $1.047R_{\odot}$ and the effective temperature was a little cool at 5640K. This was a good starting point, however, considering that the solar system is 4.55Gyr to 4.60 Gyr old and the present day solar effective temperature is given as 5787K (Cox, 2000).

The first parameters to be changed, in order to refine the model were the carbon, nitrogen and oxygen mass fractions of metals. These values were reset to 0.1516, 0.05289 and 0.5289 respectively (Jones, 1999) whilst all others remained unchanged. The difference was imperceptible with the Sun's present day luminosity being attained after 4.568Gyr, only 8 million years later than the first model, with the radius and effective temperature remaining as previous. As this change had such a small impact, these new mass fractions of metals of 0.1516 for carbon, 0.05289 for nitrogen and 0.5289 for oxygen were retained in all subsequent runs for all stellar models, as these values were obtained from a more recent source.

The second set of parameters had a different starting luminosity, effective temperature, core pressure and core temperature. Alternative values were obtained from Cox (2000), which were -0.15230, 3.7514, 17.18510 and 7.1306 respectively. This solar model gave exactly the same profile as the previous one, implying that these starting values have little or no effect on a stellar model. The starting solar luminosity at ZAMS of $0.7L_{\odot}$ (where $0.7 = 10^{-0.15230}$) is also in better agreement with accepted values. However, the program user must beware of entering arbitrary numbers here, because if the values are too far from those expected, the model will not run at all. As this second set of parameters was also obtained from a more recent source, these were used for all subsequent solar runs.

Since the metals mass fraction of the sun was set at 0.02, the only two parameters left to change, in order to obtain an accurate solar model, were the helium mass fraction and the mixing length. The effect of changing the mixing length parameter, α, was investigated first, with further runs where α was varied from between 1.7 and 2.0 at intervals of 0.1. Table 3.2 reveals how these changes affected the time required to attain present day solar luminosity and the values of the modelled solar radius and effective temperature at that time, for a constant helium mass fraction of 0.27.

Table 3.2 Effect of mixing length on the time it takes a solar model to reach the present day solar luminosity with modelled solar radius and effective temperature after that time, for a constant helium mass fraction of 0.27.

Mixing Length	Time to reach $L_{\odot}$/Ga	$R/R_{\odot}$	T_{eff}/K
1.7	4.506	1.011	5740
1.8	4.486	1.002	5767
1.9	4.467	0.993	5792
2.0	4.448	0.985	5815
Literature	4.55 – 4.60	1.000	5787*

* Cox (2000).

Increasing the mixing length clearly shortens the time it takes the model to reach the present day luminosity. This implies the core energy increases with increased mixing length, making the star smaller and hotter. As the solar radius and effective temperature were close to literature values when $\alpha = 1.9$, it was fixed at this value and the helium content was varied from a mass fraction of 0.25 to 0.30. Table 3.3 shows the effects of varying the ZAMS helium content on the model age at the present day luminosity, $L_{\odot}$, the solar model radius and effective temperature at that age.

Table 3.3 Effect of helium mass fraction on the time it takes a solar model to reach the present day solar luminosity with modelled solar radius and effective temperature after that time, for a constant mixing length of 1.9.

Mass fraction helium content	Time to reach $L_\odot$/Ga	$R/R_\odot$	T_{eff}/K
0.25	6.856	1.032	5682
0.255	6.225	1.022	5710
0.26	5.616	1.012	5738
0.265	5.031	1.002	5765
0.27	4.467	0.993	5792
0.275	3.923	0.984	5818
0.28	3.399	0.976	5843
0.285	2.894	0.968	5867
0.29	2.409	0.960	5889
0.295	1.944	0.953	5911
0.30	1.499	0.946	5933

Table 3.3 shows the drastic effect changing the solar helium content has on the time taken to attain solar luminosity, remembering that the initial solar luminosity at zero-age main sequence is $0.7L_\odot$ for all the above models. This effect of increasing helium content, resulting in a shorter time to reach solar luminosity, is expected. During a normal stellar main sequence lifetime, helium builds up in the stellar core causing the pressure and temperature to rise in order to maintain the rate of nuclear reactions. Increasing the initial helium level simply starts the star with a higher core temperature and pressure, hence increasing its core activity and shortening its main sequence life span. Recall that this has the opposite effect to when metal levels are increased (see section 2 of this chapter), which slow down nuclear reactions. More metals mean less initial hydrogen (as initial helium levels in the post solar calibration models are fixed), and a higher density. The lower hydrogen concentration coupled with the higher density of non-reactive metals will slow core nuclear reactions (Kolb, 2003).

As the models traverse the present day solar luminosity, those with higher helium contents will go through this value at a faster rate, due to their shorter main sequence lifetimes. Higher helium contents in models will give cores of higher densities, temperatures and pressures. As more material will be in the core, there will be less material in the outer envelope, and, since the same reactions are going on for the range of models in table 3.3, the envelope will be smaller. Hence higher helium stars of the same mass will be smaller and, since their luminosities are the same, higher helium will mean higher effective temperatures.

The closest best fit for a solar model was achieved when the initial helium content was a mass fraction of 0.27 for a mixing length of 1.9. To refine this slightly, a final model was run with a helium content of 0.269 for a mixing length of 1.9, in good agreement with similar previous models (Bahcall et al., 2005). This took 4.578Gyr to reach the present day solar luminosity, in the middle of the estimated 4.55Gyr to 4.60Gyr age of the solar system. The Sun's effective temperature after this time was 5787K, in agreement with the literature, and it had a radius of $0.995R_\odot$. As the temperature was in exact agreement and habitable zones are calculated from formulae not involving stellar radii, this final run was taken as our standard solar model. Table 3.4 summarises the parameters used to attain this end result.

Table 3.4 Parameters used in creating the final solar model,

Parameter	Value
Maximum Time Step / years	10^6
ZAMS Helium Content / mass fraction of Sun	0.269
ZAMS Metallicity / mass fraction of Sun	0.02
ZAMS Carbon Content / mass fraction of metals	0.1516
ZAMS Nitrogen Content / mass fraction of metals	0.05289
ZAMS Oxygen Content / mass fraction of metals	0.5289
Mixing Length (no units)	1.9
Solar Mass / $M_\odot$	1
Log_{10}(ZAMS Solar Luminosity / $L_\odot$)	-0.1523
Log_{10}(ZAMS Effective Temperature / T_{eff})	3.7514
Log_{10}(ZAMS Core Pressure / Pa)	17.1851
Log_{10}(ZAMS Core Temperature / K)	7.1306

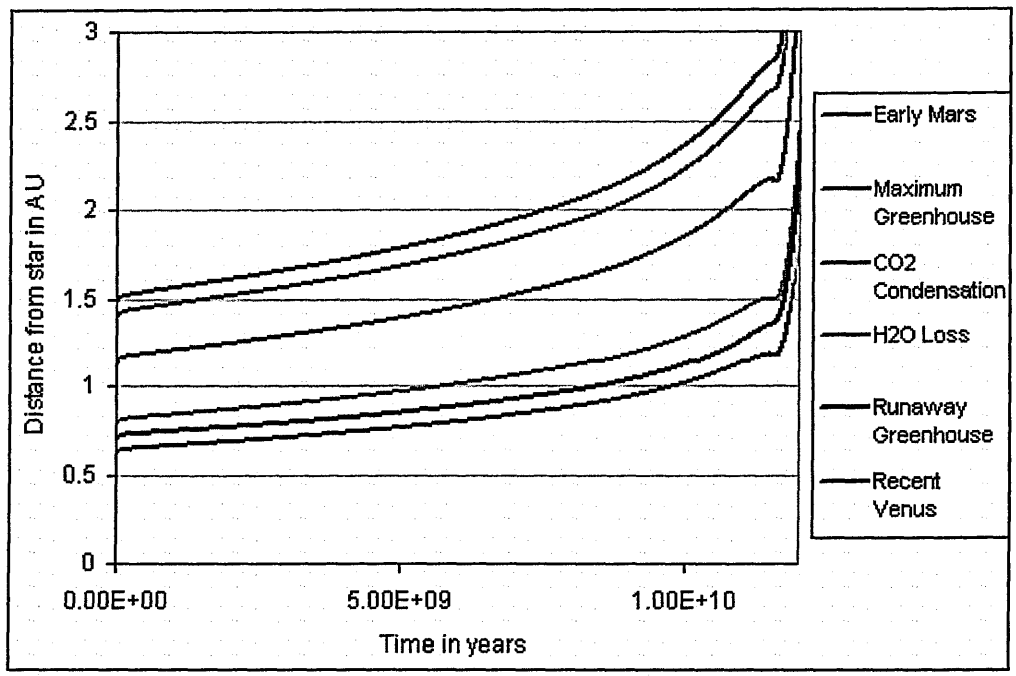

Figure 3.5 The outward movement of the six Habitable Zone boundaries during the solar main sequence lifetime.

The first seven values listed in this table, except metallicity, were used in **all** subsequent stellar simulations. The main sequence lifetime solar profile, of the model obtained from these parameters, is shown in Figure 3.2, along with the habitable zone boundaries for a runaway greenhouse effect and a maximum greenhouse effect, shown in Figure 3.3. Figure 3.5 shows all the habitable zone boundaries defined in section 1 of this chapter.

3.5.2 Creating the Stellar Grid

At the time of writing there are 156 known exoplanetary systems. One method of determining the habitable zone around each of these stars would be to model each star individually. An alternative method has been devised whereby stellar evolution simulations were performed for a selection of discrete stellar masses, with each mass having a small set of metallicities, both parameters of which would cover almost all stars in known exoplanetary systems. The mass range covered in this study was from $0.5M_\odot$ to $1.5M_\odot$, as established in section 2 of this chapter, with intervals of $0.1M_\odot$ between each

mass. Similarly, the metals mass fraction range for each mass was from 0.008 to 0.05 in equal logarithmic intervals.

The normal method in which astronomers quote stellar metallicity values is in terms of [Fe/H], the ratio of iron to hydrogen in a star, where,

$$[Fe/H] = \log_{10}[n(Fe_*)/n(H_*)] - \log_{10}[n(Fe_\odot)/n(H_\odot)] \qquad 3.11.$$

Here $n(Fe_*)$ and $n(H_*)$ is the number fraction of iron and hydrogen nuclei in a star, while $n(Fe_\odot)$ and $n(H_\odot)$ is the same fraction for the Sun. In terms of mass fraction, where m() is substituted instead of the number fraction,

$$\begin{aligned}[Fe/H] &= \log_{10}[\{m(Fe_*)/55.845\}/\{m(H_*)/1.008\}] \\ &\quad - \log_{10}[\{m(Fe_\odot)/55.845\}/\{m(H_\odot)/1.008\}] \\ &= \log_{10}[m(Fe_*)/m(H_*)] - \log_{10}[m(Fe_\odot)/m(H_\odot)] \qquad 3.12\end{aligned}$$

where 55.845 is the atomic mass of iron and 1.008 is the atomic mass of hydrogen (Young and Freedman, 2000). Since equations 3.11 and 3.12 are the same, it is clear that [Fe/H] is independent of whether it is determined by either number or mass. Now the ratio of iron to hydrogen in a star is regarded to be representative of the mass fraction of all metals, Z, i.e. all elements other than hydrogen and helium (Carroll and Ostlie, 1996). Hence for a proportionality constant, k,

$$Z = k[m(Fe_*)/m(H_*)] \qquad 3.13.$$

Iron lines are readily identified in stellar spectra and so their intensity is related to metallicity content. Hence by putting Z for $m(Fe_*)/m(H_*)$ and $Z_\odot$, the solar metallicity, for $m(Fe_\odot)/m(H_\odot)$, where similarly

$$Z_\odot = k[m(Fe_\odot)/m(H_\odot)] \qquad 3.14$$

rearranging equation 3.12 and taking exponentials gives

$$Z = Z_\odot \times 10^{[Fe/H]} \qquad 3.15.$$

In this first matrix, the Sun's mass fraction metallicity is taken as 0.02, corresponding to [Fe/H] of 0. Stellar models are also made for metallicities where [Fe/H] is equal to -0.4, -0.2, 0.2 and 0.4, corresponding to metal mass fractions of 0.007962, 0.01262, 0.03170 and 0.0524 respectively. These values were rounded to 0.008, 0.013, 0.032 and 0.05 respectively, creating the grid in figure 3.6.

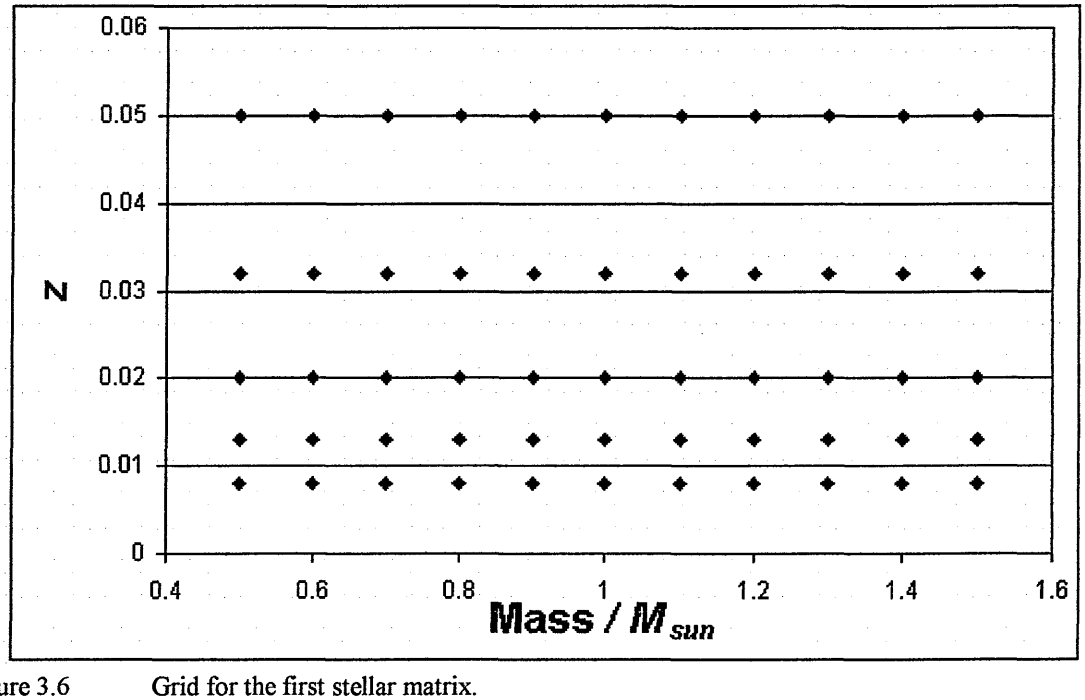

Figure 3.6 Grid for the first stellar matrix.

Table 3.5 Starting values for stellar grid models.

$M/M_{\odot}$	Metallicity mass fraction	ZAMS $\log_{10}(L/L_{\odot})$	ZAMS $\log_{10}(T_{eff})$	ZAMS $\log_{10}(P_{core}/Pa)$	ZAMS $\log_{10}(T_{core}/K)$
0.5*	0.008	-1.13600	3.6070	17.13900	7.0050
0.5*	0.013	-1.44400	3.5750	17.07700	6.9580
0.5*	0.02	-1.44400	3.5750	17.07700	6.9580
0.5*	0.032	-1.44400	3.5750	17.07700	6.9580
0.5**	0.05	-1.70000	3.4600	17.20000	6.9300
0.6*	0.008	-1.13600	3.6070	17.13900	7.0050
0.6*	0.013	-1.13600	3.6070	17.13900	7.0050
0.6**	0.02	-1.00000	3.6500	16.90000	6.9800
0.6**	0.032	-1.00000	3.6500	16.90000	6.9800
0.6**	0.05	-1.50000	3.5020	17.00000	6.9550
0.7*	0.008	-1.13600	3.6070	17.13900	7.0050
0.7*	0.013	-0.82100	3.6570	17.20500	7.0550
0.7*	0.02	-0.82100	3.6570	17.20500	7.0550
0.7*	0.032	-0.82100	3.6570	17.20500	7.0550
0.7**	0.05	-1.50000	3.5020	17.00000	6.9550
0.8***	0.008	-0.57420	3.7016	17.06510	7.0603
0.8***	0.013	-0.57420	3.7016	17.06510	7.0603
0.8***	0.02	-0.57420	3.7016	17.06510	7.0603
0.8***	0.032	-0.57420	3.7016	17.06510	7.0603
0.8***	0.05	-0.57420	3.7016	17.06510	7.0603
0.9***	0.008	-0.15230	3.7514	17.18510	7.1306
0.9***	0.013	-0.15230	3.7514	17.18510	7.1306
0.9***	0.02	-0.15230	3.7514	17.18510	7.1306
0.9***	0.032	-0.15230	3.7514	17.18510	7.1306
0.9***	0.05	-0.57420	3.7016	17.06510	7.0603
1.0***	0.008	-0.15230	3.7514	17.18510	7.1306
1.0***	0.013	-0.15230	3.7514	17.18510	7.1306
1.0***	0.02	-0.15230	3.7514	17.18510	7.1306
1.0***	0.032	-0.15230	3.7514	17.18510	7.1306
1.0***	0.05	-0.15230	3.7514	17.18510	7.1306
1.1***	0.008	-0.15230	3.7514	17.18510	7.1306
1.1***	0.013	-0.15230	3.7514	17.18510	7.1306
1.1***	0.02	-0.15230	3.7514	17.18510	7.1306
1.1***	0.032	-0.15230	3.7514	17.18510	7.1306
1.1***	0.05	-0.15230	3.7514	17.18510	7.1306
1.2**	0.008	0.22500	3.7800	17.30000	7.1700
1.2***	0.013	0.23250	3.7964	17.26540	7.1936
1.2***	0.02	0.23250	3.7964	17.26540	7.1936
1.2***	0.032	0.23250	3.7964	17.26540	7.1936
1.2***	0.05	0.23250	3.7964	17.26540	7.1936
1.3**	0.008	0.22500	3.7800	17.30000	7.1700
1.3**	0.013	0.40000	3.8100	17.29000	7.2150
1.3***	0.02	0.23250	3.7964	17.26540	7.1936
1.3***	0.032	0.23250	3.7964	17.26540	7.1936
1.3**	0.05	0.55000	3.8200	17.33000	7.2000
1.4***	0.008	0.55620	3.8355	17.32740	7.2500
1.4***	0.013	0.55620	3.8355	17.32740	7.2500
1.4***	0.02	0.55620	3.8355	17.32740	7.2500
1.4***	0.032	0.55620	3.8355	17.32740	7.2500
1.4**	0.05	0.55000	3.8200	17.33000	7.2000
1.5**	0.008	0.80000	3.8855	17.34000	7.3000
1.5***	0.013	0.55620	3.8355	17.32740	7.2500
1.5***	0.02	0.55620	3.8355	17.32740	7.2500
1.5***	0.032	0.55620	3.8355	17.32740	7.2500
1.5***	0.05	0.55000	3.8200	17.33000	7.2000

* Taken from the "starters.rk" file within the stellar evolution program.
** Estimated and extrapolated from the "starters.rk" file and from Cox, 2000.
*** Taken from Cox, 2000.

Table 3.6 Summary of the outcomes of the stellar grid models.

$M/M_{\odot}$	Metallicity mass fraction	Time on Main Sequence in Ga	Habitable Zone Distance from Star in AU, from ZAMS (top)to the onset of the red giant phase (bottom).					
			Recent Venus	Runaway Greenhouse	Water Loss	1st CO_2 Condensation	Maximum Greenhouse	Early Mars
0.5	0.008	>65.5	0.160857	0.196984	0.203482	0.298997	0.387439	0.411037
			0.209537	0.255524	0.265062	0.388885	0.502086	0.532699
0.5	0.013	>65.5	0.153179	0.188315	0.19377	0.285168	0.370819	0.393377
			0.190065	0.233093	0.24043	0.353489	0.458646	0.48657
0.5	0.02	>65.5	0.147	0.181319	0.185955	0.274057	0.357478	0.379197
			0.176925	0.217897	0.223809	0.329625	0.429339	0.45544
0.5	0.032	>65.5	0.14102	0.174545	0.17839	0.263333	0.34465	0.365557
			0.165829	0.205057	0.209774	0.309518	0.404716	0.429278
0.5	0.05	>65.5	0.136343	0.169276	0.172474	0.255001	0.334799	0.355074
			0.158168	0.196242	0.200082	0.295715	0.387986	0.411491
0.6	0.008	65.2	0.223176	0.270828	0.282314	0.413512	0.531701	0.564151
			0.810333	0.969659	1.02505	1.495272	1.90151	2.017731
0.6	0.013	>65.5	0.209662	0.255902	0.26522	0.389239	0.502922	0.53358
			0.40419	0.482445	0.511288	0.745345	0.946042	1.003871
0.6	0.02	>65.5	0.199373	0.244435	0.252205	0.370758	0.480923	0.510205
			0.32857	0.397107	0.415635	0.608013	0.779219	0.826804
0.6	0.032	>65.5	0.190168	0.234149	0.240561	0.35426	0.461323	0.489371
			0.286192	0.348948	0.362029	0.531121	0.685636	0.727443
0.6	0.05	>65.5	0.18395	0.227284	0.232696	0.343211	0.448422	0.475647
			0.266204	0.326231	0.336745	0.494955	0.641779	0.68086
0.7	0.008	36.8	0.309566	0.369148	0.391592	0.570715	0.723872	0.768121
			1.02296	1.21436	1.294012	1.883835	2.381414	2.526997
0.7	0.013	42.5	0.288862	0.34748	0.365404	0.533795	0.681569	0.723211
			0.908058	1.085236	1.148668	1.675047	2.128103	2.258182
0.7	0.02	47.5	0.273195	0.330761	0.345587	0.505816	0.64916	0.688793
			0.823769	0.989642	1.042048	1.521701	1.940993	2.059597
0.7	0.032	52.2	0.259847	0.31641	0.328702	0.482009	0.621544	0.659452
			0.753578	0.909227	0.953261	1.393771	1.783824	1.89278
0.7	0.05	54.4	0.251906	0.307916	0.318658	0.467916	0.605348	0.642236
			0.710085	0.858263	0.898243	1.314026	1.684129	1.786973
0.8	0.008	22.0	0.420102	0.488813	0.531411	0.77034	0.960075	1.018714
			1.241961	1.464279	1.571037	2.283544	2.872417	3.047999
0.8	0.013	25.4	0.391507	0.460653	0.495242	0.719529	0.90377	0.95901
			1.105386	1.311248	1.398278	2.035272	2.571469	2.728671
0.8	0.02	28.3	0.370005	0.439111	0.468045	0.681338	0.861122	0.913765
			1.006244	1.199259	1.272869	1.854853	2.351658	2.495414
0.8	0.032	31.0	0.351991	0.420777	0.445259	0.649342	0.825131	0.875566
			0.924038	1.105371	1.168883	1.704944	2.167626	2.300114
0.8	0.05	32.1	0.342245	0.410791	0.432932	0.632053	0.805652	0.854885
			0.880431	1.054397	1.113722	1.624972	2.067728	2.194103
0.9	0.008	13.7**	0.554038	0.626929	0.700825	1.011271	1.237149	1.31243
			1.189733	1.357849	1.504948	2.174363	2.674966	2.837966
0.9	0.013	16.1	0.516813	0.592369	0.653741	0.945172	1.166072	1.237171
			1.303488	1.53655	1.648866	2.396578	3.014222	3.198471
0.9	0.02	17.8	0.489046	0.566037	0.61862	0.895885	1.112524	1.180439
			1.197165	1.41716	1.514375	2.203182	2.779386	2.949297
0.9	0.032	19.4	0.465854	0.543647	0.589286	0.854722	1.06741	1.13262
			1.104701	1.31187	1.397412	2.034543	2.572611	2.729883
0.9	0.05	19.9	0.453802	0.531962	0.574042	0.833362	1.043995	1.107794
			0.955176	1.132545	1.208267	1.758511	2.221051	2.356831
1.0	0.008	9.21**	0.709453	0.781841	0.897407	1.290708	1.552649	1.646619
			1.388936	1.594677	1.756933	2.540854	3.1382	3.329589
1.0	0.013	10.5**	0.668113	0.745155	0.845118	1.217164	1.475275	1.564799
			1.268027	1.464562	1.603994	2.322031	2.87942	3.055156
1.0	0.02	11.6**	0.635918	0.715997	0.804397	1.159922	1.414431	1.500423
			1.180381	1.369321	1.493129	2.16324	2.690507	2.85479
1.0	0.032	12.6**	0.59655	0.679433	0.754603	1.08991	1.339011	1.420578
			1.106616	1.288586	1.399822	2.02949	2.530675	2.685252
1.0	0.05	12.9**	0.579354	0.663457	0.732852	1.059396	1.306213	1.385847
			1.060432	1.235403	1.341401	1.944971	2.42609	2.574285
1.1	0.008	6.41***	0.858436	0.929289	1.085851	1.55907	1.854811	1.966566
			1.631051	1.797844	2.063161	2.967437	3.570119	3.786201
1.1	0.013	7.26***	0.810047	0.887104	1.024648	1.472764	1.764714	1.871357
			1.488963	1.653909	1.883436	2.711265	3.277749	3.47648
1.1	0.02	8.00***	0.772884	0.854289	0.977643	1.406564	1.695185	1.797852
			1.384939	1.547603	1.751857	2.523671	3.062568	3.248486
1.1	0.032	8.63***	0.740982	0.825871	0.937293	1.349807	1.635348	1.734572
			1.296247	1.457411	1.639671	2.363921	2.879984	3.055029
1.1	0.05	8.84***	0.721765	0.808737	0.912986	1.315671	1.59939	1.696537
			1.239408	1.397422	1.567776	2.261123	2.759723	2.927547

$M/M_\odot$	Metallicity mass fraction	Time on Main Sequence in Ga	Habitable Zone Distance from Star in AU, from ZAMS (top)to the onset of the red giant phase (bottom).					
			Recent Venus	Runaway Greenhouse	Water Loss	1st CO_2 Condensation	Maximum Greenhouse	Early Mars
1.2	0.008	4.63***	1.018504	1.086429	1.288316	1.847659	2.178374	2.309082
			1.884876	2.053606	2.38422	3.425239	4.091177	4.338093
1.2	0.013	5.21***	0.962377	1.038023	1.217326	1.747311	2.074109	2.198954
			1.722643	1.888898	2.179013	3.13237	3.756264	3.983329
1.2	0.02	5.71***	0.919476	1.000663	1.163064	1.670719	1.994157	2.114476
			1.602757	1.767496	2.027372	2.91611	3.509412	3.721843
1.2	0.032	6.15***	0.882802	0.968579	1.116678	1.605341	1.9258	2.042231
			1.497957	1.660118	1.89481	2.726926	3.291955	3.491447
1.2****	0.05	6.43***	0.861153	0.949809	1.089297	1.566836	1.885797	1.999952
			1.431786	1.590423	1.811111	2.607156	3.151919	3.343021
1.3	0.008	3.51***	1.189285	1.252726	1.504331	2.155757	2.522246	2.673007
			2.147855	2.317865	2.716856	3.899852	4.630689	4.909459
1.3	0.013	3.93***	1.125188	1.198258	1.42326	2.040961	2.403869	2.548036
			1.967757	2.134816	2.489053	3.574471	4.258227	4.51494
1.3	0.02	4.29***	1.075937	1.155809	1.360967	1.952861	2.312342	2.45137
			1.833564	1.999022	2.319314	3.332199	3.981681	4.222028
1.3****	0.032	4.69***	1.113341	1.19854	1.408282	2.021089	2.396255	2.540414
			1.718742	1.882208	2.174078	3.124876	3.744291	3.970561
1.3****	0.05	4.88***	1.009416	1.098669	1.276831	1.834162	2.189396	2.321499
			1.642945	1.80469	2.078202	2.987988	3.587068	3.803998
1.4	0.008	2.76***	1.372595	1.42913	1.736192	2.486576	2.88897	3.061002
			2.423459	2.590954	3.06546	4.397083	5.191304	5.503001
1.4	0.013	3.07***	1.298495	1.367463	1.642471	2.353686	2.753462	2.918032
			2.23014	2.39709	2.820936	4.047961	4.794815	5.083147
1.4	0.02	3.35***	1.243009	1.320496	1.572292	2.254308	2.651199	2.810083
			2.08415	2.251634	2.636276	3.784535	4.496852	4.767647
1.4	0.032	3.60***	1.207421	1.291716	1.527281	2.190829	2.587581	2.742974
			1.956872	2.122077	2.475284	3.554561	4.233365	4.48855
1.4	0.05	3.77***	1.167631	1.256974	1.476954	2.119642	2.513089	2.664276
			1.875317	2.039745	2.372127	3.407336	4.065547	4.310809
1.5	0.008	2.20***	1.567346	1.61207	1.982522	2.838059	3.273149	3.467241
			2.706194	2.872963	3.423086	4.90771	5.7694	6.115086
1.5	0.013	2.44***	1.484311	1.546852	1.877501	2.689068	3.125944	3.312144
			2.504548	2.669205	3.168027	4.543198	5.35349	5.674627
1.5	0.02	2.64***	1.42054	1.494035	1.796844	2.574721	3.009654	3.189462
			2.349329	2.516763	2.971695	4.263214	5.039449	5.342204
1.5	0.032	2.82***	1.367383	1.449909	1.729612	2.479572	2.91281	3.087274
			2.213003	2.380352	2.799259	4.017077	4.760296	5.046609
1.5	0.05	2.89***	1.336125	1.424734	1.690078	2.423794	2.857022	3.028433
			2.125908	2.291398	2.689094	3.859619	4.579503	4.8551

N.B. Main sequence times with no asterisk qualifier were determined by the time taken from ZAMS (t = 0) to an apparent minimum effective temperature before a final effective temperature increase followed by more rapid surface cooling towards the red giant phase, see figure 3.9 (below).

* All of these models predict an initial drop in luminosity immediately after nuclear reactions commence in the stellar cores. The time to reach minimum luminosity, before helium build-up in the core causing luminosity increase, varies in the extremes from 122 million years for a $0.5M_\odot$ star with 0.05 mass fraction of metals to 7,190 years for a $1.5M_\odot$ star with 0.008 mass fraction of metals. It is the habitable zone distances when each model's luminosity is at its initial minimum, which is quoted as the ZAMS HZ distances in this table. For models with main sequence lifetimes greater than 65.5Ga, the final HZ distances quoted are those after 65.5Ga, **not** at the end of the main sequence lifetime.

** The times on the main sequence for these stellar models are determined by the time taken from ZAMS (t = 0) to the apparent minimum luminosity in the dip that follows the apparent maximum luminosity just before the onset of the red giant phase, see figure 3.8 (below).

*** The times on the main sequence for these stellar models are determined by the time taken from ZAMS (t = 0) to the minimum distances of HZs in the dip that follows the quoted maximum HZ boundary values, see figure 3.7 (below).

**** These models required maximum time steps of 10^7 years for the $1.3M_\odot$ stars and 10^8 years for the $1.2M_\odot$ star in order to complete successfully (see section 3.5.1). Normal time steps of 10^6 years for these models lead to a division by zero midway through the main sequence, hence terminating the runs.

Now the most metal rich stars have metal mass fractions, Z, of up to 0.06, but these are rare, so stellar models were created only up to 0.05 to retain a degree of logarithmic symmetry either side of the solar metallicity. Mass fractions were used for metallicities in this first stellar matrix as it is these values that are required as part of the program's input file. The starting input values of all variable parameters, with their information sources, for each of the stellar grid runs are revealed in table 3.5.

A summary of the outcomes of these stellar models, illustrating the time the models remain on the main sequence and the distance of their habitable zone boundaries determined from the formulae in section 3 of this chapter, are shown in table 3.6.

The three methods for determining the main sequence lifetime of a star, mentioned in the footnotes of table 3.6, are now described. The method used for larger mass stars, is when the distances of the habitable zone boundaries start to rapidly recede from the star. HZ boundaries are the main attribute which determines the existence of possible life in an exosystem and at the end of the main sequence lifetime of a larger star, they reach a maximum distance. This is followed by a slight movement inwards just before the onset of the red giant phase, resulting in a set of minimum distances for each of the six HZ boundaries, shown in figure 3.7. This movement mirrors the luminosity curve of the star. It is the time after zero-age main sequence, when this minimum is reached, that is taken as the main sequence lifetime of the star here. Less massive stars do not have this profile, since their habitable zone boundaries continually increase and a second method is required.

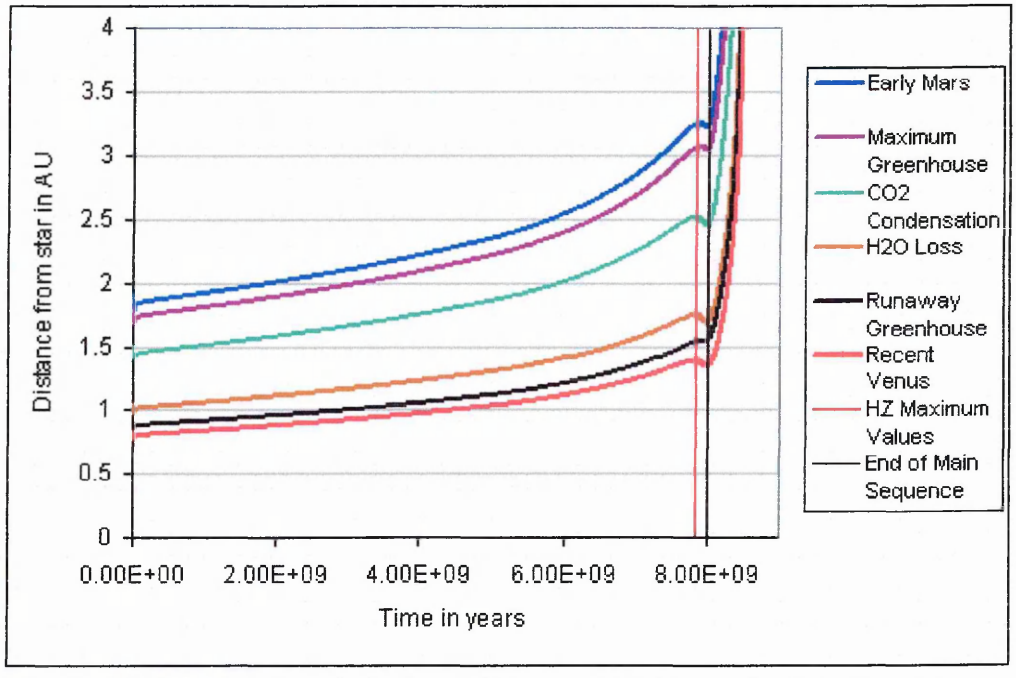

Figure 3.7 Habitable zone boundaries for a $1.1M_{\odot}$ star with 0.02 mass fraction of metals.

This second method uses the luminosity curves, from which the HZ distances are primarily calculated, since it is the rapid onset of luminosity increase which is the major factor in determining the commencement of a star's red giant phase. Luminosity changes affect habitable zones most of all and this method is employed for intermediate mass stars. Figure 3.8 shows the luminosity profile of an intermediate mass star, showing a luminosity maximum followed by a minimum just before the red giant phase starts. The time on the main sequence, shown, is from ZAMS to when this minimum is reached. Low mass stars have luminosity profiles which continually increase, so this second method can no longer be used. A third technique, of monitoring rapid changes in a star's effective temperature is

used and is the least reliable method since effective temperature only slightly affects habitable zones. It is better, however, than gauging the onset of the red giant phase of a star merely by visual inspection of a curve on a graph. Figure 3.9 shows a typical effective temperature versus time profile for a low mass star. The time on the main sequence is taken to be from ZAMS to when an effective temperature minimum is reached, before an increase in temperature followed by a subsequent further decrease as the star evolves into a red giant.

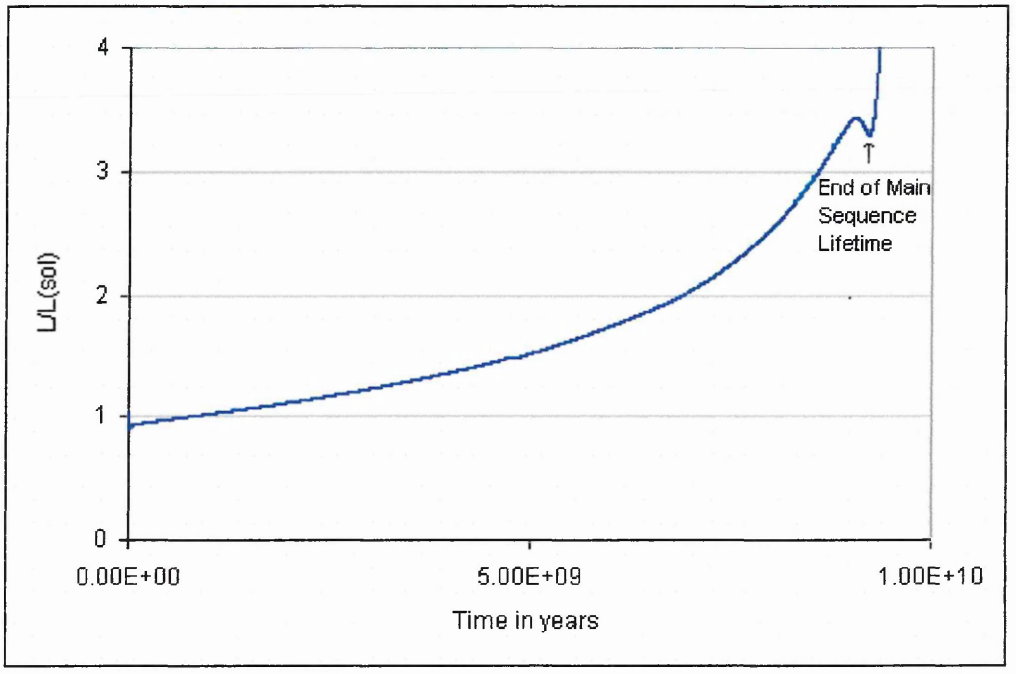

Figure 3.8 Luminosity profile over the main sequence lifetime for a $1M_{\odot}$ star with 0.008 metals mass fraction

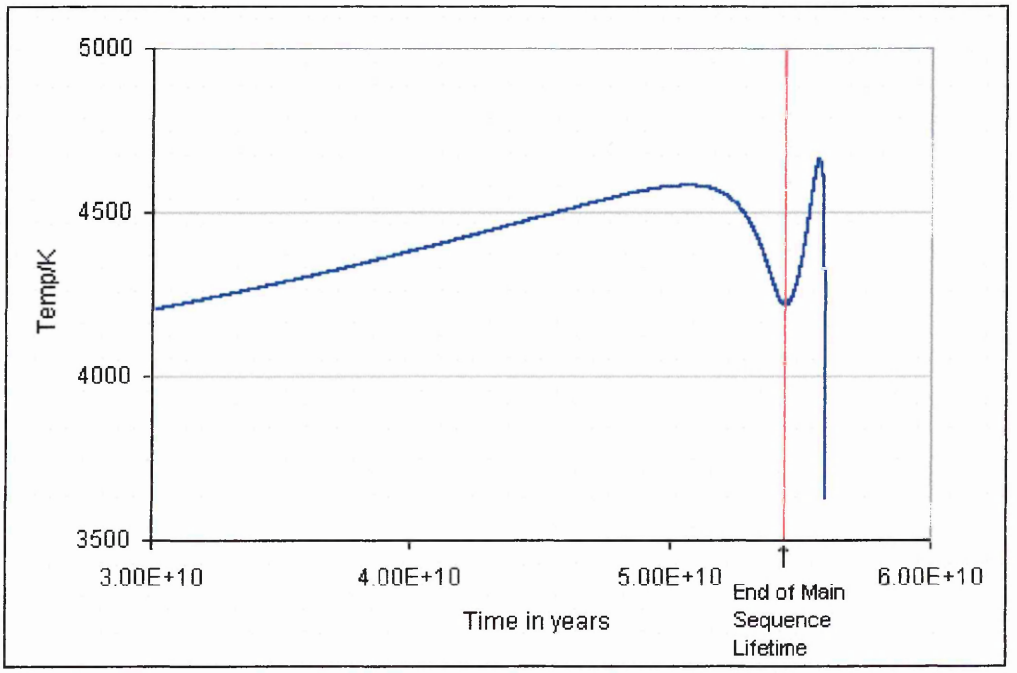

Figure 3.9 Effective temperature profile over the main sequence lifetime for a $0.7M_{\odot}$ star with 0.05 metals mass fraction.

Table 3.6 shows that for stars with the same metallicity, lifetime on the main sequence decreases with increasing mass. Also for stars with the same mass, a star's lifetime on the main sequence increases with increasing metallicity, although this trend is much less

marked than the mass effect. For lower mass stars up to $1M_{\odot}$, all five stars of different metallicity and with a lower mass have longer main sequence lifetimes than any higher mass counterpart. This is not so for stars of $1.1M_{\odot}$ and above where, for example, a heavier $1.xM_{\odot}$ star with a metallicity mass fraction of 0.05 will have a longer main sequence lifetime than a star of $1.(x\text{-}1)M_{\odot}$ with a metallicity mass fraction of 0.008. Also the ratios of distances for the same habitable zone boundary, at the end of the main sequence and ZAMS, change with increasing mass. For the lowest mass stars, the same boundaries are more than 3.5 times as far from a star at end of main sequence than at ZAMS, whereas for the highest mass stars, this ratio decreases with increasing mass to about 1.6. The trend is much less for stars with the same mass but with different metallicities, but generally, the distance ratio for the end of the main sequence and ZAMS for any same habitable zone boundary will be less for a star with a higher metallicity. Graphical representations of each of these models would require approximately 28 pages, and are hence omitted. However a flavour of their appearance is given at the end of the next section where the stars of actual exoplanetary systems are modelled and which have been studied in detail using orbital integration (Chambers, 1999).

3.5.3 Modelling Stars of Exoplanetary Systems

The exoplanetary systems studied in detail by the Open University team so far, using the Mercury Orbital Integrator (Chambers, 1999), have been 47 Ursae Majoris (Jones and Sleep, 2002), Gliese 876, Rho Coronae Borealis, Upsilon Andromedae (Jones et al., 2001), Epsilon Eridani (Jones and Sleep, 2003), and HD 72659 (Sleep, 2005). Exoplanetary systems under investigation within this study (see chapters 4 to 7) are 55 Cancri, HD 196050, HD 23079, HD 28185, HD 52265 and Tau[1] Gruis (HD 216435). In order to accurately characterise these systems, stellar evolution models of each star were made, along with the Sun. The methods used were exactly the same as already outlined in section 5.2 of this chapter, using published metallicities and masses (Schneider, 2006) unless otherwise indicated. This determined their habitable zones over the course of their main sequence lifetimes. The starting parameters of each stellar model are shown in Table 3.7. The movement of their habitable zones over their main sequence lifetimes is summarised in Table 3.8, of which examples are shown graphically in Figures 3.10 to 3.14. The Sun's HZs over its main sequence lifetime are shown in Figure 3.5.

Table 3.7 Starting values for the investigated exoplanetary system stars.

Star	$M/M_{\odot}$	Metallicity mass fraction	ZAMS $\log_{10}(L/L_{\odot})$	ZAMS $\log_{10}(T_{eff})$	ZAMS $\log_{10}(P_{core}/Pa)$	ZAMS $\log_{10}(T_{core}/K)$
47 Ursae Majoris	1.03	0.01664	-0.15230	3.7514	17.18510	7.1306
1st 55 Cancri	1.03	0.039	-0.15230	3.7514	17.18510	7.1306
2nd 55 Cancri*	0.95	0.039	-0.15230	3.7514	17.18510	7.1306
1st Epsilon Eridani	0.8	0.01589	-0.57420	3.7016	17.06510	7.0603
2nd Epsilon Eridani*	0.77	0.01589	-0.57420	3.7016	17.06510	7.0603
1st Gliese 876	0.32	0.02	-1.9020	3.5570	17.10600	6.9230
2nd Gliese 876*	0.336	0.02	-1.9020	3.5570	17.10600	6.9230
1st HD 196050**	1.1	0.03557	-0.15230	3.7514	17.18510	7.1306
2nd HD 196050**	1.1	0.02	-0.15230	3.7514	17.18510	7.1306
3rd HD 196050**	1.2546	0.03557	0.23250	3.7964	17.26450	7.1936
4th HD 196050**	1.2546	0.02	0.23250	3.7964	17.26450	7.1936
HD 23079	1.1	0.02	-0.15230	3.7514	17.18510	7.1306
HD 28185	0.99	0.03476	-0.15230	3.7514	17.18510	7.1306
HD 52265	1.13	0.02576	0.23250	3.7964	17.26450	7.1936
HD 72659	0.95	0.01449	-0.15230	3.7514	17.18510	7.1306
1st Rho Coronae Borealis	0.95	0.01291	-0.15230	3.7514	17.18510	7.1306
2nd Rho Coronae Borealis*	1.00	0.01291	-0.15230	3.7514	17.18510	7.1306
Sun	1.00	0.02	-0.15230	3.7514	17.18510	7.1306
Tau[1] Gruis	1.25	0.02825	0.23250	3.7964	17.26450	7.1936
Upsilon Andromedae	1.3	0.02	0.23250	3.7964	17.26450	7.1936

* These stellar masses are calculated from the orbital periods of the planets around the stars and differ slightly from the literature masses given by Schneider, 2006.

** HD 196050 has two literature metallicities (Schneider, 2006) and a literature mass of $1.1M_{\odot}$ The mass of $1.2546M_{\odot}$ is derived from the reported orbital period and distance of the planet (Schneider, 2006). All combinations of these masses and metallicities give four possible models for HD 196050.

Table 3.8 Summary of the outcomes of the exoplanetary system stellar models.

Star	Time on Main Sequence in Ga	Habitable Zone Distance from Star in AU, from ZAMS (top)to the onset of the red giant phase (bottom).					
		Recent Venus	Runaway Greenhouse	Water Loss	1st CO_2 Condensation	Maximum Greenhouse	Early Mars
47 Ursae Majoris	9.93	0.689877	0.769235	0.872648	1.256775	1.523043	1.61546
		1.265089	1.460931	1.600278	2.316585	2.872351	3.047652
1st 55 Cancri	11.4	0.638062	0.722248	0.807111	1.164695	1.425147	1.511873
		1.138052	1.295878	1.439573	2.079174	2.553996	2.70957
2nd 55 Cancri*	16.0*	0.522114	0.603293	0.66045	0.956175	1.186037	1.258427
		1.16781	1.383262	1.477242	2.149467	2.712837	2.87868
1st Epsilon Eridani*	26.6*	0.380961	0.450143	0.481903	0.700802	0.882915	0.936888
		0.92941	1.101016	1.175673	1.710718	2.159289	2.291293
2nd Epsilon Eridani*	31.1*	0.348561	0.414766	0.440919	0.642266	0.813336	0.863056
		1.000573	1.192255	1.265696	1.844305	2.337926	2.480844
1st Gliese 876	~500**	0.092099	0.114109	0.116505	0.172066	0.225429	0.239097
		0.257137	0.313048	0.325275	0.47695	0.614917	0.652423
2nd Gliese 876	~440**	0.095842	0.11871	0.121239	0.179032	0.234484	0.248703
		0.326699	0.397951	0.413269	0.606089	0.781771	0.829449
1st HD 196050	8.73	0.735413	0.820934	0.930249	1.339915	1.624961	1.723586
		1.280183	1.439457	1.619351	2.334649	2.844456	3.017345
2nd HD 196050	8.00	0.772884	0.854289	0.977643	1.406564	1.695185	1.797852
		1.384939	1.547603	1.751857	2.523671	3.062568	3.248486
3rd HD 196050	5.37	0.957186	1.043843	1.210766	1.739572	2.07898	2.204483
		1.596669	1.75922	2.01967	2.904757	3.493807	3.70525
4th HD 196050	4.90	1.00375	1.084312	1.26966	1.82266	2.165595	2.296001
		1.727926	1.892616	2.185695	3.141631	3.764802	3.992322
HD 23079	8.00	0.772884	0.854289	0.977643	1.406564	1.695185	1.797852
		1.384939	1.547603	1.751857	2.523671	3.062568	3.248486
HD 28185	13.2	0.579152	0.6619	0.732597	1.05869	1.303614	1.383067
		1.081324	1.240024	1.367819	1.977737	2.440765	2.589595
HD 52265	7.54	0.796345	0.880055	1.007319	1.44923	1.746399	1.852163
		1.394994	1.557254	1.764575	2.541673	3.082418	3.269503
HD 72659	13.2***	0.579249	0.656961	0.732717	1.057639	1.295799	1.37468
		1.151939	1.309578	1.457138	2.104034	2.581806	2.739034
1st Rho Coronae Borealis	12.8***	0.58825	0.665138	0.744101	1.073603	1.312757	1.392628
		1.175796	1.334187	1.487314	2.147011	2.63131	2.791503
2nd Rho Coronae Borealis	10.5	0.668662	0.745647	0.845813	1.21814	1.476308	1.565892
		1.268887	1.46209	1.60508	2.322649	2.875599	3.051053
Sun	11.6	0.626495	0.707024	0.792478	1.143097	1.395997	1.480905
		1.185545	1.34742	1.499647	2.165329	2.656553	2.818325
Tau[1] Gruis	5.27	0.966096	1.050613	1.222034	1.755308	2.094154	2.220482
		1.494219	1.722821	1.890115	2.73541	3.388065	3.594803
Upsilon Andromedae	4.29	1.075937	1.155809	1.360967	1.952861	2.312342	2.45137
		1.833564	1.999022	2.319314	3.332199	3.981681	4.222028

N.B. All main sequence lifetimes were determined using habitable zone boundary profiles unless otherwise stated below.

* The 2nd 55 Cancri model and Epsilon Eridani's main sequence lifetime were determined using their effective temperature profiles.

** The main sequence lifetime for Gliese 876 could not be determined by any of the three previously mentioned techniques using habitable zones, luminosity or effective temperature. The value here was determined by graphical inspection of its luminosity profile.

*** The main sequence lifetimes of HD 72659 and the 1st Rho Coronae Borealis model were determined using their luminosity profiles.

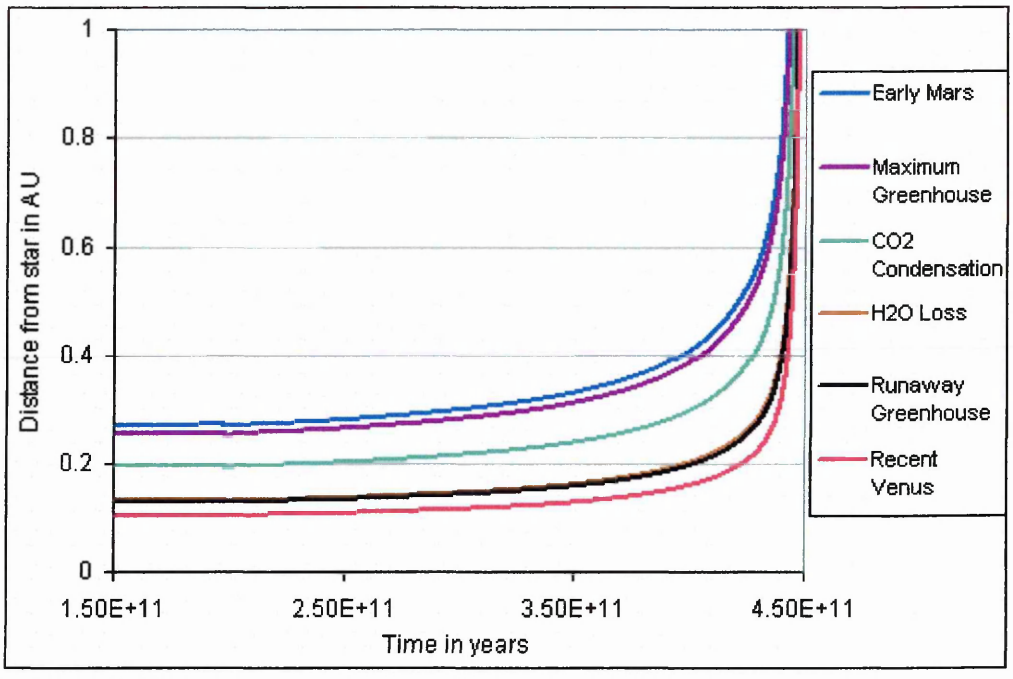

Figure 3.10 Habitable Zone boundaries for Gliese 876 over the final 290Gyr of its main sequence lifetime (The first 150Gyr show little or no change).

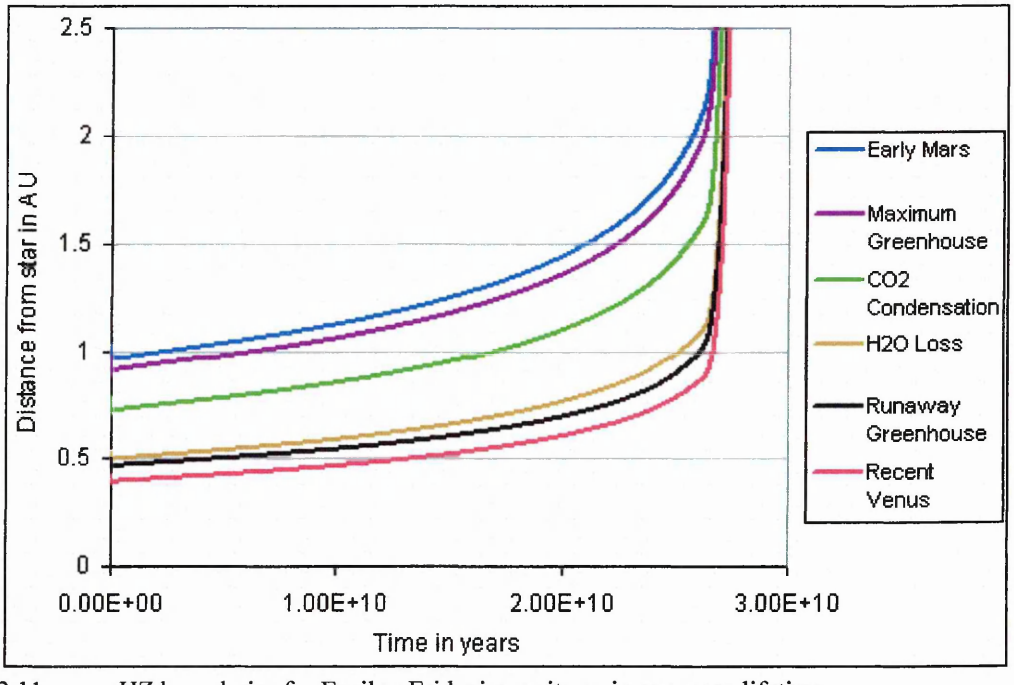

Figure 3.11 HZ boundaries for Epsilon Eridani over its main sequence lifetime.

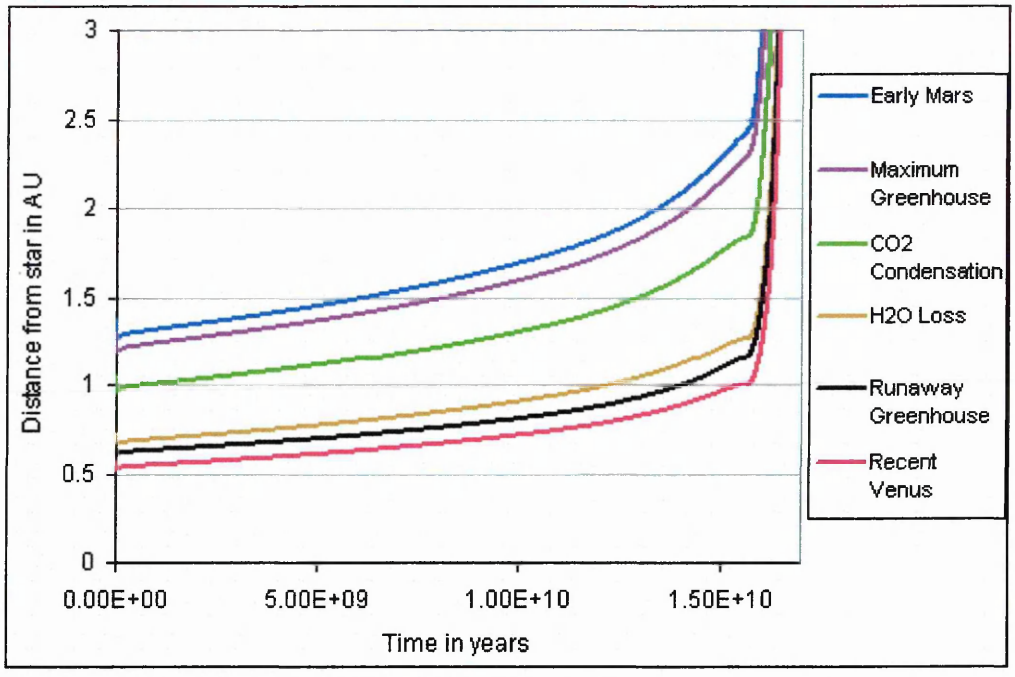

Figure 3.12 HZ boundaries for 55 Cancri ($0.95M_{\odot}$) over its main sequence lifetime.

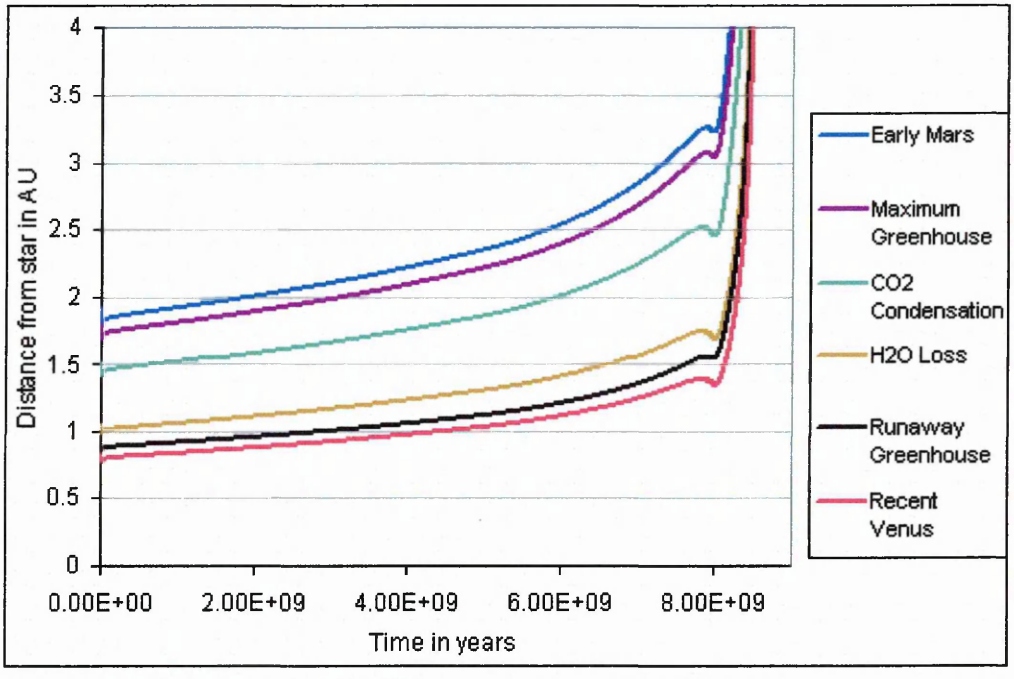

Figure 3.13 HZ boundaries for HD 23079 over its main sequence lifetime.

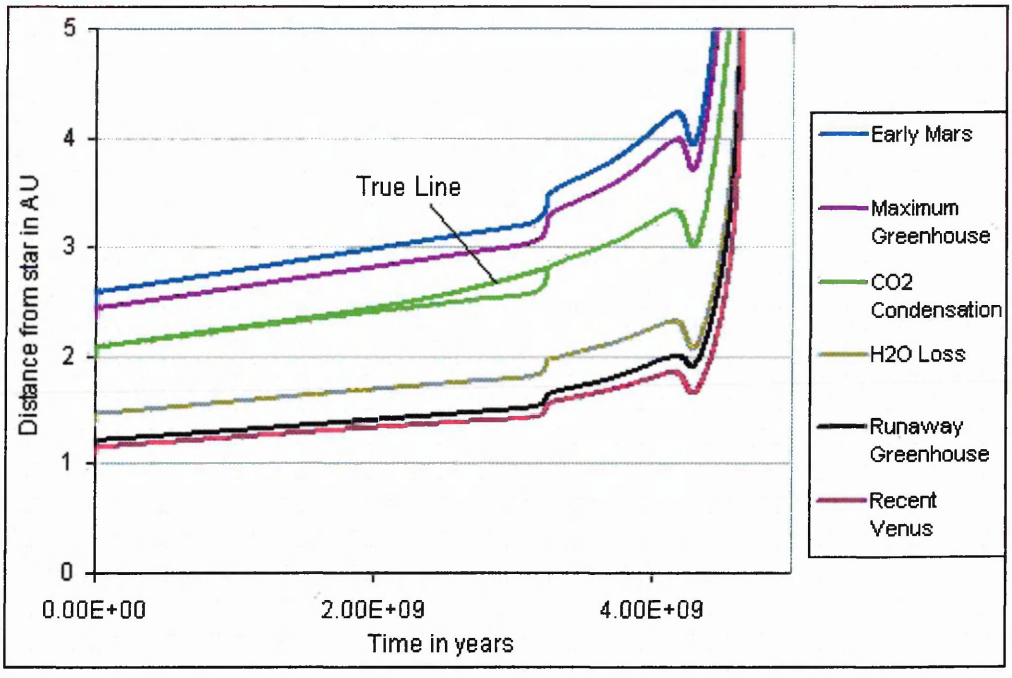

Figure 3.14 HZ boundaries for Upsilon Andromedae over its main sequence lifetime.

Notice the curious bump in each of the HZ boundaries for Upsilon Andromedae shown in Figure 3.14. This is found in all stellar models of $1.2M_{\odot}$ and above and is a peculiarity of the Mazzitelli program when modelling higher mass stars (Kolb, 2003). The true curves are the ones that connect the zero-time value with the top left-hand corner of the bump as illustrated in the figure using the CO_2 Condensation curve only for clarity. Notice that the rate of increase of HZ distances steadily increases as a model progresses along the main sequence of every other example shown in Figures 3.10 to 3.13. This is not so for Upsilon Andromedae, where the rate of increasing HZ boundary distance decreases up to about 3.2Gyr where there is a sudden sharp rise to meet the true main sequence curve. The rate of increase of HZ distance then increases as in all other models. Again this is characteristic of all stellar models above $1.2M_{\odot}$. It may initially appear that the model is correctly predicting the stellar evolution before 3.2Gyr but it is actually correct **after** 3.2Gyr in this example (and all other models showing this characteristic). This is verified when the end of main sequence HZ distances for each of the six boundaries are plotted against stellar mass for 0.02 mass fraction metal stars, shown in figure 3.15 using results extracted from table 3.6. The discontinuity between $0.9M_{\odot}$ and $1.0M_{\odot}$ is due to the change in method used for determining the end of the main sequence. Stellar masses of $0.7M_{\odot}$ to $0.9M_{\odot}$ use changes in effective temperature to determine this, $1.0M_{\odot}$ stars use luminosity, and higher stellar masses use habitable zone boundaries based primarily on luminosity. Effective temperature varies more wildly at the end of a star's main sequence, which explains the apparent discrepancy between using effective temperature and luminosity or habitable zones. However, the important trend shown in this figure is that there is **no** discontinuity between end of main sequence HZ distances of models between $1.0M_{\odot}$ and $1.5M_{\odot}$, whether there is a bump in HZ boundaries (for $1.2M_{\odot}$ to $1.5M_{\odot}$ stars) or not (for $1.0M_{\odot}$ and $1.1M_{\odot}$ stars).

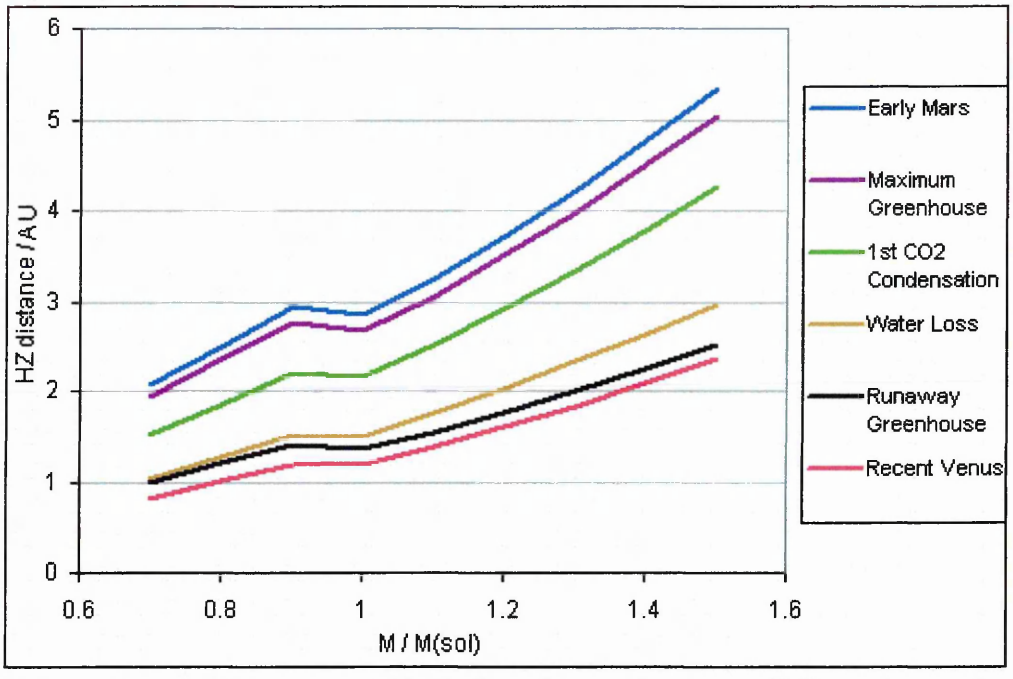

Figure 3.15 End of Main Sequence Habitable Zone distances from stars of 0.02 metals mass-fraction of different mass

Combining the 55 grid stars with the modelled stars of the investigated exoplanetary systems, the stellar grid now consisted of 75 reference points, shown in Figure 3.16. There are fewer than 75 points shown in the figure, however, as some of the grid models coincide with the modelled exoplanetary systems and some modelled exoplanetary systems coincide with each other.

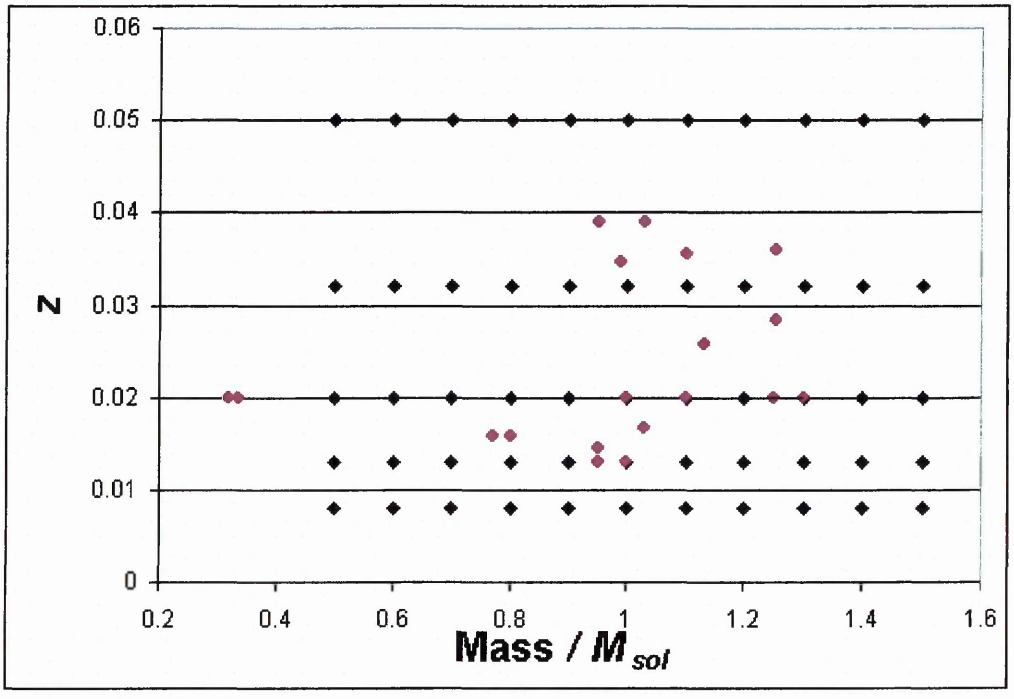

Figure 3.16 The 55 stellar grid points combined with those of the modelled (and investigated) exoplanetary system stars representing all stellar evolution simulations.

3.6 The Second Stellar Matrix

The aim of this exercise was to see the effect alternative values for solar helium and metals content had on the models in the stellar matrix, their habitable zones, and consequently the likelihood that the known exosystems could support habitable Earth-type planets. Here the

solar metallicity mass fraction is $Z_{\odot} = 0.0188$ (Cox, 2000) instead of 0.02 (Beatty, 1999). This second stellar matrix is also comprised of the same range of eleven masses as previous and five different metallicities for each mass. Whereas the helium mass fraction of all modelled stars in the first matrix were the same, at a mass fraction of 0.269, this is not so for the second. This stellar matrix allows for a change in helium mass fraction of models as metals mass fraction changes according to the relation (Pagel et al., 1992),

$$Y = Y_P + \frac{dY}{dZ} Z \qquad 3.16,$$

where Y is the stellar helium mass fraction, Y_P is the primordial helium mass fraction of the Universe and Z is stellar metals mass fraction. Here, Y_P is taken to be 0.243 (Tsangarides, 2003, Pagel et al., 1992), Y and dY/dZ remain to be determined. This empirical relationship is useful in that it represents a linear increase in helium abundance with increasing metallicity. We can thus easily calculate Y from Z.

3.6.1 Calibrating the Matrix using the Sun

The procedure here was a rerun of that carried out in section 5.1 of this chapter, starting with a solar calibration to reproduce the Sun's present day luminosity, radius and effective temperature as closely as possible for its current age. The first varied parameter was the mixing length where the initial helium mass fraction of the Sun was 0.2875 and metals mass fraction was 0.0188 (Cox, 2000). The remaining starting parameters were as in table 3.4, giving the results in table 3.9.

Table 3.9 Effect of mixing length on the time it takes a solar model to reach the present day solar luminosity with modelled solar radius and effective temperature after that time, for a constant initial helium mass fraction of 0.2875.

Mixing Length	Time to reach $L_{\odot}$/Ga	$R/R_{\odot}$	T_{eff}/K
1.6	2.472	0.988	5808
1.7	2.457	0.977	5838
1.8	2.443	0.968	5866
1.9	2.428	0.960	5891
2.0	2.413	0.953	5914
2.1	2.400	0.946	5935
Literature	4.55 – 4.60	1.000	5787*

* Cox (2000).

Clearly these values are way off the mark. The helium mass fraction of the Sun from Cox, 2000 is higher than previous solar models (Bahcall et al., 2005) and requires major adjustment as the current solar parameters would not be achievable by varying the mixing length alone. Table 3.3 shows that by maintaining the mixing length at 1.9 (the value from the first solar calibration in section 5 of this chapter), lowering the helium mass fraction of the Sun lengthens the time to reach current solar luminosity. The results of this procedure with this new solar calibration model is shown in table 3.10 indicating that the initial helium mass fraction is in agreement with models of Bahcall et al., 2005, and likely to be between 0.26 and 0.27 in order to allow the model to accurately predict the present day solar parameters. Table 3.11 verifies this by homing in on the correct helium value.

Table 3.11 shows there is good agreement with the present day solar luminosity when the helium mass fraction is 0.267 for a 0.0188 metals mass fraction sun, very similar to the

final helium mass fraction of 0.269 in the first solar calibration. However, the solar radius is too small and the effective temperature too high, so the next step is to decrease the mixing length gradually, which table 3.9 implies may correct these values. The outcome of this is shown in table 3.12.

Table 3.10 Effect of helium mass fraction on the time it takes a solar model to reach the present day solar luminosity with modelled solar radius and effective temperature after that time, for a constant mixing length of 1.9.

Mass fraction helium content	Time to reach $L_\odot$/Ga	$R/R_\odot$	T_{eff}/K
0.25	6.568	1.026	5698
0.2525	6.255	1.021	5712
0.255	5.947	1.016	5726
0.2575	5.644	1.011	5739
0.26	5.348	1.006	5753
0.2625	5.057	1.002	5767
0.265	4.771	0.997	5780
0.2675	4.491	0.993	5793
0.27	4.216	0.988	5806
0.2725	3.946	0.984	5819
0.275	3.681	0.980	5832
0.2775	3.420	0.975	5844
0.28	3.165	0.971	5856
0.2825	2.914	0.967	5868
0.285	2.668	0.964	5879
0.2875	2.428	0.960	5891

Table 3.11 Refining the effect of helium mass fraction on the time it takes a solar model to reach the present day solar luminosity with modelled solar radius and effective temperature after that time, for a constant mixing length of 1.9.

Mass fraction helium content	Time to reach $L_\odot$/Ga	$R/R_\odot$	T_{eff}/K
0.26	5.348	1.006	5753
0.261	5.231	1.005	5759
0.262	5.114	1.003	5764
0.263	4.999	1.001	5769
0.264	4.885	0.999	5775
0.265	4.771	0.997	5780
0.266	4.659	0.995	5785
0.267	4.547	0.993	5791
0.268	4.436	0.992	5796
0.269	4.325	0.990	5801
0.27	4.216	0.988	5806

Note that the time to reach $L_\odot$ is within error limits for all of these runs. The solar effective temperature according to Cox, 2000 is 5787K, however the solar radius at this temperature is a little small after 4.55Gyr. The final values taken to be those of the present day sun were where the mixing length is 1.83 and after 4.56Gyr the solar radius is 0.999 and the effective temperature is 5774K, in good agreement with other sources (5770K given by Carroll & Ostlie, 1996 and Zeilik & Gregory, 1998 and 5780K given by Beatty, 1999 and Phillips, 1994). The starting parameters used to attain this result are in table 3.13 and give solar profiles imperceptibly different from those shown in figures 3.2 and 3.3 for

the first solar matrix, including a main sequence lifetime of 11.6Gyr, the same as the first calibration model.

Table 3.12 Effect of mixing length on the time it takes a solar model to reach the present day solar luminosity for a helium mass fraction of 0.267.

Mixing Length	Time to reach $L_\odot$/Ga	$R/R_\odot$	T_{eff}/K
1.80	4.565	1.002	5767
1.81	4.563	1.001	5769
1.82	4.562	1.000	5771
1.83	4.560	0.999	5774
1.84	4.558	0.998	5776
1.85	4.556	0.998	5779
1.86	4.554	0.997	5781
1.87	4.552	0.996	5783
1.88	4.550	0.995	5786
1.89	4.549	0.994	5788
1.90	4.547	0.993	5791

Table 3.13 Parameter used in creating the final solar model for the second matrix,

Parameter	Value
Maximum Time Step / years	10^6
ZAMS Helium Content / mass fraction of Sun	0.267
ZAMS Metallicity / mass fraction of Sun	0.0188
ZAMS Carbon Content / mass fraction of metals	0.1516
ZAMS Nitrogen Content / mass fraction of metals	0.05289
ZAMS Oxygen Content / mass fraction of metals	0.5289
Mixing Length (no units)	1.83
Solar Mass / $M_\odot$	1
Log_{10}(ZAMS Solar Luminosity / $L_\odot$)	-0.1523
Log_{10}(ZAMS Effective Temperature / T_{eff})	3.7514

Putting these values into equation 3.16, where $Y_\odot = 0.267$, $Y_P = 0.243$ and $Z_\odot = 0.0188$, then $dY/dZ = 1.2766$, gives values much smaller than previously published of at least 3 (Pagel, 1992). For the use of equation 3.16 in this procedure, the solar metallicity is assumed high for its helium content in the calibration model. If the helium mass fraction were 0.2875 (Cox, 2000), then dY/dZ would be 2.367, which is closer and within the error boundaries of 2.8 ± 0.6 of Lequeux et al., 1979. The final value used here is $dY/dZ = 2$ and the solar helium mass fraction is assumed low for a metals mass fraction of 0.0188. This now allows a second stellar grid to be created.

3.6.2 Creating the Second Stellar Grid

This second stellar grid has many features which differ from the first. The main difference is that only the mixing length of all modelled stars is fixed. The metals mass fraction of the solar reference is 0.0188 instead of 0.02 and the helium mass fraction varies with metals mass fraction according to equation 3.16, where $Y_P = 0.243$ and $dY/dZ = 2$. The [Fe/H] values for each mass were again -0.4, -0.2, 0.0, 0.2 and 0.4. However when $Z_\odot = 0.0188$, then by using equation 3.15, these metallicities correspond to metals mass fractions of 0.007484, 0.01186, 0.0188, 0.0298 and 0.04722 respectively. Also by using equation 3.16, where $Y_P = 0.243$ and $dY/dZ = 2$, these models will have helium mass fractions of 0.258, 0.2667, 0.2806, 0.3026 and 0.3374 respectively. Apart from the metals mass fractions, the starting parameters for the stellar grid models are exactly the same as in table

3.5. For the correct metals mass fractions in table 3.5 for this second grid, simply substitute 0.007484 for 0.008, 0.001186 for 0.013, 0.0188 for 0.02, 0.0298 for 0.032 and 0.04722 for 0.05. A summary of the outcomes of these stellar models, illustrating the time the models remain on the main sequence and the distance of their habitable zone boundaries, determined from equations 3.3 to 3.8, are shown here in table 3.14.

Table 3.14 Summary of the outcomes of the stellar grid models.

$M/M_\odot$	Metallicity mass fraction	Time on Main Sequence in Ga	Habitable Zone Distance from Star in AU, from ZAMS (top)to the onset of the red giant phase (bottom).*					
			Recent Venus	Runaway Greenhouse	Water Loss	1st CO_2 Condensation	Maximum Greenhouse	Early Mars
0.5	0.007484	>65.5	0.158872	0.194592	0.200972	0.295331	0.382754	0.406066
			0.203278	0.248133	0.257144	0.377399	0.487663	0.517391
0.5	0.01186	>65.5	0.153852	0.189055	0.194622	0.286367	0.37222	0.394867
			0.191507	0.234737	0.242254	0.356097	0.461813	0.489933
0.5	0.0188	>65.5	0.150261	0.185205	0.190079	0.280044	0.365035	0.38722
			0.184692	0.227159	0.233634	0.3439	0.447378	0.474589
0.5	0.0298	>65.5	0.149012	0.18417	0.1885	0.278064	0.363409	0.385469
			0.184763	0.227792	0.233724	0.344387	0.449018	0.476304
0.5	0.04722	>65.5	0.152666	0.189008	0.193122	0.285116	0.373256	0.395895
			0.201765	0.248545	0.255232	0.37594	0.489769	0.519541
0.6	0.007484	>65.5	0.218976	0.266002	0.277001	0.405864	0.522307	0.554177
			0.525469	0.620027	0.664699	0.966329	1.216221	1.290566
0.6	0.01186	>65.5	0.210742	0.25708	0.266585	0.391167	0.505179	0.535978
			0.413326	0.492851	0.522845	0.761996	0.966444	1.025522
0.6	0.0188	>65.5	0.206121	0.252277	0.260741	0.383055	0.496123	0.526346
			0.382402	0.458533	0.483729	0.70602	0.899246	0.954202
0.6	0.0298	>65.5	0.206996	0.25383	0.261848	0.384962	0.499436	0.529843
			0.419433	0.501349	0.530571	0.773738	0.983128	1.04322
0.6	0.04722	59.1	0.218457	0.267506	0.276346	0.406055	0.52614	0.558187
			0.694583	0.832588	0.87863	1.282277	1.632797	1.732585
0.7	0.007484	39.0	0.302639	0.361702	0.38283	0.558268	0.709283	0.752637
			1.004222	1.1958	1.270311	1.85072	2.344887	2.488232
0.7	0.01186	42.1	0.290428	0.349116	0.367385	0.53658	0.684748	0.726587
			0.918368	1.098131	1.161711	1.694297	2.153411	2.285033
0.7	0.0188	43.1	0.284654	0.343396	0.360081	0.526454	0.673703	0.714853
			0.864818	1.03623	1.093973	1.596376	2.032133	2.156329
0.7	0.0298	40.3	0.28857	0.348326	0.365035	0.53379	0.683414	0.725154
			0.850954	1.017981	1.076434	1.570112	1.996255	2.118269
0.7	0.04722	32.3	0.310871	0.372952	0.393244	0.574034	0.731426	0.776124
			0.899451	1.067737	1.137777	1.656385	2.093879	2.221884
0.8	0.007484	23.4	0.40972	0.478308	0.518278	0.751782	0.939084	0.996457
			1.219376	1.442328	1.54247	2.243656	2.828847	3.001779
0.8	0.01186	25.2	0.393629	0.462832	0.497926	0.723322	0.908092	0.963595
			1.116117	1.325088	1.411853	2.055441	2.598549	2.757406
0.8	0.0188	25.6	0.386848	0.456625	0.489349	0.711464	0.895679	0.950431
			1.057348	1.257329	1.337513	1.947968	2.465585	2.616312
0.8	0.0298	23.8	0.39491	0.465645	0.499547	0.72612	0.913432	0.969268
			1.041981	1.236696	1.318073	1.918773	2.425228	2.57349
0.8	0.04722	19.0	0.428206	0.49995	0.541663	0.785721	0.981563	1.041531
			1.103928	1.300859	1.39643	2.029516	2.55193	2.707918
0.9	0.007484	14.9	0.539684	0.613291	0.68267	0.985682	1.209186	1.282819
			1.435304	1.688187	1.815607	2.637662	3.312202	3.514648
0.9	0.01186	15.9	0.519514	0.595113	0.657158	0.950021	1.171594	1.243023
			1.317178	1.554413	1.666184	2.422344	3.049053	3.235438
0.9	0.0188	16.2	0.512038	0.58895	0.647703	0.936982	1.158661	1.229341
			1.24836	1.475126	1.579132	2.296459	2.893318	3.070188
0.9	0.0298	15.0	0.522997	0.600613	0.661565	0.956785	1.181912	1.253996
			1.231283	1.452148	1.557529	2.264068	2.848564	3.02269
0.9	0.04722	12.0	0.558251	0.635496	0.706157	1.01986	1.252541	1.328835
			1.314994	1.540876	1.663416	2.414659	3.024136	3.208939
1.0	0.007484	9.78**	0.695705	0.769174	0.880017	1.266141	1.52619	1.618627
			1.368055	1.576295	1.730523	2.504156	3.100235	3.289394
1.0	0.01186	10.4**	0.671425	0.748483	0.849308	1.223126	1.482041	1.571966
			1.278514	1.479212	1.617261	2.341949	2.907495	3.084978
1.0	0.0188	10.5**	0.659431	0.738931	0.834139	1.202054	1.461322	1.550083
			1.221304	1.415795	1.544894	2.237948	2.782085	2.951948
1.0	0.0298	9.71**	0.666497	0.747324	0.843076	1.215033	1.477701	1.567469
			1.203643	1.393216	1.522553	2.204981	2.738288	2.905451
1.0	0.04722	7.75**	0.702619	0.783395	0.888767	1.279979	1.551103	1.645222
			1.240505	1.427028	1.569177	2.270058	2.807379	2.978635

$M/M_{\odot}$	Metallicity mass fraction	Time on Main Sequence in Ga	Habitable Zone Distance from Star in AU, from ZAMS (top)to the onset of the red giant phase (bottom).*					
			Recent Venus	Runaway Greenhouse	Water Loss	1st CO_2 Condensation	Maximum Greenhouse	Early Mars
1.1	0.007484	6.81***	0.84271	0.91504	1.06596	1.530917	1.82473	1.934762
			1.552244	1.782236	1.96351	2.839619	3.507282	3.721182
1.1	0.01186	7.22***	0.814043	0.891242	1.029702	1.479989	1.773078	1.880219
			1.449245	1.669579	1.833225	2.652698	3.283786	3.48414
1.1	0.0188	7.26***	0.800159	0.880808	1.012143	1.455555	1.749716	1.855584
			1.383109	1.596803	1.749567	2.532582	3.139614	3.331221
1.1	0.0298	6.68***	0.808283	0.890846	1.022419	1.470525	1.769072	1.876143
			1.360457	1.568563	1.720912	2.490527	3.084714	3.272941
1.1****	0.04722	5.66***	0.850954	0.933741	1.076393	1.547444	1.856476	1.968719
			1.395085	1.599867	1.764711	2.551613	3.149039	3.341059
1.2	0.007484	4.92***	1.00017	1.069833	1.265127	1.814759	2.143205	2.271907
			1.733604	1.989918	2.192921	3.171247	3.916163	4.15499
1.2****	0.01186	5.29***	0.967132	1.043003	1.22334	1.755923	2.08415	2.209595
			1.620756	1.866288	2.050177	2.966393	3.670953	3.894917
1.2	0.0188	5.20***	0.951098	1.031452	1.203061	1.727631	2.057625	2.181659
			1.53885	1.77491	1.946571	2.817287	3.490311	3.703297
1.2	0.0298	4.99***	0.96074	1.043845	1.215259	1.745435	2.081212	2.206729
			1.511505	1.741063	1.91198	2.766593	3.424458	3.633391
1.2	0.04722	4.10***	1.010333	1.094386	1.277988	1.835037	2.183941	2.315548
			1.544056	1.76942	1.95315	2.823747	3.483209	3.695585
1.3****	0.007484	3.79***	1.168327	1.233779	1.477823	2.118078	2.481979	2.630451
			1.91106	2.189499	2.417392	3.494793	4.31033	4.573128
1.3	0.01186	3.91***	1.130784	1.204052	1.430338	2.051093	2.4156	2.560465
			1.773464	2.038503	2.243343	3.244911	4.010848	4.255494
1.3****	0.0188	4.03***	1.112897	1.191938	1.407717	2.019485	2.386854	2.53024
			1.691775	1.945853	2.140011	3.095778	3.828154	4.061675
1.3	0.0298	3.72***	1.124163	1.206963	1.421969	2.040307	2.415087	2.56027
			1.656342	1.903291	2.095189	3.030457	3.745003	3.973424
1.3	0.04722	3.09***	1.182174	1.267006	1.495347	2.145308	2.53663	2.689043
			1.701991	1.946091	2.152929	3.111472	3.832503	4.066102
1.4****	0.007484	2.98***	1.348567	1.407373	1.705801	2.443307	2.842674	3.012079
			2.083545	2.380596	2.635573	3.808557	4.688822	4.974584
1.4	0.01186	3.05***	1.305305	1.374288	1.651085	2.365998	2.767441	2.932833
			1.933259	2.215309	2.445472	3.535485	4.36101	4.626904
1.4	0.0188	3.08***	1.285435	1.361827	1.625955	2.330841	2.736642	2.900511
			1.841187	2.110851	2.329007	3.367379	4.155019	4.408371
1.4	0.0298	2.87***	1.299757	1.381185	1.644073	2.357271	2.772782	2.938968
			1.809398	2.071937	2.288794	3.308601	4.079269	4.32796
1.4	0.04722	2.35***	1.367634	1.452027	1.729931	2.480231	2.915844	3.090558
			1.864556	2.125764	2.358561	3.407111	4.188596	4.443789
1.5	0.007484	2.33***	1.538582	1.585946	1.946141	2.786177	3.217536	3.408476
			2.25045	2.568183	2.846697	4.112867	5.059425	5.367718
1.5****	0.01186	2.48***	1.492324	1.554367	1.887637	2.70352	3.141724	3.32883
			2.104024	2.405816	2.661479	3.846451	4.737844	5.026626
1.5	0.0188	2.43***	1.469865	1.541484	1.859234	2.663714	3.108282	3.293812
			1.997537	2.286094	2.52678	3.652297	4.501351	4.775753
1.5	0.0298	2.24***	1.48679	1.564859	1.880645	2.694908	3.151542	3.339871
			1.966933	2.247281	2.488065	3.59538	4.426272	4.696032
1.5	0.04722	1.83***	1.566159	1.647835	1.981039	2.838716	3.319033	3.51735
			2.035769	2.316267	2.575134	3.718823	4.565736	4.843818

See table 3.6 for footnotes, with the exception that the times to reach minimum luminosity varies from 96.3 million years for a $0.5M_{\odot}$ star with 0.0298 mass fraction of metals to 7,250 years for a $1.5M_{\odot}$ star with 0.007484 mass fraction of metals.

The trends in table 3.14 are almost identical to those in the corresponding table 3.6 for the first stellar matrix. The ratio of final HZ to ZAMS HZ distances remains 3.5 for the lowest mass stars but decreases to 1.3 for the 0.04722 metallicity model of $1.5M_{\odot}$, lower than the 1.6 ratio in the first matrix. This can be attributed to the higher levels of helium in the higher metallicity models, which shortens their main sequence lifetimes considerably, as discussed in section 5.1 of this chapter. One interesting trend is that, due to the elevated helium levels in the higher metallicity stars, the most metal rich stars for the same mass do not have the longest main sequence lifetime. This is verified by figure 3.17 which shows the trends in stellar main sequence lifetime for all masses above $0.7M_{\odot}$ in a plot of main sequence lifetime versus metallicity.

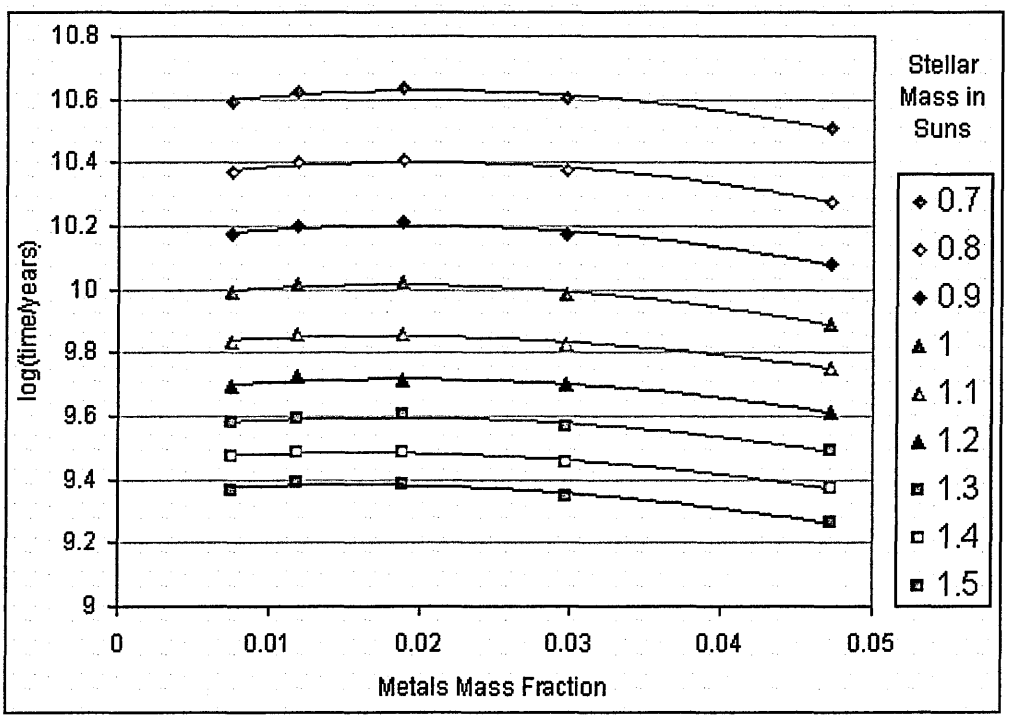

Figure 3.17 Log of time on main sequence versus metallicity for stars of the same mass.

3.6.3 Modelling Stars of Exoplanetary Systems

The stars of the exosystems listed in section 5.3 of this chapter, which have been investigated using the Mercury Orbital Integrator for the possibility that they may house habitable Earths, were also modelled using this second matrix method. This would allow a "second opinion" of their habitable zone boundaries as it does for the grid modelled stars. The starting parameters of these models are listed in table 3.7, except for the helium and metals mass fractions, which are listed in table 3.15. The outcomes of these models are listed in table 3.16 and a diagram showing the entire reference star model points are in figure 3.18.

Table 3.15 The starting helium and metals mass fractions for the stars in the exoplanetary systems using the second stellar model.

Star	Metals Mass Fraction	Helium Mass Fraction
47 Ursae Majoris	0.01564	0.2743
1st and 2nd 55 Cancri	0.03666	0.3163
1st and 2nd Epsilon Eridani	0.01493	0.2729
1st and 2nd Gliese 876	0.0188	0.2806
1st and 3rd HD 196050	0.03343	0.3099
2nd and 4th HD 196050	0.0188	0.2806
HD 23079	0.0188	0.2806
HD 28185	0.03267	0.3083
HD 52265	0.02422	0.2914
HD 72659	0.01362	0.2702
Rho Coronae Borealis	0.01214	0.2673
Sun	0.0188	0.267
Tau[1] Gruis	0.02656	0.2961
Upsilon Andromedae	0.0188	0.2806

Table 3.16 Summary of the outcomes of the exoplanetary system stellar models.

Star	Time on Main Sequence in Ga	Habitable Zone Distance from Star in AU, from ZAMS (top)to the onset of the red giant phase (bottom).					
		Recent Venus	Runaway Greenhouse	Water Loss	1st CO_2 Condensation	Maximum Greenhouse	Early Mars
47 Ursae Majoris	9.42	0.70381	0.782895	0.890272	1.28179	1.551003	1.64507
		1.289711	1.490836	1.631423	2.362083	2.93072	3.109603
1st 55 Cancri	7.98	0.720263	0.801992	0.911085	1.311909	1.588446	1.684804
		1.259251	1.451485	1.592892	2.305147	2.854588	3.028768
2nd 55 Cancri	10.8	0.603273	0.682075	0.763104	1.101009	1.346205	1.42811
		1.130399	1.279866	1.429888	2.063462	2.525312	2.678994
1st Epsilon Eridani	25.6**	0.38888	0.458341	0.491919	0.714966	0.899128	0.954089
		1.087263	1.292284	1.375355	2.002847	2.534152	2.689072
2nd Epsilon Eridani	29.7**	0.355754	0.42235	0.450017	0.655152	0.828246	0.878879
		1.027029	1.22323	1.299161	1.892856	2.398671	2.545304
1st Gliese 876	~476***	0.092623	0.114726	0.117168	0.173021	0.226615	0.240357
		0.322612	0.391372	0.408098	0.59769	0.768323	0.815216
2nd Gliese 876	~415***	0.096385	0.119348	0.121926	0.18002	0.235709	0.250005
		0.384192	0.467005	0.485997	0.712243	0.917084	0.973038
1st HD 196050	6.42	0.815218	0.89802	1.031191	1.48306	1.783568	1.891502
		1.363308	1.571675	1.724518	2.495698	3.090886	3.279487
2nd HD 196050	7.26	0.800159	0.880808	1.012143	1.455555	1.749716	1.855584
		1.383109	1.596803	1.749567	2.532582	3.139614	3.331221
3rd HD 196050	4.13****	1.057221	1.14078	1.337296	1.919576	2.279154	2.416357
		1.591783	1.827584	2.013524	2.911936	3.596538	3.81588
4th HD 196050	4.50****	1.038045	1.11783	1.313039	1.884449	2.234677	2.369127
		1.621072	1.86493	2.050576	2.966507	3.668824	3.892632
HD 23079	7.35	0.795136	0.876336	1.005789	1.446603	1.740268	1.845595
		1.369992	1.582464	1.732975	2.508788	3.111184	3.301067
HD 28185	9.78	0.65719	0.737863	0.831303	1.198272	1.458551	1.547177
		1.189164	1.371942	1.504236	2.17719	2.697778	2.862406
HD 52265	6.33	0.845323	0.927376	1.06927	1.537173	1.843923	1.955401
		1.411017	1.627755	1.784868	2.583332	3.200848	3.396175
HD 72659	12.8*	0.586392	0.664076	0.741752	1.07045	1.310231	1.389971
		1.170537	1.356138	1.480676	2.144689	2.665073	2.827782
1st Rho Coronae Borealis	12.7*	0.589998	0.667071	0.746312	1.076783	1.316589	1.396693
		1.186637	1.373805	1.501041	2.173905	2.700061	2.864894
2nd Rho Coronae Borealis	10.4	0.670546	0.747754	0.848196	1.221574	1.480477	1.570313
		1.274148	1.470806	1.611736	2.33301	2.891939	3.068428
Sun	11.6	0.63666	0.717086	0.805336	1.161331	1.416471	1.502593
		1.182424	1.375029	1.495715	2.167969	2.700878	2.865832
Tau[1] Gruis	4.44*****	1.035133	1.11759	1.309356	1.879559	2.232433	2.366844
		1.586692	1.824403	2.007086	2.90333	3.589409	3.808358
Upsilon Andromedae	4.07*****	1.106127	1.186105	1.399155	2.007381	2.374282	2.516961
		1.675898	1.926974	2.119927	3.06656	3.791211	4.02247

N.B. All main sequence lifetimes were determined using habitable zone boundary profiles unless otherwise stated below.

* The main sequence lifetimes of the 2nd 55 Cancri model, HD 72659 and the 1st Rho Coronae Borealis model were determined using their luminosity profiles.

** Epsilon Eridani's main sequence lifetimes were determined using their effective temperature profiles.

*** The main sequence lifetime for Gliese 876 could not be determined by any of the three previously mentioned techniques using habitable zones, luminosity or effective temperature. The value here was determined by graphical inspection of its luminosity profile.

**** Maximum time steps of 10^7 years were used to enable this model to complete.

***** Maximum time steps of 10^8 years were used to enable this model to complete.

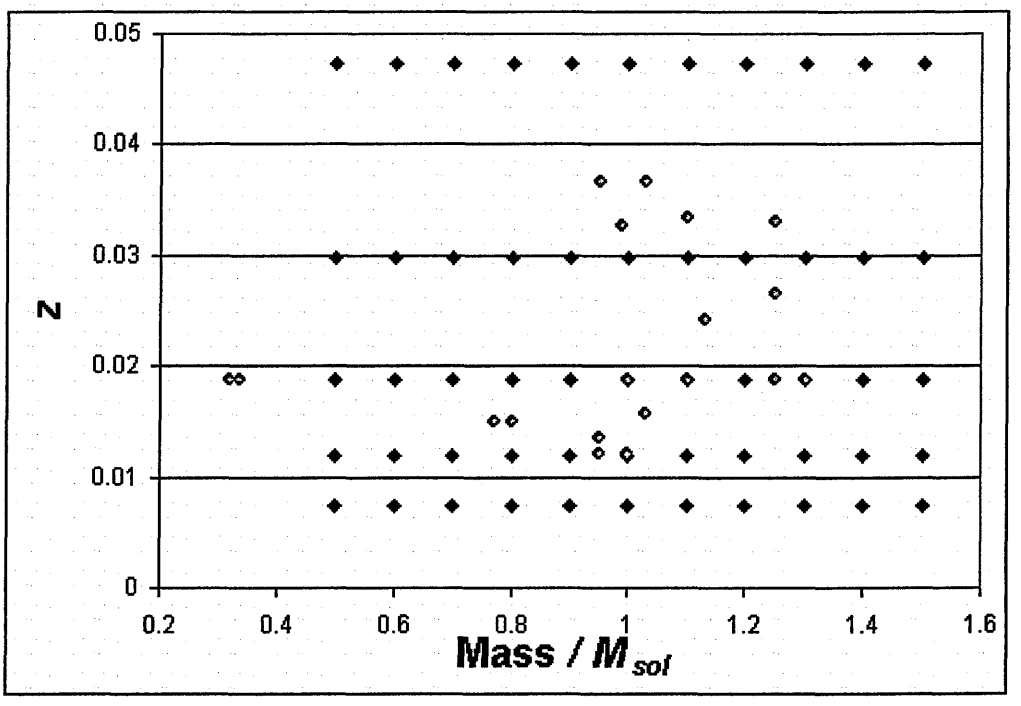

Figure 3.18 The 55 stellar grid points combined with those of the modelled (and investigated) exoplanetary system stars for the second model.

3.7 Determining Present Day Exosystem Habitable Zones from Stellar Data

A third, and probably most reliable method, of calculating present-day distances of habitable zone boundaries of known exoplanetary systems is to use data from stellar observations. Stellar parallax shifts of the nearby stars with planetary systems give their distances, with inaccuracies up to 30% (Turnbull and Tarter, 2003). The systems discovered by radial velocity changes or astrometry are all within 100 parsecs of Earth. Their bolometric luminosities can then be easily determined from the stellar apparent visual magnitude and spectral type, where bolometric refers to radiation flux over all wavelengths, not just visible. For a solar absolute bolometric magnitude, $M_{bol\odot} = 4.74$ (Cox, 2000), then we get L from

$$\frac{L}{L_{\Theta}} = 0.787 d^2 \times 10^{-0.4(M_v + BC)} \qquad 3.17,$$

Table 3.17 Effective Temperatures and Bolometric corrections for spectral stellar types (Cox, 200).

Spectral Type	Effective Temperature / K		Bolometric Correction (*BC*)	
	Luminosity Class V	Luminosity Class III	Luminosity Class V	Luminosity Class III
F0	7300	-	-0.09	-
F2	7000	-	-0.11	-
F5	6650	-	-0.14	-
F8	6250	-	-0.16	-
G0	5940	-	-0.18	-
G2	5790	-	-0.2	-
G5	5560	5050	-0.21	-0.34
G8	5310	4800	-0.4	-0.42
K0	5150	4660	-0.31	-0.5
K2	4830	4390	-0.42	-0.61
K5	4410	4050	-0.72	-1.02
M0	3840	3690	-1.38	-1.25
M2	3520	3540	-1.89	-1.62
M5	3170	3380	-2.73	-2.48

where d is the stellar distance, M_v is apparent magnitude and BC is the bolometric correction, i.e. bolometric magnitude less visual magnitude. This may not work, however, for some systems discovered by transiting, which are much further away, hence making any parallax data unreliable or non-existent. Four of these distant systems have had magnitudes measured as M_I, hence V-I corrections are required. For OGLE-TR-113 M_v - M_I = 1.06, for OGLE-TR-132 M_v - M_I = 0.47, for OGLE-TR-10 M_v - M_I = 0.89 and for OGLE-TR-111, M_v - M_I = 0.89 (Cox, 2000). The bolometric correction values for stars of different spectral type are shown in table 3.17 and graphically in figure 3.19, also with the change in effective temperature with spectral type, shown graphically in figure 3.20.

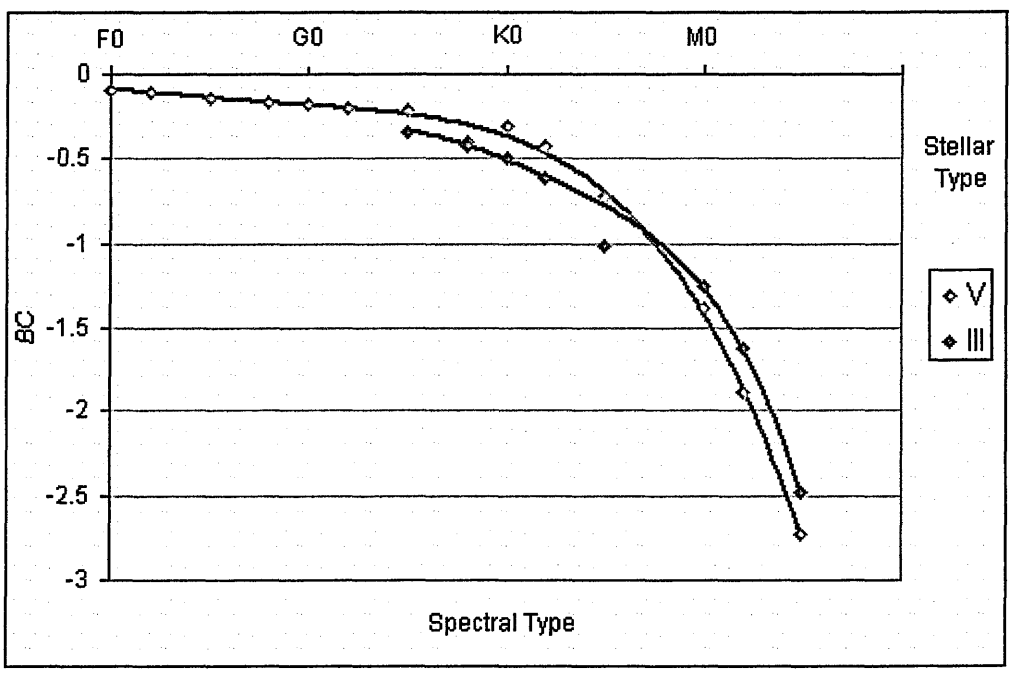

Figure 3.19 Bolometric corrections (V magnitudes) for different spectral types of star

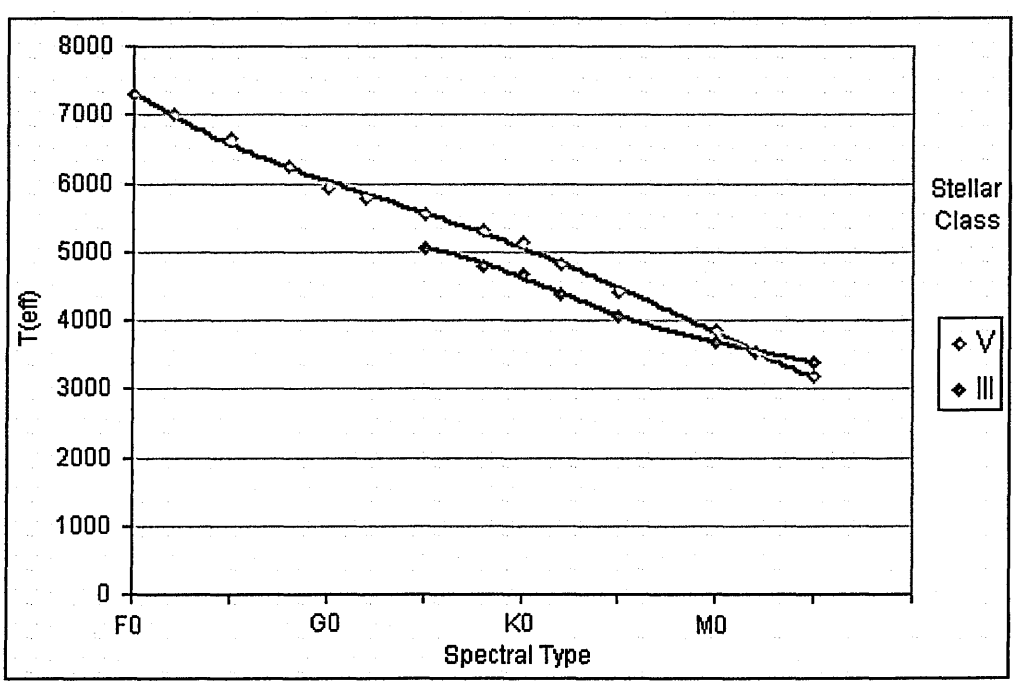

Figure 3.20 Effective temperature variation for different spectral types of star

The trend lines shown in figure 3.19 may be converted into formulae by making nomenclature substitutions by letting F=0, G=1, K=2 and M=3. Hence for the Sun of spectral type G2, the spectral type would be valued at 12, and a K7 star would have a spectral type value of 27. So for numerical spectral type being substituted by x, this gives the following two equations for luminosity class stars V and III respectively:

$$BC_V = -0.00000376337x^4 + 0.0000968025x^3 - 0.00071309x^2 - 0.00805x - 0.09006 \quad 3.18a$$

$$BC_{III} = -0.0000278623x^4 + 0.00236x^3 - 0.07606x^2 + 1.05582x - 5.61628 \quad 3.18b.$$

This enables the bolometric correction for any class V and class III star between spectral types F0 and M5 to be accurately determined. For any rare class IV star, the mean bolometric correction value of those calculated for classes V and III is taken. The formulae were determined by statistical fit, omitting the K5III star, using Microcal Origin Plot v. 6 by Microcal Software Inc, Northampton, MA, 01060 USA.

Similarly, curves may be obtained for effective temperature with spectral type, which are useful for determining the critical stellar flux, S, at the top of a planet's atmosphere, subsequently used to determine habitable zone distances with equations 3.4, 3.7 and 3.10. Again substituting numerical spectral type with x, the following two equations are obtained for spectral class type V and III stars respectively,

$$T_{eff(V)} = 0.00384x^4 - 0.33037x^3 + 8.86743x^2 - 189.4866x + 7332.32809 \quad 3.19a$$

$$T_{eff(III)} = -0.02109x^4 + 2.26609x^3 - 87.33353x^2 + 1337.084x - 1941.82128 \quad 3.19b.$$

The unclear nature of habitable zone boundaries, which are widely open to interpretation, justifies these crude methods for determining bolometric corrections and stellar effective temperature in this way. Although not entirely correct, it does enable the use of a mathematical solution to estimate these values.

3.8 Determining the Habitability of Known Exosystems

The information from the stellar grids was applied to each of the 143 exoplanetary systems known on 31st August, 2005, using the following procedure. The star of each system was matched with its nearest grid model, in terms of mass and metallicity, and the HZs of each particular nearest grid model were applied back to the corresponding starting exoplanetary system. As six habitable zone boundaries have already been defined (see section 1 of this chapter), of which three mark the internal boundaries and three the external boundaries, the middle boundary of each set of three was chosen to define the habitable zone limits of the systems, i.e. the Runaway Greenhouse and Maximum Greenhouse HZ boundaries. These two boundaries were overlaid onto the orbital and gravitational reaches of the giant(s) in each system. Regions existing beyond the reaches of any giant planet but within the habitable zones are where habitable Earth-sized planets could exist in stable orbits confined to the habitable zone. If these areas have been within the habitable zone for more than 2Gyr from the zero-age of the system or 1Gyr otherwise, then life could have existed long enough on a possible planet for it to have made an appreciable enough change in the planet's atmosphere for it to be detected. If this is the situation now, then an exoplanetary system is currently capable of supporting detectable life. If this situation arises at any time during the main sequence lifetime of a star at the centre of a system, then such a system is capable of supporting detectable life at some time in the past or future.

An alternative method to determine present-day habitable zones uses information from the observed stellar data, see table 3.18. This was applied to each of the 150 then known

exoplanetary systems, 111 of which were first investigated by P.N. Sleep, (2005), with additions and revised calculations here. Clearly there are examples where stellar distances are uncertain and these stars could not have their HZ boundaries determined by this method. The bolometric luminosity of a star is determined from its distance, apparent visual magnitude and bolometric correction from equation 3.17. The bolometric corrections and effective temperature for each star are found from their published spectral types (Schneider, 2006) using equations 3.18a & b and 3.19a & b. Using the star's bolometric luminosity and effective temperature, equations 3.4 and 3.7 will give its fluxes at the inner and outer habitable zone boundaries. Equation 3.10 is then applied to find the distances of these fluxes, and hence the **present day** inner and outer habitable zone boundary distances from the star. By comparing these with the gravitational reach of any giant planet(s) around the star, it may be determined whether the system could currently support a potentially habitable Earth-like planet. For any potentially habitable Earths, it is not possible to accurately determine whether such a planet will have been inside the HZ for the 1Gyr (or 2Gyr from ZAMS) required for life to have made an appreciable effect on the planets atmosphere to enable its detection. However, this may be estimated from the width of potentially habitable regions beyond a giant's gravitational reach.

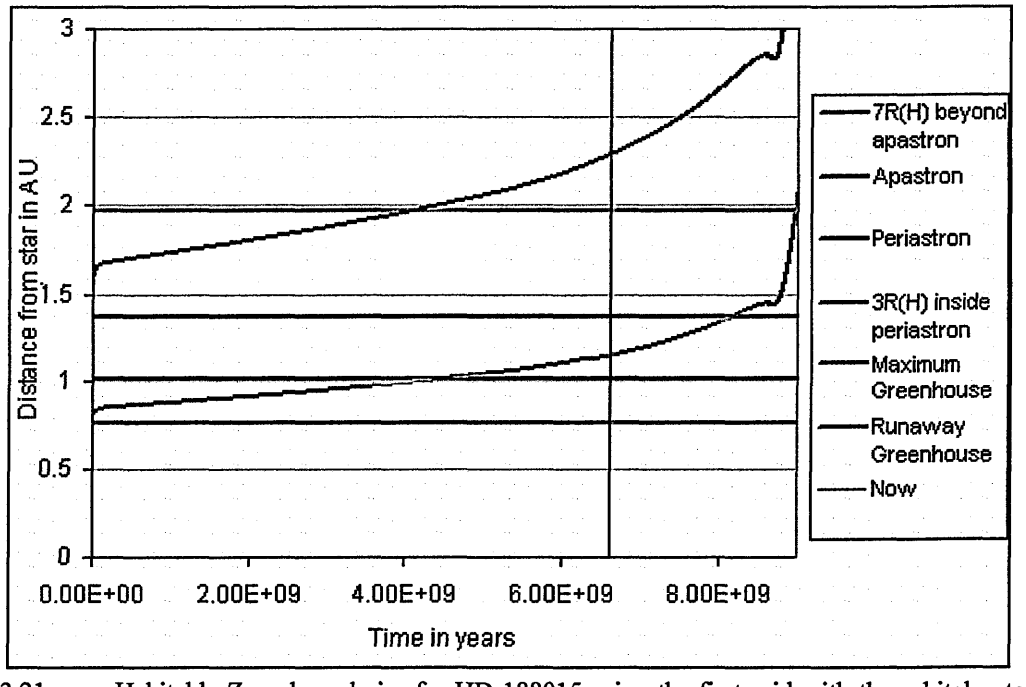

Figure 3.21 Habitable Zone boundaries for HD 188015 using the first grid with the orbital extent and limits of gravitational reach of its giant planet.

To illustrate how this works, a star, HD 188015 and its giant planet, have been randomly chosen as an example. This star has a mass of $1.08M_{\odot}$, a metallicity of [Fe/H] = 0.29 and an estimated age of 6.6Gyr (Schneider, 2006). Using equation 3.15, this metallicity is equal to a metals mass fraction of 0.039 in the first stellar grid and 0.03666 in the second stellar grid. Hence the nearest grid model for this star is that with a mass of $1.1M_{\odot}$ and metals mass fraction of 0.032 (1st grid) or 0.0298 (2nd grid). However, figure 3.16 shows a nearer point which is a model of HD 196050, with a metals mass fraction of 0.03557 or 0.03343. So the HZs of this model will be used as those for our example, HD 188015. Figure 3.21, therefore, shows the runaway greenhouse and maximum greenhouse HZ boundaries of this star, from the first stellar grid, along with the periastron and apastron limits of the giant planet's orbit. Also plotted are the internal and external limits of the giant's gravitational influence on smaller orbiting bodies, inside periastron and beyond apastron respectively (this will be explained fully in chapter 4, section 4). The plot shows that no part of the HZ could have had a habitable Earth confined to a stable orbit early in

the stars main sequence lifetime. Currently there is a narrow region beyond the limit of gravitational reach of the giant, which has been in the HZ for the last billion years (see section 1 of this chapter for more detail). So it is possible that a habitable Earth-type rocky planet could currently exist in this system, where life has lasted long enough for it to have chemically altered the planet's atmosphere. In the future and up to the end of its main sequence lifetime, this habitable narrow region will grow wider so the chance will increase that a planet may exist in a stable orbit confined to the habitable zone. This system would thus be classified as capable of housing a currently habitable planet.

In order to establish the potential habitability of each system, a list of the exoplanetary systems is now presented in Table 3.18, showing the stellar parameters and planetary parameters. The individual models for each star, from which the stellar parameters are derived, can be determined by checking the two stellar times on the main sequence, one for each model type. These can be matched with the models listed in Tables 3.6 and 3.8 for the first model type, where helium mass fractions are the same, and Tables 3.14 and 3.16 for the second model type, where helium mass fractions vary with metals mass fraction. Table 3.19 lists data of those same systems derived from Table 3.18. It shows the extent of their giant planet's gravitational reach determined from formulae 4.2 and 4.3, which will be explained in chapter 4, section 4. Planetary minimum masses were used as this minimises gravitational reach and maximises the proportion of the habitable zone offering long-term confinement. Also listed are the runaway greenhouse and maximum greenhouse habitable zone boundary distances at zero-age main sequence (ZAMS) and end of the main sequence (EoMS) for both stellar grid models. Finally the current HZ boundaries are presented, where the stellar age is known, for both stellar grids and from calculations involving measured stellar parameters.

Table 3.20 lists an assessment, from analysing the data in Table 3.19, of whether each system could house a potentially habitable Earth-like planet now and at any time during their main sequence lifetimes. Where there is a "yes" entry, then all of a star's habitable zone could house a habitable Earth-mass planet in a confined orbit either now or at any stage of a star's main sequence lifetime. A "no" entry means that no part of the habitable zone could house an Earth-like planet either now or at any stage of a star's main-sequence lifetime. A "moon" entry shows that a habitable Earth-mass satellite of a giant planet may exist within a system either now or at some time.

Entries where only part of the habitable zone may house a **detectable** habitable Earth-mass planet in a confined orbit are indicated by xI, xO or xB, where x is an integer and $1 \leq x \leq 9$. Here, "I" refers to a part of the habitable zone interior to a giant planet's orbit, "O" refers to a part of the habitable zone beyond a giant planet's orbit and "B" refers to a part between the orbits of two giants. For parts of the habitable zone capable of housing a habitable "Earth" interior to the gravitational reach of a giant for stars older than 2Gyr, the value "xI", rounded to the nearest integer, is determined by,

$$x\text{I} = 10 \times (\text{giant's inner gravitational reach} - \text{HZ inner boundary})/(\text{HZ width}) \qquad 3.20.$$

For similar regions of the habitable zone beyond the gravitational reach of a giant planet, the value "xO", to the nearest integer, is determined by,

$$x\text{O} = 10 \times (\text{HZ outer boundary} - \text{giant's outer gravitational reach})/(\text{HZ width}) \qquad 3.21.$$

In equation 3.21, however, the planet must have been within the habitable zone for 1Gyr, so the HZ outer boundary value will be that of 1Gyr prior to its present age. Regions

between two giants for stars older than 2Gyr, where habitable Earths may exist are given by,

xB = 10 × (Outer giant's inner gravitational reach − Inner giant's outer gravitational reach)/(HZ width) 3.22.

All values in these three equations are clear for each system when determining the x values for the present day boundaries where a star's age is known.

Stellar ages are taken from the literature where published. Where a star's age is not listed in the literature or its literature age is greater than the age of the Universe (13.7Gyr), it is determined from the nearest stellar models in both Mazzitelli matrices, using its observed data. The habitable zone distances determined from the observed data, using equations 3.4, 3.7 and 3.17, are matched to the same distances for the nearest model. The mean age at which these HZ distances occur in the two models is deemed to be the age of the star. If only one of the Mazzitelli models gives a sensible stellar age, that one is taken as the star's age. A star's age is not listed if the stellar data gives HZ boundaries which lie outside those ZAMs or End of Main Sequence (EoMS) boundaries as predicted by the nearest Matrix models. In such cases where the star's age is not known, the star is presently rated as not capable of supporting habitable life (in table 3.20) as it is either less than 2Gyr old (where the calculated HZ boundaries are nearer to the star than the ZAMS ones) or it is beyond the end of its main sequence life time (where the calculated HZ boundaries are beyond those at EoMS). Some stars have literature ages and ages determined from observed stellar data that are greater than that of the Universe. As this is not possible, their ages have been left blank. A small number of stars, such as Gliese 876, have an indeterminable age. However, their HZs are currently moving so slowly as to not be of any significance. In such cases the assessment of habitability is the same for both 'now' and 'at some time'.

For x calculated over the main sequence lifetime of a star, the largest and most optimistic values are taken. Any xI value is greatest after 2Gyr in any system, when the habitable zone boundaries are closest to the star and any possible life has had long enough to make detectable changes to a habitable Earth-mass planet's atmosphere. Any xO value is greatest 1Gyr before the very end of a star's main sequence lifetime, and assuming the orbits of more then one giant in a system are invariant, xB values do not change over the main sequence lifetime of a star. Where there is more than one entry in a box, then they are in chronological order. If a "moon" entry is followed by a bracketed letter, this refers to the giant planet designation in a multi-giant system around which the moon would orbit.

Table 3.18 Exoplanetary System Parameters

Star	Mass / $M_\odot$[1]	Metallicity mass fraction		Spectral Type	*BC*	*d*/Pc	m_v	Age / Gyr	MS time / Ga		Planet	Min. mass / M_{Jup}	*a* / AU	*e*	Inner Hill Radius Multiplier (n_{int})	Outer Hill Radius Multiplier (n_{ext})
		1st Model	2nd Model						1st model	2nd model						
OGLE-TR-56	1.04	-[2]		GV	-0.18	1500[3]	16.6	3[4]	11.6	10.5	b	1.45	0.0225	0	3	3
OGLE-TR-113	0.77	0.0276	0.0259	KV	-0.36	1500[3]	15.48	-[5]	31	23.8	b	1.35	0.0228	0	3	3
OGLE-TR-132	1.35	0.0538	0.0506	FV	-0.09	1500[3]	16.19	0.7[6]	3.77	2.35	b	1.19	0.0306	0	3	3
											d	*0.023*	*0.0208*	*0*	*3*	*3*
											c	*0.56*	*0.13*	*0.27*	*2.71*	*7.68*
Gliese 876	*0.32*	*0.0209*	*0.0197*	*M4V*	*-2.41*	*4.72*	*10.17*	*2.1*[7]	*500*	*476*	*b*	*1.935*	*0.208*	*0.0249*	*2.93*	*3.73*
HD 212301	1.03[48]	-[2]		F8V	-0.17	52.7	7.77	9.7[7]	11.6	10.5	b	0.045	0.036	0	3	3
HD 73256	1.05	0.0390	0.0367	G8	-0.30	36.5	8.08	0.83[8]	11.4	7.98	b	1.87	0.037	0.03	2.92	3.87
GJ 436	0.41	0.0187	0.0175	M2.5	-1.98	10.2	10.68	3[9]	440	415	b	0.067	0.0278	0.12	2.76	5.88
											e	*0.045*	*0.038*	*0.174*	*2.73*	*6.71*
											b	*0.784*	*0.115*	*0.0197*	*2.94*	*3.59*
											c	*0.217*	*0.24*	*0.44*	*2.669*	*8.595*
55 Cnc	*1.03*	*0.0390*	*0.0367*	*G8V*	*-0.30*	*13.4*	*5.95*	*5*[10]	*11.4*	*7.98*	*d*	*3.92*	*5.257*	*0.327*	*2.711*	*8.05*
HD 63454	0.8	0.0258	0.0242	K4V	-0.60	35.8	9.37	9.3[7]	31.0	23.8	b	0.38	0.036	0	3	3
HD 149026	1.3	0.0458	0.0431	G0IV	-0.18	78.9	8.15	2.4[7]	4.88	3.09	b	0.36	0.042	0	3	3
HD 83443	0.79	0.0428	0.0402	K0V	-0.36	43.54	8.23	6.5[11]	32.1	19.0	b	0.41	0.04	0.08	2.82	5.09
HD 46375	1.00	0.0356	0.0334	K1IV	-0.48	33.4	7.94	4.5	13.2	9.78	b	0.249	0.041	0.04	2.89	4.14
TrES-1	0.87	0.0200	0.0188	K0V	-0.36	157	11.79	2.5[6]	17.8	16.2	-	0.61	0.0393	0.135	2.75	6.13
HD 179949	1.24	0.0209	0.0197	F8V	-0.17	27	6.25	3.3[7]	5.71	5.2	b	0.98	0.04	0.05	2.87	4.4
HD 187123	1.06	0.0289	0.0272	G5	-0.24	50	7.86	4[12]	8.63	6.68	b	0.52	0.042	0.03	2.92	3.87
OGLE-TR-10	1.22	0.0264	0.0248	G/K	-0.24	1500	15.82	3.6[7]	6.15	4.99	b	0.54	0.04162	0	3	3
Tau Boo	1.3	0.0381	0.0358	F7V	-0.16	15	4.5	2[10]	4.69	3.72	b	4.13	0.05	0.01	2.970	3.304
HD 188753A	1.06	-[2]		K0	-0.36	44.82	7.43	5.6[13]	8.00	7.26	b	1.14	0.0446	0	3	3
HD 330075	0.95	-[2]		G5	-0.24	50.2	9.36	6.2[14]	17.8	16.2	b	0.76	0.043	0	3	3
HD 88133	1.2	0.0438	0.0411	G5IV	-0.29	74.5	8.01	3.4[15]	6.43	4.10	b	0.22	0.047	0	3	3
HD 2638	0.93	0.0289	0.0272	G5	-0.24	53.71	9.44	2.5[15]	19.4	15.0	b	0.48	0.044	0	3	3
BD-10 3166	1.1	0.0632	0.0595	G4V	-0.22	<200[16]	10.08	-[5]	8.84	5.66	b	0.48	0.046	0	3	3
HD 75289	1.05	0.0390	0.0367	G0V	-0.18	28.94	6.35	2.1[17]	11.4	7.98	b	0.42	0.046	0.054	2.863	4.494
HD 209458	1.05	0.0219	0.0206	G0V	-0.18	47	7.65	5.2[18]	11.6	10.5	b	0.69	0.045	0	3	3
HD 76700	1.00	-[2]		G6V	-0.25	59.7	8.13	11[19]	11.6	10.5	b	0.197	0.049	0	3	3
OGLE-TR-111	0.82	0.0264	0.0248	G/K	-0.24	1500	16.44	-[5]	31.0	23.8	b	0.53	0.047	0	3	3
HD 149143	1.21	0.0364	0.0342	G0IV	-0.18	63	7.9	ZAMS[7]	6.15	4.99	b	1.33	0.053	0.016	2.953	3.480
											b	*0.69*	*0.059*	*0.012*	*2.965*	*3.363*
											c	*1.89*	*0.829*	*0.28*	*2.711*	*7.755*
Ups And	*1.3*	*0.0246*	*0.0231*	*F8V*	*-0.17*	*13.47*	*4.09*	*2.6*[20]	*4.29*	*4.07*	*d*	*3.75*	*2.53*	*0.27*	*2.711*	*7.682*
51 Peg	1.0[21]	.0230[12]	.0136[12]	G2IV	-0.20	14.7	5.49	8.5[12]	11.6	10.5	b	0.468	0.052	0	3	3
HD 49674	1.00	0.0356	0.0334	G5V	-0.24	40.7	8.10	4.5[21]	13.2	9.78	b	0.12	0.0568	0	3	3
HD 109749	1.2	0.0356	0.0334	G3IV	-0.21	59	8.1	1.8[7]	6.15	4.99	b	0.28	0.0635	0.01	2.970	3.304

Star	Mass / $M_{\odot}$[1]	Metallicity mass fraction		Spectral Type	*BC*	*d*/Pc	m_v	Age / Ga	MS time / Gyr		Planet	Min. mass / M_{Jup}	*a* / AU	*e*	Inner Hill Radius Multiplier (n_{int})	Outer Hill Radius Multiplier (n_{ext})
		1st Model	2nd Model						1st model	2nd model						
Gl 581	0.31	0.0112	0.0106	M3	-2.12	6.26	10.55	<2[7]	<500	<476	b	0.056	0.041	0	3	3
HD 118203	3.1	0.0252	0.0237	K0	-0.50	88.6	8.05	EoMS[7]	<2[45]		b	1.6	0.061	0.3	2.711	7.890
HD 68988	1.2	0.0348	0.0327	G0	-0.18	58	8.21	6[22]	6.15	4.99	b	1.9	0.071	0.14	2.747	6.214
HD 168746	0.92	0.0170	0.0160	G5	-0.24	43.12	7.95	>2[23]	17.8	16.2	b	0.23	0.065	0.081	2.815	5.115
HD 217107	0.98	0.0399	0.0375	G8IV	-0.36	37	6.16	5.6[24]	12.9	7.75	b	1.37	0.074	0.13	2.755	6.051
											c	2.1	4.3	0.55	2.485	9.254
HD 162020	0.7	0.0205	0.0192	K2V	-0.46	31.26	9.18	6[25]	47.5	43.1	b	13.75	0.072	0.277	2.711	7.733
HD 160691	1.08	0.0381	0.0358	G3IV/V	-0.21	15.3	5.15	6[26]	8.73	6.42	d	0.044	0.09	-	3	3
											b	1.67	1.5	0.31	2.712	7.952
											c	3.1	4.17	0.57	2.428	9.421
HD 130322	0.79	0.0191	0.0180	K0V	-0.36	30	8.05	0.35[26]	28.3	25.6	b	1.08	0.088	0.048	2.876	4.345
HD 108147	1.27	0.0317	0.0298	F9V	-0.09	38.57	6.99	2.17[27]	5.37	4.13	b	0.4	0.104	0.498	2.596	8.899
HD 38529	1.39	0.0411	0.0386	G4IV	-0.28	42.43	5.94	-[5]	3.77	2.35	b	0.78	0.129	0.29	2.711	7.824
											c	12.7	3.68	0.36	2.708	8.222
HD 4308	0.83	0.0098	0.0092	G5V	-0.24	21.9	6.54	-[5]	22.0	23.4	b	0.047	0.114	0	3	3
Gl 86	0.79	0.0115	0.0108	K1V	-0.41	11	6.17	1[28]	25.4	25.2	b	4.01	0.11	0.046	2.880	4.295
HD 99492	0.78	0.0458	0.0431	K2V	-0.46	18	7.57	4[29]	32.1	19.0	b	0.122	0.119	0.05	2.871	4.396
HD 190360	0.96	.0356[30]	.0334[30]	G6IV	-0.30	15.89	5.71	6.7[30]	16	10.8	c	0.057	0.128	0.01	2.970	3.304
											b	1.502	3.92	0.36	2.708	8.222
HD 27894	0.75	0.0399	0.0375	K2V	-0.46	42.37	9.36	3.9[31]	52.2	40.3	b	0.62	0.122	0.049	2.873	4.371
HD 195019	1.02	-[2]		G3IV/V	-0.36	20	6.91	3.2[32]	11.6	10.5	b	3.43	0.14	0.05	2.871	4.396
HD 102117	0.95	0.0303	0.0285	G6V	-0.25	42	7.47	>10[33]	12.6	9.71	b	0.14	0.149	0	3	3
HD 6434	1.00	0.0060	0.057	G3IV	-0.21	40.32	7.72	3.7[34]	9.21	9.78	b	0.48	0.15	0.3	2.711	7.890
HD 192263	0.79	0.0126	0.0119	K2V	-0.46	19.9	7.79	1.1[35]	25.4	25.2	b	0.72	0.15	0	3	3
HD 11964	1.125	-[2]		G5	-0.29	33.98	6.42	7.5[7]	8.00	7.26	b	0.11	0.229	0.15	2.739	6.370
											c	0.7	3.167	0.3	2.711	7.890
rho CrB	*0.95*	*0.0129*	*0.0121*	*G0V*	*-0.18*	*16.7*	*5.4*	*10.0*[36]	*12.8*	*12.7*	*b*	*1.04*	*0.22*	*0.04*	*2.893*	*4.141*
HD 74156	1.05	0.0270	0.0254	G0	-0.18	64.56	7.62	7.5[7]	8.63	6.68	b	1.86	0.294	0.636	2.176	10.136
											c	6.17	3.4	0.583	2.387	9.541
HD 117618	1.05	0.0219	0.0206	G2V	-0.20	38	7.18	5.55[34]	11.6	10.5	b	0.19	0.28	0.39	2.700	8.364
HD 37605	0.8	0.0491	0.0461	K0V	-0.36	42.9	8.69	-[5]	32.1	19.0	b	2.3	0.25	0.677	1.963	10.736
HD 168443	1.01	0.0252	0.0237	G5	-0.24	33	6.92	7.8[37]	12.6	9.71	b	7.2	0.29	0.529	2.536	9.098
											c	17.1	2.87	0.228	2.712	7.322
HD 3651	0.79	0.0224	0.0211	K0V	-0.36	11	5.8	-[5]	28.3	25.6	b	0.2	0.284	0.63	2.204	10.059
HD 121504	1.00	0.0289	0.0272	G2V	-0.20	44.37	7.54	2.8[34]	12.6	9.71	b	0.89	0.32	0.13	2.755	6.051
HD 101930	0.74	0.0296	0.0278	K1V	-0.41	30.49	8.21	-[5]	52.2	40.3	b	0.3	0.302	0.11	2.775	5.697
HD 178911 B	0.87	0.0381	0.0358	G5	-0.24	46.73	7.98	13.1[7]	19.4	15.0	b	6.292	0.32	0.1243	2.760	5.954
HD 16141	1.00	0.0332	0.0312	G5IV	-0.29	35.9	6.78	6.7[34]	12.6	9.71	b	0.23	0.35	0.21	2.715	7.139
HD 114762	0.82	0.0063	0.0059	F9V	-0.17	28	7.30	5.0[38]	22.0	23.4	b	11.02	0.3	0	3	3
HD 80606	0.9	0.0538	0.0506	G5	-0.24	58.38	8.93	0.65[39]	19.9	12.0	b	3.41	0.439	0.927	-0.613	18.370

Star	Mass / $M_{\odot}$[1]	Metallicity mass fraction		Spectral Type	*BC*	*d*/Pc	m_v	Age / Gyr	MS time / Ga		Planet	Min. mass / M_{Jup}	*a* AU	*e*	Inner Hill Radius Multiplier (n_{int})	Outer Hill Radius Multiplier (n_{ext})
		1st Model	2nd Model						1st model	2nd model						
70 Vir	1.1	0.0187	0.0175	G4V	-0.22	22	5.00	EoMS[40]	8.00	7.26	b	7.44	0.48	0.4	2.695	8.410
HD 216770	0.9	0.0340	0.0319	K1V	-0.41	38	8.10	3.1[41]	19.4	15.0	b	0.65	0.46	0.37	2.706	8.271
HD 52265	*1.13*	*0.0258*	*0.0242*	*G0V*	*-0.18*	*28*	*6.30*	*3.5*[42]	*7.54*	*6.33*	*b*	*1.13*	*0.49*	*0.29*	*2.711*	*7.824*
HD 208487	0.95[33]	0.0174	0.0164	G2V	-0.20	45	7.48	8.1[33]	11.6	10.5	b	0.45	0.49	0.32	2.712	8.011
HD 34445	1.11	[2]		G0	-0.18	48	7.32	6.25[7]	8.00	7.26	b	0.58	0.51	0.4	2.695	8.410
GJ 3021	0.9	0.0317	0.0298	G6V	-0.24	17.62	6.59	<0.1[34]	19.4	15.0	b	3.32	0.49	0.505	2.584	8.941
HD 93083	0.7	0.0283	0.0266	K3V	-0.53	28.9	8.3	-[5]	52.2	40.3	b	0.37	0.477	0.14	2.747	6.214
HD 37124	0.91	0.0096	0.0090	G4V	-0.22	33	7.68	4.0[43]	13.7	14.9	b	0.61	0.53	0.055	2.861	4.519
											c	0.6	1.64	0.14	2.747	6.214
											d	0.66	3.19	0.2	2.717	7.028
HD 219449	1.7[44]	.0246[44]	.0231[44]	K0III	-0.50	45	4.21	EoMS[7]	<2[45]		b	2.9	0.3	0	3	3
HD 73526	1.02	0.0381	0.0358	G6V	-0.25	99	9.00	9.2[19]	11.4	7.98	b	3	0.66	0.34	2.711	8.121
HD 104985	1.5	0.0089	0.0084	G9III	-0.46	102	5.79	2.47[7]	2.20	2.33	b	6.3	0.78	0.03	2.917	3.874
HD 82943	1.05	0.0418	0.0393	b	1.63	1.16	0.41	2.690	8.456	7.98	c	0.88	0.73	0.54	2.510	9.177
											b	1.63	1.16	0.41	2.690	8.456
HD 169830	1.4	0.0324	0.0305	F8V	-0.17	36.32	5.90	2.6[7]	3.60	2.87	b	2.88	0.81	0.31	2.712	7.952
											c	4.04	3.6	0.33	2.711	8.067
HD 8574	1.15[46]	0.0163	0.0153	F8	-0.17	44.15	7.12	2.0[46]	5.71	5.2	b	2.23	0.76	0.4	2.695	8.410
HD 202206	1.15	0.0469	0.0441	G6V	-0.25	46.34	8.08	5.6[24]	8.84	5.66	b	17.4	0.83	0.435	2.673	8.571
											c	2.44	2.55	0.267	2.711	7.659
HD 89744	1.4	0.0303	0.0285	F7V	-0.16	40	5.74	2.04[47]	3.60	2.87	b	7.99	0.89	0.67	2.003	10.624
HD 134987	1.05	0.0340	0.0319	G5V	-0.24	25	6.45	5.8[34]	12.6	9.71	b	1.58	0.78	0.24	2.711	7.434
HD 12661	1.07	0.0393	0.0369	G6V	-0.25	37.16	7.44	8.4[34]	11.4	7.98	b	2.3	0.83	0.35	2.710	8.172
											c	1.57	2.56	0.2	2.717	7.028
HD 150706	1.06[48]	0.0148	0.0139	G0	-0.18	27.2	7.03	ZAMS[7]	7.26	7.22	b	1	0.82	0.38	2.703	8.318
HD 40979	1.08	0.0313	0.0294	F8V	-0.17	33.3	6.74	1.5[49]	8.63	6.68	b	3.32	0.811	0.23	2.712	7.342
HD 59686	1.7[44]	0.0258	0.0242	K2III	-0.60	92	5.45	EoMS[7]	<2[45]		b	5.25	0.911	0	3	3
HR 810	1.2[34]	0.0356	0.0334	G0V	-0.18	15.5	5.4	1.6[34]	6.15	4.99	b	1.94	0.91	0.24	2.711	7.434
HD 142	1.1	0.0219	0.0206	G1IV	-0.19	20.6	5.70	1.9[50]	8.00	7.26	b	1	0.98	0.38	2.703	8.318
HD 92788	1.06	0.0348	0.0327	G5	-0.24	32.82	7.31	6.4[34]	8.63	6.68	b	3.86	0.97	0.27	2.711	7.682
HD 28185	*0.99*	*0.0348*	*0.0327*	*G5*	*-0.24*	*39.4*	*7.81*	*2.9*[34]	*12.6*	*9.71*	*b*	*5.7*	*1.03*	*0.07*	*2.833*	*4.872*
HD 196885	1.27	[2]		F8IV	-0.17	33	6.39	2.18[7]	4.90	4.50	b	1.84	1.12	0.3	2.711	7.890
HD 142415	1.03	0.0324	0.0305	G1V	-0.19	34.2	7.34	1.1[41]	12.6	9.71	b	1.62	1.05	0.5	2.592	8.911
HD 177830	1.17	[2]		K0	-0.35	59	7.17	3.5[34]	5.71	5.20	b	1.28	1	0.43	2.677	8.547
HD 108874	1.00	0.0276	0.0260	G5	-0.24	68.5	8.76	7.0[21]	12.6	9.71	b	1.36	1.051	0.07	2.833	4.871
											c	1.018	2.68	0.25	2.711	7.522
HD 154857	1.17	0.0118	0.0111	G5V	-0.24	68.5	7.25	5.0[51]	5.21	5.29	b	1.8	1.11	0.51	2.575	8.972
HD 4203	1.06	0.0332	0.0312	G5	-0.24	77.5	8.68	8.7[34]	8.63	6.68	b	1.65	1.09	0.46	2.649	8.692
HD 128311	0.8	0.0240	0.0226	K0	-0.36	16.6	7.51	<2[21]	28.3	25.6	b	2.58	1.02	0.3	2.711	7.890
											c	3.21	1.76	0.17	2.728	6.655

Star	Mass / $M_{\odot}$[1]	Metallicity mass fraction		Spectral Type	*BC*	*d*/Pc	m_v	Age / Gyr	MS time / Ga		Planet	Min. mass / M_{Jup}	*a* / AU	*e*	Inner Hill Radius Multiplier (n_{int})	Outer Hill Radius Multiplier (n_{ext})
		1st Model	2nd Model						1st model	2nd model						
HD 27442	1.2	0.0317	0.0298	K2IV	-0.53	18.1	4.44	3.2[34]	6.15	4.99	b	1.28	1.18	0.07	2.833	4.872
HD 210277	0.99	0.0289	0.0272	G0	-0.18	22	6.63	6.9[34]	12.6	9.71	b	1.24	1.097	0.45	2.660	8.643
HD 19994	1.35	0.0340	0.0319	F8V	-0.17	22.38	5.07	2.4[41]	4.69	3.72	b	2	1.3	0.2	2.717	7.028
HD 188015	1.09	0.0390	0.0367	G5IV	-0.29	52.6	8.22	6.6[29]	8.63	6.68	b	1.26	1.19	0.15	2.739	6.370
HD 13189	4.5	-[2]		K2II	-0.60	185	7.57	EoMS[7]	<2[45]		b	14	1.85	0.28	2.711	7.755
HD 20367	1.04[47]	0.0252	0.0237	G0	-0.18	27	6.41	9.1[7]	11.6	10.5	b	1.07	1.25	0.23	2.712	7.342
HD 114783	0.92	0.0428	0.0402	K0	-0.36	22	7.57	4.8[34]	19.9	12	b	0.99	1.2	0.1	2.788	5.505
HD 147513	0.92	0.0187	0.0175	G3V	-0.21	12.9	5.37	0.3[41]	17.8	16.2	b	1	1.26	0.52	2.555	9.037
HIP 75458	1.05	0.0214	0.0201	K2III	-0.60	31.5	3.31	EoMS[7]	11.6	10.5	b	8.64	1.34	0.71	1.755	11.325
HD 222582	1.00	0.0195	0.0184	G5	-0.24	42	7.70	5.6[34]	11.6	10.5	b	5.11	1.35	0.76	1.373	12.422
HD 65216	0.92	0.0152	0.0143	G5V	-0.24	34.3	7.98	3.0[7]	13.2	12.8	b	1.21	1.37	0.41	2.690	8.456
HD 183263	1.17	0.0399	0.0375	G2IV	-0.20	53	7.86	8.1[29]	6.43	4.10	b	3.69	1.52	0.38	2.703	8.318
HD 141937	1.00	0.0289	0.0272	G2V	-0.20	33.46	7.25	1.6[34]	12.6	9.71	b	9.7	1.52	0.41	2.690	8.456
HD 41004 A	0.7	0.0246	0.0231	K1V	-0.41	42.5	8.65	1.6[52]	47.5	43.1	b	2.3	1.31	0.39	2.700	8.364
HD 11977	1.91	0.0123	0.0116	G8.5III	-0.44	66.5	4.7	1.25[53]	<2[45]		b	6.54	1.93	0.4	2.695	8.410
HD 47536	1.1	-[2]		K0II	-0.50	123	5.26	EoMS[7]	8.00	7.26	b	4.96	1.61	0.2	2.717	7.028
HD 23079	*1.1*	-[2]		*F9V*	*-0.17*	*34.8*	*7.1*	*3.1*[7]	*8.00*	*7.26*	*b*	*2.61*	*1.65*	*0.1*	*2.788*	*5.505*
16 Cyg B	1.01	0.0246	0.0231	G2.5V	-0.20	21.4	6.20	9.0[54]	11.6	10.5	b	1.69	1.67	0.67	2.003	10.624
HD 4208	0.93	0.0115	0.0108	G5V	-0.24	33.9	7.79	4.3[34]	16.1	15.9	b	0.8	1.67	0.05	2.871	4.396
HD 114386	0.75[48]	0.0187	0.0175	K3V	-0.53	28	8.73	8.3[7]	28.3	25.6	b	0.99	1.62	0.28	2.711	7.755
HD 45350	1.02	0.0390	0.0367	G5IV	-0.29	49	7.88	7.9[29]	11.4	7.98	b	0.98	1.77	0.78	1.195	12.938
γ Cephei A[55]	1.59	0.0303	0.0285	K0III	-0.60	11.8	3.22	EoMS[7]	<2[45]		b	1.59	2.03	0.2	2.717	7.028
HD 213240	1.22	0.0340	0.0319	G4IV	-0.28	40.75	6.80	2.7[34]	6.15	4.99	b	4.5	2.03	0.45	2.660	8.643
HD 10647	1.07	0.0214	0.0201	F8V	-0.17	17.3	5.52	4.6[56]	8.00	7.26	b	0.91	2.1	0.18	2.723	6.787
HD 10697	1.1	0.0283	0.0266	G5IV	-0.29	30	6.29	6.9[34]	8.63	6.68	b	6.12	2.13	0.11	2.775	5.697
											b	*2.54*	*2.09*	*0.061*	*2.849*	*4.663*
47 Uma	*1.03*	*0.0166*	*0.0156*	*G0V*	*-0.18*	*13.3*	*5.10*	*7.0*[38]	*9.93*	*9.42*	*c*	*0.76*	*3.73*	*0.1*	*2.788*	*5.505*
HD 190228	1.3	0.0115	0.0108	G5IV	-0.29	66.11	7.3	3.78[7]	3.93	3.91	b	4.99	2.31	0.43	2.677	8.548
HD 114729	0.93	0.0121	0.0113	G3V	-0.21	35	6.69	4.5[21]	16.1	15.9	b	0.82	2.08	0.31	2.712	7.952
HD 111232	0.78	0.0087	0.0082	G8V	-0.30	29	7.61	5.2[41]	22.0	23.4	b	6.8	1.97	0.2	2.717	7.028
HD 2039	0.98	0.0252	0.0237	G2V	-0.20	89.8	9.01	6.0[19]	11.6	10.5	b	4.85	2.19	0.68	1.946	10.786
HD 136118	1.24	0.0172	0.0162	F9V	-0.17	52.3	6.94	3.6[34]	4.90	4.50	b	11.9	2.3	0.37	2.706	8.271
HD 50554	1.1	0.0209	0.0197	F8	-0.17	31.03	6.86	4.5[34]	8.00	7.26	b	4.9	2.38	0.42	2.684	8.501
HD 196050	*1.1*	*.0399*[57]	*.0375*[57]	*G3V*	*-0.21*	*46.9*	*7.50*	*1.6*[41]	*8.00*	*7.26*	*b*	*3*	*2.5*	*0.28*	*2.711*	*7.755*
HD 216437	1.07	.0324[57]	.0305[57]	G4V	-0.22	26.5	6.06	5.8[41]	8.63	6.68	b	2.1	2.7	0.34	2.711	8.121
HD 216435	*1.25*	*0.0283*	*0.0266*	*G0V*	*-0.18*	*33.3*	*6.03*	*5.0*[58]	*5.27*	*4.44*	*b*	*1.49*	*2.7*	*0.34*	*2.711*	*8.121*
HD 106252	1.05	0.0138	0.0130	G0	-0.18	37.44	7.36	5.0[34]	9.93	9.42	b	6.81	2.61	0.54	2.510	9.177
HD 23596	1.3[59]	0.0418	0.0393	F8	-0.17	52	7.24	2.2[7]	4.88	3.09	b	7.19	2.72	0.314	2.712	7.976
14 Her	1.00	0.0448	0.0421	K0V	-0.36	18.1	6.67	7.1[34]	12.9	7.75	b	4.74	2.8	0.338	2.711	8.110
HD 142022 A	0.99	0.0310	0.0291	K0V	-0.36	35.87	7.70	7.7[7]	12.6	9.71	b	4.4	2.8	0.57	2.428	9.421

Star	Mass / $M_{\odot}$[1]	Metallicity mass fraction		Spectral Type	*BC*	*d*/Pc	m_v	Age / Gyr	MS time / Ga		Planet	Min. mass / M_{Jup}	*a* / AU	*e*	Inner Hill Radius Multiplier (n_{int})	Outer Hill Radius Multiplier (n_{ext})
		1st Model	2nd Model						1st model	2nd model						
HD 39091	1.1	0.0246	0.0231	G1IV	-0.19	20.55	5.67	5.5[7]	8.00	7.26	b	10.35	3.29	0.62	2.247	9.937
HD 70642	1.00	0.0289	0.0272	G5V	-0.24	29	7.18	4.0[60]	12.6	9.71	b	2	3.3	0.1	2.788	5.505
HD 33636	0.99	0.0148	0.0139	G0V	-0.18	28.7	7.06	2.8[34]	10.5	10.4	b	9.28	3.56	0.53	2.533	9.105
ε Eridani	*0.8*	*0.0159*	*0.0149*	*K2V*	*-0.46*	*3.2*	*3.73*	*0.7[34]*	*26.6*	*25.6*	*b*	*0.86*	*3.3*	*0.608*	*2.296*	*9.799*
HD 50499	1.27	.0399[43]	.0375[43]	G1V	-0.19	47.26	7.22	2.8[7]	5.37	4.13	b	1.71	3.86	0.23	2.712	7.342
HD 117207	1.04	0.0372	0.0350	G8V	-0.30	33	7.26	6.9[29]	11.4	7.98	b	2.06	3.78	0.16	2.733	6.516
HD 30177	0.95	0.0356	0.0334	G8V	-0.30	55	8.41	11.4[19]	19.4	15.0	b	9.17	3.86	0.3	2.711	7.890
HD 89307	1.27	-[2]		G0V	-0.18	33	7.06	ZAMS[7]	4.90	4.50	b	2.73	4.15	0.27	2.711	7.682
HD 72659	*0.95*	*0.0145*	*0.0136*	*G0V*	*-0.18*	*51.4*	*7.48*	*4.5[21]*	*13.2*	*12.8*	*b*	*2.96*	*4.16*	*0.2*	*2.717*	*7.028*

Italicised systems have been investigated using the Mercury Orbital Integrator.

1 All masses are taken from Schneider, 2006

2 For unknown stellar metallicities, the solar metallicity value is assumed. See figures 3.16 and 3.18 for nearest models

3 Light extinction due to interstellar dust is not taken into account, hence the lower magnitudes than expected for stars at these distances.

4 Sasselov, 2003

5 Stellar ages are left blank when there is no published data and either, when calculated HZ boundaries from stellar data are outside predicted ZAMS and EoMS distances, or when the determined age of the star from the matrix spreadsheet data is older than the age of the Universe (~13.7Ga).

6 Baraffe et al., 2005

7 Estimated age determined from HZs calculated from observed stellar parameters and matched with the two stellar models' spreadsheets.

8 Udry at el., 2003

9 Butler et al., 2004

10 Baliunas et al., 1997

11 Butler et al., 2002

12 Ryan, 2000

13 Konacki, 2005

14 Pepe et al., 2004

15 Estimated age determined from HZs calculated from observed stellar parameters and matched with only one of the stellar models' spreadsheets. The calculated HZ distances lie outside the ZAMS and EoMS boundaries of the other model.

16 Butler et al., 2000

17 Gonzalez and Laws, 2000

18 Cody and Sasselov, 2002

19 Tinney et al., 2003

20 Ford et al., 1999

21 Butler et al., 2003
22 Vogt et al., 2002
23 Bodenheimer et al., 2003
24 Udry et al., 2002
25 Butler et al., 2001
26 Udry et al., 2000
27 Pepe et al., 2002
28 Els et al., 2001
29 Marcy et al., 2005
30 Naef et al., 2003
31 Moutou et al., 2005
32 Fischer et al., 1999
33 Tinney et al., 2005
34 Laws et al., 2003
35 Henry et al., 2002
36 Trilling et al., 2000
37 Marcy et al., 1999
38 Henry et al., 1997
39 Wu and Murray, 2003
40 End of main sequence, Marcy and Butler, 1996
41 Mayor et al., 2004
42 Naef et al., 2001
43 Vogt et al., 2005
44 Sadakane et al., 2005
45 Age is entered as less than 2Gyr as the stellar mass is greater than $1.5M_{\odot}$, and is hence beyond the parameters of both stellar grids.
46 Reddy et al., 2002
47 Korzennik et al., 2000
48 Mass determined from giant planet's distance and orbital period.
49 Fischer et al., 2003
50 Valenti and Fischer, 2005
51 McCarthy et al., 2004
52 Santos et al., 2002
53 Setiawan et al., 2005
54 Laws and Gonzalez, 2001

[55] Mass, metallicity, and spectral type from Hatzes et al., 2003
[56] Decin et al., 2000
[57] Jones et al., 2002
[58] Jones et al., 2003
[59] Perrier et al., 2004
[60] Carter et al., 2003

Table 3.19 Habitable Zone boundary distances around each star at ZAMS, end of main sequence and now (where stellar age is known).

Star	Planet	Inner gravity reach / AU	Outer gravity reach / AU	First Stellar Grid Model (constant helium levels)						Second Stellar Grid Model (helium levels vary with metallicity						Derived from Observed Stellar Parameters	
				HZ ZAMS / AU		HZ EoMS / AU		HZ NOW / AU		HZ ZAMS / AU		HZ EoMS / AU		HZ NOW / AU		HZ NOW / AU	
				Inner	Outer	Inner	Outer	Inner	Outer	Inner	Outer	Inner	Outer	Inner	Outer	Inner	Outer
OGLE-TR-56	b	0.0174	0.0276	0.716	1.370	1.414	2.691	0.792	1.567	0.739	1.416	1.461	2.782	0.828	1.641	0.565	1.124
OGLE-TR-113	b	0.0172	0.0284	0.421	0.825	1.105	2.168	-	-	0.466	0.913	1.237	2.425	-	-	1.124	2.210
OGLE-TR-132	b	0.0246	0.0366	1.257	2.513	2.040	4.066	1.401	2.823	1.452	2.916	2.126	4.189	1.654	3.352	0.574	1.169
	d	*0.0190*	*0.0226*														
	c	*0.120*	*0.158*														
Gliese 876	*b*	*0.127*	*0.310*	*0.115*	*0.227*	*0.391*	*0.768*	*0.116*	*0.230*	*0.115*	*0.227*	*0.391*	*0.768*	*0.117*	*0.231*	*0.117*	*0.232*
HD 212301	b	0.0334	0.0386	0.716	1.370	1.414	2.691	1.093	2.170	0.739	1.416	1.461	2.782	1.258	2.497	1.128	2.250
HD 73256	b	0.0270	0.0500	0.722	1.425	1.311	2.575	0.751	1.483	0.802	1.312	1.451	2.305	0.856	1.700	0.787	1.549
GJ 436	b	0.0216	0.0372	0.119	0.234	0.398	0.782	0.122	0.241	0.119	0.236	0.467	0.917	0.123	0.243	0.162	0.321
	e	*0.0289*	*0.0507*														
	b	*0.0916*	*0.143*														
	c	*0.108*	*0.429*														
55 Cnc	d	*2.019*	*11.487*	*0.722*	*1.425*	*1.311*	*2.575*	*0.858*	*1.700*	*0.802*	*1.588*	*1.451*	*2.855*	*1.040*	*2.070*	*0.770*	*1.517*
HD 63454	b	0.0302	0.0418	0.421	0.649	1.105	1.705	0.487	0.995	0.466	0.913	1.237	2.425	0.559	1.097	0.518	1.016
HD 149026	b	0.0364	0.0476	1.099	2.189	1.805	3.587	1.323	2.649	1.267	2.537	1.946	3.833	1.633	3.269	1.456	2.896
HD 83443	b	0.0306	0.0544	0.411	0.806	1.054	2.068	0.455	0.891	0.500	0.982	1.301	2.552	0.580	1.142	0.920	1.808
HD 46375	b	0.0343	0.0499	0.662	1.304	1.240	2.441	0.767	1.515	0.738	1.459	1.372	2.698	0.886	1.758	0.858	1.685
TrES-1	-	0.0274	0.0592	0.566	1.113	1.417	2.779	0.613	1.205	0.589	1.159	1.475	2.893	0.639	1.258	0.644	1.265
HD 179949	b	0.0308	0.0531	1.001	1.994	1.767	3.509	1.264	2.533	1.031	2.058	1.775	3.490	1.326	2.656	1.163	2.322
HD 187123	b	0.0341	0.0520	0.826	1.635	1.457	2.880	0.996	1.982	0.891	1.769	1.566	3.085	1.140	2.277	1.129	2.231
OGLE-TR-10	b	0.0351	0.0481	0.969	1.926	1.660	3.292	1.215	2.428	1.044	2.08	1.741	3.424	1.376	2.753	0.867	1.712
Tau Boo	b	0.0346	0.0671	1.199	2.396	1.882	3.744	1.334	2.678	1.207	2.415	1.903	3.745	1.478	2.972	1.426	2.851
HD 188753A	b	0.0352	0.0540	0.854	1.695	1.548	3.063	1.162	2.319	0.881	1.750	1.597	3.140	1.267	2.530	1.369	2.690
HD 330075	b	0.0348	0.0512	0.566	1.113	1.417	2.779	0.670	1.320	0.589	1.159	1.475	2.893	0.706	1.393	0.568	1.123
HD 88133	b	0.0415	0.0525	0.950	1.886	1.590	3.153	-	-	1.094	2.184	1.769	3.483	1.647	3.244	1.647	3.244
HD 2638	b	0.0368	0.0512	0.544	1.067	1.312	2.573	0.586	1.158	0.601	1.182	1.452	2.849	-	-	0.586	1.158
BD-10 3166	b	0.0389	0.0531	0.809	1.599	1.397	2.760	-	-	0.934	1.856	1.600	3.149	-	-	<1.601	<3.166
HD 75289	b	0.0369	0.0589	0.722	1.425	1.311	2.575	0.780	1.542	0.802	1.588	1.451	2.855	0.900	1.790	1.224	2.434
HD 209458	b	0.0370	0.0530	0.716	1.414	1.369	2.691	0.895	1.695	0.739	1.461	1.416	2.782	0.904	1.794	1.092	2.172
HD 76700	b	0.0431	0.0548	0.716	1.414	1.369	2.691	1.264	2.505	0.739	1.461	1.416	2.782	2.943	5.776	1.210	2.388
OGLE-TR-111	b	0.0387	0.0553	0.421	0.825	1.105	2.168	-	-	0.466	0.913	1.237	2.425	-	-	0.652	1.
HD 149143	b	0.0411	0.0668	0.969	1.926	1.660	3.292	0.969	1.926	1.044	2.081	1.741	3.424	1.044	2.081	1.305	2.595
	b	*0.0486*	*0.0707*														
	c	*0.423*	*1.558*														
Ups And	*d*	*1.180*	*5.102*	*1.156*	*2.312*	*1.999*	*3.982*	*1.457*	*2.929*	*1.186*	*2.374*	*1.927*	*3.791*	*1.509*	*3.034*	*1.569*	*3.132*
51 Peg	b	0.0437	0.0603	0.716	1.414	1.369	2.691	0.924	1.829	0.739	1.461	1.416	2.782	1.100	2.187	0.948	1.880
HD 49674	b	0.0510	0.0623	0.662	1.304	1.240	2.441	0.767	1.515	0.738	1.459	1.372	2.698	0.887	1.762	0.823	1.626

Star	Planet	Inner gravity reach / AU	Outer gravity reach / AU	First Stellar Grid Model (constant helium levels)						Second Stellar Grid Model (helium levels vary with metallicity)						Derived from Observed Stellar Parameters	
				HZ ZAMS / AU		HZ EoMS / AU		HZ NOW / AU		HZ ZAMS / AU		HZ EoMS / AU		HZ NOW / AU		HZ NOW / AU	
				Inner	Outer	Inner	Outer	Inner	Outer	Inner	Outer	Inner	Outer	Inner	Outer	Inner	Outer
HD 109749	b	0.0550	0.0728	0.969	1.926	1.664	3.296	1.106	2.211	1.044	2.081	1.741	3.424	1.222	2.452	1.159	2.296
Gl 581	b	0.0363	0.0457	0.115	0.227	0.391	0.768	-	-	0.115	0.227	0.391	0.768	-	-	0.113	0.224
HD 118203	b	0.0336	0.106	-	-	-	-	-	-	-	-	-	-	-	-	2.243	4.400
HD 68988	b	0.0455	0.116	0.969	1.926	1.664	3.296	1.664	3.296	1.044	2.081	1.741	3.424	-	-	1.041	2.071
HD 168746	b	0.0519	0.0846	0.566	1.113	1.417	2.779	>0.607	>1.193	0.589	1.159	1.475	2.893	>0.632	>1.244	0.934	1.846
HD 217107	b	0.0488	0.118														
	c	0.995	10.167	0.663	1.306	1.235	2.426	0.780	1.560	0.783	1.551	1.427	2.807	1.078	2.047	2.024	3.977
HD 162020	b	0.0161	0.195	0.331	0.649	0.990	1.941	0.355	0.697	0.343	0.674	1.036	2.032	0.372	0.729	0.455	0.892
HD 160691	d	0.0837	0.0963														
	b	0.714	2.907														
	c	0.811	10.358	0.821	1.625	1.439	2.844	1.098	2.185	0.898	1.784	1.572	3.091	1.516	3.015	1.169	2.316
HD 130322	b	0.0646	0.121	0.439	0.861	1.199	2.352	0.453	0.889	0.457	0.896	1.257	2.466	0.472	0.926	0.689	1.353
HD 108147	b	0.0397	0.199	1.044	2.079	1.759	3.494	1.235	2.475	1.141	2.279	1.828	3.597	1.393	2.796	1.021	2.080
HD 38529	b	0.0719	0.223														
	c	0.933	9.323	1.257	2.513	2.040	4.066	-	-	1.452	2.916	2.126	4.189	-	-	2.413	4.757
HD 4308	b	0.105	0.123	0.489	0.960	1.464	2.872	-	-	0.478	0.939	1.442	2.829	-	-	0.908	1.794
Gl 86	b	0.06778	0.170	0.461	0.904	1.311	2.571	0.483	0.948	0.463	0.908	1.325	2.599	0.486	0.953	0.618	1.214
HD 190360	c	0.117	0.141														
	b	1.668	7.886	0.603	1.186	1.383	2.713	0.727	1.433	0.682	1.346	1.280	2.525	0.888	1.762	1.027	2.022
HD 99492	b	0.100	0.144	0.411	0.806	1.054	2.068	0.441	0.864	0.500	0.982	1.301	2.552	0.550	1.082	0.549	1.078
HD 27894	b	0.0936	0.162	0.316	0.622	0.909	1.784	0.331	0.650	0.348	0.683	1.018	1.996	0.370	0.725	0.567	1.113
HD 195019	b	0.0919	0.210	0.716	1.414	1.369	2.691	0.797	1.577	0.739	1.461	1.416	2.782	0.833	1.653	0.773	1.520
HD 102117	b	0.133	0.165	0.679	1.339	1.289	2.531	0.999	1.979	0.747	1.478	1.393	2.738	1.666	3.269	1.154	2.277
HD 6434	b	0.0833	0.258	0.782	1.553	1.595	3.138	0.920	1.834	0.769	1.526	1.576	3.100	0.896	1.785	0.944	1.869
HD 192263	b	0.120	0.180	0.461	0.904	1.311	2.571	0.484	0.949	0.463	0.908	1.325	2.599	0.486	0.955	0.549	1.077
HD 11964	b	0.175	0.309														
	c	1.716	5.573	0.854	1.695	1.548	3.063	1.463	2.909	0.881	1.750	1.597	3.140	2.230	4.377	1.562	3077
rho CrB	*b*	*0.166*	*0.293*	*0.665*	*1.313*	*1.334*	*2.631*	*0.995*	*1.976*	*0.667*	*1.317*	*1.374*	*2.700*	*1.003*	*1.991*	*1.094*	*2.175*
HD 74156	b	0.0542	0.727														
	c	0.418	9.378	0.826	1.635	1.457	2.880	1.280	2.545	0.891	1.769	1.569	3.085	-	-	1.521	3.025
HD 117618	b	0.142	0.480	0.716	1.414	1.369	2.691	0.867	1.719	0.739	1.461	1.416	2.782	0.918	1.824	1.125	2.232
HD 37605	b	0.0331	0.680	0.411	0.806	1.054	2.068	-	-	0.500	0.982	1.301	2.552	-	-	0.733	1.441
HD 168443	b	0.0400	0.790														
	c	0.851	7.208	0.679	1.339	1.289	2.531	0.896	1.774	0.747	1.478	1.393	2.738	1.010	2.185	1.149	2.270
HD 3651	b	0.078	0.586	0.439	0.861	1.199	2.352	-	-	0.457	0.896	1.257	2.466	-	-	0.712	1.398
HD 121504	b	0.221	0.489	0.679	1.339	1.289	2.531	0.753	1.487	0.747	1.478	1.393	2.738	0.840	1.667	1.113	2.208
HD 101930	b	0.226	0.422	0.316	0.622	0.909	1.784	-	-	0.348	0.683	1.018	1.996	-	-	0.670	1.315
HD 178911 B	b	0.164	0.611	0.544	1.067	1.312	2.573	-	-	0.601	1.182	1.452	2.849	0.999	1.973	0.999	1.973
HD 16141	b	0.237	0.528	0.679	1.339	1.289	2.531	0.856	1.695	0.747	1.478	1.393	2.738	1.008	2.004	1.398	2.755
HD 114762	b	0.154	0.446	0.489	0.960	1.464	2.872	0.553	1.087	0.478	0.939	1.442	2.829	0.540	1.061	0.744	1.484

Star	Planet	Inner gravity reach / AU	Outer gravity reach / AU	First Stellar Grid Model (constant helium levels)						Second Stellar Grid Model (helium levels vary with metallicity)						Derived from Observed Stellar Parameters	
				HZ ZAMS / AU		HZ EoMS / AU		HZ NOW / AU		HZ ZAMS / AU		HZ EoMS / AU		HZ NOW / AU		HZ NOW / AU	
				Inner	Outer	Inner	Outer	Inner	Outer	Inner	Outer	Inner	Outer	Inner	Outer	Inner	Outer
HD 80606	b	0.0607	1.704	0.532	1.044	1.133	2.221	0.552	1.083	0.635	1.253	1.541	3.024	0.667	1.317	0.806	1.591
70 Vir	b	0.121	1.193	0.854	1.695	1.548	3.063	1.548	3.044	0.881	1.750	1.597	3.140	1.596	3.139	1.827	3.614
HD 216770	b	0.214	0.863	0.544	1.067	1.312	2.573	0.592	1.164	0.601	1.182	1.452	2.849	0.661	1.303	0.878	1.724
HD 52265	*b*	*0.258*	*0.894*	*0.880*	*1.746*	*1.557*	*3.082*	*1.065*	*2.125*	*0.927*	*1.844*	*1.628*	*3.201*	*1.164*	*2.328*	*1.211*	*2.409*
HD 208487	b	0.262	0.856	0.716	1.414	1.369	2.691	0.977	1.940	0.739	1.461	1.416	2.782	1.064	2.115	1.161	2.302
HD 34445	b	0.230	0.950	0.854	1.695	1.548	3.063	1.234	2.462	0.881	1.750	1.597	3.140	1.377	2.748	1.298	2.582
GJ 3021	b	0.109	1.200	0.544	1.067	1.312	2.573	0.556	1.092	0.601	1.182	1.452	2.849	0.613	1.206	0.714	1.411
HD 93083	b	0.338	0.707	0.316	0.622	0.909	1.784	-	-	0.348	0.683	1.018	1.996	-	-	0.655	1.285
HD 37124	b	0.410	0.702	0.627	1.237	1.358	2.675	0.715	1.414	0.613	1.209	1.688	3.312	0.698	1.380	0.798	1.578
	c	1.143	2.475														
	d	2.020	5.203														
HD 219449	b	0.215	0.385	-	-	-	-	-	-	-	-	-	-	-	-	6.679	13.098
HD 73526	b	0.261	1.409	0.722	1.425	1.296	2.554	0.957	1.895	0.802	1.588	1.451	2.855	-	-	1.344	2.653
HD 104985	b	0.506	1.136	1.612	3.273	2.873	5.769	-	-	1.586	3.218	2.568	5.059	4.045	7.950	7.105	13.938
HD 82943	c	0.218	1.555	0.722	1.425	1.296	2.554	0.849	1.681	0.802	1.588	1.451	2.855	1.020	2.030	1.064	2.116
	b	0.438	2.411														
HD 169830	b	0.368	1.620	1.292	2.588	2.122	4.233	1.637	3.282	1.381	2.773	2.072	4.079	2.189	4.401	1.839	3.669
	c	1.463	7.611														
HD 8574	b	0.282	1.608	1.001	1.994	1.767	3.509	1.166	2.338	1.031	2.058	1.775	3.490	1.219	2.447	1.274	2.543
HD 202206	b	0.0943	2.392	0.809	1.599	1.397	2.760	1.045	2.075	0.934	1.856	1.600	3.149	1.619	3.199	0.961	1.897
	c	1.263	4.944														
HD 89744	b	0.0762	2.640	1.292	2.588	2.122	4.233	1.577	3.173	1.381	2.773	2.072	4.079	1.758	3.537	2.148	4.295
HD 134987	b	0.427	1.421	0.679	1.339	1.289	2.531	0.828	1.638	0.747	1.478	1.393	2.738	0.958	1.904	1.081	2.135
HD 12661	b	0.341	1.718	0.722	1.425	1.296	2.554	0.999	1.981	0.802	1.588	1.451	2.855	3.142	6.167	1.035	2.042
	c	1.508	4.468														
HD 150706	b	0.360	1.588	0.887	1.765	1.654	3.278	0.887	1.765	0.891	1.773	1.670	3.284	0.891	1.773	0.841	1.672
HD 40979	b	0.406	1.589	0.826	1.635	1.457	2.880	0.896	1.780	0.891	1.769	1.569	3.085	0.992	1.980	1.145	2.285
HD 59686	b	0.639	1.183	-	-	-	-	-	-	-	-	-	-	-	-	8.197	16.076
HR 810	b	0.494	1.670	0.969	1.926	1.660	3.292	1.094	2.187	1.044	2.081	1.741	3.424	1.207	2.423	1.015	2.019
HD 142	b	0.432	1.891	0.854	1.695	1.548	3.063	0.948	1.888	0.881	1.750	1.597	3.140	0.989	1.973	1.190	2.364
HD 92788	b	0.432	2.014	0.826	1.635	1.457	2.880	1.147	2.283	0.891	1.769	1.569	3.085	1.554	3.085	0.955	1.886
HD 28185	*b*	*0.601*	*1.716*	*0.679*	*1.339*	*1.289*	*2.531*	*0.755*	*1.491*	*0.747*	*1.478*	*1.393*	*2.738*	*0.844*	*1.674*	*0.911*	*1.799*
HD 196885	b	0.549	2.139	1.084	2.166	1.893	3.765	1.307	2.626	1.118	2.235	1.865	3.669	1.363	2.741	1.333	2.660
HD 142415	b	0.309	2.318	0.679	1.339	1.289	2.531	0.718	1.417	0.747	1.478	1.393	2.738	0.792	1.569	0.929	1.844
HD 177830	b	0.382	2.031	1.001	1.994	1.767	3.509	1.279	2.562	1.031	2.058	1.775	3.490	1.352	2.709	2.031	3.991
HD 108874	b	0.752	1.512	0.679	1.339	1.289	2.531	0.867	1.715	0.747	1.478	1.393	2.738	1.030	2.047	1.022	2.019
	c	1.511	4.734														
HD 154857	b	0.319	2.461	1.038	2.074	1.889	3.756	1.855	3.699	1.043	2.084	1.866	3.671	1.840	3.674	2.049	4.048
HD 4203	b	0.360	2.341	0.826	1.635	1.457	2.880	1.457	2.880	0.891	1.769	1.569	3.085	1.569	3.085	1.200	2.370
HD 27442	b	0.864	1.664	0.969	1.926	1.660	3.292	1.193	2.384	1.044	2.081	1.741	3.424	1.324	2.650	2.451	4.809

Star	Planet	Inner gravity reach / AU	Outer gravity reach / AU	First Stellar Grid Model (constant helium levels)						Second Stellar Grid Model (helium levels vary with metallicity)						Derived from Observed Stellar Parameters	
				HZ ZAMS / AU		HZ EoMS / AU		HZ NOW / AU		HZ ZAMS / AU		HZ EoMS / AU		HZ NOW / AU		HZ NOW / AU	
				Inner	Outer	Inner	Outer	Inner	Outer	Inner	Outer	Inner	Outer	Inner	Outer	Inner	Outer
	b	0.435	2.138														
HD 128311	c	0.940	3.330	0.439	0.861	1.199	2.352	<0.465	<0.911	0.457	0.896	1.257	2.466	<0.485	<0.951	0.489	0.960
HD 210277	b	0.389	2.288	0.679	1.339	1.289	2.531	0.863	1.708	0.747	1.478	1.393	2.738	1.022	2.032	0.818	1.626
HD 19994	b	0.765	2.271	1.199	2.400	1.882	3.744	1.365	2.738	1.207	2.415	1.903	3.745	1.519	3.051	1.660	3.313
HD 188015	b	0.777	1.913	0.826	1.635	1.457	2.880	1.283	2.558	0.891	1.769	1.569	3.085	1.459	2.907	1.006	1.988
HD 13189	b	0.832	3.798	-	-	-	-	-	-	-	-	-	-	-	-	6.210	12.178
HD 20367	b	0.727	2.174	0.716	1.414	1.369	2.691	1.041	2.067	0.739	1.461	1.416	2.782	1.167	2.320	1.110	2.209
HD 114783	b	0.846	1.782	0.532	1.044	1.133	2.221	0.597	1.172	0.635	1.253	1.541	3.024	0.756	1.495	0.630	1.238
HD 147513	b	0.379	2.714	0.566	1.113	1.417	2.779	0.585	1.149	0.589	1.159	1.475	2.893	0.607	1.195	0.891	1.765
HIP 75458	b	0.0644	4.383	0.716	1.414	1.369	2.691	-	-	0.739	1.461	1.416	2.782	-	-	7.520	14.747
HD 222582	b	0.106	4.348	0.716	1.414	1.369	2.691	0.869	1.723	0.739	1.461	1.416	2.782	0.921	1.829	1.021	2.017
HD 65216	b	0.533	2.798	0.657	1.296	1.310	2.582	0.730	1.442	0.664	1.310	1.356	2.665	0.739	1.460	0.733	1.448
HD 183263	b	0.531	3.363	0.950	1.886	1.590	3.152	--	-	1.094	2.184	1.769	3.483	-	-	1.147	2.276
HD 141937	b	0.301	4.014	0.679	1.339	1.289	2.531	0.728	1.437	0.747	1.478	1.393	2.738	0.806	1.597	0.959	1.903
HD 41004 A	b	0.440	2.933	0.331	0.649	0.990	1.941	0.342	0.671	0.343	0.674	1.036	2.032	0.357	0.700	0.762	1.497
HD 11977	b	0.623	4.372	-	-	-	-	-	-	-	-	-	-	-	-	7.548	14.810
HD 47536	b	0.795	3.208	0.854	1.695	1.548	3.063	-	-	0.881	1.750	1.597	3.140	-	-	11.256	22.074
HD 23079	*b*	*1.066*	*2.642*	*0.854*	*1.695*	*1.548*	*3.063*	*1.002*	*1.997*	*0.876*	*1.740*	*1.582*	*3.111*	*1.052*	*2.102*	*1.028*	*2.048*
16 Cyg B	b	0.280	4.227	0.716	1.414	1.369	2.691	1.034	2.052	0.739	1.461	1.416	2.782	1.155	2.295	1.002	1.985
HD 4208	b	1.275	2.230	0.592	1.166	1.537	3.014	0.674	1.329	0.595	1.172	1.554	3.049	0.678	1.337	0.791	1.562
HD 114386	b	0.838	3.014	0.439	0.861	1.199	2.352	0.508	0.997	0.457	0.896	1.257	2.466	0.535	1.051	0.521	1.021
HD 45350	b	0.247	4.693	0.722	1.425	1.296	2.554	0.970	1.924	0.802	1.588	1.451	2.855	1.447	2.854	1.150	2.265
Gamma Cephei	b	1.247	3.410	-	-	-	-	-	-	-	-	-	-	-	-	2.936	5.758
HD 213240	b	0.547	4.794	0.969	1.926	1.660	3.292	1.161	2.320	1.044	2.081	1.741	3.424	1.288	2.581	1.477	2.922
HD 10647	b	1.353	3.397	0.854	1.695	1.548	3.063	1.087	2.169	0.876	1.740	1.582	3.111	1.154	2.306	1.043	2.082
HD 10697	b	1.181	3.832	0.826	1.635	1.457	2.880	1.200	2.387	0.891	1.769	1.569	3.085	2.147	4.216	1.464	2.885
	b	*1.413*	*3.116*														
47 Uma	*c*	*2.716*	*5.370*	*0.769*	*1.523*	*1.461*	*2.872*	*1.055*	*2.099*	*0.783*	*1.551*	*1.491*	*2.931*	*1.106*	*2.202*	*1.000*	*1.989*
HD 190228	b	0.656	5.414	1.198	2.404	2.135	4.258	2.028	3.991	1.204	2.416	2.039	4.011	2.027	4.070	2.027	3.992
HD 114729	b	1.066	3.808	0.592	1.166	1.537	3.014	0.677	1.335	0.595	1.172	1.554	3.049	0.681	1.344	1.316	2.607
HD 111232	b	0.824	4.310	0.489	0.960	1.464	2.872	0.555	1.092	0.478	0.939	1.442	2.829	0.542	1.065	0.776	1.528
HD 2039	b	0.205	6.427	0.716	1.414	1.369	2.691	0.883	1.752	0.739	1.461	1.416	2.782	0.939	1.866	1.145	2.270
HD 136118	b	0.546	5.911	1.084	2.166	1.893	3.765	1.521	3.055	1.118	2.235	1.865	3.669	1.650	3.315	1.663	3.313
HD 50554	b	0.663	5.652	0.854	1.695	1.548	3.063	1.153	2.300	0.876	1.740	1.582	3.111	1.253	2.502	1.010	2.015
HD 196050	*b*	*1.154*	*5.049*	*0.854*	*1.695*	*1.548*	*3.063*	*0.936*	*1.863*	*0.876*	*1.740*	*1.582*	*3.111*	*0.975*	*1.945*	*1.215*	*2.406*
HD 216437	b	1.156	5.492	0.826	1.635	1.457	2.880	1.096	2.181	0.891	1.769	1.569	3.085	1.392	2.775	1.351	2.672
HD 216435	*b*	*1.252*	*5.206*	*1.051*	*2.094*	*1.723*	*3.388*	*1.765*	*3.515*	*1.118*	*2.232*	*1.824*	*3.589*	-	-	*1.631*	*3.245*
HD 106252	b	0.367	7.069	0.769	1.523	1.461	2.872	0.945	1.880	0.783	1.551	1.491	2.931	0.977	1.945	0.994	1.977
HD 23596	b	0.975	6.193	1.099	2.189	1.805	3.587	1.311	2.626	1.267	2.537	1.946	3.833	1.602	3.212	1.420	2.834
14 Her	b	0.983	6.351	0.663	1.306	1.235	2.426	0.842	1.666	0.783	1.551	1.427	2.807	1.295	2.573	0.784	1.541

Star	Planet	Inner gravity reach / AU	Outer gravity reach / AU	First Stellar Grid Model (constant helium levels)						Second Stellar Grid Model (helium levels vary with metallicity)						Derived from Observed Stellar Parameters	
				HZ ZAMS / AU		HZ EoMS / AU		HZ NOW / AU		HZ ZAMS / AU		HZ EoMS / AU		HZ NOW / AU		HZ NOW / AU	
				Inner	Outer	Inner	Outer	Inner	Outer	Inner	Outer	Inner	Outer	Inner	Outer	Inner	Outer
HD 142022 A	b	0.441	7.357	0.679	1.339	1.289	2.531	0.892	1.766	0.891	1.769	1.569	3.085	1.090	2.166	0.967	1.901
HD 39091	b	0.185	10.042	0.854	1.695	1.548	3.063	1.153	2.230	0.881	1.750	1.597	3.140	1.253	2.502	1.204	2.391
HD 70642	b	2.179	5.193	0.679	1.339	1.289	2.531	0.780	1.542	0.891	1.769	1.569	3.085	0.881	1.750	0.896	1.770
HD 33636	b	0.375	10.112	0.745	1.475	1.465	2.879	0.828	1.643	0.748	1.482	1.479	2.907	0.833	1.654	0.875	1.740
Epsilon Eridani	*b*	*0.764*	*7.568*	*0.450*	*0.883*	*1.101*	*2.159*	*0.469*	*0.919*	*0.458*	*0.899*	*1.292*	*2.534*	*0.478*	*0.937*	*0.572*	*1.123*
HD 50499	b	2.183	6.884	1.044	2.079	1.759	3.494	1.277	2.566	1.141	2.279	1.828	3.597	1.449	2.903	1.356	2.693
HD 117207	b	2.347	6.361	0.722	1.425	1.296	2.554	0.926	1.835	0.802	1.588	1.451	2.855	1.247	2.482	1.038	2.043
HD 30177	b	1.321	9.036	0.544	1.067	1.312	2.573	0.789	1.555	0.601	1.181	1.452	2.849	0.885	1.750	1.018	2.005
HD 89307	b	2.038	8.079	1.084	2.166	1.893	3.765	1.084	2.166	1.118	2.235	1.865	3.669	1.118	2.235	1.006	2.001
HD 72659	*b*	*2.201*	*7.907*	*0.657*	*1.296*	*1.310*	*2.582*	*0.762*	*1.508*	*0.664*	*1.310*	*1.356*	*2.665*	*0.773*	*1.530*	*1.292*	*2.569*

Table 3.20 Potential Habitability of the Known Exoplanetary Systems

Star	First Stellar Grid Habitability		Second Stellar Grid Habitability		Stellar Parameters Habitability
	Now	At some time	Now	At some time	Now
OGLE-TR-56	Yes	Yes	Yes	Yes	Yes
OGLE-TR-113	Yes	Yes	Yes	Yes	Yes
OGLE-TR-132	No	Yes	No	Yes	No
Gliese 87	***No***	***Yes***	***No***	***Yes***	***No***
HD 212301	Yes	Yes	Yes	Yes	Yes
HD 73256	No	Yes	No	Yes	No
GJ 436	Yes	Yes	Yes	Yes	Yes
55 Cnc	***Yes***	***Yes***	***Yes***	***Yes***	***Yes***
HD 63454	Yes	Yes	Yes	Yes	Yes
HD 149026	Yes	Yes	Yes	Yes	Yes
HD 83443	Yes	Yes	Yes	Yes	Yes
HD 46375	Yes	Yes	Yes	Yes	Yes
TrES-1	Yes	Yes	Yes	Yes	Yes
HD 179949	Yes	Yes	Yes	Yes	Yes
HD 187123	Yes	Yes	Yes	Yes	Yes
OGLE-TR-10	Yes	Yes	Yes	Yes	Yes
Tau Boo	Yes	Yes	Yes	Yes	Yes
HD 188753 A	Yes	Yes	Yes	Yes	Yes
HD 330075	Yes	Yes	Yes	Yes	Yes
HD 88133	Yes	Yes	Yes	Yes	Yes
HD 2638	Yes	Yes	Yes	Yes	Yes
BD-10 3166	Yes	Yes	Yes	Yes	Yes
HD 75289	Yes	Yes	Yes	Yes	Yes
HD 209458	Yes	Yes	Yes	Yes	Yes
HD 76700	Yes	Yes	No	Yes	Yes
OGLE-TR-111	Yes	Yes	Yes	Yes	Yes
HD 149143	No	Yes	No	Yes	No
51 Peg	Yes	Yes	Yes	Yes	Yes
Ups And	***No***	***No***	***No***	***No***	***No***
HD 49674	Yes	Yes	Yes	Yes	Yes
HD 109749	No	Yes	No	Yes	No
Gl 581	No	Yes	No	Yes	No
HD 118203	No	No	No	No	No
HD 68988	Yes	Yes	Yes	Yes	Yes
HD 168746	Yes	Yes	Yes	Yes	Yes
HD 217107	**3I**	**4I**	**No**	**1I**	**No**
HD 162020	Yes	Yes	Yes	Yes	Yes
HD 160691	**No**	**No**	**No**	**No**	**No**
HD 130322	No	Yes	No	Yes	No
HD 108147	Yes	Yes	Yes	Yes	Yes
HD 38529	**No**	**No**	**No**	**No**	**No**
HD 4308	Yes	Yes	Yes	Yes	Yes
Gl 86	No	Yes	No	Yes	No
HD 99492	Yes	Yes	Yes	Yes	Yes
HD 190360	**Yes**	**Yes**	**9I**	**Yes**	**6I**
HD 27894	Yes	Yes	Yes	Yes	Yes
HD 195019	Yes	Yes	Yes	Yes	Yes
HD 102117	Yes	Yes	Yes	Yes	Yes
HD 6434	Yes	Yes	Yes	Yes	Yes
HD 192263	No	Yes	No	Yes	No
HD 11964	**2I**	**8I**	**No**	**7I**	**1I**
rho CrB	*Yes*	*Yes*	*Yes*	*Yes*	*Yes*
HD 74156	**No**	**No**	**No**	**No**	**No**
HD 117618	Yes	Yes	Yes	Yes	Yes
HD 37605	<6O	Yes	Yes	Yes	Yes

Star	First Stellar Grid Habitability		Second Stellar Grid Habitability		Stellar Parameters Habitability
	Now	At some time	Now	At some time	Now
HD 168443	**No**	**1B**	**No**	**No**	**No**
HD 3651	<9O	Yes	Yes	Yes	Yes
HD 121504	Yes	Yes	Yes	Yes	Yes
HD 101930	<8O	Yes	Yes	Yes	Yes
HD 178911 B	Yes	Yes	Yes	Yes	Yes
HD 16141	Yes	Yes	Yes	Yes	Yes
HD 114762	Yes	Yes	Yes	Yes	Yes
HD 80606	No	3O	No	5O	No
70 Vir	Yes	Yes	Yes	Yes	Yes
HD 216770	5O	Yes	7O	Yes	Yes
HD 52265	*Yes*	*Yes*	*Yes*	*Yes*	*Yes*
HD 208487	Yes	Yes	Yes	Yes	Yes
HD 34445	Yes	Yes	Yes	Yes	Yes
GJ 3021	No	8O	No	9O	No
HD 93083	No	Moon & Yes	2O	Moon & Yes	9O
HD 37124	**6B**	**7B & Moon (c)**	**6B**	**7B & Moon (c)**	**4B**
HD 219449	No	No	No	No	No
HD 73526	4O	8O	9O	9O	Yes
HD 104985	No	Yes	No	Yes	No
HD 82943	**No**	**No**	**No**	**1O**	**No**
HD 169830	**No**	**No**	**No**	**No**	**No**
HD 8574	4O	9O	4O	9O	4O
HD 202206	**No**	**No**	**No**	**No**	**No**
HD 89744	No	4O	1O	5O	4O
HD 134987	2O	8O	4O	8O	6O
HD 12661	**No**	**No**	**No**	**No**	**No**
HD 150706	No	Yes	No	Yes	No
HD 40979	No	8O	No	8O	No
HD 59686	No	No	No	No	No
HR 810	No	8O	No	9O	No
HD 142	No	6O	No	6O	No
HD 92788	1O	4O	5O	5O	No
HD 28185	*Moon*	*Moon & 5O*	*Moon*	*Moon & 6O*	*Moon*
HD 196885	2O	7O	3O	7O	3O
HD 142415	No	No	No	1O	No
HD 177830	3O	6O	4O	7O	6O
HD 108874	**Moon (b)**	**Moon (b)**	**No**	**Moon (b)**	**No**
HD 154857	4O	4O	4O	4O	4O
HD 4203	2O	2O	3O	3O	No
HD 128311	**No**	**No**	**No**	**No**	**No**
HD 27442	5O	9O	7O	9O	9O
HD 210277	No	No	No	1O	No
HD 19994	2O	6O	4O	5O	4O
HD 188015	4O	Moon & 6O	5O	Moon & 5O	Moon
HD 13189	No	No	No	No	No
HD 20367	No	Moon & 2O	No	Moon & 2O	No
HD 114783	4I	5I, Moon & 2O	1I & Moon	2I, Moon & 4O	4I
HD 147513	No	No	No	No	No
HIP 75458	No	No	No	No	No
HD 222582	No	No	No	No	No
HD 65216	No	No	No	No	No
HD 183263	No	No	No	No	No
HD 141937	No	No	No	No	No
HD 41004 A	No	2I	No	2I	No
HD 11977	No	No	No	No	No
HD 47536	No	Moon	No	Moon	No
HD 23079	*Moon*	*1I & Moon*	*Moon*	*1I & Moon*	*Moon*

Star	First Stellar Grid Habitability		Second Stellar Grid Habitability		Stellar Parameters Habitability
	Now	At some time	Now	At some time	Now
16 Cyg B	No	No	No	No	No
HD 4208	9I	Yes & Moon	9I	Yes & Moon	6I
HD 114386	7I	8I	6I	8I	6I
HD 45350	No	No	No	No	No
Gamma Cephei	No	No	No	No	No
HD 213240	No	No	No	No	No
HD 10647	2I	4I & Moon	2I	4I & Moon	2I
HD 10697	Moon	3I & Moon	No	2I & Moon	Moon
47 UMa	***No***	***Moon (b)***	***No***	***Moon (b)***	***No***
HD 190228	No	No	No	No	No
HD 114729	6I	7I	6I	7I	No
HD 111232	5I	6I	5I	6I	1I
HD 2039	No	No	No	No	No
HD 136118	No	No	No	No	No
HD 50554	No	No	No	No	No
HD 196050	*No*	*2I*	*No*	*2I*	*No*
HD 216437	1I	3I	No	1I	No
HD 216435	*No*	*No*	*No*	*No*	*No*
HD 106252	No	No	No	No	No
HD 23596	No	No	No	No	No
14 Her	2I	4I	No	1I	3I
HD 142022 A	No	No	No	No	No
HD 39091	No	No	No	No	No
HD 70642	Yes	Yes	Yes	Yes	Yes
HD 33636	No	No	No	No	No
Epsilon Eridani	*No*	*6I*	*No*	*6I*	*No*
HD 50499	7I	8I	5I	6I	6I
HD 117207	Yes	Yes	9I	Yes	Yes
HD 30177	5I	Yes	5I	Yes	3I
HD 89307	No	6I	No	5I	No
HD 72659	*Yes*	*Yes*	*Yes*	*Yes*	*7I*

Qualification Footnotes:

Yes	The entire habitable zone may house a habitable Earth-like planet.
No	No part of the habitable zone may house a habitable Earth-like planet.
Moon	A habitable moon may exist around a giant within the habitable zone.
*x*I or *x*O	10*x*% of the habitable zone may house a habitable Earth-like planet **inside** (I) or **outside** (O) the giant planet's orbit (to the nearest 10%).
*x*B	10*x*% of the habitable zone may house a habitable Earth-like planet **between** the orbits of two giant planets (to the nearest 10%).

Bold systems have multiple planets; *italicised systems* have been studied in detail, with the orbital integrator.

Some of the stellar ages in Table 3.18 are subject to discussion and do not match the predictions of both stellar grids used here. The priority was given, however to the literature values. There appears to be no indication that one stellar grid is more "correct" than the other. Generally there is good agreement between the two, with the first grid (constant helium mass fraction) giving longer main sequence lifetimes for higher metallicity stars of the same mass. Consequently the second grid, with varying helium mass fractions, gives longer main sequence lifetimes for stars with lower metallicity.

Present day habitable zone boundaries in Table 3.19, calculated from stellar parameters, are for the most part in good agreement with those determined from both stellar grid models. However, it must be remembered that HZ boundaries are a rather imprecise concept and very much open to differing definitions and interpretation. Hence the uncertain nature of habitable zones and stellar ages must be born in mind where conflicts do occur.

Table 3.21 Assessment for the potential for habitable Earth-mass planets in new or revised exoplanetary systems discovered between 31/8/2005 and 14/6/2006.[1]

Star name	M_{star}/M_{Sun}	Spec type	BC	Age / Ga	*d*/pc	V	HZ inner /AU	HZ outer /AU	Planet	Min mass/ m_J	*a*/AU	*e*	System hab'ability now[2]	Habita-bility at some time?[2]
HD189733[3]	0.83	K1-2V?	–0.41	5[4]	19.3	7.67	0.552	1.085	b	1.15	0.0313	0	Yes	Yes
HD102195	0.928	K0V	–0.36	0.02 – 0.15[5]	28.98	8.05	0.688	1.35	b	0.48	0.049	0.06	No	Yes
Gliese581	0.31	M3V?	–2.11	>2[6]	6.26	10.55	0.113	0.224	b	0.056	0.041	0	Yes	Yes
HD118203[7]	1.23	K0V?	–0.36	EoMS[8]	88.6	8.05	2.034	3.997	b	2.13	0.07	0.309	No	Yes
HD33564	1.25	F6V	–0.15	3[9]	20.98	5.08	1.508	3.012	b	9.1	1.1	0.34	2O	2O
HD20782	1.00	G2V	–0.20	10[10]	36.02	7.38	0.973	1.929	b	1.8	1.36	0.92	No	No
HD187085	1.22	G0V	–0.18	3.6[10]	44.98	7.22	1.274	2.534	b	0.75	2.05	0.47	No	No
HD81040	0.96	G2-3V?	–0.20	0.73[11]	32.56	7.72	0.757	1.500	b	6.86	1.94	0.526	No	No
HD11964[7]	1.125	G5V?	–0.24	8.98[12]	33.98	6.42	1.490	2.943	b c gone!	0.11	0.229	0.15	Yes	Yes
HD73526[7]	1.02	G6V	–0.25	7.4 – 11.0[13]	99	9.00	1.344	2.653	b c new!	2.9 2.5	0.66 1.05	0.19 0.14	6O	6O

1 Results calculated and determined by B.W. Jones
2 Assessment determined by P.N. Sleep.
3 Inclination = 85.8°, P = 2.218573 days, star's mass calculated from P and a (Schneider, 2006)
4 Bakos et al., 2006
5 Ge et al., 2006
6 Bonfils et al., 2005
7 Parameters revised
8 Estimated age determined from HZs calculated from observed stellar parameters and matched with the two stellar models' spreadsheets.
9 Galland et al., 2005
10 Jones et al., 2006
11 Sozzetti et al., 2006
12 Saffe et al., 2005
13 Tinney et al., 2003

In determining whether systems could house habitable Earth-like planets in orbits confined within habitable zones, it is assumed that those systems with hot or warm Jupiter planets would still have smaller planets within their systems. The inward migration of the giant planets to their present positions may well have dispersed primordial protoplanets and dust. However such bodies may re-assemble in orbits within a system's ice-line, after migration, to form Earth-sized rocky planets (Fogg & Nelson, 2005 and Mandell & Sigurdsson, 2003). It is assumed, therefore, that any system with a hot or warm Jupiter planet could house habitable Earth-like planets.

It should be noted from Table 3.19 that for either stellar grid model, if the inner HZ limit (defined by the runaway greenhouse effect) at the end of the main sequence of any star is less than the outer HZ limit (defined by the maximum greenhouse effect) at ZAMS, then that star will have a continuously habitable zone bounded by these limits. However, CHZs are only found in stars of $1M_{\odot}$ or greater. As a general guiding rule, at any time during any star's main sequence lifetime, the outer HZ is approximately twice the distance from the star than the inner HZ. As a rough guide the orbital periods of planets at these boundaries for any star would be approximately 300 days at the inner HZ boundary and 600 days at the outer HZ boundary.

For Table 3.20, when determining whether an Earth-like planet may be habitable in an exoplanetary system, the only negative entry is "No". All other entries indicate possibilities for life occurring within a system. Although data in tables 3.18 and 3.19 may contain parameter errors, the inclusion of these in this analysis would have created an unmanageable amount of data which would not have had a significant effect on the overall summary statistics given in table 3.22. The most interesting systems are those which could house a detectable habitable planet and a moon at different times during their main sequences. The most interesting of all is HD 114783, which has the possibility to house a detectable habitable body throughout its main sequence lifetime from 2Gyr after ZAMS onwards, whether it is a planet inside the giant's orbit, a moon of the giant or another planet beyond the orbit of the giant. Indeed, the second stellar grid model's present day prediction is for a possible inferior detectable habitable planet to the giant **and** a detectable habitable moon.

The assessments for habitability of the ten new and revised systems in table 3.21 gave the same results for both Mazzitelli stellar models. There is no difference in the potential habitability outcomes of the three systems with updated data. Of the seven new systems, three could house a habitable Earth now, and four could at some time during their main sequence.

Table 3.22 shows a summary of the number of potentially habitable systems among the 150 examined, derived from tables 3.20 and 3.21. It also shows the number of giant planets with low eccentricity orbits confined to the habitable zone, which may house their own habitable satellites. These would be the most difficult habitable bodies to identify but are included as part of the totals of potentially habitable systems.

Table 3.22 Numbers of potentially habitable systems out of the 150 known at 14/06/2006.

Stellar Model Circumstances	Potentially Habitable Systems	Potentially Habitable Moons
1st Stellar Grid, now	85	4
1st Stellar Grid, at some time	111	13
2nd Stellar Grid, now	79	3
2nd Stellar Grid, at some time	113	13
Stellar Parameters, now	80	4

The three figures for "now" are in very close agreement, as are the two for "at some time" and show that quite different approaches to determining the number of potentially habitable systems yield very similar results. From the figures above, about 55%, or just over half, of the known planetary systems could house a habitable planet or moon now. They also show that 75%, or three-quarters, of the known systems could house a habitable planet or moon at some time during the main sequence lifetime of their stars. These results are much higher than those of Menou and Tabachnik, 2003 and Tarter and Turnbull, 2003, who both predict that about one third of systems at their time of writing could presently house a habitable planet. Menou and Tabachnik investigated the perturbations of possible terrestrial planets by the giant, but only over the short period of one million years. Their habitability criteria were also very conservative in that the planet must remain within the HZ at all times, not its semimajor axis. Tarter and Turnbull required 3Gyr for detectable habitable planets to evolve and also that the **entire** habitable zone is available for any potential Earths. However, using the same habitability criteria as here, the figures in this thesis are only slightly higher than Jones et al. (2005) and Sleep (2005) (half now, two-thirds at any time), and the same as previously quoted values of Underwood et al. (2003). Generally the fraction of habitable systems is expected to rise with time, as the majority of current exoplanet discoveries are transiting "hot Jupiters", which would have little gravitational effect on the orbits of planets within habitable zones. Perhaps in the future it may be more productive to identify new exoplanetary systems which **cannot** house a habitable Earth-like planet or moon, as it seems that this list may be shorter.

4. Modelling Exoplanetary Systems with One Giant

4.1 The Mercury Orbital Integrator

The search for extraterrestrial life will be enhanced if efforts are concentrated on stars where Earth mass planets could have existed in stable orbits confined to the habitable zone for at least the last billion years. Orbits defined as confined to the habitable zone have semimajor axes within the boundaries of this zone independent of eccentricity. This can be justified in that planets with such highly eccentric orbits would spend a relatively short time near to periastron. This may allow natural shielding phenomena, such as radiation reflecting cloud cover, to prevent overheating and planetary sterilisation. The time near to apastron would be much longer; however life can be more resistant to extremes of cold than to extremes of heat by using hibernation techniques. The stability of such orbits in exoplanetary systems can be examined in detail by using a mixed variable symplectic orbital integrator (Chambers, 1999). Phenomena such as planetary axial tilt cannot be incorporated into these analyses, however, and survival of life on Earth-like planets with high orbital eccentricities under these conditions can only be theorised using atmospheric model studies over time.

The symplectic orbital integrator used here is John Chamber's Mercury version 6.1 computer program and runs within a 32-bit DOS box in a Windows operating system on personal computers or within a Linux system on Alpha computers. The theory behind the integrator has already been comprehensively covered (Sleep, 2005 & Chambers, 1999) and will not be reproduced here. The instructions for using the program are in the files named "Mercury6.doc" and "Mercury6.man" within the zipped file which can be downloaded from the internet as part of the complete Mercury package (Chambers, 2006)

The Mercury orbital integrator contains a second-order mixed variable symplectic (MVS) integrator (Chambers, 1999), which has already been extensively tested on exoplanetary systems, as described in Chapter 1. The MVS integrator is designed to handle systems which have the largest mass at its centre, ideal for exoplanets but not satellites of giant planets. It is about 10 times faster than other integrators, which makes it an essential tool for the integration runs carried out on the exosystems investigated here. Its symplectic property, from the incorporated symplectic correctors within the algorithm (Wisdom, 1996), means there is no build up of total energy and total angular momentum of the system during runs. Time intervals between successive integration calculations of planetary positions are set to 0.05 of the smallest orbit's period, since time intervals larger than this may lead to inaccuracies in positional calculations. Planetary orbital information is stored in backup or "dump" files every 500,000 time steps. This is useful since an integration can be resumed from these files after an unscheduled termination, or continued after a termination due to a close encounter using a different integration mode and close encounter parameter value (see later). Orbital elements for the bodies are usually stored 10,000 times during the course of a 10^9 year run. One minor drawback here is that time steps need to be very short for exosystems with a giant planet in a short period orbit, and a run of 10^9 years can take many days (even weeks). The main drawback with the MVS integrator is that it cannot handle close encounters between bodies, inside the 3 Hill radii boundary of the larger body. Integrations are automatically halted at this distance, hence avoiding usage of the MVS integrator under unsuitable circumstances. The Hill radius is the distance from a body along its radius vector from the large central mass, where its gravitational attractive force on a small particle is equal to that of the central mass in its

orbital rotating frame. The Hill radius distance, R_H, (used in the Mercury Orbital Integrator, see Appendix 1) for a giant planet of mass M_p orbiting a star of mass M_* at a semimajor axis distance a, is (Murray & Dermott, 1999):

$$R_H = a\left(\frac{M_p}{3M_*}\right)^{1/3} \qquad 4.1.$$

The type of integrator used for studies of planet orbits, which cross the 3 Hill radii boundary is a "Hybrid" integrator. This is a combination of the MVS integrator and a Bulirsch-Stoer integrator (BS2), a generally robust model for N-body problems, usually used when all other integrators fail (Chambers, 1999). When a small terrestrial planet approaches to within 3 Hill radii of the giant planet the integrator automatically switches mode from MVS to BS2. Orbits can then be monitored properly throughout the entirety of any close encounters.

Previous work has shown that orbits rarely become unstable after 500Myr and of those that do, variations in orbital eccentricity are observed which get ever larger until the run terminates (Jones & Sleep, 2002, Jones et al., 2001). So if a terrestrial planet can exist in a confined orbit within the habitable zone for 1Gyr it is likely to remain there for the duration of that star's main sequence lifetime. In a normal MVS orbital integration run, the program terminates when the orbit of the Earth-mass planet has a close encounter with the giant planet, i.e. it approaches within 3 Hill radii. Under "Hybrid" runs the switch which prevents close encounters from happening may be turned off, so runs will continue until there is a possible collision between the terrestrial planet and the giant planet. If the Earth like planet collides with the star, however, the program will continue to run with solely the star and giant. This will also occur if the Earth-mass planet's distance from the star exceeds a distance of 100AU, where it is then considered to be ejected from the system.

4.2 Starting Configurations for Integration Runs

For each orbital integrator investigation, an Earth-Moon planet (a single body of the combined masses of Earth and the Moon) is launched into a range of orbits, within the habitable zone of the known exoplanetary system, and monitored for the duration of its orbital survival or up to one billion years, whichever is least. The period of one billion years was chosen as life was well established after this time in Earth's history (Ward & Brownlee, 2000). Particular interest in orbital behaviour is taken around any regions of orbital resonance, where the Earth-Moon planet would orbit the star $(p + q)/p$ times for every superior giant planet orbit, and $p/(p + q)$ times for every inferior orbit, where p and q are small positive integers. In all cases the only bodies considered in the systems are the known giant exoplanet(s), the star and the Earth-Moon planet.

The Earth-Moon orbits always have an initial eccentricity of 10^{-5} but vary in initial semimajor axis distance from the star, orbital inclination with respect to that of the giant planet and longitude of periastron, $\Delta\varpi$ (Figure 4.1), with respect to the giant planet. This is so for different configurations of the giant planet within the system, where its semimajor axis and eccentricity may be varied due to measurement errors in these parameters. The mass of the giant is usually taken to be the minimum mass but is occasionally increased to 1.5 times minimum mass to simulate an orbital inclination of $41^{O}.81$ with respect to the plane of the sky. If the orbit is stable for one billion years, it is assumed that the orbit will remain stable for the main sequence lifetime of the star.

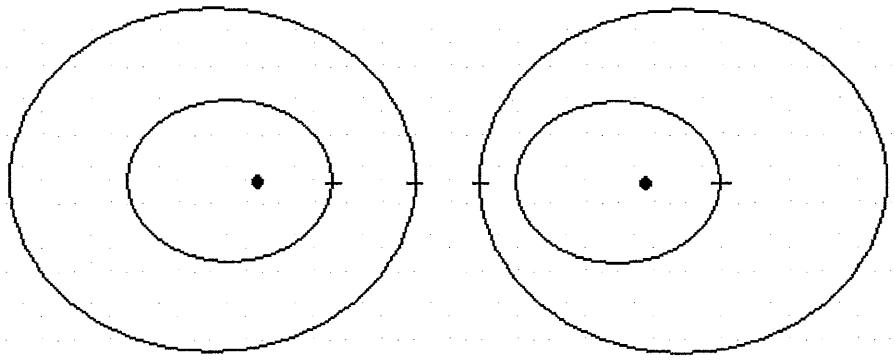

Figure 4.1. The starting positions of an Earth-Moon planet with respect to its periastron longitude relative to the giant planet's in a single giant planet system

4.3 Comparison between Computer Types

Prior to further detailed investigations of new systems, a brief study was undertaken to compare the same orbital integration runs on the two types of computer platform, PCs and Alphas. There was a mix of "stable" runs, which lasted 1 Gyr before termination and "unstable" runs which ended themselves due to some catastrophe within the system as outlined at the end of section 1 in this chapter. Times before program termination for the same initial unstable configurations may differ between the types of machine because of the number of significant figures used to calculate results within data.

Table 4.1 compares the times of unstable runs between like configurations and also illustrates agreement between the two platforms for stable runs. "Giant a" and "Giant e" are the initial semimajor axis and initial eccentricity of the giant planet (at $t = 0$) respectively, "E-M a" is the initial semimajor axis of the Earth-Moon planet (its initial eccentricity is **always** 10^{-5}), $\Delta\varpi(0)$ is the difference in periastron longitudes between the giant planet and the Earth-Moon at $t = 0$, t is the time of the integration run in years and O is the outcome of a run that terminates due to a catastrophe. Full results from runs showing variation in the Earth-Moon's semimajor axis and eccentricity during the runs has been omitted since they are not relevant to this small examination. The configurations were chosen at random from several systems to illustrate this phenomenon. The theory behind the integrator programming suggests that the same trends would remain, i.e. stable and unstable orbits on one machine would remain so on the other. The information within table 4.1 bears this out, even though two "unstable" runs for ε-Eridani had to be continued well beyond 1 Gyr before they destabilised and hence verified this. Also two runs that terminated before 1 Gyr had different catastrophic outcomes, which is unimportant as the runs were still "unstable". Any differences between the outcomes of runs with the same initial parameters were attributed to the two computer platforms using different levels of significant figures when calculating each time step. From this information, it was safe to assume that future planetary studies for any one system would be confined to either an Alpha machine or a PC to maintain consistency in results trends.

Table 4.1 Comparison between like runs performed on a PC and an Alpha computer.

Computer Type	Star	Starting Parameters				t / years	O
		Giant a / AU	Giant e	E-M a / AU	$\Delta\varpi(0)$/°		
PC	ε-Eri	3.3	0.8	8.5	0	3.147×10^8	E
Alpha	ε-Eri	3.3	0.8	8.5	0	1.085×10^8	E
PC	ε-Eri	3.3	0.8	8.5	180	$> 10^9$	-
Alpha	ε-Eri	3.3	0.8	8.5	180	$> 10^9$	-
PC	ε-Eri	3.3	0.8	8.6	0	1.496×10^8	C
Alpha	ε-Eri	3.3	0.8	8.6	0	7.511×10^7	C
PC	ε-Eri	3.3	0.8	8.6	180	$> 10^9$	-
Alpha	ε-Eri	3.3	0.8	8.6	180	$> 10^9$	-
PC	ε-Eri	3.3	0.8	8.7	0	1.818×10^9	C
Alpha	ε-Eri	3.3	0.8	8.7	0	7.511×10^8	E
PC	ε-Eri	3.3	0.8	8.7	180	5.333×10^8	C
Alpha	ε-Eri	3.3	0.8	8.7	180	4.932×10^8	C
PC	ε-Eri	3.3	0.608	7.8	0	2.964×10^9	PC
Alpha	ε-Eri	3.3	0.608	7.8	0	1.632×10^8	PC
PC	ε-Eri	3.3	0.608	7.8	180	2.195×10^8	E
Alpha	ε-Eri	3.3	0.608	7.8	180	2.911×10^8	E
PC	ε-Eri	3.3	0.608	8.2	0	1.351×10^8	E
Alpha	ε-Eri	3.3	0.608	8.2	0	8.536×10^6	E
PC	ε-Eri	3.3	0.608	8.2	180	$> 10^9$	-
Alpha	ε-Eri	3.3	0.608	8.2	180	$> 10^9$	-
PC	ε-Eri	3.3	0.608	8.3	0	3.359×10^8	E
Alpha	ε-Eri	3.3	0.608	8.3	0	2.797×10^8	PC
PC	ε-Eri	3.3	0.608	8.3	180	$> 10^9$	-
Alpha	ε-Eri	3.3	0.608	8.3	180	$> 10^9$	-
PC	HD 196050	2.5	0.28	1.75	0	$> 10^9$	-
Alpha	HD 196050	2.5	0.28	1.75	0	$> 10^9$	-
PC	HD 196050	2.5	0.28	1.75	180	4.073×10^8	E
Alpha	HD 196050	2.5	0.28	1.75	180	5.536×10^8	E
PC	HD 196050	2.5	0.28	3.45	0	$> 10^9$	-
Alpha	HD 196050	2.5	0.28	3.45	0	$> 10^9$	-
PC	HD 196050	2.5	0.28	3.45	180	7136	E
Alpha	HD 196050	2.5	0.28	3.45	180	7044	E
PC	HD 196050	2.5	0.28	3.5	0	2.799×10^4	E
Alpha	HD 196050	2.5	0.28	3.5	0	2.779×10^4	E
PC	HD 196050	2.5	0.28	3.5	180	$> 10^9$	-
Alpha	HD 196050	2.5	0.28	3.5	180	$> 10^9$	-
PC	HD 196050	2.5	0.28	4.4	0	2.169×10^4	E
Alpha	HD 196050	2.5	0.28	4.4	0	6501	E
PC	HD 196050	2.5	0.28	4.4	180	$> 10^9$	-
Alpha	HD 196050	2.5	0.28	4.4	180	$> 10^9$	-
PC	τ^1 Gruis	2.6	0.14	3.4	0	$> 10^9$	-
Alpha	τ^1 Gruis	2.6	0.14	3.4	0	$> 10^9$	-
PC	τ^1 Gruis	2.6	0.14	3.4	180	3.945×10^4	E
Alpha	τ^1 Gruis	2.6	0.14	3.4	180	4.199×10^4	E
PC	τ^1 Gruis	2.6	0.14	3.45	0	$> 10^9$	-
Alpha	τ^1 Gruis	2.6	0.14	3.45	0	$> 10^9$	-
PC	τ^1 Gruis	2.6	0.14	3.45	180	3.945×10^4	E
Alpha	τ^1 Gruis	2.6	0.14	3.45	180	5.602×10^4	E

ce Close encounter to within $3R_H$ of the giant planet.
C Earth-Moon collides with the star.
PC Earth-Moon collides with the giant planet.
E Earth-Moon is ejected from the system.

4.4 The Three Analysed Planetary Systems

Six systems have been investigated previously by the Open University Exoplanetary Team using the orbital integrator over periods of 100 million years or one gigayear. They are ρ Coronae Borealis, 47 Ursae Majoris, Gliese 876, υ Andromedae, ϵ Eridani and HD 72659

(Sleep, 2005, Jones & Sleep, 2003, Jones & Sleep, 2002, Jones et al., 2001). The new exosystems investigated in this section are τ^1 Gruis (HD 216435), HD 196050 and HD 52265, all with one giant planet each. The configurations of all nine systems are shown diagrammatically in Figure 4.2, where the giant planet's excursion, due to its orbital eccentricity, and its gravitational reach are shown with the HZ today and HZ at zero-age main sequence. The gravitational reach of each giant in the diagram is based on an invariant $3R_H$ in all cases, independent of orbital eccentricity. It has since been established (Sleep, 2005) that nR_H varies with orbital eccentricity, e, where $n = 3$ only when $e = 0$. However, n is always close to 3 or less when the Earth-Moon is interior to the giant, which is the case in all the investigated systems except ρ CrB and HD52265. When exterior to the giant, the largest value of n encountered for the systems is 7.82 for HD 52265, causing its external gravitational reach to impinge on the inner edge of the ZAMS habitable zone for a minimum mass giant. However, this is the only instance where these values, from this new research, are relevant to Earth-Moon orbital stabilities in these systems. Figure 4.2 is useful for showing everything except the external gravitational reaches of the giant planets, which extend further than shown.

The τ^1 Gruis and HD 196050 systems were investigated using PCs, where the orbital integrator program is run in a DOS window within a 32-bit Windows operating system. The study on τ^1 Gruis was initially carried out using the parameters dated prior to 11/05/2003.

The star τ^1 Gruis has a mass of $1.25 \pm 0.10 M_\odot$ and has a high metallicity, where [Fe/H] is 0.15 ± 0.04 (parameters summarised in table 4.2). It has an absolute bolometric magnitude of 3.20 ± 0.05, placing it a magnitude above the main sequence (Jones et al., 2002). It is of G0V spectral type and is believed to be near the end of its main sequence lifetime, estimated from chromospheric activity measurements of calcium II H and K lines, to be 5Gyr old (Gonzales, 1999). Its habitable zone is calculated to have moved out from 1.05AU to 2.23AU at zero age main sequence to presently be between 1.77AU and 3.52AU from the star, based on the fluxes at the limits of the Solar System habitable zone (Kasting et al., 1993). The quoted present HZ boundaries are dependent on the stellar model used and are slightly different from those in Figure 4.2, due to the star being at the end of its main sequence where the HZ is subject to rapid variation. Prior to 11/05/2003, orbital measurements gave the accompanying giant planet a minimum mass of 1.23 ± 0.18 M_J, a semimajor axis of 2.6 ± 0.6 AU, an eccentricity of 0.14 ± 0.14 and an orbital period of 1326 ± 300 days, see table 2b. The error in the eccentricity was the reason for choosing this system to compare simulation outcomes with predicted results according to equation 4.2. These orbits lie about 30% of the habitable zone's width from the inner limit and are the parameters used in this investigation. Earth-Moon orbits were placed to within 0.7AU of the star since atmospheric conditions on such a planet may allow life to yet exist. These integrations may also be useful when encountering systems with a similar giant planet configuration but with a less massive star. For a giant with a circular orbit, the gravitational field of influence leaves only the outer edge of the present day HZ free of possible perturbation effects, see Figure 4.2. This area was not investigated as the star is at the end of its main sequence lifetime and life would not have had sufficient time to evolve on a world and alter its atmosphere, in such an orbit. From 11/05/2003, the giant planet's mass and orbital parameters were modified to 1.49 M_J, at 2.7AU with an eccentricity of 0.34 (Schneider, 2006). These values placed the giant's gravitational influence across the entire habitable zone, post 2 Gyr after the star's birth. Life in this system, with these parameters, was not deemed to be possible, so orbital integrations with an Earth mass planet were not carried out.

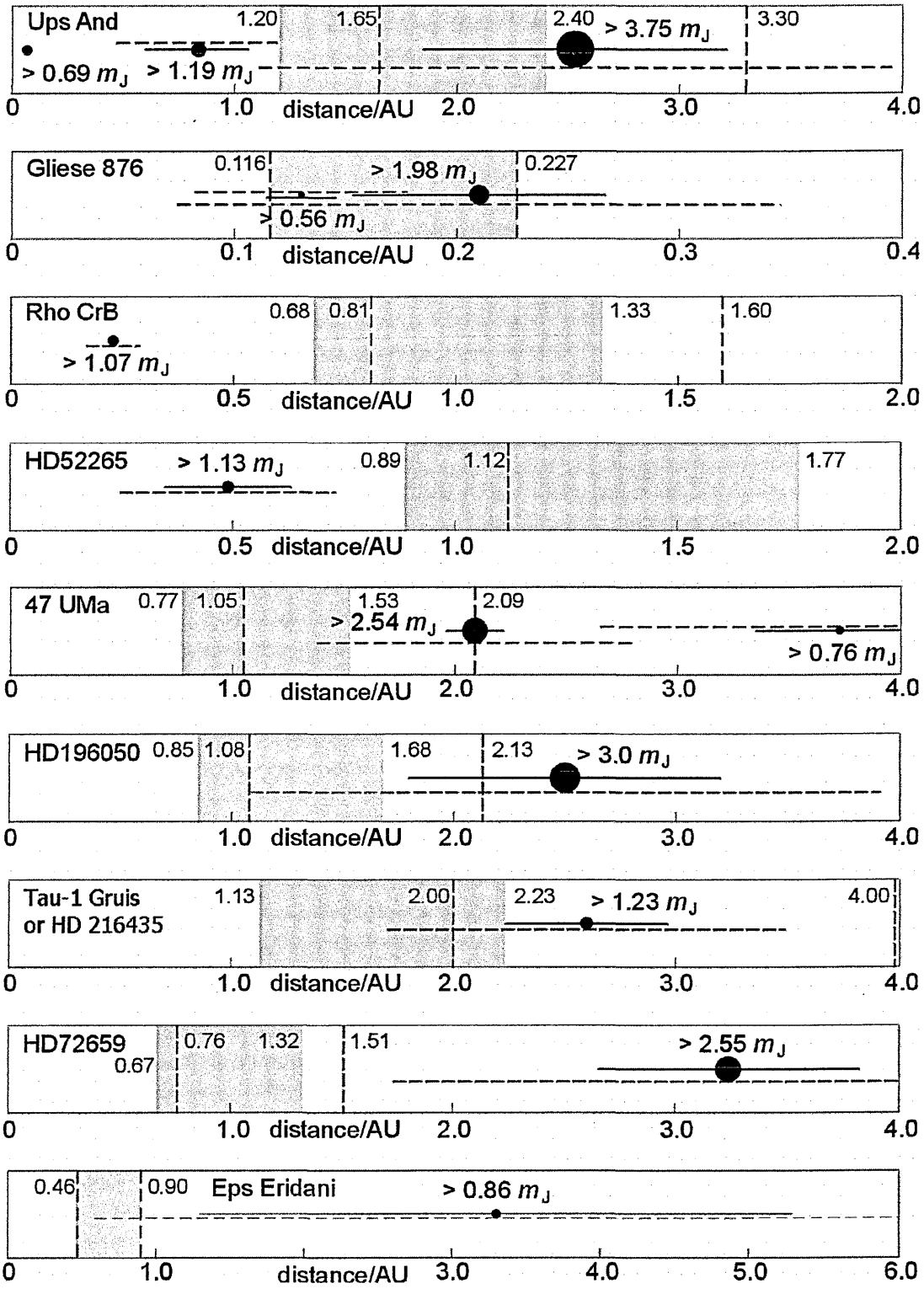

Figure 4.2. Configurations of all systems investigated by orbital integration.
The shaded region is the HZ when the star was young, and the vertical dashed lines mark its boundaries today. The solid horizontal lines extending from each giant planet show the excursion due to its orbital eccentricity, and the horizontal dashed lines extend from $[a(1-e)-3R_H]$ to $[a(1+e)+3R_H]$.

The star HD 196050 is $1.13 \pm 0.1 M_\odot$, of spectral type G3V and is heavy in metals with a [Fe/H] value of 0.3 ± 0.2 (see table 4.2). Its age is estimated to be greater than 1.6 Gyr (Mayor et al., 2004) or 3Gyr (Jones et al., 2002). Its planetary companion is of 2.8 ± 0.5 M_J with a semimajor axis of 2.4 ± 0.5 AU, taking 1300 ± 230 days to orbit with an eccentricity of 0.28, see table 4.3. The giant planet's eccentric orbit means it revolves at

the outer edge of the present day habitable zone, which is calculated to be between 0.95AU and 1.95AU dependent on the stellar model. The giant planet parameters, used for the orbital integrations, are within the errors of these values and of minimum mass $3.0M_J$, semimajor axis of 2.5AU, eccentricity of 0.28 and the stellar mass is taken as $1.1M_\odot$ (Schneider, 2006). The configuration of the HD 196050 system is similar to that of the inner giant of the previously studied system, 47 UMa (Jones & Sleep, 2002). The position of the habitable zone in HD 196050 is only marginally further out than that of 47 UMa and its planet is $3.0M_J$, 20% larger. The orbit has a semimajor axis about 15% larger at 2.5AU, putting the mean position just outside of the habitable zone as opposed to on its outer edge. The orbit is much more eccentric at $e = 0.28$, than in 47UMa, causing its 3 Hill radii inner boundary to sweep across to the inner edge of the habitable zone, see Figure 4.2. Stable orbits in 47UMa were found out to 1.2AU for a minimum mass giant. HD 196050 may be as young as 1.6Gyr (Mayor et al., 2004), so life on an Earth-like planet within the habitable zone may not yet have established itself. Whether 1.6Gyr or 3Gyr old (Jones et al., 2002), however, the purpose here was to find the extent of gravitational influence of the giant planet in HD 196050, across the outer regions of the habitable zone and its influence on Earth-mass planets within these regions.

The HD 52265 system was investigated using an Alpha machine with a Linux operating system. It is the second system, after ρ CrB, to be studied with a giant planet interior to the habitable zone region. The star HD 52265 is of $1.13M_\odot$, of spectral type G0V, has a metallicity [Fe/H] value equal to 0.11 and is approximately 3.5 Gyr old (Naef et al., 2001) (see table 4.2). The planetary companion is of $1.13 \pm 0.03\ M_J$, has a semimajor axis of 0.49AU, eccentricity of 0.29 ± 0.04 and a revolution period of 118.96 ± 0.10 days (Butler et al., 2000), see table 4.3. The present habitable zone is between 1.06AU and 2.33AU, well outside the orbit of the giant and any influence its gravity may have on any Earth-mass body in the habitable zone. The planets of ρ CrB and HD 52265 are comparable in mass but the giant in the HD 52265 system has a larger semimajor axis and a more eccentric orbit, see Figure 4.2 and will extend its gravitational influence more widely. Stable orbits were found for Earth-mass planets across the entire habitable zone for ρ CrB, even for planets as large as 8 times minimum mass. So the purpose here is to see whether the giant in HD 52265, slightly nearer to the habitable zone than that in ρ CrB, and with a greater eccentricity, does have any impact on orbits of putative terrestrial planets with semimajor axes within and near to the inner edge of the habitable zone.

Table 4.2 summarises the stellar properties of τ^1 Gruis, HD 196050 and HD 52265 as listed in table 3.18. Also summarised are the habitable zone distances from the stars at ZAMS (zero-age main sequence), now and at EoMS (end of main sequence), as listed in table 3.19. Table 4.3 gives the giant planet minimum mass and orbital data, including the extent of its gravitational reach as calculated from,

$$n_{\text{int}} = -12.686\, e^3 + 10.883\, e^2 - 3.085\, e + 3 \qquad 4.2$$

$$n_{\text{ext}} = 53.479\, e^3 - 65.169\, e^2 + 31.036\, e + 3 \qquad 4.3,$$

where n_{int} is the inner Hill radius multiplier, n_{ext} is the outer Hill radius multiplier and e is orbital eccentricity (Sleep, 2005).

Table 4.2. Stellar properties of τ^1 Gruis, HD 196050 and HD 52265

Parameter	τ^1 Gruis	HD 196050	HD 52265
$M_*/ M_\odot$	1.25 ± 0.10	1.13 ± 0.10	1.13
Metallicity / [Fe/H]	0.15 ± 0.04	0.3 ± 0.2	0.11
Metallicity / % (1st & 2nd model)	2.83 & 2.66	3.99 & 3.75	2.58 & 2.42
Spectral Type	G0V	G3V	G0V
Bolometric Correction	-0.18	-0.21	-0.18
Age / Gyr	5.0*	1.6	3.5
Distance / pc	33.3	46.9	28
Apparent Visual Magnitude	6.03	7.6	6.30
$L/L_\odot$	4.00	2.10	2.20
T_{eff}/K	6032	5751	6032
1st model inner HZ ZAMS / AU	1.051	0.854	0.880
1st model outer HZ ZAMS / AU	2.094	1.695	1.746
1st model inner HZ now / AU	1.765	0.936	1.065
1st model outer HZ now / AU	3.515	1.863	2.125
1st model inner HZ EoMS / AU	1.723	1.548	1.557
1st model outer HZ EoMS / AU	3.388	3.063	3.082
2nd model inner HZ ZAMS / AU	1.118	0.876	0.927
2nd model outer HZ ZAMS / AU	2.232	1.74	1.844
2nd model inner HZ now / AU	-*	0.975	1.164
2nd model outer HZ now / AU	-*	1.945	2.328
2nd model inner HZ EoMS / AU	1.824	1.582	1.628
2nd model outer HZ EoMS / AU	3.589	3.111	3.201
Stellar parameters inner HZ now / AU	1.631	1.215	1.211
Stellar parameters outer HZ now / AU	3.245	2.406	2.409

* The age of the star is older than that of the predicted main-sequence lifetime for this model.
ZAMS = zero-age main sequence
EoMS = end of main sequence

Table 4.3. Orbital Properties of the exoplanets τ^1 Gruis b, HD 196050b and HD 52265b.

Parameter	τ^1 Gruis b		HD 196050 b	HD 52265 b
	Old	New		
$M_p \sin i_0 / M_J$	1.23 ± 0.18	1.49	3.0	1.13 ± 0.06
Semimajor axis/AU	2.6 ± 0.6	2.70	2.5	0.49 ± 0.008
Orbital Eccentricity	0.14 ± 0.14	0.34	0.28	0.29 ± 0.04
Period / days	1326 ± 300	1442.919	1289	118.96 ± 0.10
Inner R_H multiplier, n_{int}	e=0, 3 e=0.14, 2.75 e=0.28, 2.71	2.71	2.71	2.71
Outer R_H multiplier, n_{ext}	e=0, 3 e=0.14, 6.21 e=0.28, 7.75	8.12	7.75	7.82
Inner gravitational reach / AU	e=0, 2.07 e=0.14, 1.75 e=0.28, 1.39	1.25	1.18	0.26
Outer gravitational reach / AU	e=0, 3.13 e=0.14, 4.06 e=0.28, 4.70	5.21	4.97	0.89

4.5 Outcome of the System Investigations

4.5.1 τ^1 Gruis

The details of all orbital runs, using the MVS integrator in the Mercury program for an Earth-Moon planet within this system are given in tables 4.4, 4.5 and 4.6. Table 4.4 lists the outcomes of the orbital integration runs within the inner habitable zone region up to the giant's gravitational field of influence for giant orbital eccentricities of 0, 0.14 and 0.28, corresponding to the old uncertainty limits (table 4.3). Earth-Moon orbits were found to be stable from 0.7AU to 2.0AU, for a minimum mass giant planet with a circular orbit. The orbits were only stable out to 1.7AU when the giant's orbital eccentricity was 0.14 with the outer stability limit further decreased to 1.3AU when the giant's orbital eccentricity was 0.28. These values are in excellent agreement with the predicted theoretical values determined from previous results (Sleep, 2005), shown in table 4.3. Clearly it is the presence of the giant over a wider region around the star due to its orbital eccentricity which causes this. These destabilising limits correspond to values of n in $n\mathrm{R_H}$ of 3.4 for $e = 0$, 3.0 for $e = 0.14$ and 3.2 for $e = 0.28$, when using formula 4.1. All are similar, close to $n = 3$ and show no trend with increasing orbital eccentricity.

For all results for the three giant orbital eccentricities, the variation of orbital eccentricity and semimajor axis of the Earth-Moon slowly increases with increasing starting distance from the star. This is due to an increase in the giant's influence on the smaller body as its initial orbital parameters move nearer to the giant. For the initially circular giant orbits, which acquire a very small eccentricity immediately, the difference in the longitude of periastron, $\Delta\varpi$, between the giant and Earth-Moon revolves around a full 360^{O} out to 1.5AU. Beyond this distance, the value is constrained between limits, as are all Earth-Moon orbits when the giant has an orbital eccentricity of 0.14 and 0.28, see figures 4.3 and 4.4. The implication here is that orbits with a revolving $\Delta\varpi$ may be more stable than those where $\Delta\varpi$ are constrained, whether $\Delta\varpi(0)$ is 0^{O} or 180^{O}.

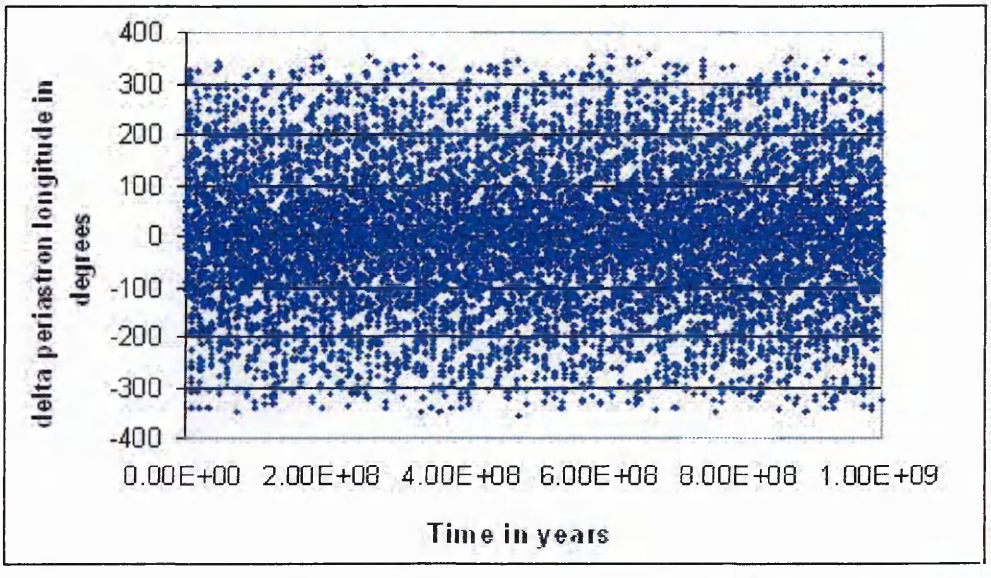

Figure 4.3. Free revolving delta periastron longitude values with time between an Earth-Moon body and a giant planet ($\Delta\varpi = 0^{\mathrm{O}}$, Giant $e = 0$, E-M $a = 1.0$AU all at $t = 0$).

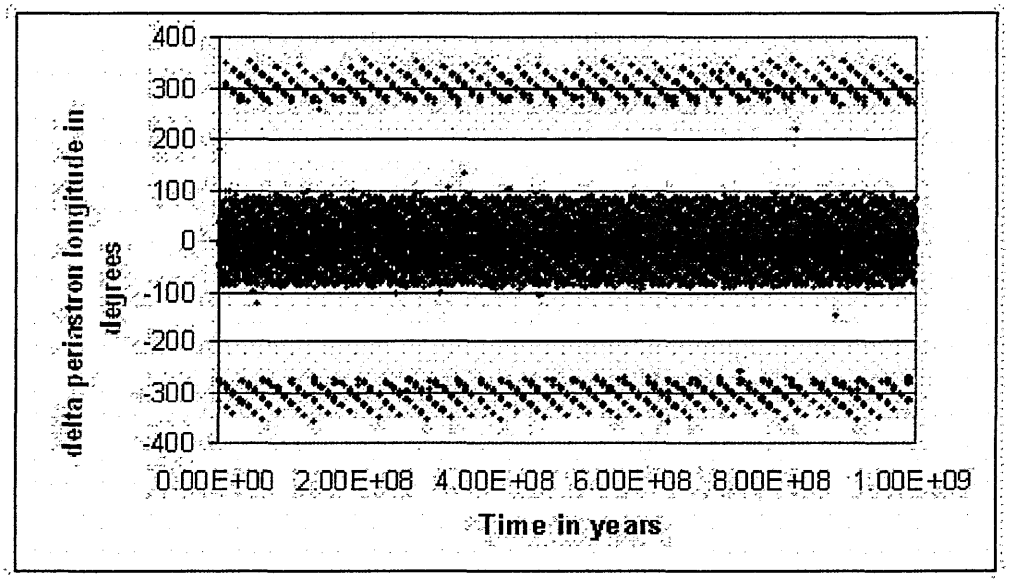

Figure 4.4. Constrained $\Delta\varpi$ with time between an Earth-Moon body and a giant planet. (Note that $\Delta\varpi$ values greater than 260^{O} and less than -260^{O} correspond to those between $\pm 100^{O}$.) ($\Delta\varpi = 180^{O}$, Giant $e = 0.14$, E-M $a = 1.1$AU all at $t = 0$).

Although the initial semimajor axes for both $\Delta\varpi(0) = 0°$ and 180°, for each semimajor axis run are initially the same, the mean values over a stable run's 1Gyr period differ slightly. The orbits always have a mean semimajor axis value slightly less than the starting value, where the largest value is often the initial one. This implies an initial potential energy loss by the Earth-Moon, since orbital potential energy, PE $\propto -1/a$. This initial potential energy loss is not always due to a similar gain by the giant planet and increases as the Earth-Moon's semimajor axis increases towards that of the giant, possibly due to the decreasing stability of the orbits. The orbital integration runs launched where $\Delta\varpi(0) = 180^{O}$ always have larger mean semimajor axis values compared to those where $\Delta\varpi(0) = 0^{O}$. This may be due to the Earth-Moon being on the opposite side of the star from the giant when it is launched at its apastron position. There will be less energy interaction between the bodies during the first orbit of the inner of the two planets as they are initially much further apart. A second explanation may be resonance effects between the two planets, causing small orbital shifts until they find their most stable configuration. These phenomena may be due to the programming of the Mercury Orbital Integrator, however they are minor and do not detract from the bigger picture of the study of orbital stabilities.

Another trend in Earth-Moon orbital properties is an increase in their orbital eccentricity with increasing initial giant orbital eccentricity when started with the same semimajor axis. This phenomenon is known as "pumping up" the eccentricity of the Earth-Moon by the giant and is illustrated by examining any set of three outcomes for Earth-Moon integrations with the same semimajor axis over the giant eccentricities of 0, 0.14 and 0.28 in table 4.4. In all integrations, when the giant's orbital eccentricity was initially significant, the Earth-Moon would rapidly oscillate between its minimum and maximum values, no matter how large, throughout the run, whilst the orbital semimajor axis remained almost constant (see Figures 4.5 and 4.6).

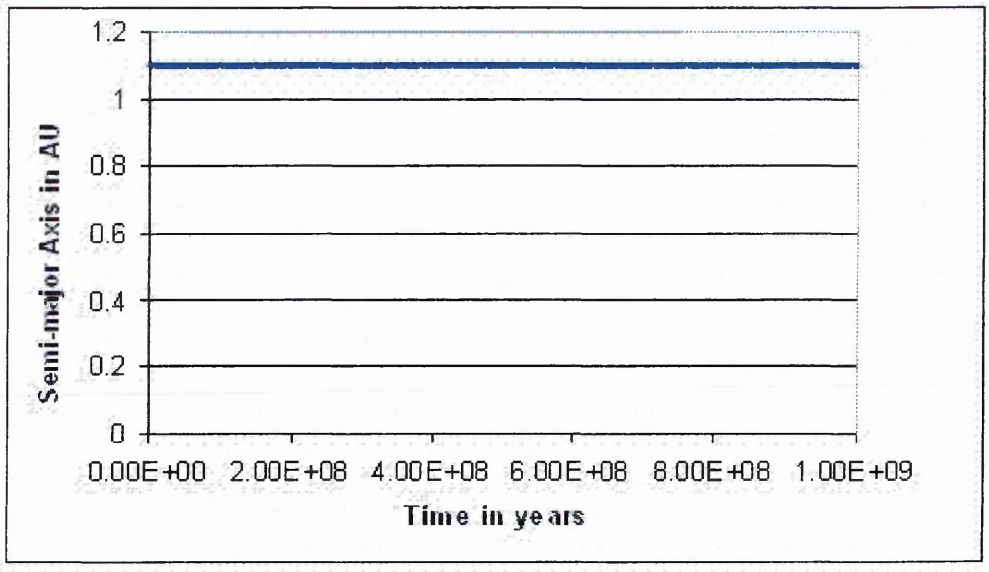

Figure 4.5 Variation of semimajor axis with time for a stable orbit around τ^1 Gruis ($\Delta\varpi = 0^O$, Giant $e = 0.14$, E-M $a = 1.1$AU all at $t = 0$).

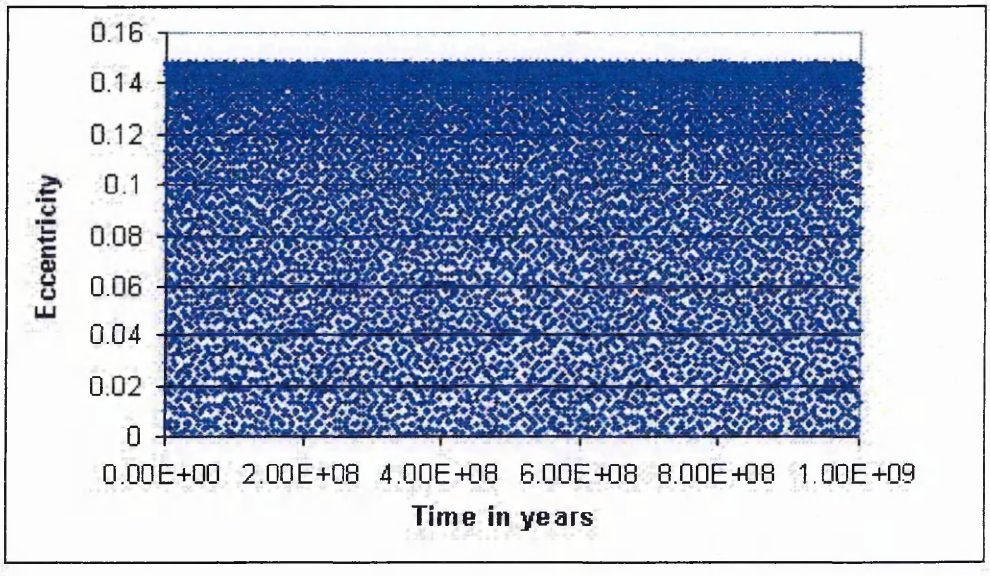

Figure 4.6 Variation of eccentricity with time for a stable orbit around τ^1 Gruis ($\Delta\varpi = 0^O$, Giant $e = 0.14$, E-M $a = 1.1$AU all at $t = 0$).

When the giant's mass was increased to 1.5 times its minimum, i.e. where the $e = 0.14$ orbit of the giant is inclined at $41^O.81$ to the plane of the sky instead of 90^O in the case of the minimum mass studies, the stability region for Earth-Moon orbits was narrowed slightly, as would be expected, from 0.7AU – 1.7AU to 0.7AU – 1.6AU. All trends discussed for the case of the minimum mass giant were also followed here. Two of three orbital runs, where the Earth-Moon orbit was inclined at 10^O to that of the giant, showed no $\Delta\varpi$ constraint, contrary to the constrained orbits for all the runs in the plane of the giant's orbit. This may imply more stable orbits when inclined. However the third run at initially 1.7AU had the same remarkably short unstable lifetime, of less than one day, as the run which was not inclined. Inclining the Earth-Moon orbit to the giant's was not pursued further as previous work (Jones & Sleep, 2002) has shown that this has little effect on the overall outcomes in orbital stability trends.

Table 4.4 Orbital runs for an Earth-Moon planet in the habitable zone of τ^1 Gruis in the presence of the minimum mass giant ($1.23M_J$) at 2.6AU.

Starting Parameters			Parameter variation during a run			t / years	O
Giant e	E-M a / AU	$\Delta\varpi(0)$/°	Earth-Moon e	Earth-Moon a / AU	$\Delta\varpi$/°		
0	0.7	0	10^{-5} – 0.000106	0.69997 ± 0.00003	0 - 360	$>10^9$	-
0	0.7	180	10^{-5} – 0.000156	0.69999 ± 0.00003	0 - 360	$>10^9$	-
0	0.8	0	10^{-5} – 0.000189	0.79995 ± 0.00005	0 - 360	$>10^9$	-
0	0.8	180	10^{-5} – 0.000251	0.79998 ± 0.00005	0 - 360	$>10^9$	-
0	0.9	0	10^{-5} – 0.000319	0.89991 ± 0.00009	0 - 360	$>10^9$	-
0	0.9	180	10^{-5} – 0.000389	0.89998 ± 0.00009	0 - 360	$>10^9$	-
0	1.0	0	10^{-5} – 0.000524	0.99985 ± 0.00015	0 - 360	$>10^9$	-
0	1.0	180	10^{-5} – 0.000594	0.99998 ± 0.00015	0 - 360	$>10^9$	-
0	1.1	0	10^{-5} – 0.000853	1.09976 ± 0.00024	0 - 360	$>10^9$	-
0	1.1	180	10^{-5} – 0.000903	1.09998 ± 0.00024	0 - 360	$>10^9$	-
0	1.2	0	10^{-5} – 0.001400	1.19962 ± 0.00038	0 - 360	$>10^9$	-
0	1.2	180	10^{-5} – 0.001392	1.20000 ± 0.00038	0 - 360	$>10^9$	-
0	1.3	0	10^{-5} – 0.002322	1.29941 ± 0.00059	0 - 360	$>10^9$	-
0	1.3	180	10^{-5} – 0.002242	1.30004 ± 0.00059	0 - 360	$>10^9$	-
0	1.4	0	10^{-5} – 0.004304	1.39991 ± 0.00091	0 - 360	$>10^9$	-
0	1.4	180	10^{-5} – 0.004027	1.40012 ± 0.00091	0 - 360	$>10^9$	-
0	1.5	0	10^{-5} – 0.009186	1.49858 ± 0.00142	0 - 360	$>10^9$	-
0	1.5	180	10^{-5} – 0.008615	1.50025 ± 0.00142	0 - 360	$>10^9$	-
0	1.6	0	10^{-5} – 0.034789	1.59705 ± 0.00295	100 - 260	$>10^9$	-
0	1.6	180	10^{-5} – 0.035601	1.59967 ± 0.00300	0 - 360	$>10^9$	-
0	1.7	0	10^{-5} – 0.030925	1.69599 ± 0.00401	140 - 220	$>10^9$	-
0	1.7	180	10^{-5} – 0.031973	1.70021 ± 0.00410	150 - 210	$>10^9$	-
0	1.8	0	10^{-5} – 0.011761	1.79503 ± 0.00509	120 - 240	$>10^9$	-
0	1.8	180	10^{-5} – 0.018040	1.80192 ± 0.00547	150 - 210	$>10^9$	-
0	1.9	0	10^{-5} – 0.016687	1.89198 ± 0.00802	140 - 220	$>10^9$	-
0	1.9	180	10^{-5} – 0.024278	1.90347 ± 0.00906	150 - 210	$>10^9$	-
0	2.0	0	10^{-5} – 0.088900	1.97348 ± 0.02652	160 - 200	$>10^9$	-
0	2.0	180	10^{-5} – 0.120915	1.98087 ± 0.04037	160 - 200	$>10^9$	-
0	2.1	0	10^{-5}	2.1	-	0.003	ce
0	2.1	180	10^{-5}	2.1	-	4.947	ce
0.14	0.7	0	10^{-5} – 0.107322	0.69995 ± 0.00005	± 90*	$>10^9$	-
0.14	0.7	180	10^{-5} – 0.107122	0.69998 ± 0.00005	± 100*	$>10^9$	-
0.14	0.8	0	10^{-5} – 0.114842	0.79990 ± 0.00010	± 100*	$>10^9$	-
0.14	0.8	180	10^{-5} – 0.114525	0.79998 ± 0.00010	± 90*	$>10^9$	-
0.14	0.9	0	10^{-5} – 0.125010	0.89983 ± 0.00017	± 100*	$>10^9$	-
0.14	0.9	180	10^{-5} – 0.124861	0.89997 ± 0.00017	± 100*	$>10^9$	-
0.14	1.0	0	10^{-5} – 0.135969	0.99966 ± 0.00034	± 100*	$>10^9$	-
0.14	1.0	180	10^{-5} – 0.134082	0.99996 ± 0.00034	± 90*	$>10^9$	-
0.14	1.1	0	10^{-5} – 0.148153	1.09948 ± 0.00052	± 100*	$>10^9$	-
0.14	1.1	180	10^{-5} – 0.147033	1.09998 ± 0.00051	± 90*	$>10^9$	-
0.14	1.2	0	10^{-5} – 0.152636	1.19894 ± 0.00106	± 100*	$>10^9$	-
0.14	1.2	180	10^{-5} – 0.147269	1.20000 ± 0.00102	± 90*	$>10^9$	-
0.14	1.3	0	10^{-5} – 0.184591	1.29853 ± 0.00147	± 90*	$>10^9$	-
0.14	1.3	180	10^{-5} – 0.187741	1.29980 ± 0.00147	± 100*	$>10^9$	-
0.14	1.4	0	10^{-5} – 0.197111	1.39666 ± 0.00334	± 100*	$>10^9$	-
0.14	1.4	180	10^{-5} – 0.197268	1.39909 ± 0.00345	± 100*	$>10^9$	-
0.14	1.5	0	10^{-5} – 0.204329	1.49613 ± 0.00387	± 100*	$>10^9$	-
0.14	1.5	180	10^{-5} – 0.197837	1.50056 ± 0.00393	± 90*	$>10^9$	-
0.14	1.6	0	10^{-5} – 0.201793	1.58943 ± 0.01056	± 110*	$>10^9$	-
0.14	1.6	180	10^{-5} – 0.153179	1.60180 ± 0.00961	± 90*	$>10^9$	-
0.14	1.7	0	10^{-5} – 0.221941	1.69339 ± 0.01263	± 80*	$>10^9$	-
0.14	1.7	180	10^{-5} – 0.037228	1.69169 ± 0.01002	–	18.841	ce
0.14	1.8	0	10^{-5}	1.8	–	0.003	ce
0.14	1.8	180	10^{-5}	1.8	–	7.708	ce
0.28	0.7	0	10^{-5} – 0.233718	0.69988 ± 0.00012	± 100*	$>10^9$	-
0.28	0.7	180	10^{-5} – 0.232762	0.69997 ± 0.00012	± 90*	$>10^9$	-
0.28	0.8	0	10^{-5} – 0.246661	0.79978 ± 0.00022	± 90*	$>10^9$	-
0.28	0.8	180	10^{-5} – 0.246837	0.79994 ± 0.00021	± 90*	$>10^9$	-

Starting Parameters			Parameter variation during a run			t / years	O
Giant e	E-M a / AU	$\Delta\varpi(0)$/°	Earth-Moon e	Earth-Moon a / AU	$\Delta\varpi$/°		
0.28	0.9	0	10^{-5} – 0.264826	0.89962 ± 0.00056	± 90*	$>10^9$	-
0.28	0.9	180	10^{-5} – 0.267871	0.89982 ± 0.00055	± 100*	$>10^9$	-
0.28	1.0	0	10^{-5} – 0.284248	0.99903 ± 0.00097	± 100*	$>10^9$	-
0.28	1.0	180	10^{-5} – 0.279454	0.99997 ± 0.00097	± 90*	$>10^9$	-
0.28	1.1	0	10^{-5} – 0.321646	1.09863 ± 0.00137	± 100*	$>10^9$	-
0.28	1.1	180	10^{-5} – 0.322328	1.09956 ± 0.00138	± 100*	$>10^9$	-
0.28	1.2	0	10^{-5} – 0.334178	1.19688 ± 0.00312	± 100*	$>10^9$	-
0.28	1.2	180	10^{-5} – 0.321600	1.20026 ± 0.00280	± 90*	$>10^9$	-
0.28	1.3	0	10^{-5} – 0.393050	1.29546 ± 0.00453	± 80*	$>10^9$	-
0.28	1.3	180	10^{-5} – 0.403962	1.30014 ± 0.00418	± 100*	$>10^9$	-
0.28	1.4	0	10^{-5}	1.4	–	0.001	ce
0.28	1.4	180	10^{-5}	1.4	–	3.642	ce

Table 4.5 Orbital runs for an Earth-Moon planet in the habitable zone of τ^1 Gruis in the presence of a 1.5 times minimum mass giant ($1.84M_J$) at 2.6AU and $e = 0.14$.

Starting Parameters		Parameter variation during a run			t / years	O
E-M a / AU	$\Delta\varpi(0)$/°	Earth-Moon e	Earth-Moon a / AU	$\Delta\varpi$/°		
0.7	0	10^{-5} – 0.114478	0.69999 ± 0.00001	± 100*	$>10^9$	-
0.7	180	10^{-5} – 0.114148	0.69998 ± 0.00008	± 100*	$>10^9$	-
0.8	0	10^{-5} – 0.118157	0.79986 ± 0.00014	± 100*	$>10^9$	-
0.8	180	10^{-5} – 0.117653	0.79997 ± 0.00014	± 90*	$>10^9$	-
0.9	0	10^{-5} – 0.126620	0.89974 ± 0.00026	± 100*	$>10^9$	-
0.9	180	10^{-5} – 0.126349	0.89995 ± 0.00026	± 90*	$>10^9$	-
1.0	0	10^{-5} – 0.136496	0.99948 ± 0.00052	± 100*	$>10^9$	-
1.0	180	10^{-5} – 0.133721	0.99994 ± 0.00050	± 90*	$>10^9$	-
1.1	0	10^{-5} – 0.148347	1.09992 ± 0.00078	± 100*	$>10^9$	-
1.1	180	10^{-5} – 0.146618	1.09998 ± 0.00077	± 90*	$>10^9$	-
1.2	0	10^{-5} – 0.149118	1.19841 ± 0.00159	± 120*	$>10^9$	-
1.2	180	10^{-5} – 0.140811	1.20000 ± 0.00151	± 90*	$>10^9$	-
1.3	0	10^{-5} – 0.189934	1.29778 ± 0.00222	± 90*	$>10^9$	-
1.3	180	10^{-5} – 0.194630	1.29968 ± 0.00224	± 100*	$>10^9$	-
1.4	0	10^{-5} – 0.201447	1.39518 ± 0.00481	± 100*	$>10^9$	-
1.4	180	10^{-5} – 0.202092	1.39869 ± 0.00513	± 100*	$>10^9$	-
1.5	0	10^{-5} – 0.207774	1.49428 ± 0.00572	± 120*	$>10^9$	-
1.5, inclined 10°	0	10^{-5} – 0.207715	1.49454 ± 0.00546	0 – 360	$>10^9$	-
1.5	180	10^{-5} – 0.197992	1.50086 ± 0.00582	± 90*	$>10^9$	-
1.6	0	10^{-5} – 0.208080	1.58509 ± 0.01491	± 120*	$>10^9$	-
1.6, inclined 10°	0	10^{-5} – 0.202604	1.58570 ± 0.01430	0 – 360	$>10^9$	-
1.6	180	10^{-5} – 0.141116	1.60151 ± 0.01254	± 90*	$>10^9$	-
1.7	0	10^{-5}	1.7	-	0.002	ce
1.7, inclined 10°	0	10^{-5}	1.7	-	0.002	ce
1.7	180	10^{-5}	1.7	-	14.615	ce

A third study was undertaken of mean motion resonance between the two planets. This is when the Earth-Moon's orbital period is a simple fraction of that of the outer giant. This was a search for regions of instability at distances from the star where orbits would normally be expected to be stable, as is the case for regions of instability within the asteroid belt in the solar system, caused by resonance effects with Jupiter.

Table 4.6 Orbital resonance runs for an Earth-Moon planet in the habitable zone of τ^1 Gruis in the presence of the minimum mass giant ($1.23M_J$) at 2.6AU with an orbital eccentricity of 0.14.

Start Parameters			Parameter variation during a run			*t / years*	*O*
r	**E-M *a* / AU**	**$\Delta\varpi(0)$/°**	**Earth-Moon *e***	**Earth-Moon *a* / AU**	**$\Delta\varpi$/°**		
2	1.6379	0	10^{-5} – 0.218077	1.61696 ± 0.02094	± 120*	$>10^9$	-
2	1.6379	180	10^{-5} – 0.330311	1.63770 ± 0.03397	± 150*	$>10^9$	-
2.5	1.41149716	0	10^{-5} – 0.226943	1.40604 ± 0.00546	± 110*	$>10^9$	-
2.5	1.41149716	180	10^{-5} – 0.244101	1.40917 ± 0.00737	± 100*	9.361×10^6	ce
3	1.245	180	10^{-5} – 0.043128	1.24486 ± 0.00140	± 90*	$>10^9$	-
3	1.2486	180	10^{-5} – 0.065844	1.24694 ± 0.00296	± 100*	$>10^9$	-
3	1.2487	180	10^{-5} – 0.063792	1.24687 ± 0.00274	± 90*	$>10^9$	-
3	1.2488	180	10^{-5} – 0.062525	1.24687 ± 0.00263	± 100*	$>10^9$	-
3	1.2489	180	10^{-5} – 0.063232	1.24696 ± 0.00276	± 100*	$>10^9$	-
3	1.2490	0	10^{-5} – 0.094400	1.24496 ± 0.00404	± 120*	$>10^9$	-
3	1.2490	180	10^{-5} – 0.064195	1.24705 ± 0.00294	± 110*	$>10^9$	-
3	1.2491	180	10^{-5} – 0.182755	1.24878 ± 0.00674	0 – 360	9.580×10^7	ce
3	1.2492	180	10^{-5} – 0.193210	1.24918 ± 0.00729	0 – 360	7.983×10^7	ce
3	1.2493	180	10^{-5} – 0.193342	1.24903 ± 0.00730	± 110*	2.218×10^8	ce
3	1.2494	180	10^{-5} – 0.195834	1.24918 ± 0.00693	± 100*	5.442×10^7	ce
3	1.2495	180	10^{-5} – 0.193249	1.24907 ± 0.00681	0 – 360	1.580×10^7	ce
3	1.2496	180	10^{-5} – 0.183615	1.24890 ± 0.00699	0 – 360	7.686×10^7	ce
3	1.2497	180	10^{-5} – 0.194250	1.24866 ± 0.00611	0 – 360	1.104×10^7	ce
3	1.2498	180	10^{-5} – 0.201588	1.24870 ± 0.00691	± 120*	3.172×10^7	ce
3	1.2499	180	10^{-5} – 0.181811	1.24926 ± 0.00714	0 – 360	2.266×10^7	ce
3	1.24995	0	10^{-5} – 0.097791	1.24542 ± 0.00453	± 120*	$>10^9$	-
3	1.24995	180	10^{-5} – 0.181096	1.24883 ± 0.00706	± 70*	1.097×10^8	ce
3	1.25	0	10^{-5} – 0.097905	1.24543 ± 0.00457	± 120*	$>10^9$	-
3	1.25	180	10^{-5} – 0.194152	1.24883 ± 0.00668	0 – 360	1.672×10^7	ce
3	1.2501	180	10^{-5} – 0.195076	1.24925 ± 0.00709	0 – 360	5.344×10^7	ce
3	1.2502	180	10^{-5} – 0.190571	1.24896 ± 0.00753	± 110*	1.271×10^8	ce
3	1.2503	180	10^{-5} – 0.193210	1.24904 ± 0.00742	± 120*	6.055×10^8	ce
3	1.2504	180	10^{-5} – 0.187097	1.24897 ± 0.00712	± 120*	3.178×10^8	ce
3	1.2505	180	10^{-5} – 0.188622	1.24907 ± 0.00729	± 110*	2.110×10^8	ce
3	1.2506	180	10^{-5} – 0.184171	1.24890 ± 0.00711	± 120*	1.549×10^8	ce
3	1.2507	180	10^{-5} – 0.183177	1.24892 ± 0.00747	0 – 360	$>10^9$	-
3	1.2508	180	10^{-5} – 0.179605	1.24888 ± 0.00749	0 – 360	$>10^9$	-
3	1.2509	180	10^{-5} – 0.177213	1.24889 ± 0.00749	0 – 360	$>10^9$	-
3	1.251	0	10^{-5} – 0.102874	1.24589 ± 0.00511	± 120*	$>10^9$	-
3	1.251	180	10^{-5} – 0.170234	1.24895 ± 0.00724	0 – 360	$>10^9$	-
3	1.255	180	10^{-5} – 0.156189	1.24884 ± 0.00928	0 – 360	$>10^9$	-
3	1.26	180	10^{-5} – 0.193507	1.25883 ± 0.00365	± 110*	$>10^9$	-
3.5	1.1278759	0	10^{-5} – 0.156484	1.12684 ± 0.00104	± 110*	$>10^9$	-
3.5	1.1278759	180	10^{-5} – 0.151966	1.12836 ± 0.00092	± 90*	$>10^9$	-
4	1.03181	0	10^{-5} – 0.128379	1.03127 ± 0.00299	0 – 360	$>10^9$	-
4	1.03181	180	10^{-5} – 0.066470	1.03114 ± 0.00159	0 – 360	$>10^9$	-
4.5	0.95389	0	10^{-5} – 0.131109	0.95372 ± 0.00028	± 90*	$>10^9$	-
4.5	0.95389	180	10^{-5} – 0.130283	0.95389 ± 0.00024	± 90*	$>10^9$	-
5	0.8891875	0	10^{-5} – 0.168027	0.88888 ± 0.00096	± 130*	$>10^9$	-
5	0.8891875	180	10^{-5} – 0.159414	0.88887 ± 0.00087	0 – 360	$>10^9$	-
5.5	0.834446	0	10^{-5} – 0.118475	0.83433 ± 0.00012	± 90*	$>10^9$	-
5.5	0.834446	180	10^{-5} – 0.117989	0.83442 ± 0.00012	± 90*	$>10^9$	-
6	0.787419	0	10^{-5} – 0.138894	0.78715 ± 0.00042	± 120*	$>10^9$	-
6	0.787419	180	10^{-5} – 0.140751	0.78717 ± 0.00041	0 – 360	$>10^9$	-
6.5	0.746500	0	10^{-5} – 0.110437	0.74643 ± 0.00007	± 90*	$>10^9$	-
6.5	0.746500	180	10^{-5} – 0.110161	0.74648 ± 0.00007	± 90*	$>10^9$	-
7	0.7105713	0	10^{-5} – 0.106846	0.71052 ± 0.00007	± 90*	$>10^9$	-
7	0.7105713	180	10^{-5} – 0.107287	0.71049 ± 0.00007	± 100*	$>10^9$	-

Table 4.6 reveals the outcomes of Earth-Moons launched at distances from the star such that it orbits from twice to seven times, at half orbit intervals, whilst the giant orbits once. All runs started with $\Delta\varpi(0) = 0^{O}$ last the duration of the 1Gyr integration. Of those started with $\Delta\varpi(0) = 180°$, only two did not last the full 1Gyr, those being the 5:2 and 3:1 resonance runs. The width of the unstable region at the 3:1 resonance was then determined by launching Earth-Moons at successive distances from the star starting from 1.245AU, through the resonance distance at 1.24995AU and finishing at 1.26AU, with distances differing by 10^{-4}AU at the finest resolution. Figure 4.7 shows the outcome of this investigation, revealing an unstable region from 1.2490AU to 1.2508AU, equivalent to 270,000km or less than 0.15% its distance from the star. This is centred at 1.2499AU, just inside the actual resonance position by 0.00005AU (7,500km) or approximately one Earth radius. This clearly shows the tiny region where this instability occurs. Figure 4.8 shows the distances at which the Earth-Moon orbits settled for each of their starting distances. They tend towards a distance at 1.249AU, just less than that of the resonance, when originally launched between 1.249AU and 1.251AU of this position. This implies that the unstable resonance region may be narrower than figure 4.7 originally suggests. Clearly this is an opportunity for further study beyond the scope of this thesis.

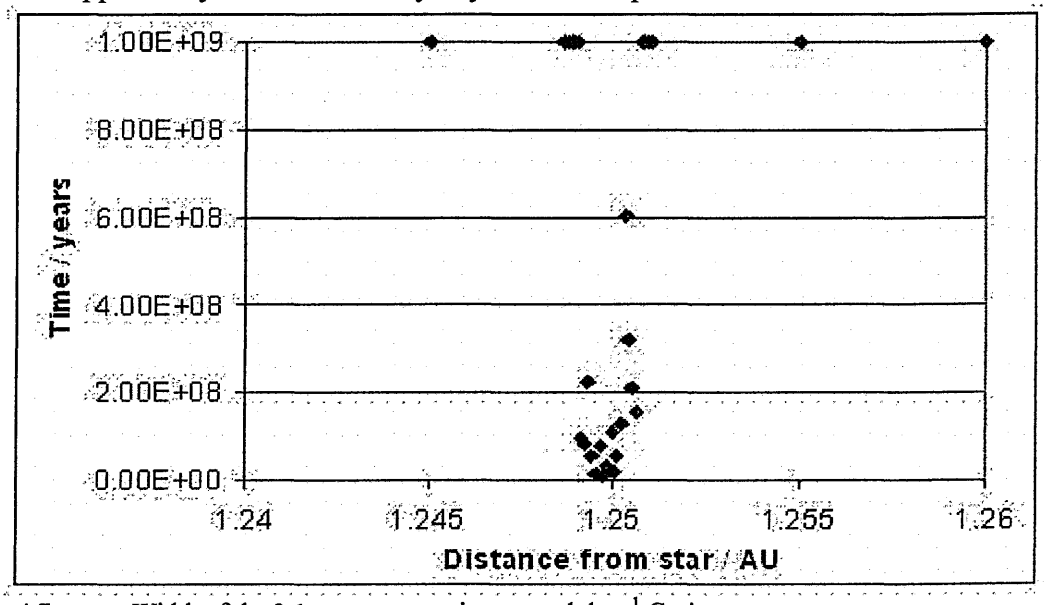

Figure 4.7 Width of the 3:1 resonance region around the τ^{1} Gruis system.

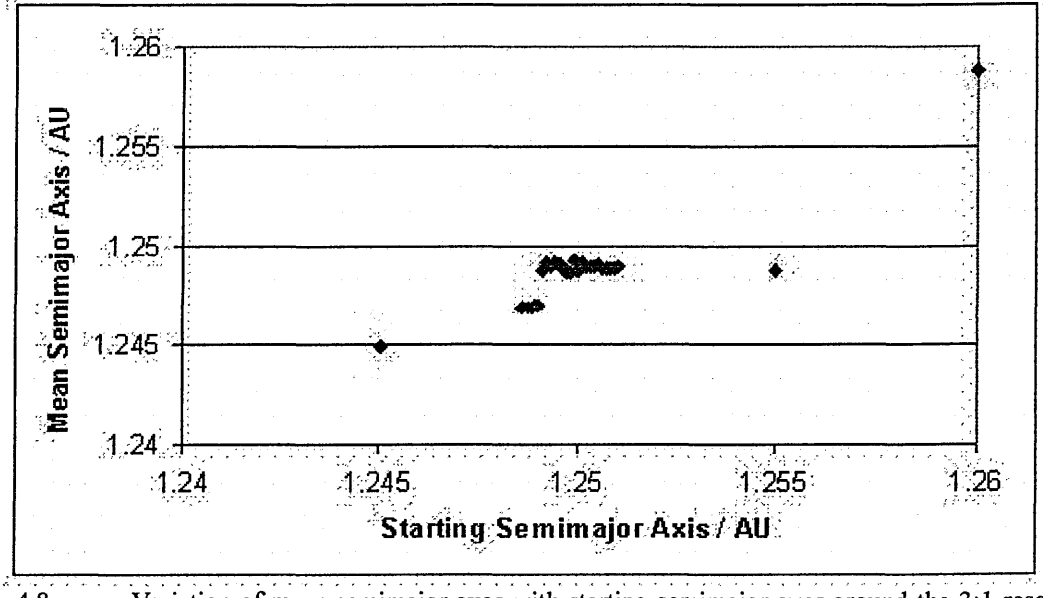

Figure 4.8 Variation of mean semimajor axes with starting semimajor axes around the 3:1 resonance region in the τ^{1} Gruis system.

A final investigation was carried out for the Earth-Moon integrations at 1.7AU with a minimum mass giant with an orbital eccentricity 0.14, which gave two very different results. When $\Delta\varpi(0) = 180°$, the terrestrial planet's orbit lasted 18.841 years, when $\Delta\varpi(0) = 0°$ the orbit remained stable and confined for more than 6.28Gyr, longer than the main sequence lifetime of the star. This difference was the result of the first configuration causing the terrestrial planet to pass closer to the giant when its apastron longitude was almost coincident with the giant's periastron longitude, hence the slight instability required to take it within 3 Hill radii of the giant in a very short time. In the second case, reducing the interval between data output to 1,000 years instead of the usual 100,000, revealed the Earth-Moon had caused the giant's periastron longitude to precess at a constant rate, taking 2.964Myr for one revolution, setting up an intricate libration of periastron longitudes between itself and the giant, resulting in stability. The blue line in Figure 4.9 shows the precession of the giant surrounded by the red perihelia longitudes of the terrestrial planet. The libration of the Earth-Moon periastron longitude oscillated mainly $\pm 50^{O}$ either side of the giant's, where a further reduction in data output intervals to one year, showed a slow move forward over ~1,200 years followed by a more rapid swing back over ~400 years, see Figure 4.10. This coincided with large and regular oscillatory changes in the eccentricity of the terrestrial planet (Figure 4.11). The difference in periastron longitudes between the two planets has a clear effect on the orbital eccentricity range of the Earth-Moon (Figure 4.12) and may well be a contributing factor to the stability of the system. These results also show the power of the Mercury Orbital Integrator in its accuracy when predicting outcomes of Earth-Moons within planetary systems. The libration effects of the terrestrial planet seen here are similar to effects seen previously in orbital simulations of the outer two giants of υ Andromedae (Lissauer & Rivera, 2001) and are a good example of a secular resonance.

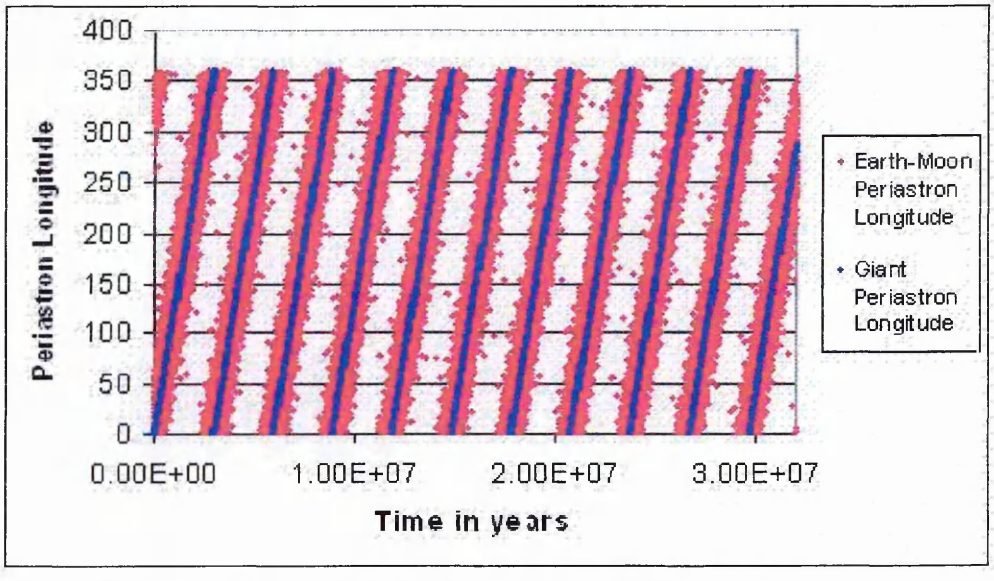

Figure 4.9 Precession of periastron longitudes (E-M, a = 1.7AU)

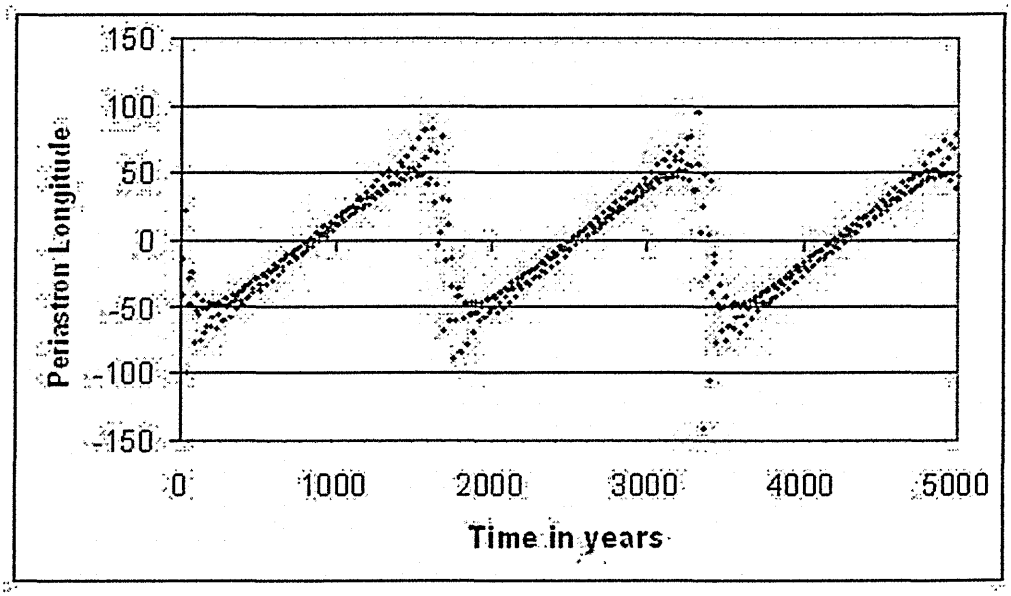

Figure 4.10. Libration of $\Delta\varpi$ (a = 1.7AU)

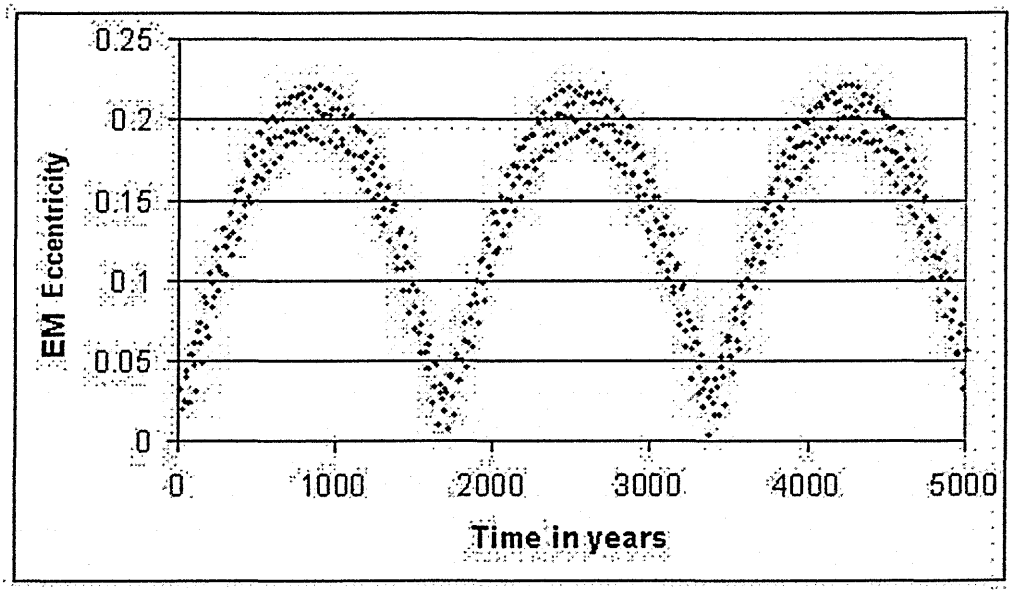

Figure 4.11. Change in Earth-Moon orbital eccentricity with time (E-M, a = 1.7AU)

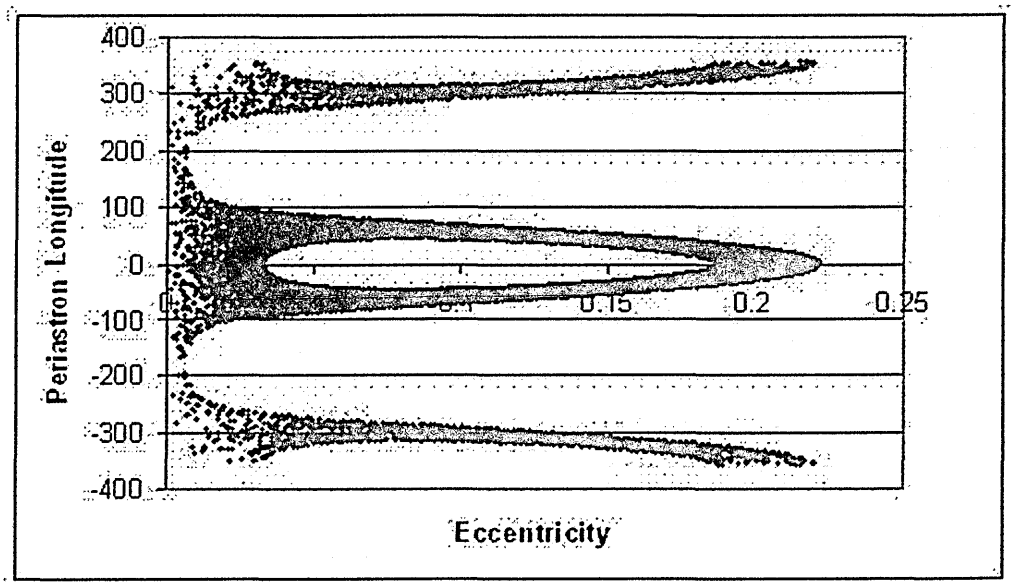

Figure 4.12. $\Delta\varpi$ v. eccentricity (a = 1.7AU)

The results indicate an Earth-Moon mass planet could exist in a confined orbit for 1Gyr about τ^1 Gruis, but only at the inner edge of the habitable zone at zero-age main sequence (Figure 4.2). The giant would have to have a low eccentricity but could be up to 1.5 times its minimum mass. The only detrimental resonance effects occurred in a narrow region around 1.25AU, when the Earth-Moon's orbital period was three times the giant's and when $\Delta\varpi(0) = 180°$. Shortly after these analyses, new observations of the star, revealed on 11/05/2003, changed the giant's mass and orbital parameters. The minimum mass is now $1.49M_J$ and the planet has a semimajor axis of 2.7AU and eccentricity of 0.34 (Schneider, 2006). Although the mass and distance changes have no effect on the trends described here, the eccentricity draws the planet right across the habitable zone making this an uninhabitable system. The findings here could possibly be of use for similar systems, yet to be discovered, and the resonance study may well be confirmed in other systems to be investigated in the future.

4.5.2 HD 196050

The orbital run details for an Earth-Moon planet within this system are listed in tables 4.7 and 4.8. As the giant planet lies on the outer edge of the present habitable zone (Figure 4.2), only inferior orbits plus a resonance study of Earth-Moon planets were investigated. Stable orbits were restricted to a narrow band between 0.75AU and 1.0AU, although orbit stability at 1.0AU was dependent on $\Delta\varpi(0)$ and was only stable for $\Delta\varpi(0) = 0$. The semimajor axes of the runs followed the same trends as those of τ^1 Gruis, i.e. Earth-Moons launched with $\Delta\varpi(0) = 0$ had a slightly less long term mean semimajor axis than those launched with $\Delta\varpi(0) = 180^O$. The causes of instabilities at 0.7AU are unknown as the orbital periods at this distance are not in any resonance with the giant, but both periastron longitude integrations had constant semimajor axes as each eccentricity grew until a close encounter within 3 Hill radii of the giant occurred. Increasing the mass of the giant to 1.5 times minimum mass made the entire region to 0.75AU of the star unsuitable for confined orbits.

The resonance investigation showed a mix of stable and unstable orbits from 7:2 to 7:1, with no obvious trends. The two runs at the 7:2 resonance may have been destabilised because they were too close to the giant, however in all other cases, orbital stability was dependent on $\Delta\varpi(0)$. A value of 0° led to stable integrations at 4:1, but unstable integrations at 5:1, 6:1 and 7:1. Their counterparts, 180°, were all stable as were all of the resonance runs for both $\Delta\varpi(0)$ values at 9:2, 11:2 and 13:2.

The outcome of this brief investigation was that Earth-Moons could exist in stable orbits inferior to the giant planet only if the giant was near its minimum mass. They would, however, be stable only inside the 1.0AU distance of the inner edge of the habitable zone. The unstable orbits in this region occur around the n:1 period resonances (where n is an integer and $4 < n < 8$) only when $\Delta\varpi(0) = 0$. The closer regular approach to the giant planet's periastron position of the terrestrial planet at apastron, caused by the 4:1 resonance, was enough to destabilise the orbit, but not so when $\Delta\varpi(0) = 0$. For a larger planet at 1.5 times minimum mass, the giant's gravitational influence would stretch across this entire region and no stable orbits would be possible at all. The outcome is that detectable life is unlikely to exist on the surface of any terrestrial planets within this system, especially as one literature age is only 1.6Gyr (Mayor et al., 2004), compared to the literature age, when the study was undertaken, of greater than 3Gyr (Jones et al., 2002).

Table 4.7 Orbital runs for an Earth-Moon planet in the habitable zone of HD 196050 in the presence of the giant planet at 2.5AU with an eccentricity of 0.28.

Starting Parameters			Parameter variation during a run			*t* / *years*	*O*
m	E-M *a* / AU	$\Delta\varpi(0)$/°	Earth-Moon *e*	Earth-Moon *a* / AU	$\Delta\varpi$/°		
1	0.7	0	10^{-5} – 0.679452	0.78682 ± 0.09133	20 - 100	1.299×10^{4}	ce
1	0.7	180	10^{-5} – 0.742235	0.72790 ± 0.09133	20 - 100	1.331×10^{4}	ce
1	0.75	0	10^{-5} – 0.289947	0.74931 ± 0.00078	± 100*	$>10^{9}$	-
1	0.75	180	10^{-5} – 0.278335	0.74987 ± 0.00080	± 90*	$>10^{9}$	-
1	0.8	0	10^{-5} – 0.285713	0.79920 ± 0.00080	± 100*	$>10^{9}$	-
1	0.8	180	10^{-5} – 0.282439	0.79980 ± 0.00080	± 100*	$>10^{9}$	-
1	0.9	0	10^{-5} – 0.289716	0.89865 ± 0.00135	± 100*	$>10^{9}$	-
1	0.9	180	10^{-5} – 0.287588	0.89983 ± 0.00134	± 100*	$>10^{9}$	-
1	1.0	0	10^{-5} – 0.204465	0.99900 ± 0.00567	± 100*	$>10^{9}$	-
1	1.0	180	10^{-5}	1.0	-	3.468×10^{4}	ce
1	1.1	0	10^{-5}	1.1	-	0.001	ce
1	1.1	180	10^{-5}	1.1	-	22.585	ce
1.5	0.75	180	10^{-5} – 0.515651	0.75491 ± 0.00793	20 - 100	6967	ce
1.5	0.75	0	10^{-5} – 0.536091	0.72813 ± 0.02321	20 - 80	7911	ce

Table 4.8 Orbital resonance runs for an Earth-Moon planet in the habitable zone of HD 196050 with the giant planet at 2.5AU and an eccentricity of 0.28.

Starting Parameters			Parameter variation during a run			*t* / *years*	*O*
r	E-M *a* / AU	$\Delta\varpi(0)$/°	Earth-Moon *e*	Earth-Moon *a* / AU	$\Delta\varpi$/°		
3.5	1.084486	0	10^{-5} – 0.372586	1.07739 ± 0.00710	± 100*	3.987×10^{7}	ce
3.5	1.084486	180	10^{-5} – 0.387705	1.08155 ± 0.00294	0 – 360	1.653×10^{5}	ce
4	0.993	0	10^{-5} – 0.162063	0.98605 ± 0.00695	± 130*	$>10^{9}$	-
4	0.993	180	10^{-5} – 0.283944	0.99036 ± 0.00653	± 100*	4.047×10^{7}	ce
4	0.9921266	0	10^{-5} – 0.161457	0.98560 ± 0.00958	0 – 360	$>10^{9}$	-
4	0.9921266	180	10^{-5} – 0.268618	0.99043 ± 0.00958	0 – 360	7.964×10^{6}	ce
4	0.992	0	10^{-5} – 0.161251	0.98556 ± 0.00644	± 100*	$>10^{9}$	-
4	0.992	180	10^{-5} – 0.262232	0.99099 ± 0.00942	0 – 360	1.487×10^{7}	ce
4.5	0.9172	0	10^{-5} – 0.309187	0.91468 ± 0.00252	± 100*	$>10^{9}$	-
4.5	0.9172	180	10^{-5} – 0.301787	0.91838 ± 0.00218	± 90*	$>10^{9}$	-
5	0.856	0	10^{-5} – 0.305843	0.85422 ± 0.00592	0 – 360	1.045×10^{8}	ce
5	0.856	180	10^{-5} – 0.112413	0.85384 ± 0.00403	0 – 360	$>10^{9}$	-
5	0.855	0	10^{-5} – 0.3093661	0.85401 ± 0.00622	0 – 360	9.481×10^{8}	ce
5	0.855	180	10^{-5} – 0.112294	0.85373 ± 0.00366	0 – 360	$>10^{9}$	-
5	0.854988	0	10^{-5} – 0.309693	0.85405 ± 0.00451	0 – 360	1.972×10^{6}	ce
5	0.854988	180	10^{-5} – 0.113645	0.85373 ± 0.00369	0 – 360	$>10^{9}$	-
5	0.854	0	10^{-5} – 0.125599	0.85169 ± 0.00282	± 100*	$>10^{9}$	-
5	0.854	180	10^{-5} – 0.052917	0.85297 ± 0.00164	± 110*	$>10^{9}$	-
5.5	0.802359	0	10^{-5} – 0.291080	0.80127 ± 0.00109	± 110*	$>10^{9}$	-
5.5	0.802359	180	10^{-5} – 0.281495	0.80253 ± 0.00080	± 90*	$>10^{9}$	-
6	0.7571336	0	10^{-5} – 0.354543	0.75639 ± 0.00302	0 – 360	4.079×10^{7}	ce
6	0.7571336	180	10^{-5} – 0.098519	0.75630 ± 0.00204	0 – 360	$>10^{9}$	-
6.5	0.71779	0	10^{-5} – 0.313536	0.71746 ± 0.00041	± 100*	$>10^{9}$	-
6.5	0.71779	180	10^{-5} – 0.309237	0.71773 ± 0.00041	± 90*	$>10^{9}$	-
7	0.6831897	0	10^{-5}	0.6831897	-	1.558×10^{4}	ce
7	0.6831897	180	10^{-5} – 0.030159	0.68250 ± 0.00079	0 – 360	$>10^{9}$	-

4.5.3 HD 52265

A detailed listing of the terrestrial planet's orbital runs within this system, are in table 4.9. Orbits within 0.9AU are unstable due to their proximity to the giant. At 0.9AU for a minimum mass giant, the planet's orbital stability is dependent on $\Delta\varpi(0)$. Figure 4.13 shows the stable E-M orbit, which lasts longer than 1Gyr and the unstable orbit lasting just 22.8Myr before a close encounter between it and the giant. The diagram also illustrates the nature of eccentricity variation between stable and unstable orbits. Stable orbits usually have eccentricities that change by only small amounts, whereas unstable ones have eccentricities that often fluctuate wildly. The semimajor axis, though, is usually constant for stable and unstable orbits until a cataclysmic termination event occurs.

Since the giant planet lies interior to the habitable zone, all of the Earth-Moon's investigated orbits were in superior orbits. The giant's gravitational influence extends to ~0.95AU from the star, at and beyond which, all orbits are stable, compared to the theoretical limit of 0.89AU as determined by equation 4.3. For higher giant masses, table 4.9 shows the gravitational influence slowly extends to ~1.1AU for an 8 times minimum mass planet (1.15AU according to equation 4.3). This is still interior to the current inner habitable zone limit of the system, hence this would be a good candidate for housing a habitable Earth-mass planet, provided it survived the inward migration of the giant (Mandell & Sigurdsson, 2003 and Fogg & Nelson, 2005). All semimajor axes of stable orbits oscillate about their starting distance with no perceptible trend with increasing values. Their pumped up eccentricities vary rapidly between their starting and maximum values, where variation shows a weak trend decreasing with increasing semimajor axis.

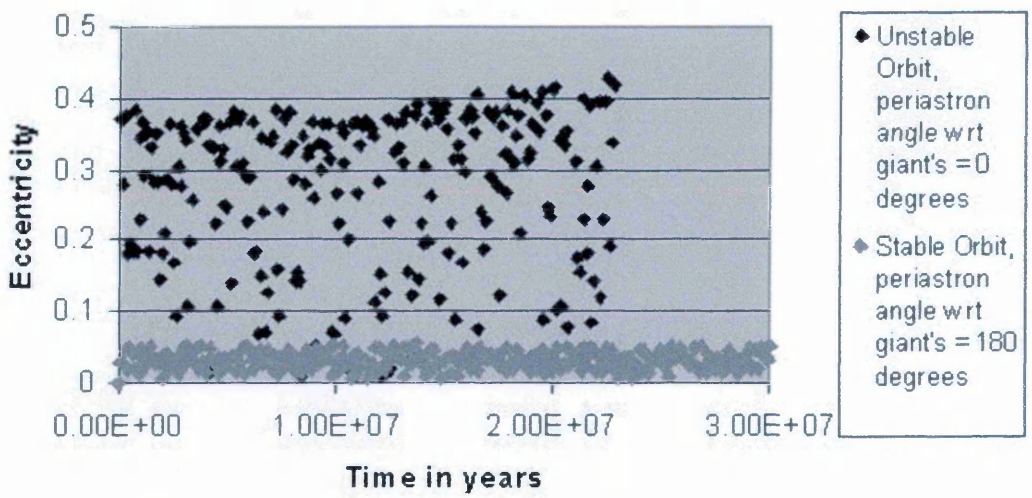

Figure 4.13. Stability comparison of two orbits around HD 52265, each of semimajor axis 0.9AU but with different $\Delta\varpi(0)$.

The resonance study, results shown in table 4.10 revealed instabilities at 2:1 and 5:2 orbital period resonance and both were periastron longitude dependent. Stable orbits occurred at 0.77783AU (2:1) for $\Delta\varpi(0) = 180°$, which is surprising considering its proximity to the giant. There is clearly a resonance stabilising effect here possibly due to tidal effects caused by the combined gravitational attraction of the giant planet and the star. The 5:2 resonance distance at 0.90259AU is very close to the orbital run at 0.9AU and shows similar trends. The instabilities at the 5:2 resonance and 0.9AU are most likely to be due to the regular and slightly closer approach of the terrestrial planet when at periastron corresponding to when the giant is at apastron.

Table 4.9 Orbital runs for an Earth-Moon planet in the habitable zone of HD 52265 with the giant planet at 0.49AU with an eccentricity of 0.29.

Start Parameters			Parameter variation during a run			*t* / *years*	*O*
m	E-M *a* / AU	$\Delta\varpi(0)$/°	Earth-Moon *e*	Earth-Moon *a* / AU	$\Delta\varpi$/°		
1	0.8	0	10^{-5}	0.8	-	348.2	ce
1	0.8	180	10^{-5}	0.8	-	149.4	ce
1	0.85	0	10^{-5} – 0.110245	0.84190 ± 0.00810	0 – 360	9.449×10^{5}	ce
1	0.85	180	10^{-5} – 0.403628	0.85955 ± 0.00955	0 – 360	1.192×10^{6}	ce
1	0.9	0	10^{-5} – 0.054844	0.90440 ± 0.01540	90 – 270	$>10^{9}$	-
1	0.9	180	10^{-5} – 0.430162	0.90410 ± 0.01590	± 100*	2.285×10^{7}	ce
1	0.95	0	10^{-5} – 0.140937	0.94415 ± 0.00665	70 – 290	$>10^{9}$	-
1	0.95	180	10^{-5} – 0.364881	0.95515 ± 0.00725	± 100*	$>10^{9}$	-
1	1.0	0	10^{-5} – 0.321610	0.99235 ± 0.00855	± 90*	$>10^{9}$	-
1	1.0	180	10^{-5} – 0.350930	1.02195 ± 0.02495	0 – 360	$>10^{9}$	-
1	1.1	0	10^{-5} – 0.297425	1.09690 ± 0.00710	± 110*	$>10^{9}$	-
1	1.1	180	10^{-5} – 0.292378	1.10525 ± 0.00695	± 100*	$>10^{9}$	-
1.5	0.8	0	10^{-5}	0.8	-	172	ce
1.5	0.8	180	10^{-5}	0.8	-	84.6	ce
1.5	0.9	0	10^{-5}	0.9	-	1.243×10^{4}	ce
1.5	0.9	180	10^{-5} – 0.390835	0.90340 ± 0.01340	0 – 360	6.928×10^{5}	ce
1.5	1.0	0	10^{-5} – 0.329699	0.98910 ± 0.01220	± 100*	$>10^{9}$	-
1.5	1.0	180	10^{-5} – 0.229272	1.02365 ± 0.02475	± 100*	$>10^{9}$	-
1.5	1.1	0	10^{-5} – 0.297274	1.09575 ± 0.01065	± 110*	$>10^{9}$	-
1.5	1.1	180	10^{-5} – 0.288712	1.10795 ± 0.01025	± 110*	$>10^{9}$	-
1.5	1.2	0	10^{-5} – 0.274038	1.19360 ± 0.01050	± 110*	$>10^{9}$	-
1.5	1.2	180	10^{-5} – 0.254980	1.20940 ± 0.01090	± 110*	$>10^{9}$	-
2	0.8	0	10^{-5}	0.8	-	711	ce
2	0.8	180	10^{-5}	0.8	-	61.1	ce
2	0.9	0	10^{-5}	0.9	-	1124	ce
2	0.9	180	10^{-5} – 0.414276	0.90935 ± 0.01995	± 90*	2.563×10^{6}	ce
2	1.0	0	10^{-5} – 0.339992	0.98585 ± 0.01565	± 100*	$>10^{9}$	-
2	1.0	180	10^{-5} – 0.228969	1.02520 ± 0.02640	0 – 360	$>10^{9}$	-
2	1.1	0	10^{-5} – 0.295805	1.09430 ± 0.01410	± 120*	$>10^{9}$	-
2	1.1	180	10^{-5} – 0.286175	1.11075 ± 0.01365	± 100*	$>10^{9}$	-
3	0.8	0	10^{-5}	0.8	-	50.6	ce
3	0.8	180	10^{-5}	0.8	-	39.2	ce
3	0.9	0	10^{-5}	0.9	-	312	ce
3	0.9	180	10^{-5}	0.9	-	1.735×10^{4}	ce
3	1.0	0	10^{-5} – 0.364210	0.98015 ± 0.02285	± 90*	$>10^{9}$	-
3	1.0	180	10^{-5} – 0.225929	1.02825 ± 0.02915	± 130*	$>10^{9}$	-
3	1.1	0	10^{-5} – 0.295436	1.09240 ± 0.02160	± 110*	$>10^{9}$	-
3	1.1	180	10^{-5} – 0.282615	1.11625 ± 0.2025	± 110*	$>10^{9}$	-
4	0.8	0	10^{-5}	0.8	-	1194	ce
4	0.8	180	10^{-5}	0.8	-	37.8	ce
4	0.9	0	10^{-5}	0.9	-	278	ce
4	0.9	180	10^{-5}	0.9	-	224	ce
4	1.0	0	10^{-5}	1.0	-	4621	ce
4	1.0	180	10^{-5} – 0.223174	1.03150 ± 0.03190	0 – 360	$>10^{9}$	-
4	1.1	0	10^{-5} – 0.296882	1.09085 ± 0.02915	± 120*	$>10^{9}$	-
4	1.1	180	10^{-5} – 0.281205	1.12205 ± 0.02685	± 100*	$>10^{9}$	-
6	0.9	0	10^{-5}	0.9	-	66.2	ce
6	0.9	180	10^{-5}	0.9	-	47.6	ce
6	1.0	0	10^{-5}	1.0	-	5157	ce
6	1.0	180	10^{-5} – 0.216563	1.03750 ± 0.03750	0 – 360	$>10^{9}$	-
6	1.1	0	10^{-5} – 0.315529	1.09080 ± 0.04710	0 – 360	$>10^{9}$	-
6	1.1	180	10^{-5} – 0.281560	1.13360 ± 0.03980	± 120*	$>10^{9}$	-
8	0.9	0	10^{-5}	0.9	-	6.97	ce
8	0.9	180	10^{-5}	0.9	-	18.3	ce
8	1.0	0	10^{-5}	1.0	-	760.7	ce
8	1.0	180	10^{-5} – 0.225262	1.04375 ± 0.04375	0 – 360	$>10^{9}$	-
8	1.1	0	10^{-5}	1.1	-	6.779×10^{5}	ce
8	1.1	180	10^{-5} – 0.284350	1.14435 ± 0.05315	± 120*	$>10^{9}$	-
8	1.2	0	10^{-5} – 0.328517	1.17460 ± 0.05710	0 – 360	$>10^{9}$	-
8	1.2	180	10^{-5} – 0.219175	1.26225 ± 0.06225	0 – 360	$>10^{9}$	-

Table 4.10 Orbital resonance runs for an Earth-Moon planet in the habitable zone of HD 52265 with the giant planet at 0.49AU and an eccentricity of 0.29.

Start Parameters			Parameter variation during a run			*t / years*	*O*
r	E-M *a* / AU	$\Delta\varpi(0)$/°	Earth-Moon *e*	Earth-Moon *a* / AU	$\Delta\varpi$/°		
1.5	0.64208	0	10^{-5}	0.64208	-	216	ce
1.5	0.64208	180	10^{-5}	0.64208	-	0.484	ce
2	0.77783	0	10^{-5}	0.77783	-	482	ce
2	0.77783	180	10^{-5} – 0.573999	0.78005 ± 0.00895	0 – 360	$>10^9$	-
2.5	0.90259	0	10^{-5} – 0.388353	0.90450 ± 0.01260	± 110*	$>10^9$	-
2.5	0.90259	180	10^{-5} – 0.408870	0.90500 ± 0.01720	± 120*	3.592×10^8	ce
3	1.01924	0	10^{-5} – 0.238411	1.00880 ± 0.01170	± 80*	$>10^9$	-
3	1.01924	180	10^{-5} – 0.172071	1.02425 ± 0.01015	± 90*	$>10^9$	-
3.5	1.12956	0	10^{-5} – 0.295297	1.12630 ± 0.00680	± 110*	$>10^9$	-
3.5	1.12956	180	10^{-5} – 0.289615	1.13550 ± 0.00680	± 110*	$>10^9$	-
4	1.23472	0	10^{-5} – 0.288458	1.23945 ± 0.00710	0 – 360	$>10^9$	-
4	1.23472	180	10^{-5} – 0.131547	1.23740 ± 0.00960	± 110*	$>10^9$	-

5. Modelling 55 Cancri with Three Giants

5.1 System Characteristics

This study uses the Mercury Orbital Integrator, as outlined at the beginning of chapter 4 in the single giant system investigations. It is based on the system characteristics of 55 Cancri as published on the Schneider Exoplanet web site on 24th January, 2004 (Marcy, 2002). First inspection of these characteristics revealed a discrepancy in the literature mass of the star. Although quoted as $1.03M_{\odot}$, a simple calculation of its mass from the semimajor axes and orbital periods of the planets from table 5.1 indicated the mass to be less. Rearranging Newton's Law of Gravitation gives,

$$\frac{M_*}{M_{\odot}} = \frac{a^3}{P^2} \qquad 5.1.$$

Here M is the stellar mass, $M_{\odot}$ is solar mass, a is the planet's semimajor axis in astronomical units and P is the planet's orbital period in years. The data for the planets 55 Cancri b, c and d gives a stellar mass of $0.945M_{\odot}$, $0.953M_{\odot}$ and $0.954M_{\odot}$ respectively. The mean of these is 0.95 $M_{\odot}$, in agreement with Marcy et al., 2002, and orbital integrations for this system were carried out on both masses, with the majority on the lesser. Hence table 5.1 shows the orbital properties of the planets of 55 Cancri plus their gravitational reaches (with the Hill radius multipliers calculated from equations 4.2 and 4.3) for both the published and recalculated masses. Figure 5.1 gives a diagrammatical representation of the orbital extremes of each of the giants and their gravitational reach overlaying the outward movement of the habitable zone for a $0.95M_{\odot}$ star, as determined by the second Mazzitelli model, with the star's present age revealed at 5Gyr. The diagram shows the HZ to be free of any giant planet gravitational perturbation effects; the planet distances on the y-axis are logarithmic to enhance the detail of the inner giant orbits. Table 5.2 shows the stellar properties of 55 Cancri, again with habitable zones determined for both stellar masses.

Table 5.1. Orbital Properties of the exoplanets in the 55 Cancri exosystem used in this investigation.

Parameters before 11/4/2005	Planet		
	b	c	d
$M_p \sin i_0 / M_J$	0.84	0.21	4.05
Semimajor axis/AU	0.115	0.241	5.9
Orbital Eccentricity	0.02	0.339	0.16
Period / days	14.653	44.276	5360
Inner R_H multiplier	2.717	2.711	2.733
Outer R_H multiplier	7.028	8.115	6.516
$1.03M_{\odot}$ Inner gravitational reach / AU	0.072	0.133	3.219
$1.03M_{\odot}$ Outer gravitational reach / AU	0.190	0.401	10.987
$0.95M_{\odot}$ Inner gravitational reach / AU	0.072	0.132	3.171
$0.95M_{\odot}$ Outer gravitational reach / AU	0.191	0.403	11.100

The stellar data in table 5.2 reveals the star to be similar to the Sun but with a higher metallicity, which is common for the known stars with planets. The age of 55 Cancri is similar to the Sun at 5Gyr as derived from the H and K chromospheric emission levels. It is slightly redder than the Sun, with a main sequence life time of 16Gyr or 11.5Gyr for masses of $0.95M_{\odot}$ or $1.03M_{\odot}$ respectively according to the first Mazzitelli stellar model, or 11.4 Gyr or 8 Gyr respectively according to the second Mazzitelli model.

Table 5.2. Stellar properties of 55 Cancri

Parameter	Schneider Mass[1]	Calculated Mass[2]
$M_*/M_\odot$	1.03	0.95
Metallicity / [Fe/H]	0.29	0.29
Metallicity / % (1st & 2nd model)	3.90 & 3.67	3.90 & 3.67
Spectral Type, luminosity class	G8V	G8V
Bolometric Correction	-0.30	-0.30
Age / Gyr	5.0	5.0
Distance / pc	13.4	13.4
Apparent Visual Magnitude	5.95	5.95
$L/L_\odot$	0.77	0.77
T_{eff}/K	5271	5271
1st model inner HZ ZAMS / AU	0.722	0.603
1st model outer HZ ZAMS / AU	1.425	1.186
1st model inner HZ now / AU	0.858	0.695
1st model outer HZ now / AU	1.700	1.368
1st model inner HZ EoMS / AU	1.311[3]	1.383[4]
1st model outer HZ EoMS / AU	2.575[3]	2.713[4]
2nd model inner HZ ZAMS / AU	0.802	0.682
2nd model outer HZ ZAMS / AU	1.588	1.346
2nd model inner HZ now / AU	1.040	0.826
2nd model outer HZ now / AU	2.070	1.637
2nd model inner HZ EoMS / AU	1.451[3]	1.280[5]
2nd model outer HZ EoMS / AU	2.855[3]	2.525[5]
Stellar parameters inner HZ now / AU	0.770	0.770
Stellar parameters outer HZ now / AU	1.517	1.517

1 Schneider, 2006
2 Mean mass calculated from the three planet orbital periods
3 Determined using HZ profiles as described in chapter 3, section 5.2
4 Determined using Effective Temperature profiles as described in chapter 3, section 5.2
5 Determined using Luminosity profiles as described in chapter 3, section 5.2

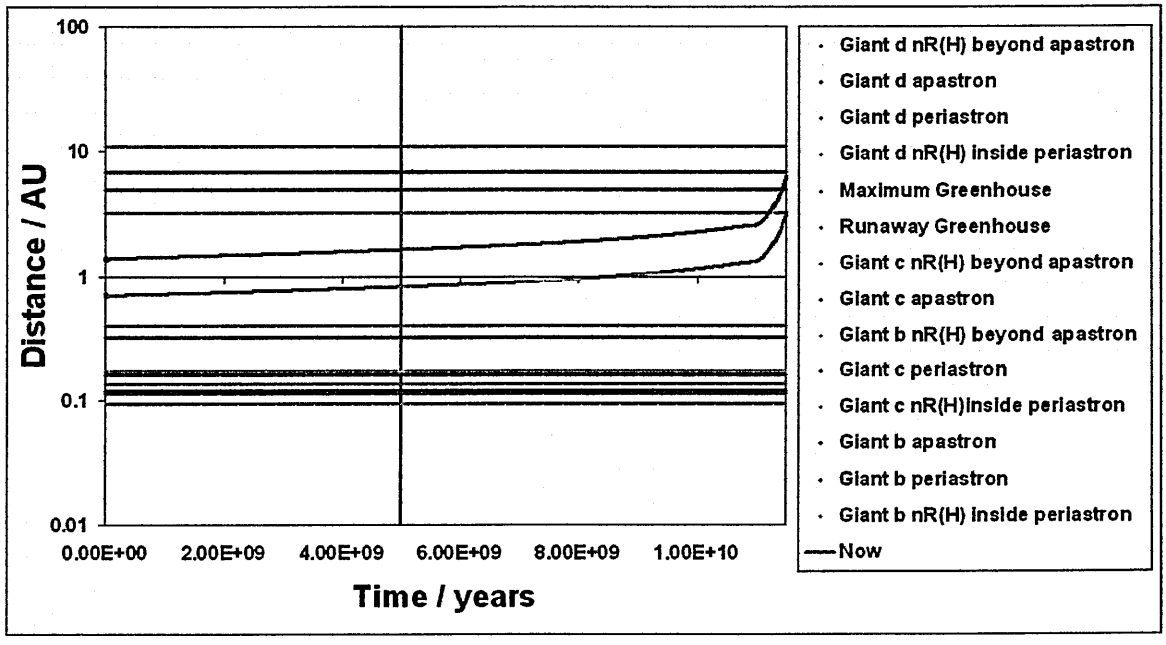

Figure 5.1 Movement of the Habitable Zone for the main sequence life time of a $0.95M_\odot$ 55 Cancri star (as determined by the second Mazzitelli model), overlaying the apastra, periastra and gravitational reaches of the three giant planets. For each "n" value, see table 5.1

5.2 Determining the Stability of the 55 Cancri System

Before inserting Earth-Moon planets within the habitable zone of this system, an initial study was undertaken to investigate the stability of the system with just the three giants. As there is more than one giant, their initial positions relative to each other must be determined at a specific time, in this case Julian Date 2450000. The periastra longitudes are relative to one ascending node, which is sufficient as all three planets are deemed to lie in one plane. The mean anomalies are determined from the time after Julian Date 2450000, when each planet was next at periastron (Marcy et al., 2002). For a mean anomaly in degrees, M, Julian date of periastron, JD and orbital period in days, P,

$$M = 360\left(1 - \frac{(JD - 2450000)}{P}\right) \qquad 5.2.$$

The times of periastron and calculated mean anomalies for each giant are given in table 5.3, with their periastron longitude. These are entered into the Mercury Orbital Integrator starting parameters for these and all subsequent runs, so that the program places the giants in their correct relative positions at the start of each run. These positions are shown diagrammatically in Figure 5.2, where the distances of the inner giants from the star have been magnified by 10 for clarity. The inclination angle of the system was gradually increased from the plane of the sky, hence reducing the planets' masses. This would determine the maximum masses of the planets the system is capable of supporting before its gravitational forces cause destabilisation, the results of which are shown in table 5.4

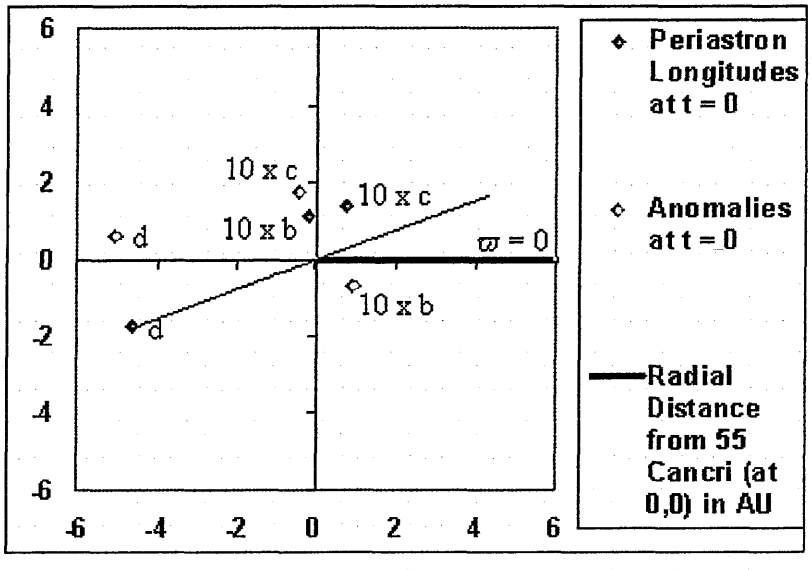

Figure 5.2 The relative starting positions (Anomalies) and initial periastra longitudes of the three giants. The distances of giants b and c are magnified by 10 for clarity. Earth-Moons are subsequently launched within the HZ (0.6AU to 3AU) on the line shown from giant d's periastron, through the origin (star) and beyond.

Table 5.3 Starting positions of the three giants at Julian Date 2450000 (1200, 09/10/1995).

Giant	Periastron Longitude / ^{o}	Julian Date of Periastron	Mean Anomaly / ^{o}
b	99	2450001.479	323.66
c	61	2450031.4	104.69
d	201	2452785	172.95

Table 5.4 Verification of the stability of the 55 Cancri system around a $1.03M_{\odot}$ star

Inclination angle / ^{O}	Minimum mass multiplier	Time before system collapse / years	Circumstances of system collapse
90	1	$>10^{9}$	-
56.44	1.2	2.704×10^{8}	Giant c ejected
50.28	1.3	1.203×10^{8}	Giant c ejected
45.58	1.4	5.549×10^{7}	Giant c falls into the star
41.81	1.5	4.029×10^{7}	Giant b falls into the star
35	1.7434	2.635×10^{7}	Giant c ejected
30	2	5.332×10^{5}	Giant c falls into the star
25	2.3662	3.565×10^{5}	Giant c ejected
20	2.9238	1.228×10^{4}	Giant c ejected
15	3.8637	8175	Giant c ejected
10	5.7588	1191	Giant c ejected
5	11.4737	41.19	Giant c ejected

The table reveals that the system must be inclined at an angle higher than $56^{O}.44$ with the plane of the sky for it to be stable; hence from equation 1.1, the maximum masses of the planets must be less than 1.2 times their minimum mass. By equation 4.1, this would imply a maximum increase in gravitational reach of 6% from each planet greater than those quoted for the minimum mass giants. This finding effectively rules out any studies using yet greater planet masses due to the inclination of the system being unknown. Also, a similar stability run at 1.1 times the giants' minimum mass was ruled out as unnecessary for the same reason. This result does contradict, however, a previously deduced inclination of 27^{O} of the system to the plane of the sky, determined from the shape of a surrounding dust ring (Trilling et al, 2000).

The properties of the giants' orbits at unit minimum mass over the next 1Gyr, showed no association between the outer giant, d and the inner two, b and c. Indications of periastra longitude constraints between the inner two giants (Figure 5.3), however, back up previous investigations into probable resonance phenomena due to the orbital period of giant c being almost exactly three times that of b (Zhou et al., 2004, Beauge et al., 2003 Ji et al., 2003).

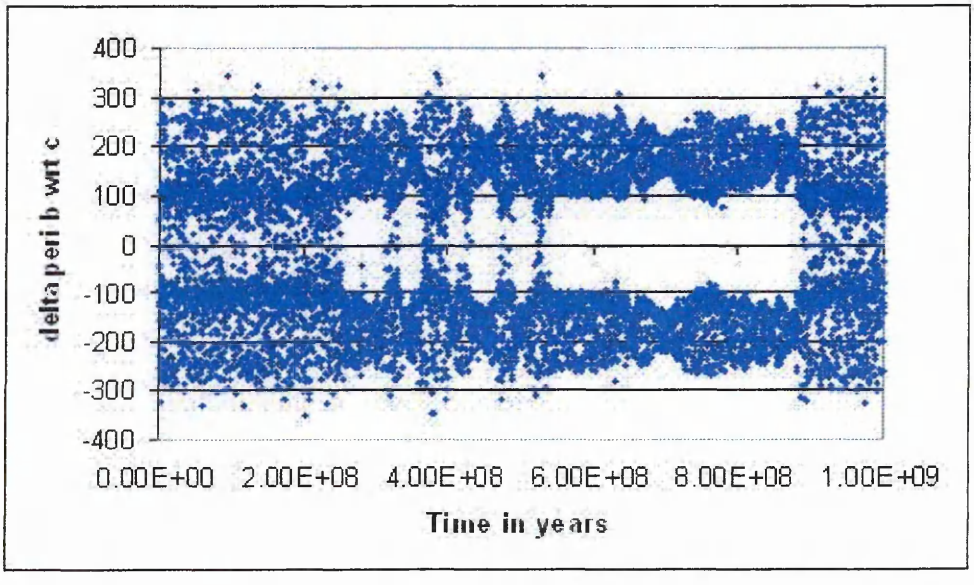

Figure 5.3 Difference in periastra longitudes between giants b and c within the 55 Cancri system over the next 1Gyr, assuming minimum mass giants.

Table 5.5 $\Delta\varpi$ between each pair of the three minimum mass planets over the 1Gyr run.

b, c $\Delta\varpi$	b, d $\Delta\varpi$	c, d $\Delta\varpi$
0 – 360*	0 – 360	0 – 360
0 – 360*	0 – 360	0 – 360
0 – 360*	0 – 360	0 – 360

* Secular tendencies are present, where $\Delta\varpi = 90^{O}$ to 270^{O}, from 2.5 x 10^{8} to 9 x 10^{8} years over this 10^{9} year integration.

5.3 Outcome of the System Investigations with a 1.03 $M_{\odot}$ Star

The previously mentioned 1Gyr run to determine the stability of the 55 Cancri system took 55 days to complete on a 1.8GHz PC computer. This was far too long a time for subsequent 1Gyr integrations to determine whether Earth-Moon planet orbits were stable and confined to the habitable zone. Hence the integration time for each run in this study was cut to 100Myr, where each run took a more manageable 5.5 days.

Integrations were carried out with Earth-Moons at 0.1AU intervals from 0.7AU to 2.0AU plus further runs at 2.5AU and 3.0AU. Table 5.2 shows that this covers the habitable zone tabulated for the various cases. Two runs were carried out at each distance with Earth-Moon periastron longitudes of 21^{O} and 201^{O} such that one initial $\Delta\varpi = 180^{O}$ with the periastron of giant d at 21^{O} longitude and the second initial $\Delta\varpi = 0^{O}$ at 201^{O} longitude. In all integrations, the Earth-Moon terrestrial planet had an initial orbital eccentricity of 10^{-5} and orbited in the same plane as the giants.

The integration results from table 5.6 reveal stable Earth-Moon orbits confined to the habitable zone from 0.9AU to 2.5AU, i.e. over virtually all of the Habitable Zone as determined for this 1.03 $M_{\odot}$ star over the whole of the main sequence lifetime, using the first Mazzitelli model (see Table 5.2). As this was the only model at the time of these integrations, subsequent more detailed studies of the outer habitable zone, as predicted by the second Mazzitelli model, were not carried out due to time constraints. These stable orbits are characterised by semimajor axes that vary by less than 1% of the initial value (Figure 5.4) and consistent variations in orbital eccentricity (Figure 5.5). At the limits of the habitable zone, the outcome of the unstable orbit at 3.0AU is due to a close approach of giant d. This occurred when the initial periastra of giant d and Earth-Moon were coincident. In the other integration at 3.0AU where the periastra of the two bodies were initially 180^{O} apart, strong libration constraints of $\pm$ 70^{O} occurred which resulted in stabilisation over the entire 10^{8} years, the fine detail of which was not pursued here (see τ^{1} Gruis in chapter 4). Unstable orbits or destabilised orbits at the inner edge of the habitable zone at 0.7AU and 0.8AU were attributed to gravitational perturbations of giant c. The destabilised orbits may last 100Myr but irregular changes in orbital eccentricity, shown in Figure 5.6, reveal underlying chaotic tendencies which may lead to instability. This is despite the orbits lying well beyond the outer gravitational reach of Giant c, as shown in table 5.1 and in Figure 5.1. There is also the possibility that this may be due to higher order resonance effects of giant d, ca. (20-25):1, which were not studied for this stellar mass, but were investigated for the 0.95 $M_{\odot}$ star (see section 5.4).

Table 5.6 Orbital runs for an Earth-Moon planet in the habitable zone of a $1.03M_{\odot}$ 55 Cancri star in the presence of minimum mass giants.

Start Parameters		Parameter variation during a run					t / years	O
E-M a / AU	$P/^{O}$	Earth-Moon e	Earth-Moon a / AU	b $\Delta\varpi^{\square}$	c $\Delta\varpi^{O}$	d $\Delta\varpi^{O}$		
0.7	21	10^{-5} – 0.017084	0.69856 ± 0.00455	0 – 360	0 – 360	0 – 360	$>10^{8**}$	-
0.7	201	10^{-5} – 0.560690	0.81063 ± 0.15634	0 – 360	0 – 360	0 – 360	3.511×10^{6}	c ce
0.8	21	10^{-5} – 0.015912	0.79797 ± 0.00485	0 – 360	0 – 360	± 90*	$>10^{8}$	-
0.8	201	10^{-5} – 0.019265	0.80190 ± 0.00509	0 – 360	0 – 360	0 – 360	$>10^{8**}$	-
0.9	21	10^{-5} – 0.023479	0.89742 ± 0.00576	0 – 360	0 – 360	± 70*	$>10^{8}$	-
0.9	201	10^{-5} – 0.027770	0.90241 ± 0.00572	0 – 360	0 – 360	± 100*	$>10^{8}$	-
1.0	21	10^{-5} – 0.037720	0.99753 ± 0.00658	0 – 360	0 – 360	± 80*	$>10^{8}$	-
1.0	201	10^{-5} – 0.037914	1.00280 ± 0.00705	0 – 360	0 – 360	± 80*	$>10^{8}$	-
1.1	21	10^{-5} – 0.048686	1.09648 ± 0.00782	0 – 360	0 – 360	± 70*	$>10^{8}$	-
1.1	201	10^{-5} – 0.052081	1.10350 ± 0.00767	0 – 360	0 – 360	± 80*	$>10^{8}$	-
1.2	21	10^{-5} – 0.062947	1.19639 ± 0.00869	0 – 360	0 – 360	± 80*	$>10^{8}$	-
1.2	201	10^{-5} – 0.065089	1.20400 ± 0.00868	0 – 360	0 – 360	± 80*	$>10^{8}$	-
1.3	21	10^{-5} – 0.076195	1.29582 ± 0.00985	0 – 360	0 – 360	± 80*	$>10^{8}$	-
1.3	201	10^{-5} – 0.080137	1.30523 ± 0.01018	0 – 360	0 – 360	± 100*	$>10^{8}$	-
1.4	21	10^{-5} – 0.086753	1.39643 ± 0.01177	0 – 360	0 – 360	± 70*	$>10^{8}$	-
1.4	201	10^{-5} – 0.090211	1.40441 ± 0.01156	0 – 360	0 – 360	± 100*	$>10^{8}$	-
1.5	21	10^{-5} – 0.097204	1.49452 ± 0.01250	0 – 360	0 – 360	± 80*	$>10^{8}$	-
1.5	201	10^{-5} – 0.100611	1.50534 ± 0.01249	0 – 360	0 – 360	± 90*	$>10^{8}$	-
1.6	21	10^{-5} – 0.107438	1.59391 ± 0.01377	0 – 360	0 – 360	± 80*	$>10^{8}$	-
1.6	201	10^{-5} – 0.110417	1.60663 ± 0.01382	0 – 360	0 – 360	± 90*	$>10^{8}$	-
1.7	21	10^{-5} – 0.116019	1.69339 ± 0.01519	0 – 360	0 – 360	± 80*	$>10^{8}$	-
1.7	201	10^{-5} – 0.120300	1.70737 ± 0.01532	0 – 360	0 – 360	± 90*	$>10^{8}$	-
1.8	21	10^{-5} – 0.124701	1.79308 ± 0.01691	0 – 360	0 – 360	± 80*	$>10^{8}$	-
1.8	201	10^{-5} – 0.127734	1.80708 ± 0.01717	0 – 360	0 – 360	± 90*	$>10^{8}$	-
1.9	21	10^{-5} – 0.132626	1.89120 ± 0.01799	0 – 360	0 – 360	± 100*	$>10^{8}$	-
1.9	201	10^{-5} – 0.136314	1.90783 ± 0.01866	0 – 360	0 – 360	± 90*	$>10^{8}$	-
2.0	21	10^{-5} – 0.134602	1.99204 ± 0.01987	0 – 360	0 – 360	± 90*	$>10^{8}$	-
2.0	201	10^{-5} – 0.183940	2.00625 ± 0.02445	0 – 360	0 – 360	0 – 360	$>10^{8}$	-
2.5	21	10^{-5} – 0.174989	2.48959 ± 0.03035	0 – 360	0 – 360	± 90*	$>10^{8}$	-
2.5	201	10^{-5} – 0.172101	2.51234 ± 0.02897	0 – 360	0 – 360	± 90*	$>10^{8}$	-
3.0	21	10^{-5} – 0.237500	2.98950 ± 0.04590	0 – 360	0 – 360	± 70*	$>10^{8}$	-
3.0	201	10^{-5}	3.0	-	-	-	77	d ce

Footnotes for all subsequent tables:

r orbital period resonance ratio

a Earth-Moon's (E-M) semimajor axis distance from the star in AU

p longitude of periastron of Earth-Moon with respect to that of the system (^{O})

e orbital eccentricity

$x\ \Delta\varpi$ periastron longitude difference between the giant x and Earth-moon

t time of run to completion or termination in years

O outcome of run termination if applicable where 'x ce' is a close encounter with a giant planet and x is either b, c or d.

* Libration of the Earth-Moon periastron longitude is evident relative to that of the giant.

** Indications of instability are evident in the orbital eccentricity.

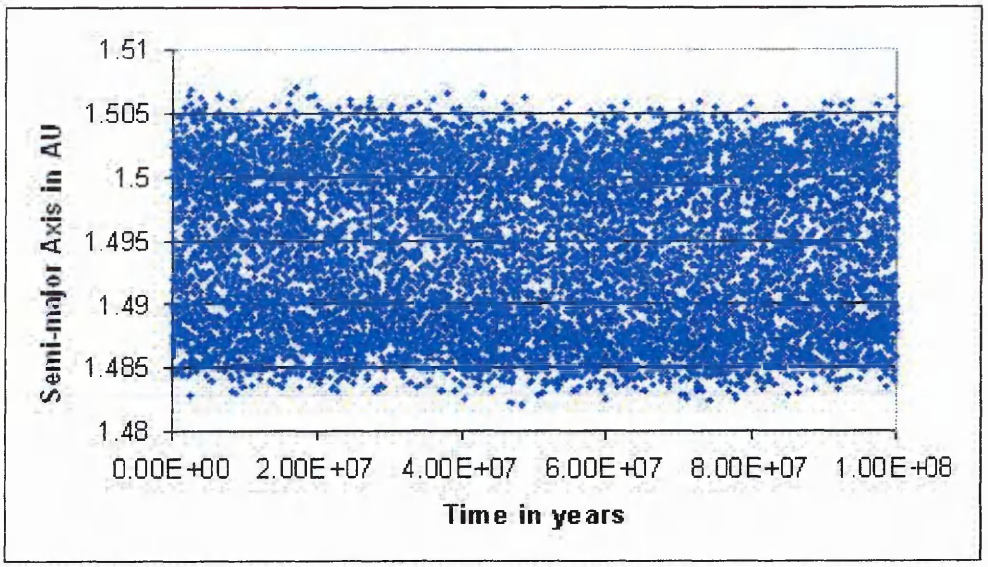

Figure 5.4 Variation of semimajor axis of a stable Earth-Moon orbit at 1.5AU with time, where $\Delta\varpi(0) = 180^{O}$.

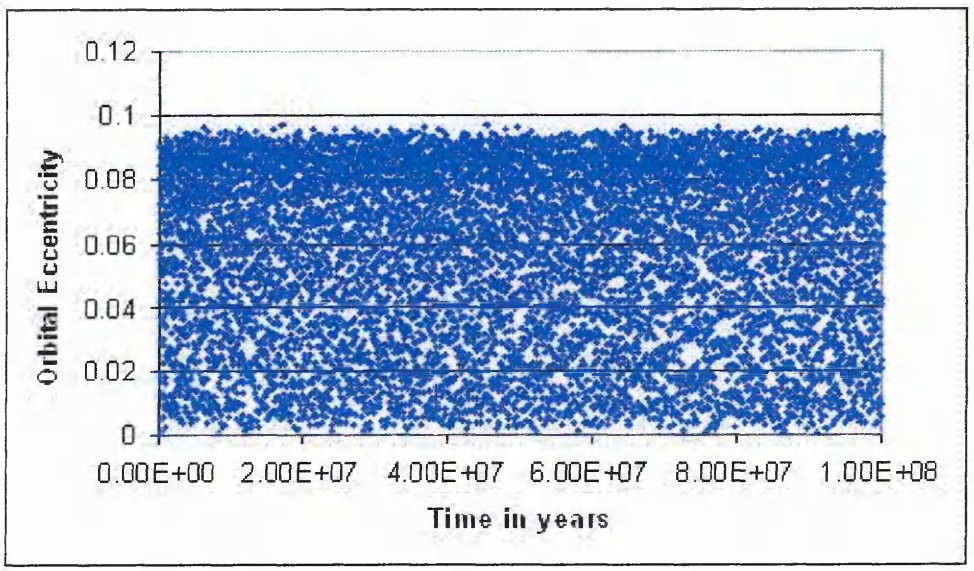

Figure 5.5 Variation of eccentricity of a stable Earth-Moon orbit at 1.5AU with time, where $\Delta\varpi(0) = 180^{O}$.

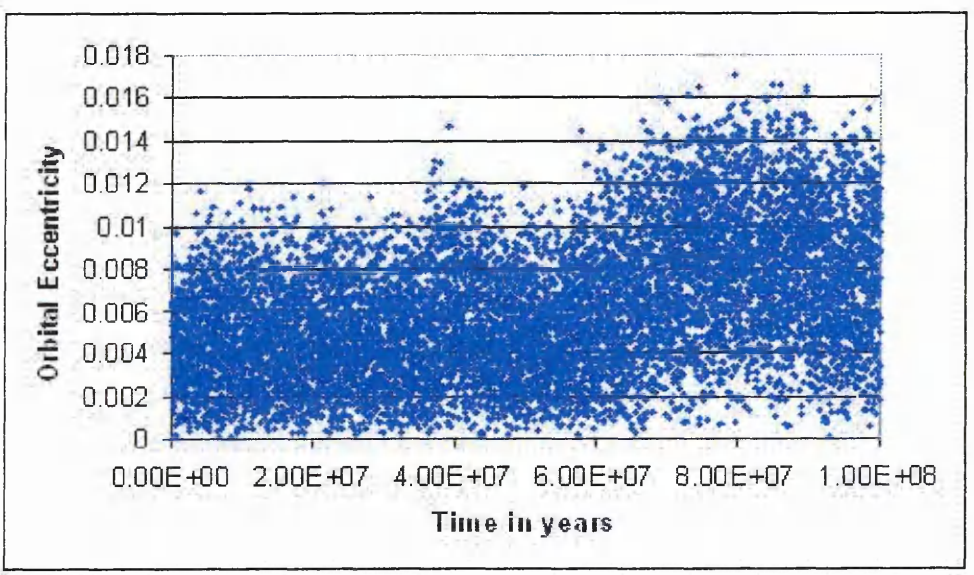

Figure 5.6 Variation of eccentricity of an unstable Earth-Moon orbit at 0.7AU with time, where $\Delta\varpi(0) = 180^{O}$.

Of the stable Earth-Moon orbits with initial semimajor axes between 0.9AU and 2.5AU inclusive, confined to the habitable zone, all had small semimajor axis variations, with percentage variation increasing from 0.63% to 1.22% as initial semimajor axis values increased from 0.9AU to 2.5AU. Eccentricity varied consistently for all integrations (see Figure 5.5), and this variation also increased with increasing semimajor axis, from a maximum value of 0.0235 at 0.9AU to 0.184 at 2.4AU. Both of these effects are attributed to the ever increasing gravitational perturbation effects of the most massive outer giant d, as the initial Earth-Moon semimajor axis increases. All periastron libration effects, when present in Earth-Moon orbits, were connected with giant d and in no case were there any such effects with the less massive inner two giants. Of the runs at the same initial semimajor axis, those with initially coincident periastra between the Earth-Moon and giant d had slightly larger variations in eccentricity and settled into orbits with slightly larger mean semimajor axes with greater variation. These variations were in low single figures percentages for eccentricity and fractions of a percent for semimajor axes, but consistent nonetheless. They were also opposite to similar trends found in the single planet systems, where coincident initial periastra between a giant and Earth-Moon yielded slightly 'tighter' Earth-Moon orbits. The possible reason for this is that during all integration launches, the mean anomaly of the giant d is $172^{O}.95$, hence at coincident periastra longitudes, the initial positioning of the Earth-Moon, always at a mean anomaly of 0^{O}, and giant d is almost on opposite sides of the star. Thus it appears that subtle differences in orbital characteristics with the same initial semimajor axis may not rely on initial relative periastra but on the actual initial locations of the planets relative to each other in their orbits.

5.4 Outcome of the System Investigations with a $0.95M_{\odot}$ Star

As mentioned in section 5.1, the orbital periods and semimajor axes of the giant planets in 55 Cancri are actually consistent with a star of mass $0.95M_{\odot}$ (Marcy et al., 2002). The outcomes of all subsequent integrations of Earth-Moon planets within this system are all based on the star having this mass. The runs to determine the stable orbits confined to the entire habitable zone over all the star's main sequence life time (see table 5.2) are revealed in table 5.7.

Initial inspection of the table reveals stable orbits from 0.8AU to 2.7AU, with the stable runs at 2.8AU and 2.9AU being dependent on the periastron longitude of the Earth-Moon relative to that of giant d. This range covers the entire habitable zone with the exception of the innermost region between 0.6AU and 0.8AU, implying that 55 Cancri could be an excellent candidate for housing a habitable terrestrial planet. Previous orbital integrations limited to 1AU only, by Marcy et al., 2002, found stable orbits for an Earth type planet with eccentricity variations with a maximum of 0.03 over 27,000years. The type of integrator used and details of the integration runs are not stated in their paper, but it implies that their integration time may have been much shorter than 100Myr with much more frequent time steps than 10^{4} years. This would give them the more detailed eccentricity oscillation information, as was so for τ^{1} Gruis where an Earth-Moon was launched at 1.7AU at $\Delta\varpi = 0$, discussed in chapter 4, section 5.1. Their findings are in good agreement with those here, where eccentricities oscillated from 10^{-5} to 0.032 before instabilities occurred after 76Myr and 86Myr for Earth-Moon periastron launch angles of 201^{O} and 21^{O} respectively. There were even indications from our results of a possible eccentricity cycle of 28,300 years, although this is inconclusive due to the density of results being insufficient for this level of refinement.

Although the orbital integrations lasted for 100Myr in all cases between 0.8AU and 2.7AU, many runs were such that their orbital elements were not stable over the period. This occurred at 1.0AU and between 1.3AU and 1.8AU. Examples of the semimajor axis and

eccentricity from a stable orbit are shown in figures 5.4 and 5.5. Examples of each parameter, from a potentially unstable orbit lasting 100Myr, are shown in figures 5.7 and 5.8.

Table 5.7 Orbital runs for an Earth-Moon planet in the habitable zone of a $0.95M_{\odot}$ 55 Cancri star in the presence of minimum mass giants.

Start Parameters		Parameter variation during a run					t / years	O
E-M a / AU	p/°	Earth-Moon e	Earth-Moon a / AU	b $\Delta\varpi^{\square}$	c $\Delta\varpi^{O}$	d $\Delta\varpi^{O}$		
0.6	21	10^{-5} – 0.414577	0.58091 ± 0.01969	0 – 360	0 – 360	0 – 360	5.150×10^{7}	c ce
0.6	201	10^{-5} – 0.616838	0.60205 ± 0.00413	90 - 270	0 – 360	0 – 360	1.047×10^{7}	c ce
0.7	21	10^{-5} – 0.738540	0.69820 ± 0.01949	0 – 360	0 – 360	0 – 360	6.001×10^{7}	c ce
0.7	201	10^{-5} – 0.728394	0.83046 ± 0.16025	0 – 360	0 – 360	0 – 360	5.211×10^{6}	c ce
0.8	21	10^{-5} – 0.016081	0.79783 ± 0.00515	0 – 360	0 – 360	± 90*	$>10^{8}$	-
0.8	201	10^{-5} – 0.017504	0.80214 ± 0.00562	0 – 360	0 – 360	± 100*	$>10^{8}$	-
0.9	21	10^{-5} – 0.024046	0.89706 ± 0.00624	0 – 360	0 – 360	± 70*	$>10^{8}$	-
0.9	201	10^{-5} – 0.026110	0.90257 ± 0.00619	0 – 360	0 – 360	± 100*	$>10^{8}$	-
1.0	21	10^{-5} – 0.156186	0.99576 ± 0.00836	0 – 360	0 – 360	0 – 360	$>10^{8}$**	-
1.0	201	10^{-5} – 0.292038	1.00492 ± 0.01158	0 – 360	0 – 360	0 – 360	$>10^{8}$***	-
1.1	21	10^{-5} – 0.049109	1.09654 ± 0.00822	0 – 360	0 – 360	± 70*	$>10^{8}$	-
1.1	201	10^{-5} – 0.052920	1.10414 ± 0.00854	0 – 360	0 – 360	± 90*	$>10^{8}$	-
1.2	21	10^{-5} – 0.064163	1.19592 ± 0.00944	0 – 360	0 – 360	± 80*	$>10^{8}$	-
1.2	201	10^{-5} – 0.066714	1.20406 ± 0.00974	0 – 360	0 – 360	± 80*	$>10^{8}$	-
1.3	21	10^{-5} – 0.098239	1.29460 ± 0.01093	0 – 360	0 – 360	0 – 360	$>10^{8}$**	-
1.3	201	10^{-5} – 0.079410	1.30609 ± 0.01157	0 – 360	0 – 360	± 80*	$>10^{8}$	-
1.4	21	10^{-5} – 0.333734	1.39448 ± 0.01414	0 – 360	0 – 360	0 – 360	$>10^{8}$**	-
1.4	201	10^{-5} – 0.187047	1.40411 ± 0.01258	0 – 360	0 – 360	0 – 360	$>10^{8}$**	-
1.5	21	10^{-5} – 0.097517	1.49629 ± 0.01486	0 – 360	0 – 360	± 80*	$>10^{8}$	-
1.5	201	10^{-5} – 0.101465	1.50571 ± 0.01382	0 – 360	0 – 360	± 90*	$>10^{8}$**	-
1.6	21	10^{-5} – 0.108703	1.59443 ± 0.01562	0 – 360	0 – 360	± 80*	$>10^{8}$**	-
1.6	201	10^{-5} – 0.153377	1.60760 ± 0.01602	0 – 360	0 – 360	0 – 360	$>10^{8}$**	-
1.7	21	10^{-5} – 0.116455	1.69405 ± 0.01651	0 – 360	0 – 360	± 80*	$>10^{8}$	-
1.7	201	10^{-5} – 0.126223	1.70750 ± 0.01641	0 – 360	0 – 360	± 100*	$>10^{8}$**	-
1.8	21	10^{-5} – 0.158991	1.79264 ± 0.01843	0 – 360	0 – 360	0 – 360	$>10^{8}$**	-
1.8	201	10^{-5} – 0.128942	1.80805 ± 0.01845	0 – 360	0 – 360	± 90*	$>10^{8}$	-
1.9	21	10^{-5} – 0.134290	1.89185 ± 0.02044	0 – 360	0 – 360	± 80*	$>10^{8}$	-
1.9	201	10^{-5} – 0.137034	1.90931 ± 0.01983	0 – 360	0 – 360	± 90*	$>10^{8}$	-
2.0	21	10^{-5} – 0.134721	1.99254 ± 0.02175	0 – 360	0 – 360	± 80*	$>10^{8}$	-
2.0	201	10^{-5} – 0.186826	2.00495 ± 0.02596	0 – 360	0 – 360	0 – 360	$>10^{8}$	-
2.1	21	10^{-5} – 0.145480	2.09048 ± 0.02278	0 – 360	0 – 360	± 80*	$>10^{8}$	-
2.1	201	10^{-5} – 0.156286	2.10934 ± 0.02394	0 – 360	0 – 360	± 90*	$>10^{8}$	-
2.2	21	10^{-5} – 0.150108	2.18924 ± 0.02591	0 – 360	0 – 360	± 80*	$>10^{8}$	-
2.2	201	10^{-5} – 0.154504	2.21178 ± 0.02582	0 – 360	0 – 360	± 90*	$>10^{8}$	-
2.3	21	10^{-5} – 0.131308	2.28874 ± 0.02708	0 – 360	0 – 360	± 70*	$>10^{8}$	-
2.3	201	10^{-5} – 0.107933	2.30993 ± 0.02843	0 – 360	0 – 360	± 130*	$>10^{8}$	-
2.4	21	10^{-5} – 0.177633	2.38612 ± 0.03035	0 – 360	0 – 360	± 90*	$>10^{8}$	-
2.4	201	10^{-5} – 0.177592	2.41143 ± 0.02901	0 – 360	0 – 360	± 80*	$>10^{8}$	-
2.5	21	10^{-5} – 0.175388	2.48709 ± 0.03236	0 – 360	0 – 360	± 80*	$>10^{8}$	-
2.5	201	10^{-5} – 0.172198	2.51342 ± 0.03162	0 – 360	0 – 360	± 80*	$>10^{8}$	-
2.6	21	10^{-5} – 0.172255	2.58549 ± 0.03345	0 – 360	0 – 360	± 90*	$>10^{8}$	-
2.6	201	10^{-5} – 0.165352	2.61473 ± 0.03333	0 – 360	0 – 360	± 90*	$>10^{8}$	-
2.7	21	10^{-5} – 0.154435	2.68417 ± 0.03574	0 – 360	0 – 360	± 100*	$>10^{8}$	-
2.7	201	10^{-5} – 0.129438	2.71721 ± 0.03812	0 – 360	0 – 360	± 90*	$>10^{8}$	-
2.8	21	10^{-5} – 0.111313	2.78027 ± 0.04517	0 – 360	0 – 360	0 – 360	$>10^{8}$	-
2.8	201	10^{-5} – 0.172150	2.81451 ± 0.01451	-	-	-	1.546×10^{4}	d ce
2.9	21	10^{-5} – 0.237020	2.88543 ± 0.05575	0 – 360	0 – 360	± 80*	$>10^{8}$	-
2.9	201	10^{-5}	2.9	-	-	-	51	d ce
3.0	21	10^{-5}	3.0	-	-	-	124	d ce
3.0	201	10^{-5}	3.0	-	-	-	81	d ce

Footnotes as for table 5.6 plus,

*** Indications of instability are evident in the orbital semimajor axis and eccentricity.

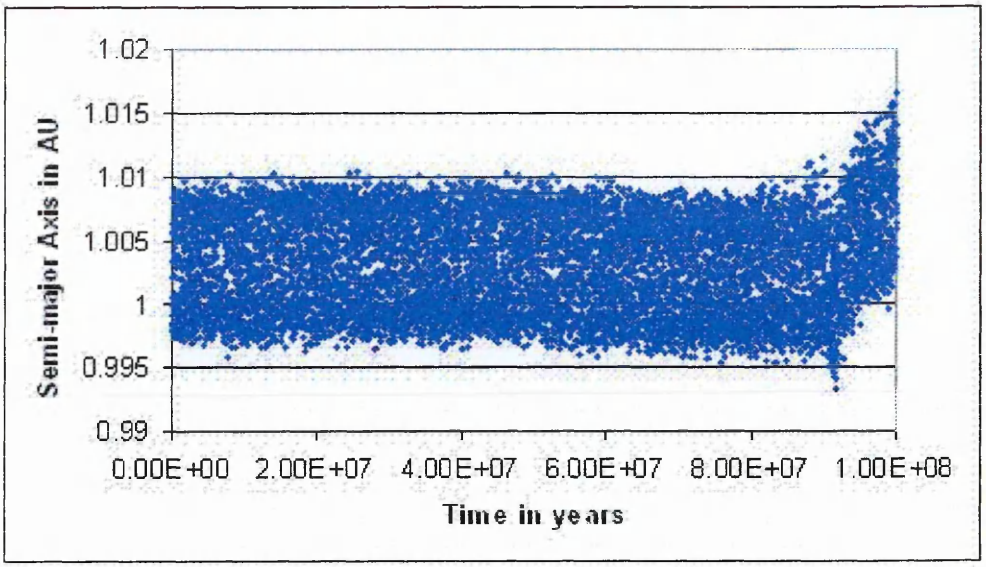

Figure 5.7 Semimajor axis v time for an Earth-Moon planet originally at 1AU and periastron longitude of 201^{O}.

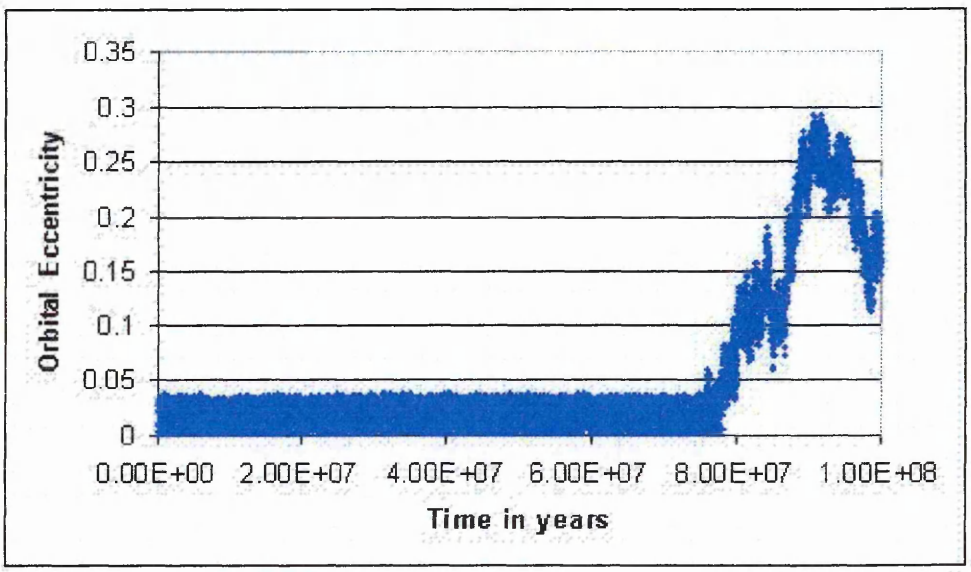

Figure 5.8 Eccentricity v time for an Earth-Moon planet originally at 1AU and periastron longitude of 201^{O}.

Orbital stability from these two figures seems assured until a considerable fraction of the 100Myr has passed, with the implication that such integrations may not last 1Gyr. Most of these potentially unstable orbits are only revealed through anomalies in eccentricity; it is a rare occurrence for the semimajor axis also to reveal this. One reason for these instabilities may be due to the fine balance the three giants have in order to exist alone in their stable orbits. This is manifested in the on-off libration phenomenon of giants b and c as shown in Figure 5.3 plus the integration result showing that the system destabilises entirely if the giant masses are only 1.2 times their minimum mass. It implies that the entire system may exist on a fine balance between order and chaos. This suggests that the system may not be as habitable as it would be if the giant orbits were completely stable. It also draws the possibility to the reader as to how many others of the known multiple giant systems may exist in a similar 'knife-edge' state, be they potentially habitable or not.

5.5 Resonance Investigation with a $0.95M_{\odot}$ Star

To check whether there are resonance effects behind the irregular behaviour of some of the table 5.7 orbits, a detailed study is summarised in table 5.8, where orbital period resonance orders were studied from 3:1 to 25:1 and from 7:2 to 25:2 for an Earth-Moon with giant d.

The resonance ratio is r, this being the ratio of the orbital period of the Earth-Moon to that of giant d. Table 5.9 also details integration runs where initial semimajor axes were mid-way between higher resonance orders x:1 and (x+1):1 where x is from 13 to 24 inclusive.

Table 5.8 Orbital resonance runs for an Earth-Moon planet in the habitable zone of a $0.95M_{\odot}$ 55 Cancri star in the presence of minimum mass giants.

Start Parameters			Parameter variation during a run					t / years	O
r	E-M a / AU	P / ^{O}	Earth-Moon e	Earth-Moon a / AU	b $\Delta\varpi^{O}$	c $\Delta\varpi^{O}$	d $\Delta\varpi^{O}$		
3	2.836424	21	10^{-5} – 0.219816	2.81346 ± 0.08048	0 – 360	0 – 360	0 – 360	$>10^{8}$	-
3	2.836424	201	10^{-5}	2.836424	-	-	-	5306	d cc
3.5	2.55941	21	10^{-5} – 0.598416	2.55168 ± 0.05235	0 – 360	0 – 360	0 – 360	$>10^{8}$	-
3.5	2.55941	201	10^{-5} – 0.172977	2.57320 ± 0.03340	0 – 360	0 – 360	± 90*	$>10^{8}$	-
4	2.34142	21	10^{-5} – 0.148445	2.32430 ± 0.03415	0 – 360	0 – 360	0 – 360	$>10^{8}$**	-
4	2.34142	201	10^{-5} – 0.170149	2.35342 ± 0.03026	0 – 360	0 – 360	± 100*	$>10^{8}$	-
4.5	2.1646	21	10^{-5} – 0.150620	2.15654 ± 0.02474	0 – 360	0 – 360	± 80*	$>10^{8}$	-
4.5	2.1646	201	10^{-5} – 0.153928	2.17360 ± 0.02566	0 – 360	0 – 360	± 90*	$>10^{8}$	-
5	2.01777	21	10^{-5} – 0.197444	2.00564 ± 0.02763	0 – 360	0 – 360	0 – 360	$>10^{8}$**	-
5	2.01777	201	10^{-5} – 0.148854	2.02699 ± 0.02272	0 – 360	0 – 360	± 100*	$>10^{8}$	-
5.5	1.89355	21	10^{-5} – 0.131979	1.88637 ± 0.01976	0 – 360	0 – 360	± 80*	$>10^{8}$	-
5.5	1.89355	201	10^{-5} – 0.136580	1.90230 ± 0.01950	0 – 360	0 – 360	± 90*	$>10^{8}$	-
6	1.78683	21	10^{-5} – 0.128759	1.78042 ± 0.01828	0 – 360	0 – 360	± 90*	$>10^{8}$**	-
6	1.78683	201	10^{-5} – 0.127881	1.79448 ± 0.01836	0 – 360	0 – 360	± 90*	$>10^{8}$	-
6.5	1.693986	21	10^{-5} – 0.116489	1.68772 ± 0.01613	0 – 360	0 – 360	± 80*	$>10^{8}$	-
6.5	1.693986	201	10^{-5} – 0.119959	1.70145 ± 0.01685	0 – 360	0 – 360	± 90*	$>10^{8}$	-
7	1.61233	21	10^{-5} – 0.108682	1.60618 ± 0.01566	0 – 360	0 – 360	± 80*	$>10^{8}$	-
7	1.61233	201	10^{-5} – 0.114268	1.61940 ± 0.01587	0 – 360	0 – 360	± 90*	$>10^{8}$	-
7.5	1.53985	21	10^{-5} – 0.101409	1.53587 ± 0.01500	0 – 360	0 – 360	± 80*	$>10^{8}$	-
7.5	1.53985	201	10^{-5} – 0.104906	1.54593 ± 0.01481	0 – 360	0 – 360	± 90*	$>10^{8}$	-
8	1.475	21	10^{-5} – 0.116723	1.46815 ± 0.01339	0 – 360	0 – 360	0 – 360	$>10^{8}$**	-
8	1.475	201	10^{-5} – 0.100418	1.48128 ± 0.01367	0 – 360	0 – 360	± 80*	$>10^{8}$	-
8.5	1.4165744	21	10^{-5} – 0.089676	1.41331 ± 0.01331	0 – 360	0 – 360	± 80*	$>10^{8}$	-
8.5	1.4165744	201	10^{-5} – 0.145244	1.42084 ± 0.01305	0 – 360	0 – 360	0 – 360	$>10^{8}$**	-
9	1.36361	21	10^{-5} – 0.084037	1.35797 ± 0.01187	0 – 360	0 – 360	± 80*	$>10^{8}$	-
9	1.36361	201	10^{-5} – 0.129287	1.36814 ± 0.01226	0 – 360	0 – 360	0 – 360	$>10^{8}$**	-
9.5	1.3153347	21	10^{-5} – 0.214557	1.31075 ± 0.01151	0 – 360	0 – 360	0 – 360	$>10^{8}$**	-
9.5	1.3153347	201	10^{-5} – 0.131567	1.31979 ± 0.01159	0 – 360	0 – 360	0 – 360	$>10^{8}$**	-
10	1.2711	21	10^{-5} – 0.072612	1.26678 ± 0.01042	0 – 360	0 – 360	± 80*	$>10^{8}$	-
10	1.2711	201	10^{-5} – 0.162456	1.27588 ± 0.01130	0 – 360	0 – 360	0 – 360	$>10^{8}$**	-
10.5	1.230436	21	10^{-5} – 0.065924	1.22661 ± 0.00991	0 – 360	0 – 360	± 80*	$>10^{8}$	-
10.5	1.230436	201	10^{-5} – 0.070271	1.23394 ± 0.01062	0 – 360	0 – 360	± 100*	$>10^{8}$	-
11	1.192862	21	10^{-5} – 0.073798	1.18891 ± 0.00960	0 – 360	0 – 360	± 90*	$>10^{8}$**	-
11	1.192862	201	10^{-5} – 0.064313	1.19718 ± 0.00938	0 – 360	0 – 360	± 90*	$>10^{8}$	-
11.5	1.158031	21	10^{-5} – 0.057085	1.15429 ± 0.00886	0 – 360	0 – 360	± 80*	$>10^{8}$	-
11.5	1.158031	201	10^{-5} – 0.062372	1.16222 ± 0.00895	0 – 360	0 – 360	± 100*	$>10^{8}$	-
12	1.1256357	21	10^{-5} – 0.052986	1.12167 ± 0.00868	0 – 360	0 – 360	± 70*	$>10^{8}$	-
12	1.1256357	201	10^{-5} – 0.031084	1.12604 ± 0.01332	0 – 360	0 – 360	0 – 360	$>10^{8}$***	-
12.5	1.095415	21	10^{-5} – 0.049107	1.09167 ± 0.00823	0 – 360	0 – 360	± 80*	$>10^{8}$	-
12.5	1.095415	201	10^{-5} – 0.058734	1.09935 ± 0.00843	0 – 360	0 – 360	0 – 360	$>10^{8}$**	-
13	1.0671442	21	10^{-5} – 0.045701	1.06355 ± 0.00795	0 – 360	0 – 360	± 80*	$>10^{8}$	-
13	1.0671442	201	10^{-5} – 0.048298	1.07077 ± 0.00833	0 – 360	0 – 360	± 100*	$>10^{8}$	-
14	1.0157	21	10^{-5} – 0.037463	1.01221 ± 0.00741	0 – 360	0 – 360	± 80*	$>10^{8}$	-
14	1.0157	201	10^{-5} – 0.407524	1.02447 ± 0.01335	0 – 360	0 – 360	0 – 360	$>10^{8}$***	-
15	0.97	21	10^{-5} – 0.032829	0.96729 ± 0.00698	0 – 360	0 – 360	± 80*	$>10^{8}$	-
15	0.97	201	10^{-5} – 0.347137	0.96155 ± 0.02749	0 – 360	0 – 360	0 – 360	$>10^{8}$***	-
16	0.92919	21	10^{-5} – 0.027853	0.92595 ± 0.00692	0 – 360	0 – 360	± 80*	$>10^{8}$**	-
16	0.92919	201	10^{-5} – 0.065237	0.93229 ± 0.00645	0 – 360	0 – 360	± 110*	$>10^{8}$**	-
17	0.892386	21	10^{-5} – 0.579325	0.88197 ± 0.03308	0 – 360	0 – 360	0 – 360	9.531×10^{7}	c ce
17	0.892386	201	10^{-5} – 0.329252	0.86075 ± 0.04139	0 – 360	0 – 360	0 – 360	$>10^{8}$***	-
18	0.859	21	10^{-5} – 0.019910	0.85637 ± 0.00579	0 – 360	0 – 360	± 80*	$>10^{8}$	-
18	0.859	201	10^{-5} – 0.026709	0.86072 ± 0.00641	0 – 360	0 – 360	0 – 360	$>10^{8}$**	-
19	0.828609	21	10^{-5} – 0.020146	0.82625 ± 0.00571	0 – 360	0 – 360	± 120*	$>10^{8}$	-
19	0.827	201	10^{-5} – 0.771357	0.86018 ± 0.22919	0 – 360	0 – 360	0 – 360	7.568×10^{7}	c ce
19	0.828	201	10^{-5} – 0.019199	0.83118 ± 0.00643	0 – 360	0 – 360	± 100*	$>10^{8}$	-
19	0.828609	201	10^{-5} – 0.659626	0.84415 ± 0.02676	0 – 360	0 – 360	0 – 360	3.617×10^{7}	c ce
19	0.829	201	10^{-5} – 0.021976	0.83127 ± 0.00557	0 – 360	0 – 360	0 – 360	$>10^{8}$	-
19	0.830	201	10^{-5} – 0.021789	0.83249 ± 0.00578	0 – 360	0 – 360	0 – 360	$>10^{8}$	-
20	0.8	21	10^{-5} – 0.016081	0.79783 ± 0.00515	0 – 360	0 – 360	± 90*	$>10^{8}$	-
20	0.8	201	10^{-5} – 0.017504	0.80214 ± 0.00562	0 – 360	0 – 360	± 100*	$>10^{8}$	-

Start Parameters			Parameter variation during a run					t / years	O
r	E-M a / AU	$P/^{O}$	Earth-Moon e	Earth-Moon a / AU	b $\Delta\varpi^{\square}$	c $\Delta\varpi^{O}$	d $\Delta\varpi^{O}$		
21	0.7751263	21	10^{-5} – 0.018022	0.77254 ± 0.00521	0 – 360	0 – 360	0 – 360	$>10^{8}$	-
21	0.7751263	201	10^{-5} – 0.025427	0.77669 ± 0.00604	0 – 360	0 – 360	0 – 360	$>10^{8}$**	-
22	0.751456	21	10^{-5} – 0.040111	0.82609 ± 0.08436	0 – 360	0 – 360	0 – 360	$>10^{8}$***	-
22	0.751456	201	10^{-5} – 0.022969	0.75376 ± 0.00572	0 – 360	0 – 360	0 – 360	$>10^{8}$***	-
23	0.7295137	21	10^{-5} – 0.553030	0.74690 ± 0.06373	0 – 360	0 – 360	0 – 360	2.868×10^{7}	c ce
23	0.7295137	201	10^{-5} – 0.036125	0.73344 ± 0.00591	0 – 360	0 – 360	0 – 360	$>10^{8}$***	-
24	0.709106	21	10^{-5} – 0.015656	0.70684 ± 0.00449	0 – 360	0 – 360	0 – 360	$>10^{8}$**	-
24	0.709106	201	10^{-5} – 0.434608	0.69146 ± 0.05014	0 – 360	0 – 360	0 – 360	7.492×10^{7}	c ce
25	0.69	21	10^{-5} – 0.663430	0.70538 ± 0.04424	0 – 360	0 – 360	0 – 360	3.488×10^{7}	c cc
25	0.69	201	10^{-5} – 0.090460	0.68772 ± 0.00818	0 – 360	0 – 360	0 – 360	$>10^{8}$***	-

Footnotes as for table 5.6 plus,
*** Indications of instability are evident in the orbital semimajor axis and eccentricity.

Table 5.9 Orbital runs for an Earth-Moon planet in the habitable zone of a $0.95M_{\odot}$ 55 Cancri star in the presence of minimum mass giants, for an initial E-M orbital distance midway between higher order resonances.

Start Parameters			Parameter variation during a run					t / years	O
r	E-M a / AU	$P/^{O}$	Earth-Moon e	Earth-Moon a / AU	b $\Delta\varpi^{\square}$	c $\Delta\varpi^{O}$	d $\Delta\varpi^{O}$		
13-14	1.0414	21	10^{-5} – 0.040357	1.03803 ± 0.00756	0 – 360	0 – 360	± 70*	$>10^{8}$	-
13-14	1.0414	201	10^{-5} – 0.045048	1.04504 ± 0.00772	0 – 360	0 – 360	± 100*	$>10^{8}$	-
14-15	0.993	21	10^{-5} – 0.035796	0.99013 ± 0.00739	0 – 360	0 – 360	± 80*	$>10^{8}$	-
14-15	0.993	201	10^{-5} – 0.033591	0.99939 ± 0.01097	0 – 360	0 – 360	0 – 360	$>10^{8}$***	-
15-16	0.9496	21	10^{-5} – 0.029611	0.95668 ± 0.00692	0 – 360	0 – 360	± 80*	$>10^{8}$	-
15-16	0.9496	201	10^{-5} – 0.032846	0.95290 ± 0.00679	0 – 360	0 – 360	± 120*	$>10^{8}$	-
16-17	0.91079	21	10^{-5} – 0.732507	1.07647 ± 0.21943	0 – 360	0 – 360	0 – 360	3.022×10^{7}	d ce
16-17	0.91079	201	10^{-5} – 0.279634	0.92667 ± 0.02022	0 – 360	0 – 360	0 – 360	$>10^{8}$***	-
17-18	0.8757	21	10^{-5} – 0.021278	0.87309 ± 0.00580	0 – 360	0 – 360	± 60*	$>10^{8}$	-
17-18	0.8757	201	10^{-5} – 0.166329	0.87620 ± 0.00841	0 – 360	0 – 360	0 – 360	$>10^{8}$***	-
18-19	0.8438	21	10^{-5} – 0.019747	0.84148 ± 0.00566	0 – 360	0 – 360	± 100*	$>10^{8}$	-
18-19	0.8438	201	10^{-5} – 0.025020	0.84704 ± 0.00601	0 – 360	0 – 360	0 – 360	$>10^{8}$	-
19-20	0.8143	21	10^{-5} – 0.016980	0.81190 ± 0.00558	0 – 360	0 – 360	± 70*	$>10^{8}$	-
19-20	0.8143	201	10^{-5} – 0.027628	0.81694 ± 0.00563	0 – 360	0 – 360	0 – 360	$>10^{8}$**	-
20-21	0.787563	21	10^{-5} – 0.751848	1.29478 ± 0.52070	0 – 360	0 – 360	0 – 360	3.335×10^{7}	c ce
20-21	0.787563	201	10^{-5} – 0.017186	0.78953 ± 0.00521	0 – 360	0 – 360	± 110*	$>10^{8}$**	-
21-22	0.763291	21	10^{-5} – 0.573153	0.79732 ± 0.27302	0 – 360	0 – 360	0 – 360	6.093×10^{7}	c ce
21-22	0.763291	201	10^{-5} – 0.759373	0.84731 ± 0.16378	0 – 360	0 – 360	0 – 360	4.701×10^{7}	c ce
22-23	0.740485	21	10^{-5} – 0.042841	0.74038 ± 0.00766	0 – 360	0 – 360	0 – 360	$>10^{8}$***	-
22-23	0.740485	201	10^{-5} – 0.645459	0.69538 ± 0.06357	0 – 360	0 – 360	0 – 360	2.363×10^{7}	c ce
23-24	0.71931	21	10^{-5} – 0.775365	1.10940 ± 0.40283	0 – 360	0 – 360	0 – 360	4.216×10^{7}	d ce
23-24	0.71931	201	10^{-5} – 0.031075	0.72183 ± 0.00528	0 – 360	0 – 360	0 – 360	$>10^{8}$***	-
24-25	0.7	21	10^{-5} – 0.738540	0.69820 ± 0.01949	0 – 360	0 – 360	0 – 360	6.001×10^{7}	c ce
24-25	0.7	201	10^{-5} – 0.728394	0.83046 ± 0.16025	0 – 360	0 – 360	0 – 360	5.211×10^{6}	c ce

Footnotes as for table 5.6 plus,
*** Indications of instability are evident in the orbital semimajor axis and eccentricity.

Both tables reveal that almost all of the habitable zone resonances permit stable confined Earth-Moon orbits. The first exception is the very inner region inside 0.75AU, lying in the system's habitable zone during its first 7.8Gyr or 2.2Gyr depending on the first or second Mazzitelli stellar model respectively. Of these unstable orbits, some are dependent on $\Delta\varpi$ with giant d. The reason for their instability is almost certainly due to the proximity of the orbit of the inner giant c more than any resonance effects. The very outer region at 2.8AU and beyond, which applies to the system after the end of its main sequence lifetime for this mass star, also has unstable orbits almost certainly due to the proximity of the orbit of outer giant d. The only possible instabilities appear to occur at the very high 17:1 and 19:1 resonances plus the midway point between the 16:1 and 17:1 resonances, and are dependent on the periastron longitude and/or mean anomaly of giant d. There seems to be no explanation for these exceptions.

There also appears to be many examples of Earth-Moon orbits which have chaotic eccentricity variations or chaotic eccentricity and semimajor axis variations. These are liberally spread throughout the habitable zone, including within the region between 1.9AU and 2.7AU, which from table 5.7 was originally thought to be stable. In all of the 121 integrations from tables 5.7, 5.8 and 5.9 that lasted the course of 100Myr, 41 showed chaotic tendencies, i.e. just over one third. With this percentage of Earth-Moon orbits which may not potentially last 1Gyr, the habitability of the system appears to rely on initial orbital elements and circumstances that are extra to the configurations of the giant planets. As stated previously at the end of section 4 of this chapter, this may be due to the fine gravitational balance of the system between order and chaos.

5.6 System Investigations with a 0.95 $M_{\odot}$ Star and Four Giants

The configuration of the three planets within 55 Cancri until 11th April, 2005 is shown in table 5.1 (Schneider, 2005) and has formed the basis of the study in the previous sections. Subsequently, a fourth planet, 55 Cancri e, has been confirmed and added to the system (McArthur et al., 2004). This has changed orbital parameters and physical properties of the previously known three giant planets. These new properties are shown in table 5.10.

Table 5.10. Current orbital Properties of the exoplanets in the 55 Cancri exosystem.

Parameters from 11/4/2005	Planet			
	e	b	c	d
$M_p \sin i_0 / M_J$	0.045 ± 0.01	0.784 ± 0.09	0.217 ± 0.04	3.92 ± 0.52
Semimajor axis/AU	0.038	0.115	0.24	5.257
Orbital Eccentricity	0.174 ± 0.127	0.0197 ± 0.012	0.44 ± 0.08	0.327 ± 0.28
Period / days	2.81	14.67	43.93	4517.4
Inner R_H multiplier	2.726	2.943	2.669	2.711
Outer R_H multiplier	6.709	3.587	8.595	8.050
1.03$M_{\odot}$ Inner gravitational reach / AU	0.029	0.092	0.108	2.019
1.03$M_{\odot}$ Outer gravitational reach / AU	0.051	0.143	0.429	11.487
0.95$M_{\odot}$ Inner gravitational reach / AU	0.029	0.091	0.108	1.977
0.95$M_{\odot}$ Outer gravitational reach / AU	0.051	0.144	0.432	11.610

The errors on all parameters other than minimum mass and eccentricity are less than 4% and are not considered in this short study. Both mass and eccentricity errors in table 5.10 will have a significant effect on inner and outer gravitational reaches of the giants. Despite the stellar mass still quoted as 1.03$M_{\odot}$ on the Schneider Exoplanet web site (Schneider, 2006), the mass calculated from the orbital elements used in equation 5.1 gave stellar masses of 0.927$M_{\odot}$, 0.943$M_{\odot}$, 0.956$M_{\odot}$ and 0.950$M_{\odot}$ for giants e, b, c and d respectively, giving a mean mass of 0.943$M_{\odot}$.

Table 5.11 Starting positions of the four giants at Julian Date 2450000.

Giant	Periastron Longitude / ^{o}	Julian Date of Periastron	Mean Anomaly / ^{o}
e	261.65 ± 41.14	2453295.31	105.05
b	131.49 ± 33.27	2453021.08	23.07
c	244.39 ± 10.65	2453028.63	20.81
d	234.73 ± 6.74	2452837.69	133.86

The stability of this new system configuration was tested in the absence of an Earth-Moon. The relative starting positions of the four giants are shown in table 5.11. To give the

arrangement every chance of showing stability, the hybrid integrator was used with close encounters stopping the run when planets passed within $0.1R_H$ of each other. The integration with these conditions and parameters, also using a stellar mass of $0.95M_\odot$ for consistency with the main study, lasted 2681 years before a close encounter occurred between giant b and giant c. In order to minimise the Hill radii distances between the planets, the masses and eccentricities were given their lowest values within the error limits from table 5.10 and the original stellar mass of $1.03M_\odot$ was used. Also the periastra longitudes were optimised within the errors so as to be closest to the arrangement with three planets in data prior to 11/04/05 (which was known to be stable). This planetary setup resulted in a hybrid integration run that lasted just over 31Myr before the giant e collided with the central body. Clearly the new planetary data for 55 Cancri yields a system that is not stable and may require reviewing, bringing into question whether or not giant e exists at all. This new four planet setup was not pursued further.

6. Theoretical integrations on satellites

The extensive integration studies in the previous chapters have investigated the orbital stabilities of Earth-like planets in or near the habitable zones (HZ) of known systems. The accompanying giant planet(s) in these systems have orbits that are interior to the HZ (HD 52265), exterior to the HZ (τ^1 Gruis, HD 196050) or both (55 Cancri) where there is more than one giant. The investigations have been carried out exclusively with the Fortran 77 Mercury Orbital Integrator program (Chambers, 1999 and Chambers & Migliorini, 1997) using the mixed-variable symplectic and hybrid integrators, which are designed to run with the largest body at the centre of the system.

The two systems to be studied in this chapter (HD 23079 and HD 28185) each have a giant planet within the HZ. This effectively negates any possibility of an Earth-type planet existing within the HZ of these systems in a stable orbit. There is a small chance that such planets could exist as Trojans to the giant. Laughlin & Chambers, 2002, regard this as viable, but there are no occurrences of such a phenomenon in the solar system involving large body Trojans, hence it is regarded as unlikely. A possibility does exist, however, of Earth-sized habitable satellites of the giant planets in these systems. To investigate this arrangement using the same program, however, there needs to be a shift from astrocentric systems to ones of a planetocentric nature, the same as the geocentric system as perceived by ancient civilisations. The relative motions of all bodies are still the same, but from the program's perspective the star orbits the planet, hence the largest body is no longer at the system's centre. Personal communication with the program writer (Chambers, 2004) revealed that the 15th order RADAU integrator could be used for this study (Everhart, 2002 & 1974). First, though, this integrator needed to be tested on a known stable satellite system to prove it can handle such configurations, of which the Galilean satellites of the Jovian system were chosen. Secondly it needed to be tested on a theoretical system to ensure results were within the bounds of physical laws and that the outcomes for satellites in their orbits were as predicted by the restricted three-body problem theory. One major difference to be noted with the RADAU Integrator is that it sets its own time step interval between each positioning of bodies within their orbits, provided that the initial time step is set sufficiently small, i.e. 1/20th the period of the smallest initial orbit. Hence if there are many interactions between bodies in very small orbits, the RADAU integrator will allow for this and adjust its time step to be as small as is required. In contrast, the time step for the MVS or Hybrid Integrators is set by the user to be 1/20th the period of the smallest initial orbit and is invariant, leading to possible errors when close encounters between bodies occur.

6.1 Previous work

In contrast to the extensive research into the stability of possible Earth-type planets within the HZ of known extrasolar planetary systems, there is much less on the study of orbital stability of possible satellites of giant planets within the HZ. This may be due to the problem of detecting Earth-sized satellites being more challenging than for Earth-sized planets. As an example, Jupiter causes the Sun to orbit their common centre of gravity at an average speed of 12.46ms^{-1}. An Earth-mass satellite of Jupiter orbiting at the distance of Ganymede would cause small oscillations in the Sun's motion with an amplitude of 0.033ms^{-1}. Thus the chances of detecting such a satellite's influence on astrometric measurements or the Doppler shift of stellar spectral lines would go unnoticed, even with the new generation of space telescopes due for launch. Despite the overwhelming brilliance of the star, direct observation may be possible with these new space telescopes (Darwin or the James Webb Space Telescope), as would be transits. For orbits inclined at or close to 90^{O} to the celestial sphere, the relative drop in light level from the star due to an

Earth-sized satellite would be 0.01% to 0.001% and it may be possible to detect such transits with forthcoming instruments due to be commissioned over the next five to fifteen years. The easiest detection method for satellites of giant planets would be by gravitational microlensing. Unfortunately there would be no way, in such one off events, of knowing whether the small light spikes close to that of the giant planet(s) were caused by satellites or other similar Earth-sized planets within the system that happen to be in alignment with the giant.

There is much research using numerical analysis into the behaviour of satellite orbits in general, including solar system and artificial satellites, however this only takes into account the orbits of the satellites around the large central body, which is the planet. Much of the previous numerical analyses of satellite orbits, such as the Kozai formalism (Kozai, 1962) of Cuk and Burns (2004) does not allow for the presence of the star within the system. The Poisson's small parameter method of Kudryavtsev (1995), the Runge-Kutta-Nystrom numerical analysis method of Hadjifotinou and Harper (1995) and the recurrent power series method of Hadjifotinou (2000) are more concerned with the effects of planet oblateness on satellite orbits, while Mikkola's (1999) symplectic methods is specific to modelling atmospheric drag. None of these analyses pursue true satellite orbits around a central planet in the presence of the star.

Using an extensive numerical investigation method, Ichtiaroglou and Voyatzis (1990) did allow for the effects of the star in their study of the effect of elliptical parent planet orbits on their satellites, finding that most orbits are unstable and/or chaotic. Barnes and O'Brien (2002) used tidal theory and numerical orbital integrations, also incorporating the star, to investigate the effects of tides on satellite orbits, finding that Earth-sized moons of Jovian planets could exist in stable orbits within the HZ for 5 Gyr in systems with a star of mass greater than $0.15M_{\odot}$. Weiss and Stewart (2002) also used numerical integrations to investigate the fate of satellites of giant planets during inward planetary migration. Their results show that Earth-sized satellites would remain in orbit around the giant provided planet migration halted within the HZ. Although Williams, Kasting and Wade (1997) perform no orbital studies of potentially habitable satellites of giant planets, they give a brief account of the hurdles, which must be overcome for life to arise on such bodies. Additional to those experienced by planets they also discuss the necessity of satellites to have a strong magnetic field, required to prevent atmospheres being lost due to the constant bombardment of energetic ions from the giant's magnetosphere. The work undertaken here may be the first in depth study into the long term stability of satellites, over 100Myr, of giant planets in orbits confined to the habitable zone

6.2 Initial testing of the RADAU integrator on a satellite system

The Jovian system consists of 62 satellites as at 18/01/05 (Jacobsen, 2005), of which the four Galilean satellites are considerably more massive than the rest. Table 6.1 shows distances from Jupiter, radii and masses of the Galilean moons, Io, Europa, Ganymede, Callisto along with, for contrast, the fifth and sixth largest satellites, Amalthea and Himalia.

The table clearly shows the distinction in size between Io, Europa, Ganymede and Callisto and the largest of the rest. The masses of Himalia and Amalthea are so small compared to the Galilean moons that for the purpose of this investigation, they, with the remaining moons, will not be considered.

Table 6.1 Essential physical data for the six largest Jovian satellites.

Satellite	Distance from Jupiter (km)	Radius (km)	Density ($H_2O = 1$)	Mass (10^{20} kg)	Mass (Europas)
Amalthea	181,300	86	1.8 *	0.0717 *	0.00015
Io	421,600	1,821	3.55 *	893.3	1.862
Europa	670,900	1,565	3.01 *	479.7	1.000
Ganymede	1,070,000	2,634	1.94 *	1482	3.089
Callisto	1,883,000	2,403	1.86 *	1076	2.243
Himalia	11,480,000	85	2.8 *	0.0956 *	0.00020

(Murray and Dermott, 1999)
* (Hamilton, 2005)

Table 6.2 Starting condition of the Jovian satellite orbits, with the Sun, for each of the integrations (Jacobsen, 2005).

"Satellite"	Semimajor Axis (AU)	Orbital Eccentricity	Inclination (°)	Longitude of Perijove (°)	Longitude of Ascending Node (°)	Mean Anomaly (°)
Io	0.00282	0.0041	0.036	83.898	44.208	342.021
Europa	0.00449	0.0094	0.469	88.684	219.383	171.016
Ganymede	0.00716	0.0011	0.170	203.214	63.692	306.589
Callisto	0.0126	0.0074	0.187	57.714	294.195	180.997
Sun	1.0 or 5.2	0.0484	3.12	0	0	0

The initial starting condition for each of the integrations, shown in Table 6.2, was obtained from NASA (Jacobsen, 2005) and is the real positions of the satellites within the Jovian system as at 16th January 1997. Previous studies on planetary systems would have the orbital integrator stop when there are close encounters between two bodies, which pass within $3R_H$ (Hill radii) of each other, according to the Hill radius formula in chapter 4, section 1. However to test the stability of the satellite system thoroughly, the integrator was programmed not to stop on a close encounter and to allow collisions between any of the bodies. The close encounter distance for each body was changed from $3R_H$ to $0.1R_H$ to minimise the size of the file that records close encounters, "ce.out". As satellite orbit parameters evolve during a run, of which the semimajor axes and eccentricities are most important, many close encounters may ensue and would lead to the generation of a large close encounter file. This would slow the program during each writing procedure to this file. The $0.1R_H$ distance is less than 1% of the initial nearest neighbour distance, which is why it was used. Table 6.3 shows multiples of the Hill radii of each satellite, with respect to Jupiter, compared to the distances of closest approach between each body's nearest neighbours, according to the initial conditions and allowing for orbital eccentricity of each body (see table 6.2). It shows that the $3R_H$ distance is an appreciable fraction of the initial nearest neighbour distance whereas the $0.1R_H$ distance is a small fraction.

Table 6.3 Comparison of Hill radius multiples with distances of closest approach

"Satellite"	0.1 R_H/AU	1 R_H /AU	3 R_H /AU	Nearest Neighbour's Distance /AU
Io	7.06×10^{-6}	7.06×10^{-5}	2.12×10^{-4}	1.62×10^{-3}
Europa	9.14×10^{-6}	9.14×10^{-5}	2.74×10^{-4}	1.62×10^{-3}
Ganymede	2.12×10^{-5}	2.12×10^{-4}	6.37×10^{-4}	2.62×10^{-3}
Callisto	3.36×10^{-5}	3.36×10^{-4}	1.01×10^{-3}	5.34×10^{-3}
Sun at 5.2 AU	3.662	36.62	109.9	4.936
Sun at 1.0AU	0.704	7.042	21.13	0.939

The Hill radius quoted for the Sun shows that the version of the Hill radius formulae, used in the orbital integrator (equation 4.1), is inappropriate when the orbiting body is anything but small compared to the central body (here the orbiting body is much larger and so $M_*/3M_p >> 1$, where M_* is the Sun's mass and M_p is the central body's or planet's mass). Clearly, the Hill radius, the distance between two orbiting bodies where gravitational

forces balance in the rotating orbital frame, cannot be beyond the distance between the two bodies. A second version of the Hill radius formula, equation 6.1 (Murray & Dermott, 1999), is derived from equations of motion in the rotating frame, see Appendix 3, where R_H cannot be greater than $0.6934a$. This would be more appropriate for satellite integrations where for a central mass M_p and orbiting mass M_* with semimajor axis a,

$$R_H = a\left(\frac{M_*}{3(M_* + M_p)}\right)^{1/3} \qquad 6.1$$

Four orbital integrations of the Jovian system, using the initial parameters displayed in Tables 6.1 and 6.2 were run over the next ten million years. Jupiter's semimajor axis was 5.2AU and 1AU, and the J_2 moment of Jupiter, valued at 0.014736 (Murray & Dermott, 1999) is included and excluded in each case. The J_2 term is a measure of a planet's oblateness caused by its rotation. For a planet that is axially symmetric about its rotation axis it is given by,

$$J_2 = \frac{C - A}{M_p r^2} \qquad 6.2,$$

where C and A are the moments of inertia about the polar and equatorial axes respectively, M_p is the planet's mass and r is its equatorial radius. All runs lasted the course of the integration and in all runs, each of the semimajor axes were unchanging. Figure 6.1 shows the evolution of the eccentricity when J_2 effects are included and Figure 6.2 shows the eccentricity evolution when J_2 effects are absent. It is clear that the inclusion of the J_2 term in the central body has an effect of retaining the original eccentricity of the satellites, whereas its absence results in slightly more circularised orbits with less variation. There is no change in the solar eccentricity as it is too far away from Jupiter, since the J_2 effect decreases with the inverse square of an orbiting bodies distance (Murray & Dermott, 1999, page 151). For similar runs with the Sun-Jupiter distance initially at 1AU, all semimajor axes were again invariant and the same eccentricity effect was seen when the J_2 term was present and absent. The major difference in the eccentricity was its greater variation, presumably due to the more powerful gravitational perturbation effects of the Sun on the satellites (Figure 6.3).

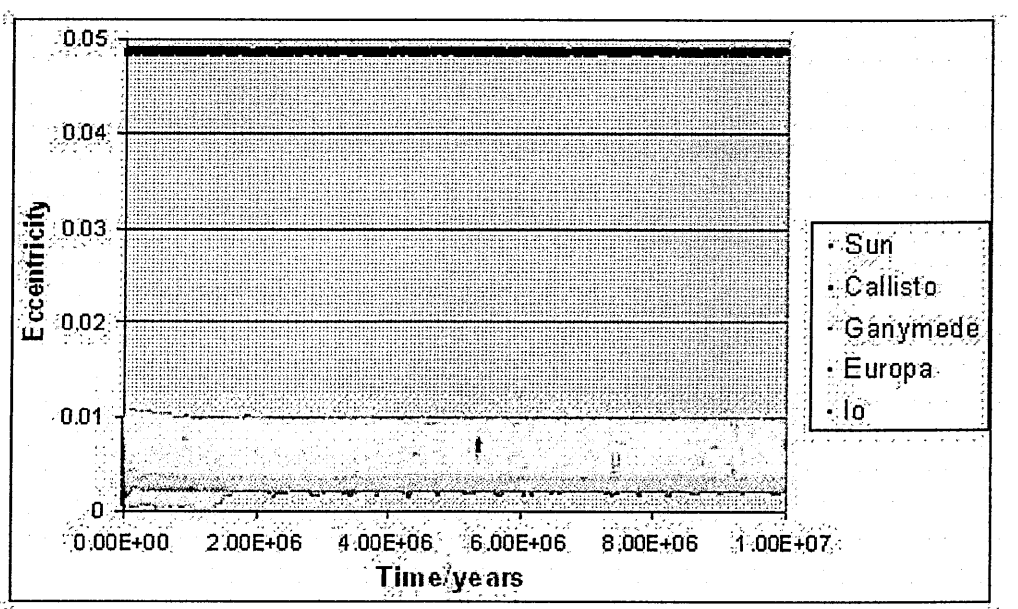

Figure 6.1 Eccentricity of the Galilean satellites with time, with Jupiter's J_2 moment, over the next 10 million years using the Mercury 6_1 RADAU integrator.

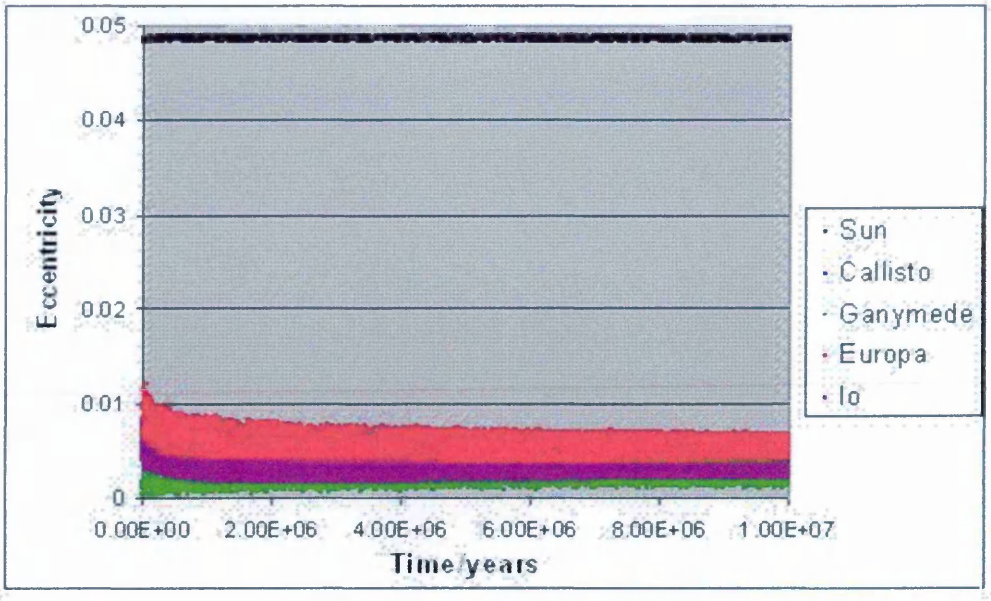

Figure 6.2 Eccentricity of the Galilean satellites with time, without Jupiter's J_2 moment, over the next 10 million years using the Mercury 6_1 RADAU integrator.

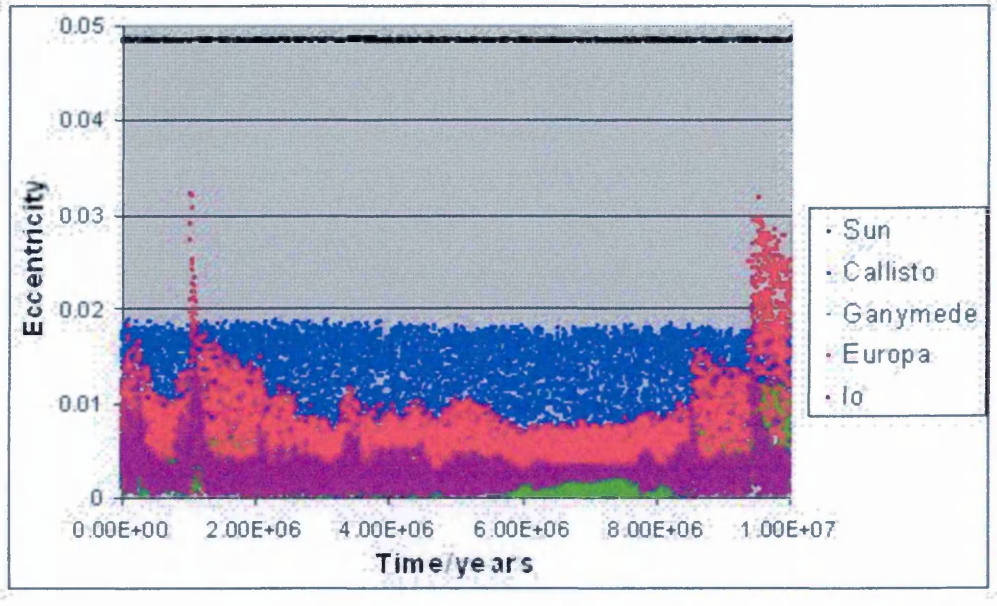

Figure 6.3 Eccentricity of the Galilean satellites with time, without Jupiter's J_2 moment, at 1AU from the Sun using the Mercury 6_1 RADAU integrator.

A final feasibility test was carried out to see if a planet as large as Earth, hence capable of supporting life, could exist as a satellite with a stable orbit of a giant within the habitable zone. This involved two further integration runs, with and without Jupiter's J_2 moment, where the giant was 1AU from the Sun and an Earth-Moon planet replaced the orbit of the outermost Galilean satellite, Callisto, with no other satellites present. The integration lasted its 10Myr term and was completely stable in both cases. Figure 6.4 shows the variation of eccentricity for Sun and Earth-Moon with time, revealing stable limits within the variation, which oscillated once between maximum values over a period of ca. 9,000 years. A virtually identical outcome was obtained for a similar integration where Jupiter's J_2 moment was absent.

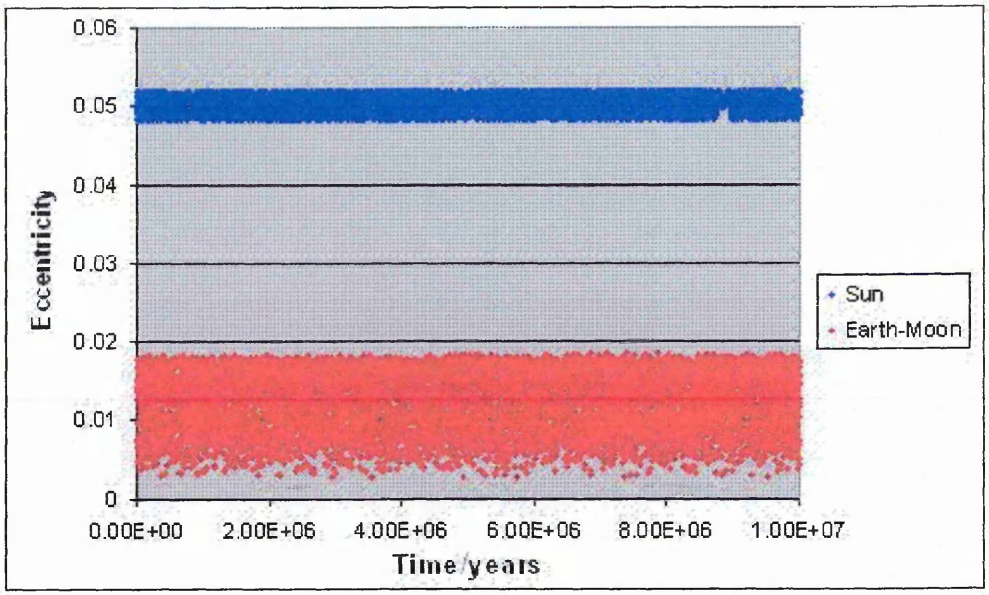

Figure 6.4 Eccentricity of an Earth-Moon orbiting Jupiter with time at 1AU from the Sun, with Jupiter's J_2 moment, as determined by Mercury6_1 RADAU integrator.

This initial investigation shows that the Mercury RADAU integrator can be used to determine the outcome of satellite orbits around giant planets. It also reveals that an Earth-Moon-mass satellite will have a stable orbit when 0.0126AU from a Jupiter mass body, which is itself 1AU from a solar mass star. This is as expected since the Hill radius of the giant in this situation, and under heliocentric circumstances, according to equation 4.1, is 0.0682AU.

6.3 Theory of the Restricted Three-Body Problem

The next stage is to test the RADAU integrator as to whether it predicts the correct outcome of a satellite in orbits of varying distances around a giant planet. Before this, however, it is necessary to determine what these outcomes should be by investigating the "restricted three-body problem". The orbital mechanics of three bodies can be used to determine gravitational zero-velocity curves for different pseudo-potentials, of a system in which two of the bodies are massive and in circular orbits about their centre of mass, and the third body is of negligible mass. These pseudo-potentials have a direct effect on the trajectory of the third body, which is free to roam the system but must remain in the same plane as the orbits of the two major bodies if launched in that plane. The term pseudo-potential is used because the entire frame of reference, in which they lie, is rotating with respect to a fixed X-Y coordinate set. The two main bodies, on the x-axis, rotate about their common centre of gravity ($0 = X = Y = x = y$) at the same rate as the x-y reference frame (Figure 6.5). They allow predictions to be made, from curves of zero-velocity in the rotating frame, as to the fate of small satellite bodies within the system. Pseudo-potentials are, therefore, used to see whether a satellite, orbiting at certain initial distances from the giant planet, would remain in orbit around the giant or whether it could break from its orbit and become another planet. If orbits are unstable, it would be possible to predict whether satellites would have only one fate of colliding with the planet or whether it could also collide with the star or be ejected from the system.

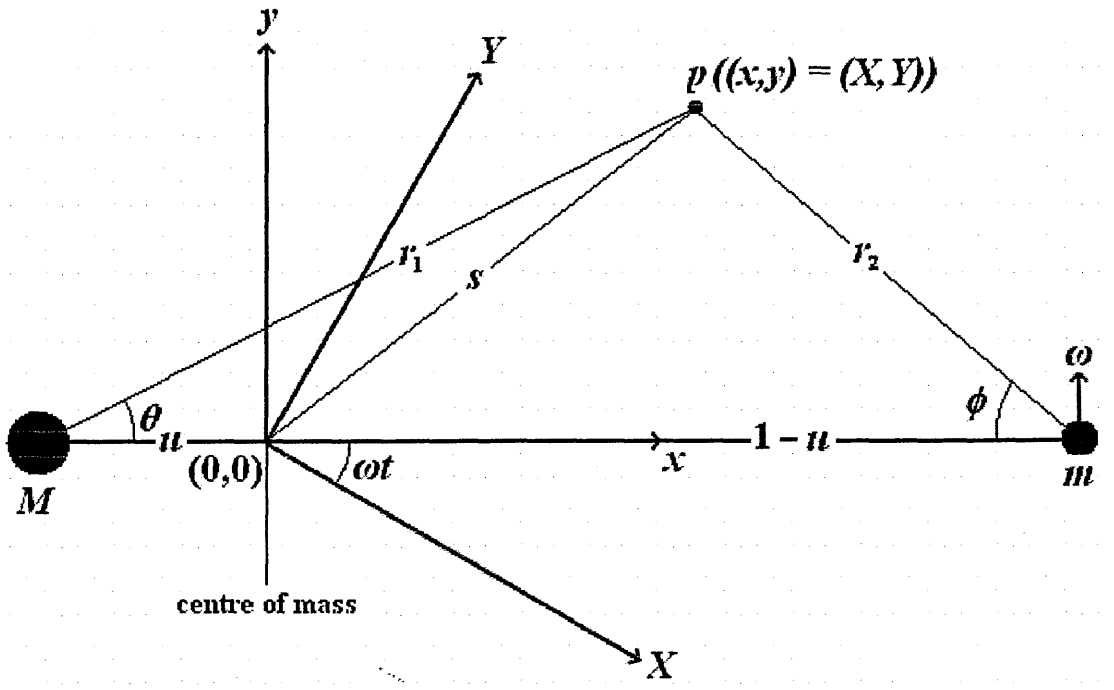

Figure 6.5 The configuration for determining pseudo-gravitational potentials.

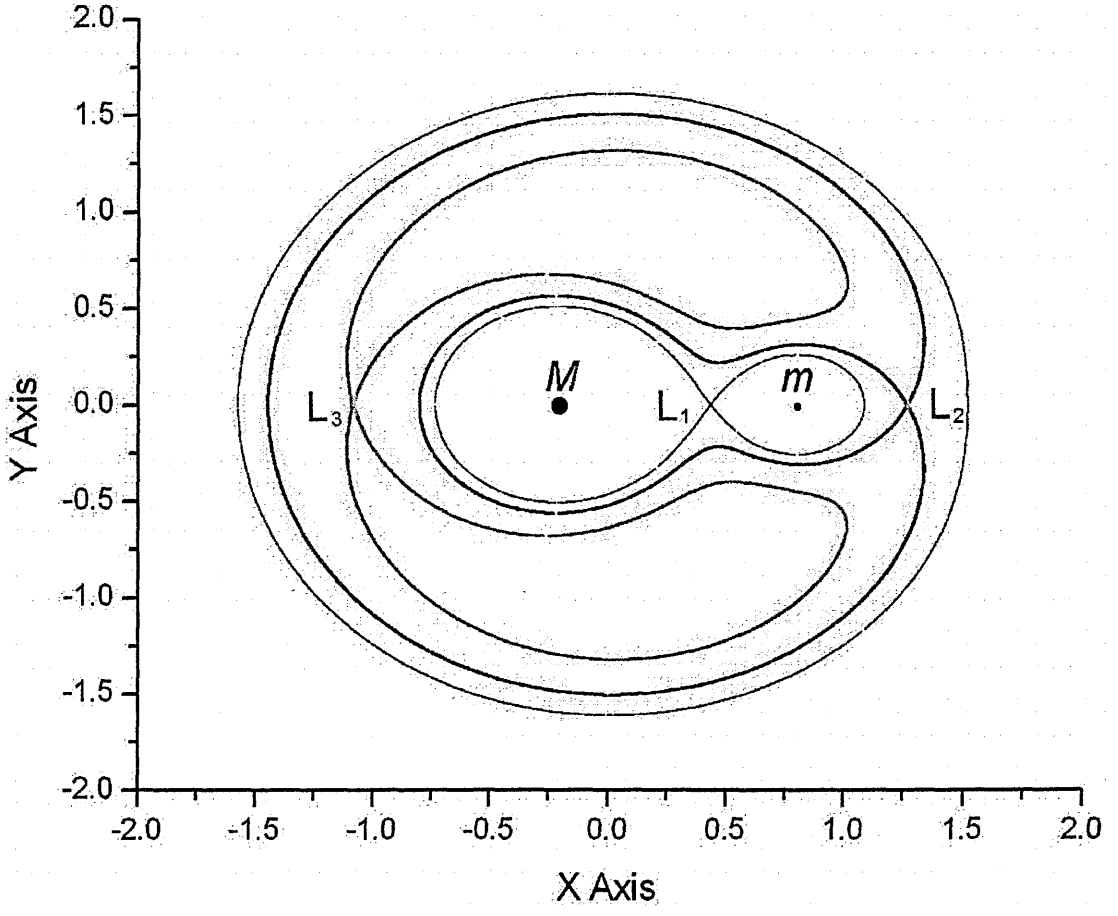

Figure 6.6 Zero-velocity curves passing through the x-axis Lagrangian points of a binary system where $m/(M + m) = u = 0.2$. The Jacobian constants, C_J (see equation 6.2), for the L_1, L_2 and L_3 are 3.805, 3.552 and 3.197 respectively.

Figure 6.6 shows three critical zero-velocity curves for a binary star system where, for the purpose of clarity, the secondary, m, is much more massive than a planet. The figure helps to illustrate the fates of small third bodies within this system. Particles launched in orbits closer to M or m than the black line will remain in stable orbits about those respective

bodies or collide with those respective bodies. Particles launched in orbits closer to M or m than the inner red line, but outside the black line, will orbit about either of those bodies or collide with either of those bodies. Particles launched in orbits outside the inner red line will remain in a distant orbit about both bodies, collide with either of those bodies or be ejected from the system. Particles launched within the green boundary may settle in orbits around mass M, bounded by the green boundary. These would then become Trojans of the second body in the system provided $m/M < 0.03852$. The outer black curve has the same Jacobian Constant, C_J (see equation 6.2), as the curve passing through the L_1 point but is on the outer side of the L_2 and L_3 points. For a giant planet orbiting around a star, $m/(M + m)$, or u, is of the order of 0.001 and the L_1 point will be less than 10% distant from the planet of its semimajor axis. A three dimensional profile of zero-velocity curves, for the same mass ratios used for Figure 6.6, are shown in figure 6.7, revealing a zero-velocity surface. This is a plot of Jacobian Constants, C_J, along the x-y rotating plane, where when $v = 0$, $C_J = 2U_J$ (see Appendix 2) and U_J is pseudo-potential. The plot is upside down for clarity. The larger and smaller masses are depicted by the larger and smaller wells respectively. The L_1 position is the saddle point between the masses, the L_2 position is the saddle point nearer the smaller mass and the L_3 position is the saddle point nearer the larger mass. As these Lagrangian points are saddles, they are unstable. The two 'peaks' either side of the smaller mass are the L_4 and L_5 positions, which are stable only if $m/M < 0.03852$.

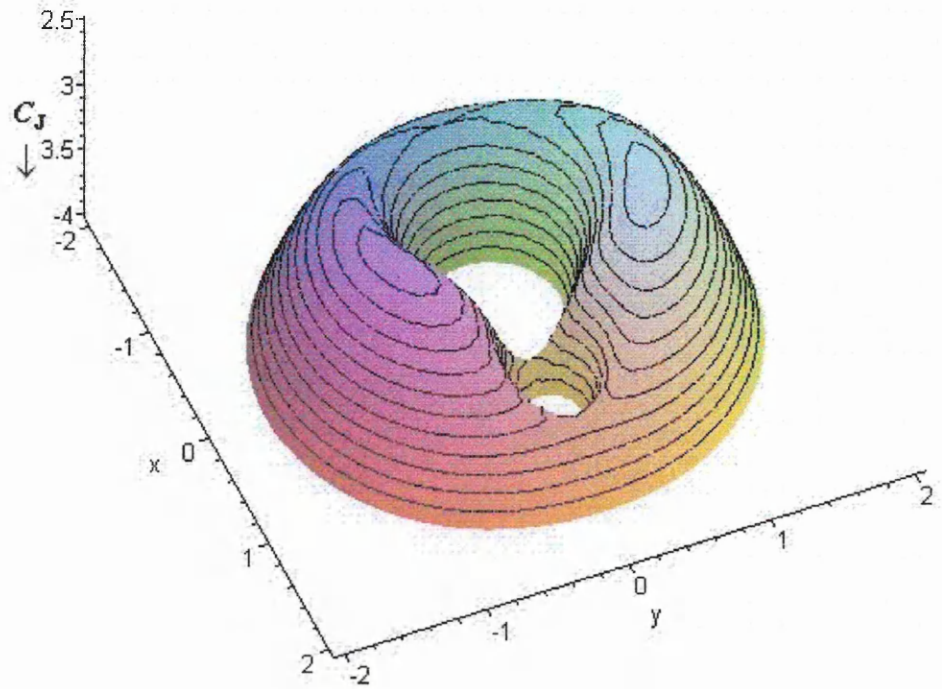

Figure 6.7 Zero-velocity surface of a binary system where $m/(M + m) = u = 0.2$.

Equation 6.3 is used to produce these curves and surfaces and is derived in Appendix 2 as equation A2.32,

$$C_J = x^2 + y^2 + 2\frac{(1-u)}{\sqrt{(x+u)^2 + y^2}} + 2\frac{u}{\sqrt{(x-1+u)^2 + y^2}} \qquad 6.3.$$

It is a considerably simplified equation in that the giant planet's semimajor axis and the angular velocity of the rotating frame are always unity. Also the mass of the system is defined such that $G(M + m) = 1$, where G is the Universal Gravitational Constant. These steps avoid the unnecessary and complicating use of constants in the derivation. The positions on the x-axis of the three Lagrangian points can be found from equation 6.3, where, since $y = 0$,

$$C_J = x^2 + 2\frac{(1-u)}{\sqrt{(x+u)^2}} + 2\frac{u}{\sqrt{(x-1+u)^2}} \qquad 6.4.$$

Differentiating equation 6.4 with respect to x and letting $dC_J/dx = 0$ gives each Lagrangian point depending on the associated sign taken from the square roots of the denominators. The equations, derived in Appendix 2 as equation A2.34, to find the x-coordinates for the L_1, L_2 and L_3 points respectively are given by,

$$\frac{dC_J}{dx} = f_1(x) = x - \frac{(1-u)}{(x-u)^2} + \frac{u}{(x-1+u)^2} = 0 \qquad 6.5,$$

$$\frac{dC_J}{dx} = f_2(x) = x - \frac{(1-u)}{(x-u)^2} - \frac{u}{(x-1+u)^2} = 0 \qquad 6.6,$$

and

$$\frac{dC_J}{dx} = f_3(x) = x + \frac{(1-u)}{(x-u)^2} + \frac{u}{(x-1+u)^2} = 0 \qquad 6.7,$$

These equations can only be solved using iteration techniques, of which the Newton-Raphson method is used here. The iteration starts on the line $y = f_l(x)$ (l = 1, 2 or 3) at a point (x_1,y_1) near to the x-axis where the line $y = f_l(x)$ crosses, as shown in Figure 6.8. Since $y_1 = f_l(x_1)$, the tangent of the curve at this point crosses the x-axis at $(x_2,0)$ and the slope of this tangent, $f_l'(x_1)$, is $f_l(x_1)/(x_1 - x_2)$. The same procedure is then repeated at the point (x_2,y_2) so that $f_l'(x_2) = f_l(x_2)/(x_2 - x_3)$. Hence at the point (x_n,y_n), then $f_l'(x_n) = f_l(x_n)/(x_n - x_{n+1})$. Simple rearrangement of this gives,

$$x_{n+1} = x_n - \frac{f_l(x_n)}{f_l'(x_n)} \qquad 6.8.$$

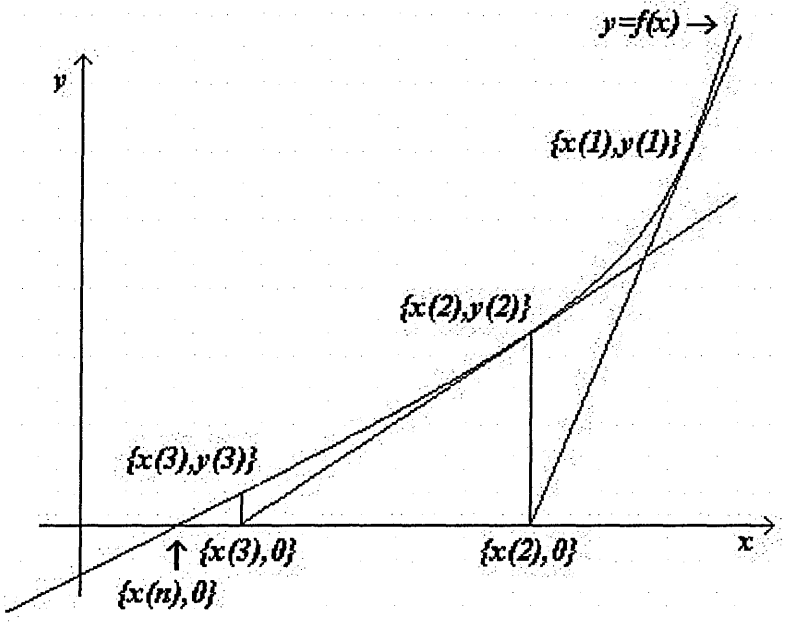

Figure 6.8 Diagramatic outline of the Newton-Raphson iteration technique.

So the iteration equations for the L_1, L_2 and L_3 points respectively are,

$$(L_1) \quad x_{n+1} = x_n - \frac{x_n - \frac{(1-u)}{(x_n-u)^2} + \frac{u}{(x_n-1+u)^2}}{1 + \frac{2(1-u)}{(x_n-u)^3} - \frac{2u}{(x_n-1+u)^3}} \qquad 6.9,$$

$$(L_2) \quad x_{n+1} = x_n - \frac{x_n - \dfrac{(1-u)}{(x_n-u)^2} - \dfrac{u}{(x_n-1+u)^2}}{1 + \dfrac{2(1-u)}{(x_n-u)^3} + \dfrac{2u}{(x_n-1+u)^3}} \qquad 6.10,$$

and

$$(L_3) \quad x_{n+1} = x_n - \frac{x_n + \dfrac{(1-u)}{(x_n-u)^2} + \dfrac{u}{(x_n-1+u)^2}}{1 - \dfrac{2(1-u)}{(x_n-u)^3} - \dfrac{2u}{(x_n-1+u)^3}} \qquad 6.11.$$

The iterations should converge to an x-value and is stopped when the difference between the two x_{n+1} and x_n is less than 0.0001, i.e. too small to be of any significance. This final x-value is the solution of the equation. The iteration must be started near to the solution value otherwise the wrong result for x may be obtained.

6.4 Determining the Starting Points of the Iteration Process to find the Lagrangian Points L_1, L_2 and L_3.

In order to find the Lagrangian points in the line of the two bodies, the best starting point for the iterations in equations 6.9 and 6.10, is to use the two Hill radii distances either side of the secondary mass. The best starting point for iteration equation 6.11 is the point opposite the primary mass from the secondary at the same distance as the secondary. These three different points are required since equations 6.9 to 6.11, which determine L_1, L_2 and L_3 respectively, are discontinuous functions with discontinuities at the coordinates of the two bodies. If the iteration starting points were too distant from their respective Lagrangian points, the iterations may diverge or converge to the wrong value. The point opposite the planet, used to start the iteration to find L_3, is perfectly adequate for this purpose and requires no investigation here. The iteration starting points for L_1 and L_2, however, do require further investigation, as now outlined.

The Hill radius formula used within the Mercury Orbital Integrator and previously (Jones et al., 2001, Barnes and O'Brien, 2002), has been derived in Appendix 1, where, for a body separation distance, a, and Hill radius, R_H,

$$R_H = a\left(\frac{m}{3M}\right)^{1/3} \qquad 6.12$$

A second version derived in Appendix 3, where $u = m/(M+m)$ is,

$$R_H = a\left(\frac{u}{3}\right)^{1/3} \qquad 6.13.$$

For small values of u, this will be very close to the first Hill radius approximation in equation 6.12, since when m is small, $m/M \approx m/(M+m)$. As these equations are only guidelines to start the L_1 and L_2 iterations, this second Hill radius formula in equation 6.13, could be more useful since, even if the assumption that $m \ll M$ is not met and m is comparable to M, u is never greater than 0.5, i.e. R_H/a is never greater than 0.550. This is an advantage since from equation 6.12, R_H/a would be as high as 0.693 for a system where two masses are equal, yet the true distance of balancing gravitational forces is 0.5, then equation 6.13 gives a much better Hill radius approximation even for comparable masses. So for iterations to determine L_1, and L_2, then equation 6.13 would be a better choice of Hill radius, as an indicator as to where to start. This is important as too large an inaccuracy in the iteration starting point may cause the iteration to diverge or converge to the incorrect L_1 and L_2 positions.

Comparing the two versions of the Hill radius formulae, table 6.4 shows the calculated values of R_H/a, for different orders of u.

Table 6.4, Comparison of Hill radii as determined from different formulae versions.

u	$(R_H/a) =$		L_1	L_2	Mean L_1 & L_2
	$(u/3)^{1/3}$	$(m/3M)^{1/3}$			
0.5	0.550	0.693	0.5	0.698	0.599
0.1	0.322	0.333	0.291	0.360	0.325
10^{-2}	0.149	0.150	0.142	0.157	0.149
10^{-3}	0.0693	0.0694	0.0677	0.0709	0.0693
10^{-4}	0.0322	0.0322	0.0318	0.0325	0.0322
10^{-5}	0.0149	0.0149	0.0149	0.0150	0.0149
10^{-6}	0.0069	0.0069	0.0069	0.0069	0.0069

The table shows that the established Hill radii formulae, in equations 6.12 and 6.13, give excellent agreement with the mean of the L_1 and L_2 points (all three columns of which are shaded) for increasing values of u, up to $u = 0.1$, when the error is 1% in equation 6.13 and 2.5% in equation 6.12. Indeed, equation 6.13 is the best approximation of all, giving better agreement than equation 6.12 up to $u = 0.5$. This justifies its choice to start iteration convergences to determine the L_1 and L_2 positions. Note also that for very small u, the distances of the L_1 and L_2 positions from the secondary are virtually equal but start to diverge when $u = 10^{-4}$, until the difference of each from the mean, when u = 0.5 is 16.53%.

6.5 Boundaries for Particles defined by Zero-Velocity Curves

Having established the formulae to determine the zero-velocity curves for a range of pseudo-potentials within a binary system, we can now briefly explore the meaning of these curves and what they imply for small bodies or particles orbiting close to the secondary mass. From section 3 of this chapter, zero-velocity curves are imaginary lines around a binary system where the purely pseudo-potential energy, U_H, of a much smaller particle having no kinetic energy in the rotating frame, or zero-velocity, is the same.

So far the Maple V Release 5 program (Waterloo Maple Inc. November 27th 1997) has been used to obtain and analyse zero-velocity curves for particular systems. This method is rather cumbersome and not widely known, so four programs were written in the 'C' computer language to make such analyses more accessible.

6.6 Computer Programs determining Zero-Velocity Curves

There are four computer programs described in this section, all written by me in the C programming language. All can be compiled and run on a Unix or Linux system or within a DOS box on any 32-bit Windows operating system. For the purpose of writing, compiling and checking each program, a Microsoft Windows compatible C-compiler was used, supplied as freeware by Digital Mars at www.digitalmars.com by Walter Bright Copyright (c) 1997-2003. All four programs have clearly labelled comment lines to explain the function of each section. Each program is written specifically to be used most easily with binary systems where the primary body is a star and the secondary is a planet. All programs have fail-safes for each input value, so that generated results have physical meaning. Potentially useful information is displayed on-screen such as mass fraction of the secondary in the system, the secondary's Hill radius details, locations of Lagrangian points and Jacobian constants at these points. Zero-velocity data is written to an output file, which resides in the same directory as the program. The user sets the resolution in each program, which determines the amount of data, printed to file and the length of time the program takes to run. All programs are processor intensive and not reliant on random access memory or hard disk space. The programs were tested at their highest resolution on a 1.2GHz AMD processor, the first of which takes just one second to run, creating a data file of 4.6 megabytes. The second program takes 50 seconds to run, creating a data file of 1.13 megabytes and the third and fourth programs take 8 seconds to run, creating data files

of 1.3 megabytes. This data can be imported into a program of the user's choice for visual representation. Some final on-screen footnotes advise how best to proceed. All calculations in each program are exact, only the Hill radii are approximations, as determined from equation 6.13.

6.6.1 Zero-Velocity Surfaces

This first program creates a three-dimensional view of many zero-velocity curves in a binary system, i.e. a zero-velocity surface, an example of which is shown in Figure 6.7. The code for the program is presented in Appendix 4 as program A4.1, under the name "zvcurves.c", the name of the file containing the source code. The program will start by typing "zvcurves" at the command prompt. The operator is asked to enter a mass for the primary body, in terms of solar masses, followed by a mass for the secondary body, in terms of Jupiter masses, and finally the distance between the two bodies, in Astronomical Units. Each of these values must be within boundaries, beyond which the program will stop with an appropriate message advising the user how best to proceed next time. The mass of the primary must be greater than zero solar masses, the mass of the secondary must be greater than zero and up to the primary's mass, and the distance between the bodies must be greater than zero astronomical units. The program then prints to the monitor screen the mass fraction of the secondary body in the system followed by the distance of the Hill radius from the planet according to equation 6.13. The distances are displayed of the Hill radius on either side of the secondary along the x-axis, with the x-coordinate of the point equidistant from the primary and secondary but on the other side of the primary. The positions of the L_1, L_2 and L_3 Lagrangian points are determined using the Newton-Raphson iteration technique of equations 6.9, 6.10 and 6.11 respectively. There are 100 iteration steps, which is sufficient for obtaining the Lagrangian positions accurately enough, considering that for planets as secondary masses where usually $0.001 < u < 0.01$, the starting iteration point is extremely close to the true Lagrangian position, see Table 6.4. The Jacobian constants, C_J, for the curves that pass through the three points L_1, L_2 and L_3 are then calculated from equation 6.4 (with the appropriate signage for each Lagrangian point determined from equations 6.5, 6.6 and 6.7) and displayed on-screen. The user is requested to enter the number of plotted points (10 to 100) between each body, i.e. a value which determines the size of the data output file and the resolution of the zero-velocity surface. The program then uses equation 6.2 to calculate the Jacobian constants over a grid of x- and y-values, where $(-2,-2) \leq (x,y) \leq (2,2)$. The Jacobian constants are plotted with increasing values in the $-z$ direction, so that when represented graphically, the potentials around the masses are represented as wells and not peaks. The x- and y-values are printed to the file with a Jacobian constant for each x,y coordinate. The program tells the user that it has successfully completed its tasks and gives the file-name where the data is stored, in the same directory as the execution program. The file-name must then be renamed otherwise the next program run will overwrite the data. Finally the program tells the user the command to operate the program, which determines single zero-velocity curves for any one particular Jacobian constant.

An example of a graphical representation of data, where $u = 0.2$, $a = 1$, with a resolution of 20 points between the two masses, is shown in figure 6.9. This was obtained using Microcal Origin Version 6.0, copyright © 1991-1999, Microcal Software Inc., Northampton, MA, USA. The diagram has the same data as Figure 6.7 obtained using the Maple V program and clearly shows the larger pseudo potential well of the primary and the smaller well of the secondary. This depiction is good for showing potential wells for bodies of similar masses. Figure 6.10 shows a similar zero-velocity surface where the resolution and semimajor axis are the same but u is 0.001. The potential well of the primary is clearly evident but that of the planet has almost disappeared, and is actually a small hole to the lower right of the star. The planet is uncovered in figure 6.11, when the

resolution is taken to the maximum 50 points between the two masses and the area around the planet is magnified.

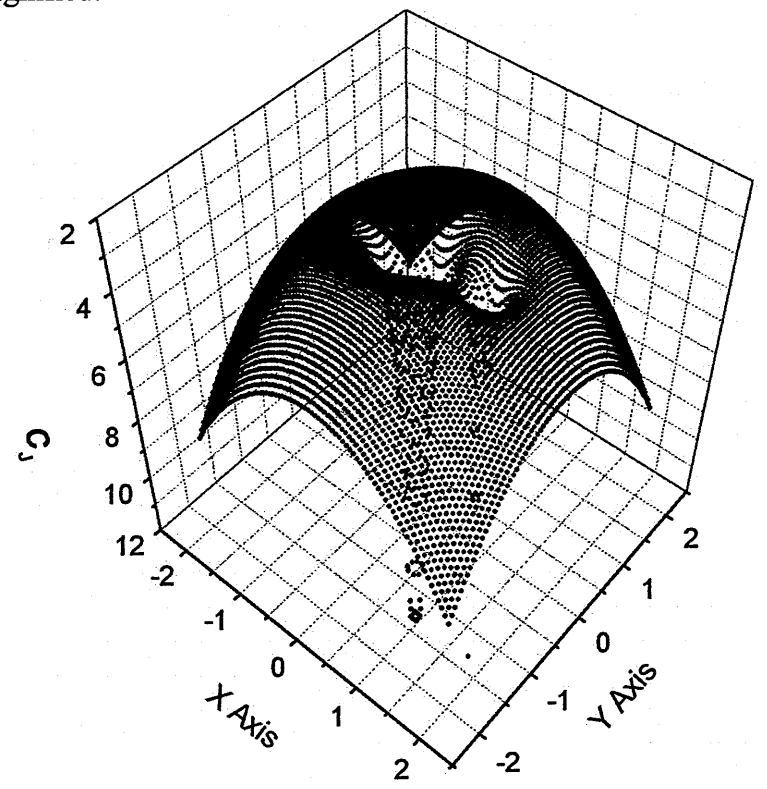

Figure 6.9 Zero-velocity surface for a binary system where $u = 0.2$ and $a = 1$.

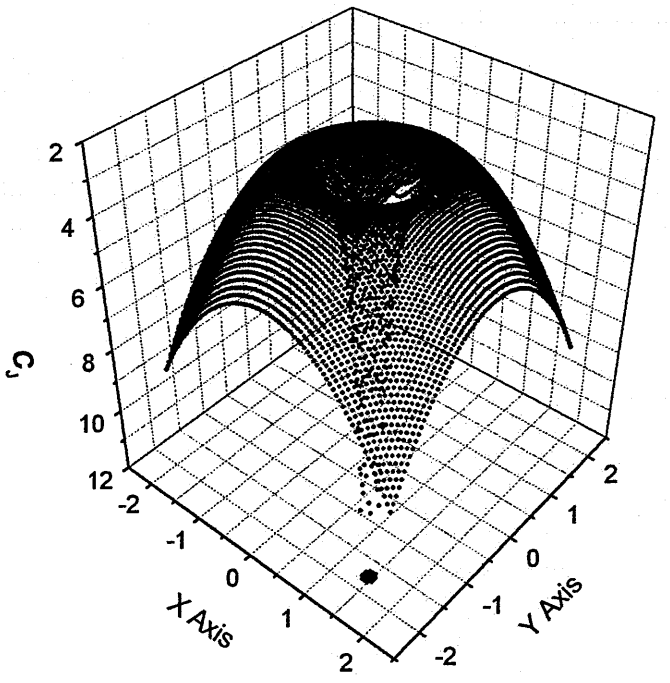

Figure 6.10 Zero-velocity surface for a binary system where $u = 0.001$ and $a = 1$.

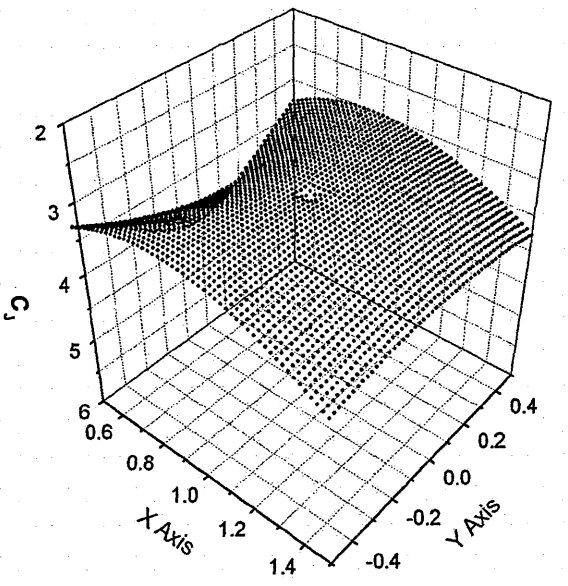

Figure 6.11 Zero-velocity surface for a binary system where $u = 0.001$ and $a = 1$, concentrated around the planet.

6.6.2 Two-Dimensional Zero-Velocity Curves

This second program is very similar in its make-up and operation to the previous one. The code for this program is presented in Appendix 4 as program A4.2 under the name "2dcurves.c", the name of the file containing the source code. For each run it creates a two dimensional zero-velocity curve in a binary system which has a specified Jacobian constant, three special cases of which are shown in figures 6.6. The program will start by typing "2dcurves" at the command prompt. As above, primary and secondary masses are requested plus their separation distance, however this time with an added request for a Jacobian constant. Any value may be entered provided $C_J \geq 3$, since below this value curves either do not exist or are of no interest. The program then proceeds exactly as above until it calculates the Jacobian constants for each of the x,y values. The resolution option here is for much higher values than the first program, between 1000 and 5000, due to the need for the higher density of points required in plotting the curves. Instead of printing all data to file, there are conditional lines whereby only calculated C_J values within 0.0001 of the input Jacobian constant are printed. The numbers of points in the data file are displayed and the program closes as above with a final line informing the user of the command they should enter to determine zero-velocity surfaces.

Again we use as an example of a graphical representation of data, a system where $u = 0.2$, $a = 1$, but with a resolution of 5000 points between the two masses. Three zero-velocity curves of particular interest are plotted for this system in figure 6.6, i.e. those that pass through the L_1, L_2 and L_3 points. This was also plotted using Microcal Origin Version 6.0. Figure 6.6 shows the same outcome as the zero-velocity curves in Figure 3.7 on Page 81 of Solar System Dynamics by Murray and Dermott, Cambridge University Press, 1999. Figure 6.12 shows a zero-velocity curve for $C_J = 3.05$, where the resolution and semimajor axis are the same but u is 0.001. The values of C_J, here, gives curves which are in each body's gravity well, plus the outside curve that surrounds them, and is hence lower than the Lagrangian point values for this system, where at L_1, $C_J = 3.039$, at L_2, $C_J = 3.037$ and at L_3, $C_J = 3.001$. The black dots at the centre of the gravity wells are the locations of the bodies. Note that in this system, where u is much smaller than the first example, the Jacobian constant values of the zero-velocity curves passing through the Lagrangian points are lower. This is expected, as the distortion of a smaller secondary on the overall shape of a zero-velocity surface will be less than the distortion of a larger secondary.

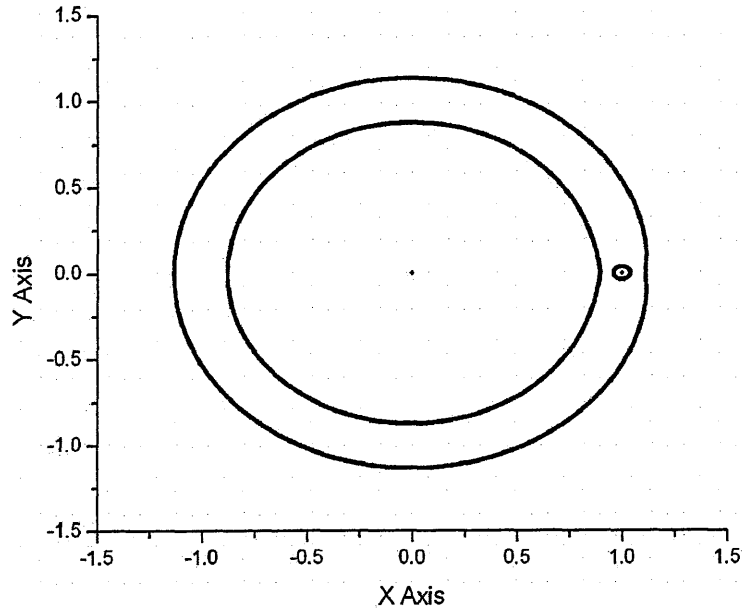

Figure 6.12 Zero-velocity curve, for $C_J = 3.05$, of a binary system where $u = 0.001$ and $a = 1$.

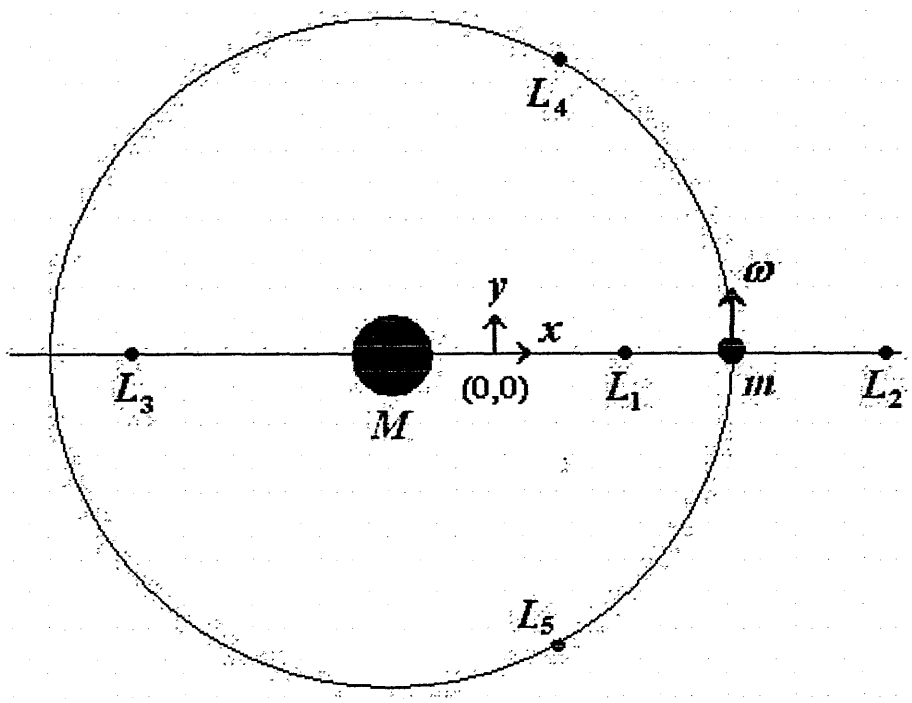

Figure 6.13 Locations of the Lagrangian equilibrium points.

Indeed, the lowest C_J values are at the L_4 and L_5 positions (Murray and Dermott, 1999 page 80), shown in Figure 6.13, and will vary according to the mass fraction of the secondary. They occur at x-coordinates midway between the two bodies, so $x = 1 - u - ½ = ½ - u$, and they make equilateral triangles with the two main bodies, so $y = (\sqrt{3})/2$. Putting these values into equation 6.3 gives,

$$C_J = \frac{11}{4} + \left(\frac{1}{2} - u\right)^2 \qquad 6.14.$$

Clearly this has a maximum when u approaches 0, which is $C_J = 3$, and a minimum when $u = ½$, which is $C_J = 2.75$. In the extreme case when $u = 0$, then equation 6.3 becomes,

$$C_J = x^2 + y^2 + \frac{2}{\sqrt{x^2 + y^2}} \qquad 6.15.$$

This has a minimum value when its differential with respect to x or y is zero, since the equation is symmetrical. So this minimum occurs when either $0 = 2x - \frac{2x}{(x^2 + y^2)^{3/2}}$ or $0 = 2y - \frac{2y}{(x^2 + y^2)^{3/2}}$, i.e. when $x^2 + y^2 = 1$, and so in equation 6.15, $C_J = 3$.

6.6.3 The L_1 and L_2 Zero-Velocity Curve close to the Planet

These third and fourth programs use the same method as the program in Section 6.6.2 to determine the zero-velocity curves around the planet (secondary), which pass through the L_1 and L_2 points respectively. The grid of x- and y-values here only covers the boundary just beyond the Hill radius, determined by equation 6.13. These are of particular interest as the L_1 curve is the most distant zero-velocity curve around the planet that confines a small body to this region. Such particles are bound to the planet and, barring any energy exchanges, will either orbit only the planet or collide with it, and can never do otherwise. The L_2 curve is the one beyond which a satellite may be ejected from the system.

The codes for these programs are presented in Appendix 4 as programs A4.3 and A4.4, under the names "l1curve.c" and "l2curve.c" respectively, the names of the files containing the source code. The programs will start by typing either "l1curve" or "l2curve" at the command prompt. Again, primary and secondary masses are requested plus their separation distance. The upper planet size limit here is 15 Jupiter masses and the lower star size limit is 0.08 solar masses. These boundaries were chosen since the primary will no longer be a star below 0.08 solar masses, and the secondary becomes a brown dwarf above 15 Jupiter masses. The programs then proceed by calculating the Jacobian constants for each of the x,y values within the Hill radius, as defined by equation 6.13, of the planet. The resolution option here is highest of the four programs, i.e. 10,000 to 50,000 points between the masses, however the calculations only cover the region around the planet. As in program 6.6.2, instead of printing all data to file, there are conditional lines whereby only calculated C_J values within 0.0001 of the input Jacobian constant are printed. The "l1curve.c" program gives the distance of the L_1 point from the planet with the distance of the L_1 zero-velocity curve at quadrature and on the far side of the planet. The "l2curve.c" program gives the distance of the L_2 point from the planet with the distance of the L_2 zero-velocity curve at quadrature. The numbers of points in the data file are displayed and the program closes informing the user of the name of that file.

An example of the shape and extent of the zero-velocity curve which passes through the L_1 point of a planet, where $u = 0.001$, $a = 1$ and the resolution is 30,000, is shown in figure 6.14, where the planet is shown as the small dot. It is easily seen that the curve shape is by no means circular. The distance of the curve at the quadrature positions from the planet is least. This may imply that this is the easiest route for a small particle to escape orbit from the planet. However, the shape of the L_1 curve may lead to particles with initially circular orbits close to this curve becoming elliptical immediately. The aim of the study in the next section of this chapter is to find what the Mercury orbital integrator tells us about the evolution of such orbits, which are exclusively in the x-y plane of the giant's orbit. Since there is initially no z-component to the giant planet's or small body's motion, both bodies will acquire no z-direction motion and hence will remain in the x-y plane.

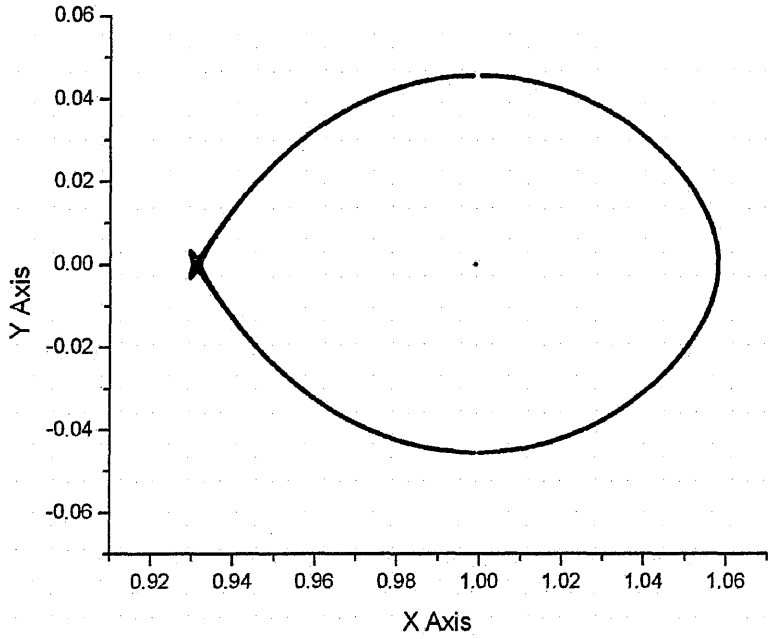

Figure 6.14 The L_1 zero-velocity curve around a planet where $u = 0.001$ and $a = 1$.

6.7 Applying the Theory to a Theoretical System

HD 28185 is one of the satellite systems investigated and it is this system that was adapted for this theoretical analysis. Although the giant has an eccentricity of 0.07, this was set to zero. Its semimajor axis was left unchanged at 1.03AU. The giant planet mass is $5.7M_J$ or $0.00544M_\odot$ and the stellar mass is $0.99M_\odot$, so from equation 6.12 or 6.13, the Hill radius of the giant is 0.126AU to three significant figures. Each of the integrations had a maximum run time of 100Myr due to the small time-step of $1/20^{th}$ of the satellites orbital period; 1Gyr would have taken too much computer time. The Hill radii close encounter multiples of the star and Earth-Moon were set at 0.01 and 1.0 respectively, to minimise close encounter terminations and maximise the time before any possible cataclysmic event could occur during runs.

Due to the shape of the zero-velocity curve around the planet that passes through the L_1 point, see Figure 6.14 which equally applies here where $u = 0.00547$, Earth-Moon satellites were launched in the x,y plane at increasing distances from the giant in circular orbits at longitudes 0^O, 90^O, 180^O and 270^O with respect to the line from the giant to the star. Although at 90^O and 270^O the distances of the satellite as a fraction of the L_1 zero-velocity curve are the same, differences are observed in orbital evolution due to it either initially moving towards (270^O) or away (90^O) from the star. At these longitudes the L_1 zero-velocity curve is 0.0816AU from the planet, whereas at 180^O the curve is 0.1020AU distant and at the L_1 point itself (0^O) it is 0.1206AU distant. As this study is purely theoretical, the J_2 effect of the giant was not incorporated into these integrations. Table 6.5 shows the integration time and their outcomes only, as this is the critical data required here.

Table 6.5 Theoretical satellite runs with $J_2 = 0$ for the giant planet

Satellite Distance from Giant / AU	Launch Longitude (Star = 0^0)	Run Completion Time / years	Run Outcome
0.05	0	$>10^8$	-
0.05	90	$>10^8$	-
0.05	180	$>10^8$	-
0.05	270	$>10^8$	-
0.051	90	$>10^8$	-
0.051	270	$>10^8$	-
0.052	90	$>10^8$	-
0.052	270	$>10^8$	-
0.0521	90	$>10^8$	-
0.0521	270	$>10^8$	-
0.0522	90	$>10^8$	-
0.0522	270	$>10^8$	-
0.0523	90	$>10^8$	-
0.0523	270	$>10^8$	-
0.0524	90	$>10^8$	-
0.0524	270	$>10^8$	-
0.0525	90	$>10^8$	-
0.0525	270	$>10^8$	-
0.0526	90	170	C
0.0526	270	164	C
0.0527	90	113	C
0.0527	270	150	C
0.0528	90	16	C
0.0528	270	68	C
0.0529	90	174	C
0.0529	270	103	C
0.053	90	220	C
0.053	270	58	C
0.054	90	370	C
0.054	270	369	C
0.055	0	$>10^8$	-
0.055	90	50	C
0.055	180	$>10^8$	-
0.055	270	139	C
0.056	0	$>10^8$	-
0.056	90	19	C
0.056	180	$>10^8$	-
0.056	270	392	C
0.057	0	$>10^8$	-
0.057	90	135	C
0.057	180	$>10^8$	-
0.057	270	56	C
0.058	0	$>10^8$	-
0.058	90	879	C
0.058	90	338*	C
0.058	90	96**	C
0.058	180	$>10^8$	-
0.058	270	340	E
0.058	270	1675*	E
0.058	270	2141**	E
0.0581	0	$>10^8$	-
0.0581	180	$>10^8$	-
0.0582	0	$>10^8$	-
0.0582	180	290	C
0.0583	0	$>10^8$	-
0.0583	180	718	C
0.0584	0	$>10^8$	-

Satellite Distance from Giant / AU	Launch Longitude (Star = 0^{O})	Run Completion Time / years	Run Outcome
0.0584	180	49	C
0.0585	0	$>10^{8}$	-
0.0585	180	81	C
0.0586	0	$>10^{8}$	-
0.0586	180	16	C
0.0587	0	$>10^{8}$	-
0.0587	180	16	C
0.0588	0	1477	C
0.0588	180	145	C
0.0589	0	1711	C
0.0589	180	41	C
0.059	0	307	C
0.059	90	692	E
0.059	180	135	C
0.059	270	35	C
0.0591	0	209	C
0.0591	180	54	C
0.0592	0	414	C
0.0592	180	243	C
0.0593	0	71	C
0.0593	180	56	C
0.0594	0	50	C
0.0594	180	$>10^{8}$	-
0.0595	0	56	C
0.0595	180	$>10^{8}$	-
0.0596	0	227	C
0.0596	180	$>10^{8}$	-
0.0597	0	28	C
0.0597	180	$>10^{8}$	-
0.0598	0	48	C
0.0598	180	$>10^{8}$	-
0.0599	0	932	C
0.0599	180	$>10^{8}$	-
0.06	0	69	C
0.06	90	453	E
0.06	180	$>10^{8}$	-
0.06	270	390	C
0.0601	0	268	C
0.0601	180	$>10^{8}$	-
0.0602	0	106	C
0.0602	180	$>10^{8}$	-
0.0603	0	77	C
0.0603	180	$>10^{8}$	-
0.0604	0	210	C
0.0604	180	$>10^{8}$	-
0.0605	0	10	C
0.0605	180	$>10^{8}$	-
0.0606	0	15	C
0.0606	180	$>10^{8}$	-
0.0607	0	46	C
0.0607	180	$>10^{8}$	-
0.0608	0	70	C
0.0608	180	$>10^{8}$	-
0.0609	0	71	C
0.0609	180	$>10^{8}$	-
0.061	0	412	C
0.061	90	40	C
0.061	180	$>10^{8}$	-
0.061	270	56	C

Satellite Distance from Giant / AU	Launch Longitude (Star = 0^{O})	Run Completion Time / years	Run Outcome
0.0611	0	336	C
0.0611	180	$>10^8$	-
0.0612	0	150	C
0.0612	180	$>10^8$	-
0.0613	0	204	C
0.0613	180	$>10^8$	-
0.0614	0	7	C
0.0614	180	$>10^8$	-
0.0615	0	641	C
0.0615	180	$>10^8$	-
0.0616	0	44	C
0.0616	180	$>10^8$	-
0.0617	0	12	C
0.0617	180	$>10^8$	-
0.0618	0	112	C
0.0618	180	$>10^8$	-
0.0619	0	62	C
0.0619	180	$>10^8$	-
0.062	0	188	C
0.062	90	285	C
0.062	180	$>10^8$	-
0.062	270	21	C
0.0621	0	65	C
0.0621	180	$>10^8$	-
0.0622	0	191	C
0.0622	180	$>10^8$	-
0.0623	0	8	C
0.0623	180	$>10^8$	-
0.0624	0	105	C
0.0624	180	$>10^8$	-
0.0625	0	92	C
0.0625	180	$>10^8$	-
0.0626	0	7	C
0.0626	180	$>10^8$	-
0.0627	0	143	C
0.0627	180	7.372×10^5	C
0.0628	0	72	C
0.0628	180	$>10^8$	-
0.0629	0	234	C
0.0629	180	$>10^8$	-
0.063	0	65	C
0.063	90	1766	E
0.063	180	$>10^8$	-
0.063	270	13	C
0.0631	0	20	C
0.0631	180	172	C
0.0632	0	70	C
0.0632	180	135	C
0.0633	0	44	C
0.0633	180	1289	C
0.0634	0	87	C
0.0634	180	35	C
0.0635	0	23	C
0.0635	180	89	C
0.064	0	7	C
0.064	90	891	E
0.064	180	277	C
0.064	270	182	C
0.065	0	53	C

Satellite Distance from Giant / AU	Launch Longitude (Star = 0°)	Run Completion Time / years	Run Outcome
0.065	90	59	C
0.065	180	13	C
0.065	270	2	C
0.066	0	120	C
0.066	90	234	C
0.066	180	125	C
0.066	270	5	C
0.067	0	194	C
0.067	90	1657	E
0.067	180	440	E
0.067	270	0	C
0.068	0	71	C
0.068	90	1009	E
0.068	180	280	C
0.068	270	0	C
0.069	0	110	C
0.069	90	0	C
0.069	180	1127	E
0.069	270	19	C
0.07	0	71	C
0.07	90	6	C
0.07	180	103	C
0.07	270	21	C
0.071	0	89	C
0.071	90	522	E
0.071	180	1899	E
0.071	270	10	C
0.072	0	205	C
0.072	90	134	C
0.072	180	177	C
0.072	270	100	C
0.073	0	2	C
0.073	90	24	C
0.073	180	537	E
0.073	270	90	C
0.074	0	977	E
0.074	90	61	C
0.074	180	515	E
0.074	270	253	C
0.075	0	94	C
0.075	90	846	C
0.075	180	382	E
0.075	270	14	C
0.08	0	493	C
0.08	90	724	E
0.08	180	27	C
0.08	270	61	C
0.085	0	18	C
0.085	90	187	C
0.085	180	989	E
0.085	270	209	E
0.09	0	1361	E
0.09	90	164	C
0.09	180	4	C
0.09	270	199	E
0.095	0	61	C
0.095	90	116	C
0.095	180	398	C
0.095	270	5	C

Satellite Distance from Giant / AU	Launch Longitude (Star = 0^O)	Run Completion Time / years	Run Outcome
0.1	0	28	C
0.1	90	177	C
0.1	180	427	E
0.1	270	778	C

C Collided with the giant planet
E Ejected from the system
* Initial time step set at 1 day instead of 0.05 of satellite orbital period (3.45 days)
** Initial time step set at 0.1 day instead of 0.05 of satellite orbital period (3.45 days)

From the theory, all integrations in table 6.5 should either last their 100Myr term or should collide with the giant. However, those launched with an initial longitude of 90^O or 270^O with respect to the star at an initial distance of 0.085AU could collide with the star, being between the L_1 and L_2 zero-velocity curves. Those launched with the same initial longitudes at 0.9AU and beyond could also be ejected from the system. The table shows that of the 162 runs that terminate prematurely, the outcomes of 20 of these unstable orbital runs contradict the theory. For these satellites to be ejected, they must acquire sufficient energy. This must be acquired from the giant planet in the form of "sling-shot" events or gravity assists. As discussed in section 6.3, small satellite bodies must cross the zero-velocity curve passing through the L_2 point to escape the system. The nearest initial satellite distance from the giant where an ejection occurs is at 0.058AU for a launch longitude of 270^O and 0.059AU for a launch longitude of 90^O, compared to the L_2 curve's distance from the giant at these longitudes of 0.086AU. At a launch longitude of 180^O the nearest initial satellite distance from the giant where an ejection occurs is at 0.067AU, just over half the distance to the L_2 point at 0.126AU. There is no point between the star and giant planet where the L_2 curve crosses. As the satellite distance at 0.058AU was the first time this unexpected phenomenon was encountered, the initial time-step of the integrations was reduced from 0.05 of an orbit (3.45 days) to 1 day and then 0.1 day. This was checked through personal communication with the program writer (Chambers, 2004), who suggested that initial time steps that are initially too large, may lead to inaccurate results. Here, however, this proved not to be the case.

The stability of satellite orbits was also dependent on their launch longitude for any one particular distance from the giant. Table 6.6 shows the initial Jacobian constants, C_J, at which satellite orbits initially become unstable at their respective launch longitudes and also where they are able to escape from the system. Due to the resolution of the zero-velocity surface used to determine these C_J values, they can only be accurately quoted to three decimal places.

Table 6.6 Critical Jacobean constants for satellite orbit outcomes

Initial launch longitude with respect to the star	Orbital destabilisation		Satellite ejection	
	Initial satellite distance from the giant / AU	C_J	Initial satellite distance from the giant / AU	C_J
90 or 270	0.0525	3.193	0.058 – 0.059	3.172 – 3.169
180	0.0581	3.181	0.067	3.158
0	0.0588	3.180	0.074	3.146

The implication here is that provided the initial Jacobian constant of a satellite is 3.193 or more, then its orbit will be stable. The C_J of the L_1 point within this theoretical system is 3.116, so the difference in Jacobian constants where the shape of the gravity well is sufficiently distorted for orbital destabilisation to occur is 0.064 to 0.077. Similarly, the C_J of the L_2 point is 3.109, so the difference in Jacobian constants where a satellite can escape from orbit is 0.037 to 0.063. It appears, on this brief analysis, that there is an energy

barrier where a satellite can overcome a C_J difference of 0.063 or less by gravitational assists and escape the system. It also appears that C_J differences between 0.064 and 0.077 cannot be overcome by the satellite sufficiently to escape the system, but they can attain enough energy to destabilise their orbits. Satellites further down the giant planet gravity well than a C_J difference of 0.078 or more remain in stable orbits. Clearly a greater in-depth analysis would be required to verify these figures and outcomes.

There appears to be an island of stability for satellites launched with a longitude difference of 180^O, with respect to the star, from 0.0594AU to 0.0630AU (with one exception at 0.0627AU). This is too wide to be an orbital resonance effect and the Jacobian constants of the satellite starting positions are between 3.177.and 3.168 respectively. Again further investigation would be required here to resolve this phenomenon.

An alternative and disturbing explanation for the system ejection outcomes is that there may be a bug in the programming of the Mercury Orbital Integrator. This is doubtful; however, as the program is widely used and any such discrepancies are highly likely to have been already found. The chance of an odd result is always present, which may be enhanced by the fact that in these satellite runs, the Integrator is being abused somewhat as the largest body in the system is not at its centre. As previously discussed in section 6.4, this does not sit well with the usage of the less reliable of the two Hill radius formulae versions, given in equation 6.12. Indeed, the usage of the Mercury Integrator so far, in the planetary studies for which it is designed, suggests that it is robust and reliable. Initial experiments with satellite integrations using the Jovian Galilean system with the MVS, Bulirsch Stoer, Conservative Bulirsch-Stoer and Hybrid Integrators, lead to nothing but failure. The RADAU integrator was the only one that worked for the unusual configurations required for satellite runs when using Mercury.

6.8 Conclusion

The outcomes of all but 20 of the 238 integrations on this theoretical system were as predicted by the theory. As discussed in section 7 of this chapter, there is sufficient evidence to suggest that the 20 unexpected system ejections are due to energy exchanges between the satellite, giant and star. Hence, on this premise, the Mercury Orbital RADAU Integrator is appropriate to continue with the satellite studies on real systems.

7. Real Integrations on Satellite Systems

7.1 System Characteristics

These studies use the Mercury Orbital RADAU Integrator as verified in chapter 6 for its use on satellites of giant planets within exosystems. The two systems investigated here have their stellar parameters shown in table 7.1 and the orbital parameters of the giant planet within each system, shown in table 7.2.

Table 7.1. Stellar properties of HD 23079 and HD 28185

Parameter	HD 23079	HD 28185
$M_*/M_\odot$	1.1	0.99
Metallicity / [Fe/H]	-	0.24
Metallicity / % (1st & 2nd model)	-	3.48 & 3.27
Spectral Type	F9V	G5
Bolometric Correction	-0.17	-0.24
Age / Gyr	3.1	2.9
Distance / pc	34.8	39.4
Apparent Visual Magnitude	7.1	7.81
$L/L_\odot$	1.62	1.14
T_{eff}/K	6130	5565
1st model inner HZ ZAMS /AU	0.854	0.679
1st model outer HZ ZAMS /AU	1.695	1.339
1st model inner HZ now /AU	1.002	0.755
1st model outer HZ now /AU	1.997	1.491
1st model inner HZ EoMS /AU	1.548	1.289
1st model outer HZ EoMS /AU	3.063	2.531
2nd model inner HZ ZAMS /AU	0.876	0.747
2nd model outer HZ ZAMS /AU	1.74	1.478
2nd model inner HZ now /AU	1.052	0.844
2nd model outer HZ now /AU	2.102	1.674
2nd model inner HZ EoMS /AU	1.582	1.393
2nd model outer HZ EoMS /AU	3.111	2.738
Stellar params inner HZ now /AU	1.028	0.911
Stellar params outer HZ now /AU	2.048	1.799

Table 7.2. Orbital Properties of the exoplanets HD 23079 b and HD 28185 b.

Parameter	HD 23079 b	HD 28185 b
$M_p \sin i_0 / M_J$	2.61	5.7
Semimajor axis/AU	1.65	1.03
Orbital Eccentricity	0.1	0.07
Period / days	738.459	383
Inner R_H multiplier	2.788	2.833
Outer R_H multiplier	5.505	4.872
Inner gravitational reach / AU	1.066	0.601
Outer gravitational reach / AU	2.642	1.716

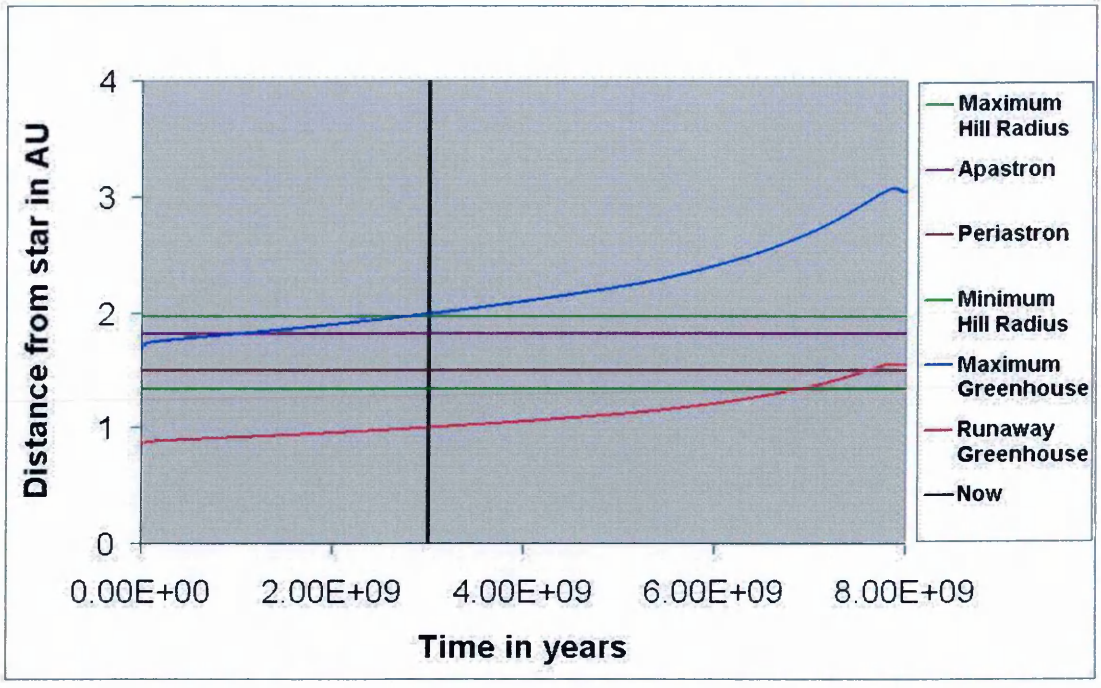

Figure 7.1 HZ movement over the main sequence lifetime for HD 23079 according to the second Mazzitelli model. The green lines are the Hill radii of the giant beyond apastron and inside periastron, between which a satellite must orbit.

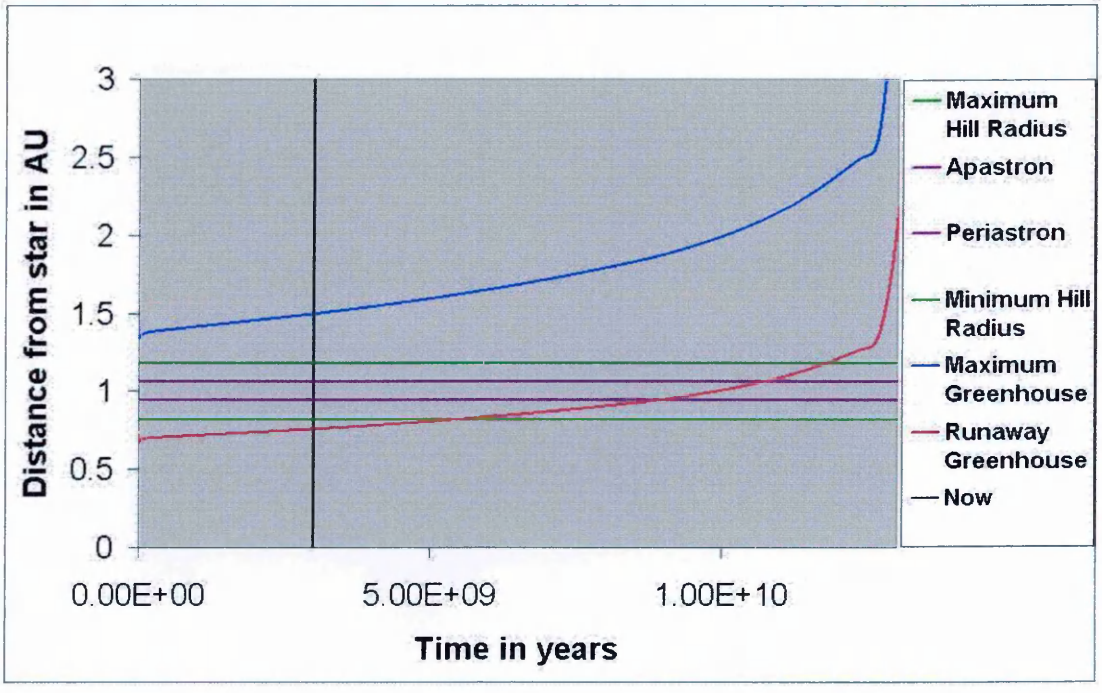

Figure 7.2 HZ movement over the main sequence lifetime for HD 28185 according to the first Mazzitelli model. The green lines are the Hill radii of the giant beyond apastron and inside periastron, between which a satellite must orbit.

The eccentricity of both giants is low, keeping them well within the boundaries of the habitable zone as defined by the runaway greenhouse and maximum greenhouse boundaries defined in chapter 3, section 1. Figures 7.1 and 7.2 shows the movement of the habitable zones, within these systems, over each stars main sequence lifetime.

Both Mazzitelli Stellar models were used to show the HZ movement as there was little difference between each model for either star. Figure 7.1 shows that a satellite of the HD

23079 giant could be capable of supporting life after 1Gyr, based on the semimajor axis of the giant lying within the HZ. Although at this time, the eccentricity of the giant would mean a satellite would spend some time beyond the HZ, this time would be small. Bearing in mind that life takes 2Gyr to make an appreciable alteration to any host planet's atmosphere, then for a satellite orbiting HD 23079b, such changes could have happened 1Gyr ago. Life on a satellite today can still look forward to 5Gyr existence before the star reaches its end of main sequence. During the last 1Gyr on the main sequence, any habitable satellites will drift inside the outwardly moving inner HZ boundary. Cloud reflection effects could possibly protect the satellite beyond this time and life could exist until the end of the star's main sequence lifetime. Figure 7.2 shows that a satellite of HD 28185b could also have supported life from the end of any early bombardment period. An atmosphere of such a satellite should now have been altered and life can expect to exist for at least another 5Gyr, possibly 7Gyr, before the inner HZ passes over the giant's orbit, rendering any satellite uninhabitable. It is unlikely, though, that a satellite could support life to the end of the star's main sequence life time.

7.2 Outcome of the HD 23079 Integrations

As with the orbital integrations on the theoretical HD 28185 system, each integration in these studies was terminated after 100Myr due to the time required for each run. The distance of the Earth-Moon sized satellite was increased from the planet until orbital destabilisation started to occur and just beyond. As the orbits of the giant planet around the star and Earth-Moon satellite around the giant were eccentric, the four periplanet launch longitudes were as defined for the planetary integrations. As previously explained in chapter 6, however, the giant and star have swapped places with the giant being at the centre of the system for these investigations. Consequently, due to the Integrators use of Hill radius formula 6.12, the close encounter run termination distance was set to $0.1R_H$ for the star and $1.0R_H$ for the Earth-Moon both orbiting the central planet. Any close encounter run termination distance greater than $0.1705R_H$ for the star results in an immediate end to an integration, as this distance, as determined by equation 6.12, is the planet's periastron. This also leads to different terminology, where periplanet is the point of closest approach of the satellite or star to the planet, so the star's periplanet is the same as the planet's periastron.

Notes for all subsequent tables:

e	orbital eccentricity
a	Earth-Moon's (E-M) semimajor axis distance from the planet in AU
p	longitude of periastron of Earth-Moon with respect to that of the star (^{O})
$\Delta\varpi$	periastron longitude difference between the giant and Earth-moon
t	time of run to completion or termination in years
O	outcome of run termination if applicable where 'ce' is a close encounter within 0.1 of the star's Hill radius, as determined by equation 6.12.
**	possible libration between these relative periastron longitudes

Table 7.3 Orbital runs for an Earth-Moon satellite orbiting the minimum mass giant HD 23079b in the habitable zone of its star, excluding J_2 effects.

Starting Parameters		Parameter variation during a run			t/years	O
E-M a / AU	p / °	Earth-Moon e	Earth-Moon a / AU	$\Delta\varpi$ / °		
0.01	0	0.000365 – 0.001027*	0.01002 ± 0.00003	±30**	$>10^8$	-
0.01	180	0.000386 – 0.001045*	0.01002 ± 0.00003	±30**	$>10^8$	-
0.02	0	10^{-5} – 0.009804	0.01995 ± 0.00005	0 - 360	$>10^8$	-
0.02	180	10^{-5} – 0.005733	0.01995 ± 0.00005	0 - 360	$>10^8$	-
0.03	0	10^{-5} – 0.019598	0.02983 ± 0.00018	0 - 360	$>10^8$	-
0.03	180	10^{-5} – 0.018269	0.02983 ± 0.00018	0 - 360	$>10^8$	-
0.04	0	10^{-5} – 0.044000	0.03943 ± 0.00057	0 - 360	$>10^8$	-
0.04	180	10^{-5} – 0.044074	0.03947 ± 0.00058	0 - 360	$>10^8$	-
0.05	0	10^{-5} – 0.090538	0.04856 ± 0.00144	0 - 360	$>10^8$	-

Starting Parameters		Parameter variation during a run			t / years	O
E-M a / AU	p / °	Earth-Moon e	Earth-Moon a / AU	$\Delta\varpi$ / °		
0.05	90	10^{-5} – 0.230003	0.05187 ± 0.00233	0 - 360	$>10^8$	-
0.05	180	10^{-5} – 0.095664	0.04868 ± 0.00146	0 - 360	$>10^8$	-
0.05	270	10^{-5} – 0.229403	0.05186 ± 0.00232	0 - 360	$>10^8$	-
0.051	90	10^{-5} – 0.268221	0.05311 ± 0.00271	0 - 360	$>10^8$	-
0.051	270	10^{-5} – 0.267623	0.05312 ± 0.00271	0 - 360	$>10^8$	-
0.052	90	10^{-5} – 0.306473	0.05438 ± 0.00315	0 - 360	$>10^8$	-
0.052	270	10^{-5} – 0.306859	0.05439 ± 0.00317	0 - 360	$>10^8$	-
0.053	90	10^{-5} – 0.375008	0.05570 ± 0.00386	0 - 360	$>10^8$	-
0.053	270	10^{-5} – 0.374362	0.05576 ± 0.00385	0 - 360	$>10^8$	-
0.054	90	10^{-5} – 0.441299	0.05710 ± 0.00435	0 - 360	4.271×10^6	ce
0.054	270	10^{-5} – 0.461856	0.05717 ± 0.00444	0 - 360	1.063×10^7	ce
0.055	0	10^{-5} – 0.125242	0.05287 ± 0.00213	0 - 360	$>10^8$	-
0.055	90	10^{-5}	0.055	-	2797	ce
0.055	180	10^{-5} – 0.131335	0.05308 ± 0.00218	0 - 360	$>10^8$	-
0.055	270	10^{-5}	0.055	-	374	-
0.056	0	10^{-5} – 0.132178	0.05372 ± 0.00228	0 - 360	$>10^8$	-
0.056	90	10^{-5}	0.056	-	131	ce
0.056	180	10^{-5} – 0.142858	0.05394 ± 0.00235	0 - 360	$>10^8$	-
0.056	270	10^{-5}	0.056	-	342	ce
0.057	0	10^{-5} – 0.138775	0.05455 ± 0.00245	0 - 360	$>10^8$	-
0.057	90	10^{-5}	0.057	-	497	ce
0.057	180	10^{-5} – 0.152136	0.05482 ± 0.00253	0 - 360	$>10^8$	-
0.057	270	10^{-5}	0.057	-	45	ce
0.058	0	10^{-5} – 0.148082	0.05538 ± 0.00262	0 - 360	$>10^8$	-
0.058	90	10^{-5}	0.058	-	11	ce
0.058	180	10^{-5} – 0.162231	0.05566 ± 0.00272	0 - 360	$>10^8$	-
0.058	270	10^{-5}	0.058	-	5	ce
0.059	0	10^{-5} – 0.169127	0.05618 ± 0.00282	0 - 360	$>10^8$	-
0.059	90	10^{-5}	0.059	-	10	ce
0.059	180	10^{-5} – 0.183434	0.05657 ± 0.00297	0 - 360	$>10^8$	-
0.059	270	10^{-5}	0.059	-	302	PC
0.06	0	10^{-5} – 0.369886	0.05765 ± 0.00431	0 - 360	$>10^8$	-
0.06	90	10^{-5}	0.060	-	9	ce
0.06	180	10^{-5} – 0.403908	0.05810 ± 0.00476	0 - 360	$>10^8$	-
0.06	270	10^{-5}	0.060	-	13	ce
0.061	0	10^{-5}	0.061	-	1148	ce
0.061	180	10^{-5}	0.061	-	735	ce
0.062	0	10^{-5}	0.062	-	1911	ce
0.062	180	10^{-5}	0.062	-	2219	ce
0.063	0	10^{-5}	0.063	-	1172	ce
0.063	180	10^{-5}	0.063	-	670	ce
0.064	0	10^{-5}	0.064	-	19	ce
0.064	180	10^{-5}	0.064	-	21	ce
0.065	0	10^{-5}	0.065	-	9	ce
0.065	180	10^{-5}	0.065	-	51	ce
0.066	0	10^{-5}	0.066	-	9	ce
0.066	180	10^{-5}	0.066	-	7	ce
0.067	0	10^{-5}	0.067	-	25	ce
0.067	180	10^{-5}	0.067	-	7	ce
0.068	0	10^{-5} – 0.263696	0.06305 ± 0.00495	0 - 360	$>10^8$	-
0.068	180	10^{-5}	0.068	-	17	ce
0.069	0	10^{-5}	0.069	-	1.671×10^4	E
0.069	180	10^{-5}	0.069	-	161	PC
0.07	0	10^{-5} – 0.341246	0.06444 ± 0.00556	0 - 360	$>10^8$	-
0.07	180	10^{-5}	0.070	-	25	ce
0.08	0	10^{-5}	0.080	-	640	PC
0.08	180	10^{-5}	0.080	-	65	ce

* Measurements taken after the first 10^7 years to allow for orbital stabilisation.
ce Close encounter to within $0.1R_H$ of the star
PC Earth-Moon satellite collides with its parent planet.
E Earth-Moon is ejected from the system.

Table 7.3 shows the results for integrations where the J_2 effect was not included. As the giant is now in an eccentric orbit about the star the integrations are always started with the star at periplanet. This is to play devil's advocate with satellite orbital stabilities as the stellar gravitational influence will be initially greatest. There are two distinct categories of orbits, as discovered in chapter 6. For orbits launched at different periplanet longitudes, those launched at 90^O and 270^O destabilise nearer to the planet than those launched at 0^O and 180^O. This is because, for orbits launched at the same distance from the giant, those initially at quadrature have lower pseudo-potentials and are, therefore, more prone to destabilisation as discussed in chapter 6, section 7.

The orbits of the satellites launched at quadrature destabilise at a launch distance of 0.054AU and have close encounters with the star. As one of the footnotes in table 7.3 explains, close encounters occur within $0.1R_H$ of the star, or 0.871AU as determined by equation 6.12, as used in the Mercury Orbital Integrator. When the giant is at periastron it is 0.614AU from the star's $0.1R_H$ distance, which is well beyond the L_1 or L_2 points of the giant, at 0.131AU and 0.138AU from the giant respectively. The satellite must, therefore have gained sufficient energy through gravitational assists to escape the giant and pass too close to the star. The orbits of satellites launched at 0^O and 180^O periastron longitude destabilise at 0.061AU, although two more stable orbits appear at 0.068AU and 0.070AU, both at 0^O launch longitude. These orbits are close to the 11:2 resonance with the star (where the satellite orbits eleven times for every two star orbits), but not significantly so for them to be stable for this reason, particularly as the orbit launched at 0.069AU is unstable.

The stable orbits of Earth-Moon satellites show similar trends with increasing distance from the giant, as do the Earth-Moon exoplanets in the previous investigations of chapters 4 and 5. The distance from the giant remains constant for all, although the variation in this distance increases with increasing distance from the giant. The eccentricity oscillation span also increases with increasing satellite distance. These effects are due to greater influence from the star as the initial pseudo-potential of the satellite decreases. Satellites launched at the same distance from the giant also have increasing eccentricity with decreasing initial pseudo-potentials or C_J value, as seen from satellites launched at 0.05AU in table 7.3. The run that had an initial periastron launch longitude of 0^O has the highest C_J and consequently its largest eccentricity value is lowest. The run with an initial periastron launch longitude of 180^O has a slightly lower C_J and its largest eccentricity value is slightly higher. Those launched at 90^O and 270^O have a considerably lower C_J and their largest eccentricity is considerably higher. Figures 7.3, 7.4 and 7.5 show, for a stable orbit, the typical variation in the distance of the satellite from the giant, changes in the satellite's eccentricity and in its periastron longitude with time respectively. Only the closest satellite integration initially at 0.01AU showed any signs of its periplanet longitude librating about that of the star's (periastron) (Figure 7.6), no such phenomena were present in the rest.

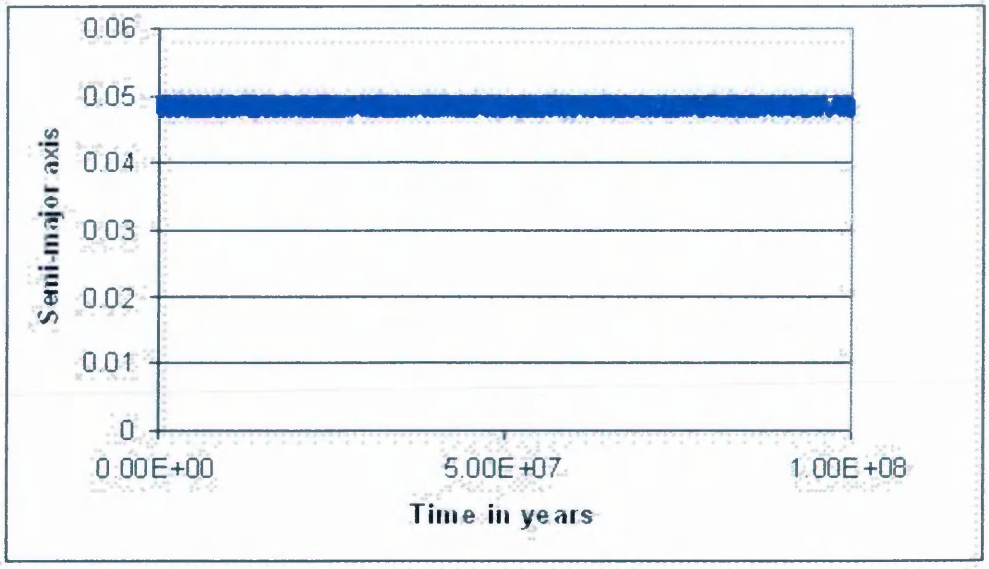

Figure 7.3 Variation in distance from the giant planet with time for a satellite in a stable orbit around HD 23079b at 0.05AU.

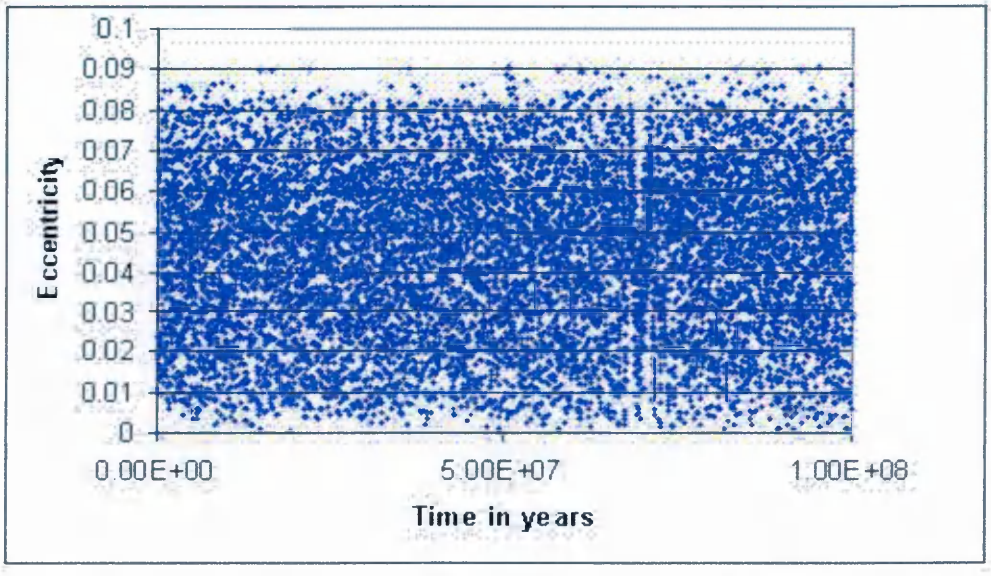

Figure 7.4 Eccentricity change with time for a satellite in a stable orbit around HD 23079b at 0.05AU.

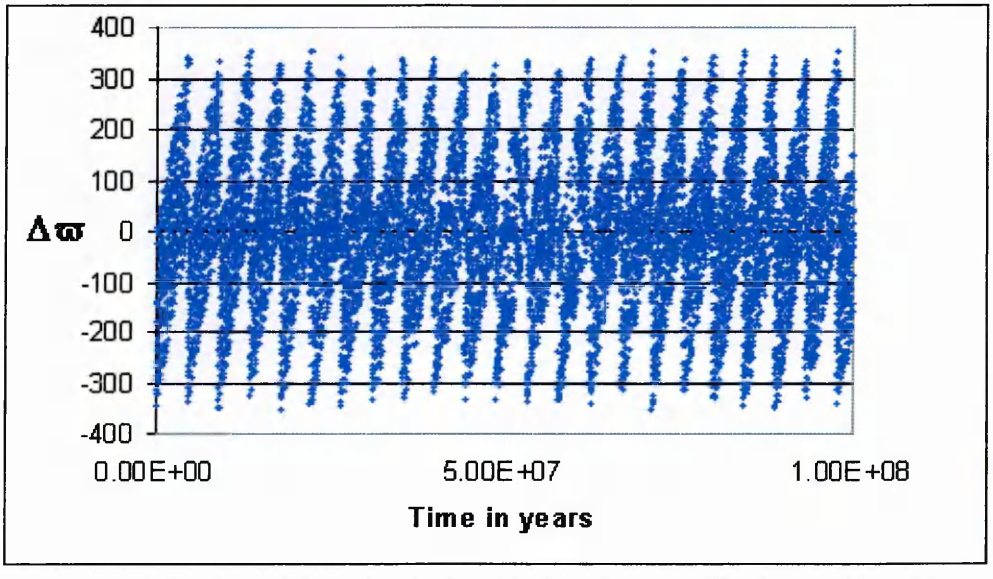

Figure 7.5 Variation in periplanet longitude with time for a satellite in a stable orbit around HD 23079b at 0.05AU.

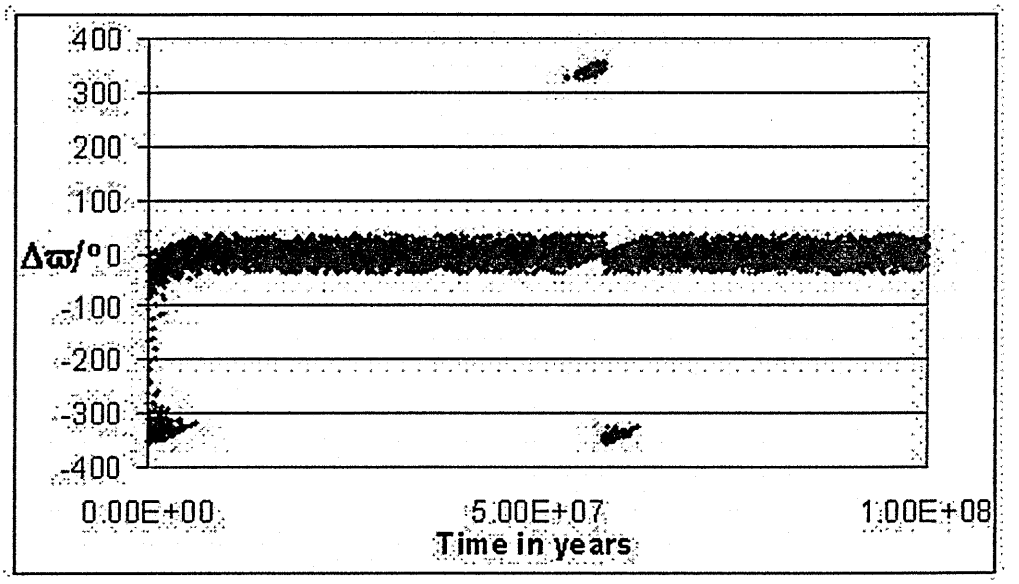

Figure 7.6 Variation in periplanet longitude ($\Delta\varpi$ in degrees) with time for a satellite in a stable orbit around HD 23079b at 0.01AU, illustrating possible libration about the 0^{O} periplanet longitude of the star.

7.3 Outcome of the HD 28185 Integrations – no J_2 Effect

This system was investigated with much more rigour than HD 23079. In addition to finding the distance from the giant where Earth-sized satellite orbits destabilise, investigations were undertaken as to the effects on orbital stability of satellite size and the J_2 effect from the giant. Also investigated was satellite orbital inclination with respect to the plane of the giant planet's orbit around its star, and the equatorial plane of the giant (more relevant in the presence of the J_2 effect in section 1 of this chapter). The close encounter run termination distance was again $0.1R_H$ for the star and $1.0R_H$ for the satellite since the distance of the giant's periastron is $0.2367R_H$ of the star as determined by equation 6.12. Consequently, entering a stellar Hill radius termination multiple larger then this results in immediate termination of any runs.

As with HD 23079, the satellites were launched at four periplanet launch longitudes, i.e. 0^{O}, 90^{O}, 180^{O}, and 270^{O} with respect to the periastron of the giant. The satellite was also given initial orbital inclinations of 0^{O}, 30^{O}, 60^{O}, 75^{O}, 90^{O} and 180^{O} to the plane of the star's orbit around the giant planet (from the perspective of the integrator). These were investigated with either the satellite orbits being inclined or the star's orbit being inclined. When the satellite orbits were inclined, the effect would be of it orbiting the giant out of the plane of its rotation, which is contrary to theories of satellite system formation (but like the Earth-Moon system orbiting the Sun). When the "star's orbit" is inclined, the perspective is that the satellites orbit in the plane of the giant planet's rotation, as in most satellite systems within the Solar System (see Figure 7.7). It is within the inclination investigation when the giant's J_2 value would be expected to have a significant effect, as this incorporates giant planet rotation induced oblateness.

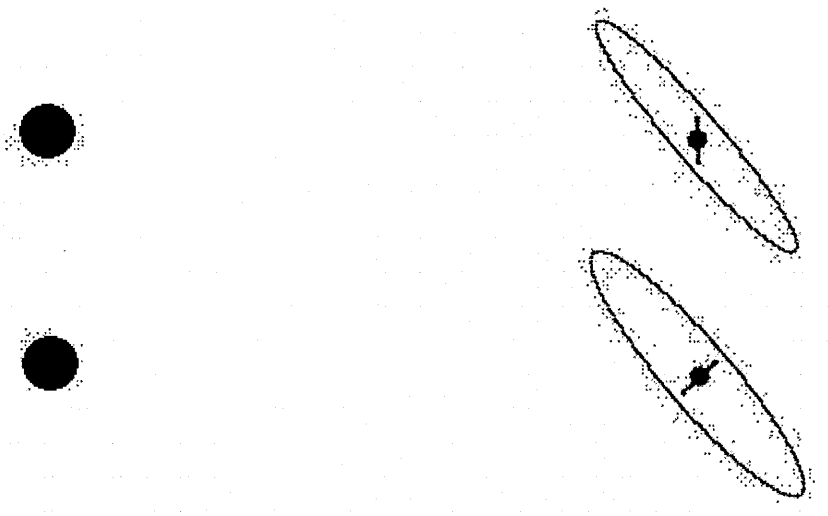

Figure 7.7 The two configurations for inclined satellite orbits. Top illustrates orbits inclined out of the plane of the giant's orbital and rotation plane, i.e. Type 1. Bottom illustrates orbits inclined out of the plane of the giant's orbit but in the plane of its rotation, i.e. Type 2.

The greatest gravitational perturbation effects on any satellite orbits will occur at the giant planet's periastron, when it is 0.9579AU from the star. At this distance the L_1 curve crosses the L_1 point at 0.1122AU from the giant, is 0.0948AU opposite the giant and is 0.0759AU from the giant at quadrature. All satellites that are launched in the plane of the giant's orbit within this boundary, for this study, remain in this orbital plane. They also should have either stable orbits or should collide with the giant. A brief glance at Table 7.5 reveals, however, that there are many satellite close encounters with the star, implying that gravitational assists have taken place with the giant enabling the satellite to cross the L_1 boundary.

As with HD 23079b, satellites launched within the giant's orbital plane fall into two categories. Those launched at quadrature are stable to an initial distance of 0.046AU from the giant, whereas those launched at 180^{O} with respect to the star's periplanet are stable to 0.050AU, and those launched at 0^{O} remain stable to 0.051AU with an island of stability between 0.055AU and 0.057AU, similar to that in HD 23079b. Trends of increasing eccentricity and variation in planet distance with initial planet distance are also the same and the only instance of satellite periplanet libration effects about the star's periplanet (periastron) occur very close to the giant at 0.01AU (see Figure 7.6).

Table 7.5 Orbital runs for an Earth-Moon satellite orbiting the minimum mass giant HD 28185b in the habitable zone of its star, excluding J_2 effects.

Starting Parameters			Parameter variation during a run				t / years	O
E-M a / AU	p / °	i / °	Earth-Moon e	Earth-Moon a / AU	$\Delta\varpi$ / °	ΔI / °		
0.01	0	0	0.000210 – 0.001300*	0.01	± 50*	0	>10^8	-
0.01	180	0	0.000230 – 0.001315*	0.01	± 50*	0	>10^8	-
0.02	0	0	10^{-5} – 0.010307	0.01995 ± 0.00005	0 - 360	0	>10^8	-
0.02	180	0	10^{-5} – 0.008791	0.01995 ± 0.00005	0 - 360	0	>10^8	-
0.03	0	0	10^{-5} – 0.028774	0.02973 ± 0.00028	0 - 360	0	>10^8	-
0.03	180	0	10^{-5} – 0.029221	0.02975 ± 0.00028	0 - 360	0	>10^8	-
0.03	0	60	10^{-5} – 0.764627	0.02975 ± 0.00041	0 - 360	41 - 60	>10^8	-
0.03	180	60	10^{-5} – 0.761804	0.02976 ± 0.00040	0 - 360	42 - 60	>10^8	-
0.03	0	75	10^{-5} – 0.956810	0.02011 ± 0.00997	0 - 360	40 - 76	>10^8	-
0.03	180	75	10^{-5} – 0.955582	0.02258 ± 0.00744	0 - 360	40 - 75	>10^8	-
0.03	0	75s*	10^{-5} – 0.954014	0.02571 ± 0.00431	0 - 360	0 - 150	>10^8	-
0.03	180	75s*	10^{-5} – 0.953695	0.02394 ± 0.00606	0 - 360	0 - 150	>10^8	-
0.031	0	60	10^{-5} – 0.761850	0.03073 ± 0.00046	0 - 360	41 - 60	>10^8	-
0.031	180	60	10^{-5} – 0.754320	0.03073 ± 0.00045	0 - 360	42 - 60	>10^8	-
0.031	0	75	10^{-5} – 0.956478	0.02673 ± 0.00430	0 - 360	41 - 76	>10^8	-
0.031	180	75	10^{-5} – 0.963502	0.01769 ± 0.01332	0 - 360	41 - 76	>10^8	-
0.032	0	60	10^{-5} – 0.760352	0.03167 ± 0.00051	0 - 360	41 - 60	>10^8	-
0.032	180	60	10^{-5} – 0.752940	0.03169 ± 0.00051	0 - 360	42 - 60	>10^8	-
0.032	0	75	10^{-5} – 0.957903	0.02503 ± 0.00697	0 - 360	40 - 75	>10^8	-
0.032	180	75	10^{-5} – 0.956337	0.02928 ± 0.00697	0 - 360	41 - 76	>10^8	-
0.033	0	60	10^{-5} – 0.763812	0.03264 ± 0.00059	0 - 360	42 - 60	>10^8	-
0.033	180	60	10^{-5} – 0.760943	0.03268 ± 0.00058	0 - 360	42 - 60	>10^8	-
0.033	0	75	10^{-5} – 0.956376	0.03186 ± 0.00117	0 - 360	41 - 75	>10^8	-
0.033	180	75	10^{-5} – 0.956337	0.02928 ± 0.00280	0 - 360	41 - 76	>10^8	-
0.034	0	60	10^{-5} – 0.758834	0.03358 ± 0.00065	0 - 360	42 - 60	>10^8	-
0.034	180	60	10^{-5} – 0.765982	0.03365 ± 0.00067	0 - 360	42 - 60	>10^8	-
0.034	0	75	10^{-5} – 0.896462	0.03371 ± 0.00042	0 - 360	46 - 76	1.064 x 10^5	PC
0.034	180	75	10^{-5} – 0.920713	0.03362 ± 0.00038	0 - 360	46 - 76	5.149 x 10^5	PC
0.035	0	60	10^{-5} – 0.758390	0.03455 ± 0.00074	0 - 360	42 - 60	>10^8	-
0.035	180	60	10^{-5} – 0.779766	0.03459 ± 0.00075	0 - 360	42 - 61	>10^8	-
0.035	0	75	10^{-5} – 0.976355	0.01889 ± 0.01614	0 - 360	41 - 78	>10^8	-
0.035	180	75	10^{-5} – 0.969166	0.03403 ± 0.00116	0 - 360	42 - 78	2.668 x 10^6	PC
0.036	0	60	10^{-5} – 0.758138	0.03551 ± 0.00083	0 - 360	42 - 60	>10^8	-
0.036	180	60	10^{-5} – 0.780089	0.03552 ± 0.00085	0 - 360	42 - 62	>10^8	-
0.037	0	60	10^{-5} – 0.753744	0.03642 ± 0.00090	0 - 360	42 - 60	>10^8	-
0.037	180	60	10^{-5} – 0.785278	0.03649 ± 0.00091	0 - 360	42 - 63	>10^8	-
0.04	0	0	10^{-5} – 0.070014	0.03909 ± 0.00091	0 - 360	0	>10^8	-
0.04	180	0	10^{-5} – 0.076334	0.03919 ± 0.00093	0 - 360	0	>10^8	-
0.04	0	60s*	10^{-5} – 0.737202	0.03922 ± 0.00129	0 - 360	0 - 120	>10^8	-
0.04	180	60s*	10^{-5} – 0.719168	0.03938 ± 0.00129	0 - 360	0 - 119	>10^8	-
0.04	0	75	10^{-5} – 0.952143	0.03919 ± 0.00114	0 - 360	42 - 78	5.548 x 10^6	PC
0.04	180	75	10^{-5} – 0.958669	0.03931 ± 0.00113	0 - 360	42 - 76	5.500 x 10^6	PC
0.04	0	75s*	0.122473 – 0.967971*	0.02897 ± 0.01103	0 - 360	0 - 151	>10^8	-
0.04	180	75s*	0.122473 – 0.968175	0.03498 ± 0.00543	0 - 360	0 - 150	>10^8	-
0.041	0	60	10^{-5} – 0.922033	0.03977 ± 0.00157	0 - 360	43 - 78	4.594 x 10^7	PC
0.041	180	60	10^{-5} – 0.708347	0.04047 ± 0.00149	0 - 360	43 - 60	>10^8	-
0.042	0	60	10^{-5} – 0.811431	0.04081 ± 0.00181	0 - 360	43 - 64	>10^8	-
0.042	180	60	10^{-5} – 0.802937	0.04093 ± 0.00169	0 - 360	42 - 62	>10^8	-
0.043	0	60	10^{-5} – 0.962749	0.04168 ± 0.00237	0 - 360	42 - 77	6.822 x 10^7	PC
0.043	180	60	10^{-5} – 0.966664	0.04176 ± 0.00232	0 - 360	41 - 77	5.439 x 10^7	PC
0.044	0	60	10^{-5} – 0.952204	0.04151 ± 0.00268	0 - 360	42 - 77	2.999 x 10^7	PC
0.044	180	60	10^{-5} – 0.853002	0.04421 ± 0.00335	0 - 360	43 - 71	1.416 x 10^7	ce
0.045	0	0	10^{-5} – 0.102278	0.04354 ± 0.00146	0 - 360	0	>10^8	-
0.045	90	0	10^{-5} – 0.331487	0.04715 ± 0.00286	0 - 360	0	>10^8	-
0.045	180	0	10^{-5} – 0.116740	0.04373 ± 0.00153	0 - 360	0	>10^8	-
0.045	270	0	10^{-5} – 0.329032	0.04713 ± 0.00283	0 - 360	0	>10^8	-
0.045	0	30	10^{-5} – 0.111407	0.04356 ± 0.00144	0 - 360	27 - 30	>10^8	-
0.045	180	30	10^{-5} – 0.111076	0.04370 ± 0.00142	0 - 360	27 - 30	>10^8	-
0.045	0	60	10^{-5} – 0.968916	0.04197 ± 0.00439	0 - 360	37 - 78	5.392 x 10^7	PC
0.045	180	60	10^{-5} – 0.901277	0.04483 ± 0.00308	0 - 360	39 - 69	3.566 x 10^7	ce
0.045	0	60s*	10^{-5} – 0.910163	0.04474 ± 0.00246	0 - 360	0 - 131	2.556 x 10^6	PC
0.045	180	60s*	10^{-5} – 0.934926	0.04498 ± 0.00303	0 - 360	0 - 127	4.536 x 10^6	PC
0.045	0	90s*	10^{-5}	0.045	-	-	3	PC
0.045	180	90s*	10^{-5}	0.045	-	-	3	PC
0.046	0	0	10^{-5} – 0.109786	0.04440 ± 0.00160	0 - 360	0	>10^8	-
0.046	90	0	10^{-5} – 0.473136	0.04860 ± 0.00393	0 - 360	0	>10^8	-

Starting Parameters			Parameter variation during a run				t/years	O
E-M a / AU	p / °	i / °	Earth-Moon e	Earth-Moon a / AU	$\Delta\varpi$ / °	ΔI / °		
0.046	180	0	10^{-5} – 0.128529	0.04462 ± 0.00167	0 - 360	0	>10^8	-
0.046	270	0	10^{-5} – 0.470541	0.04853 ± 0.00393	0 - 360	0	>10^8	-
0.046	0	60	10^{-5} – 0.861739	0.04499 ± 0.00256	0 - 360	41 - 69	5.871 x 10^6	ce
0.046	180	60	10^{-5} – 0.862022	0.04483 ± 0.00205	0 - 360	43 - 71	1.909 x 10^6	ce
0.047	0	0	10^{-5} – 0.118713	0.04526 ± 0.00175	0 - 360	0	>10^8	-
0.047	90	0	10^{-5}	0.047	-	-	3724	ce
0.047	180	0	10^{-5} – 0.135634	0.04550 ± 0.00182	0 - 360	0	>10^8	-
0.047	270	0	10^{-5}	0.047	-	-	4929	ce
0.048	0	0	10^{-5} – 0.126773	0.04610 ± 0.00190	0 - 360	0	>10^8	-
0.048	90	0	10^{-5}	0.048	-	-	143	ce
0.048	180	0	10^{-5} – 0.147506	0.04640 ± 0.00201	0 - 360	0	>10^8	-
0.048	270	0	10^{-5}	0.048	-	-	98	ce
0.049	0	0	10^{-5} – 0.135435	0.04694 ± 0.00206	0 - 360	0	>10^8	-
0.049	90	0	10^{-5}	0.049	-	-	51	ce
0.049	180	0	10^{-5} – 0.160667	0.04727 ± 0.00219	0 - 360	0	>10^8	-
0.049	270	0	10^{-5}	0.049	-	-	34	ce
0.05	0	0	10^{-5} – 0.145817	0.04775 ± 0.00225	0 - 360	0	>10^8	-
0.05	90	0	10^{-5}	0.050	-	-	4	ce
0.05	180	0	10^{-5} – 0.218670	0.04826 ± 0.00263	0 - 360	0	>10^8	-
0.05	270	0	10^{-5}	0.050	-	-	34	ce
0.05	0	0a	10^{-5} – 0.144050	0.04777 ± 0.00223	0 - 360	0	>10^8	-
0.05	180	0a	10^{-5} – 0.173154	0.04816 ± 0.00241	0 - 360	0	>10^8	-
0.05	0	30	10^{-5} – 0.154684	0.04778 ± 0.00222	0 - 360	27 - 30	>10^8	-
0.05	180	30	10^{-5} – 0.157057	0.04806 ± 0.00223	0 - 360	27 - 30	>10^8	-
0.05	0	30s*	10^{-5} – 0.153606	0.04780 ± 0.00220	0 - 360	0 - 60	>10^8	-
0.05	180	30s*	10^{-5} – 0.153891	0.04808 ± 0.00224	0 - 360	0 - 60	>10^8	-
0.05	0	60	10^{-5} – 0.596807	0.04801 ± 0.00199	0 - 360	51 - 60	2.542 x 10^4	E
0.05	180	60	10^{-5} – 0.636765	0.04881 ± 0.00119	0 - 360	48 - 63	4.004 x 10^4	ce
0.05	0	60s*	10^{-5} – 0.517730	0.04796 ± 0.00204	0 - 360	0 - 110	4.532 x 10^4	ce
0.05	180	60s*	10^{-5} – 0.258152	0.04874 ± 0.00126	0 - 360	0 - 85	1.740 x 10^4	ce
0.051	0	0	10^{-5} – 0.383854	0.04920 ± 0.00366	0 - 360	0	>10^8	-
0.051	180	0	10^{-5} – 0.295583	0.04953 ± 0.00270	0 - 360	0	1.118 x 10^5	ce
0.052	0	0	10^{-5}	0.052	-	-	779	ce
0.052	180	0	10^{-5}	0.052	-	-	679	ce
0.053	0	0	10^{-5}	0.053	-	-	1421	ce
0.053	180	0	10^{-5}	0.053	-	-	246	ce
0.054	0	0	10^{-5}	0.054	-	-	22	ce
0.054	180	0	10^{-5}	0.054	-	-	136	ce
0.055	0	0	10^{-5} – 0.268010	0.05167 ± 0.00333	0 - 360	0	>10^8	-
0.055	180	0	10^{-5}	0.055	-	-	8	ce
0.056	0	0	10^{-5} – 0.248973	0.05259 ± 0.00370	0 - 360	0	>10^8	-
0.056	180	0	10^{-5}	0.056	-	-	16	ce
0.057	0	0	10^{-5} – 0.234917	0.05323 ± 0.00177	0 - 360	0	>10^8	-
0.057	180	0	10^{-5}	0.057	-	-	15	ce
0.058	0	0	10^{-5}	0.058	-	-	29	ce
0.058	180	0	10^{-5}	0.058	-	-	10	ce
0.059	0	0	10^{-5}	0.059	-	-	5	ce
0.059	180	0	10^{-5}	0.059	-	-	5	ce
0.06	0	0	10^{-5}	0.060	-	-	15	PC
0.06	180	0	10^{-5}	0.060	-	-	5	ce
0.065	0	0	10^{-5}	0.065	-	-	2	ce
0.065	180	0	10^{-5}	0.065	-	-	4	ce
0.07	0	0	10^{-5}	0.070	-	-	13	PC
0.07	180	0	10^{-5}	0.070	-	-	19	PC

* Measurements taken after the first 10^7 years to allow for orbital stabilisation.
s* Star is inclined to the equator of the giant planet.
a Satellite was launched at apoplanet, the farthest distance from the giant in its orbit
ce Close encounter to within $0.1R_H$ of the star.
PC Earth-Moon satellite collides with its parent planet.
E Earth-Moon is ejected from the system.

Inclining the satellite orbits out of the plane of the giant's orbit opens up a new vista of orbital trends with time. Satellite orbital inclinations are of two types as illustrated in Figure 7.7. Type 1 is when the giant rotates in the plane of its orbit and satellites orbit out of this plane, Type 2 is when the satellites orbit in the plane of rotation of the giant, which itself is inclined to its orbital plane (achieved by inclining the "star's orbit" within the Integrator). Satellites were launched only at 0^O and 180^O to the star's periplanet position.

Table 7.6 shows the distance from the giant where orbits remain stable with both instances of inclination and both instances of periastron launch longitude. There is clearly some connection between satellite inclination angle and orbit stability distance, although there are too few points to establish any mathematical relationship. As there is no J_2 effect from the giant, the results should theoretically be the same for both types of satellite orbital inclination.

Table 7.6 Distances of inclined satellite orbits out to which stable orbits are maintained.

Launch Longitude / ^{O} →	0	180	0	180
Orbital Inclination / ^{O} ↓	Distance from the giant to which satellite orbits are stable out of the plane of the giant's rotation / AU		Distance from the giant to which satellite orbits are stable in the plane of the giant's rotation / AU	
0	0.051	0.050	0.051	0.050
30	0.050	0.050	0.050	0.050
60	0.042	0.042	0.040	0.040
75	0.033	0.033	0.040	0.040
90	0	0	0	0

So this study could also be regarded as a robustness test for the Mercury Orbital Integrator. Results from table 7.5 show there are clear differences between the two types of inclinations excepting, for the same semimajor axis, variations in distance from the planet and eccentricity, which are very similar. Type 1 inclinations have a much less and more believable variation, from approximately 40^{O} up to just more than the original inclination angle. Type 2 inclinations vary much more widely, from 0^{O} (i.e within the giant's orbital plane) to more than twice the original inclined angle. A further investigation, which gives more credibility to type 1 inclinations, relates satellite orbital eccentricity with inclination angle over integration time. Kozai (1962) showed that for asteroids under the attraction of the Sun and Jupiter, a relation exists such that for eccentricity, e, inclination, I and a constant k, then

$$\sqrt{1-e^2}\cos I = k \qquad 7.1.$$

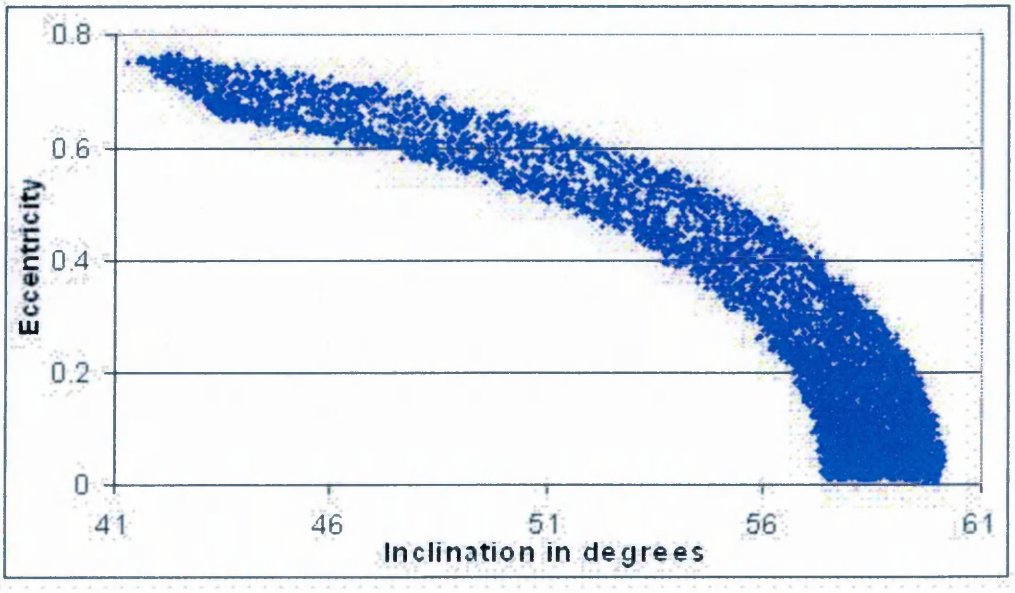

Figure 7.8 Variation of eccentricity v. inclination for a satellite orbiting HD 28185b initially 60^{O} out of the orbital plane of the giant, as in Type 1.

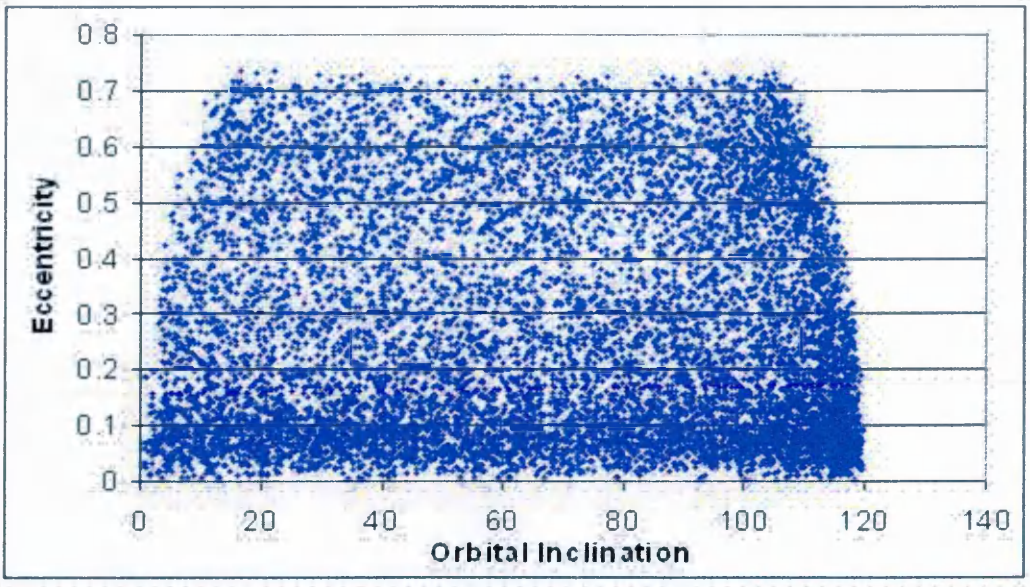

Figure 7.9 Variation of eccentricity v. inclination for a satellite orbiting HD 28185b initially 60^{O} out of the orbital plane of the giant, as in Type 2.

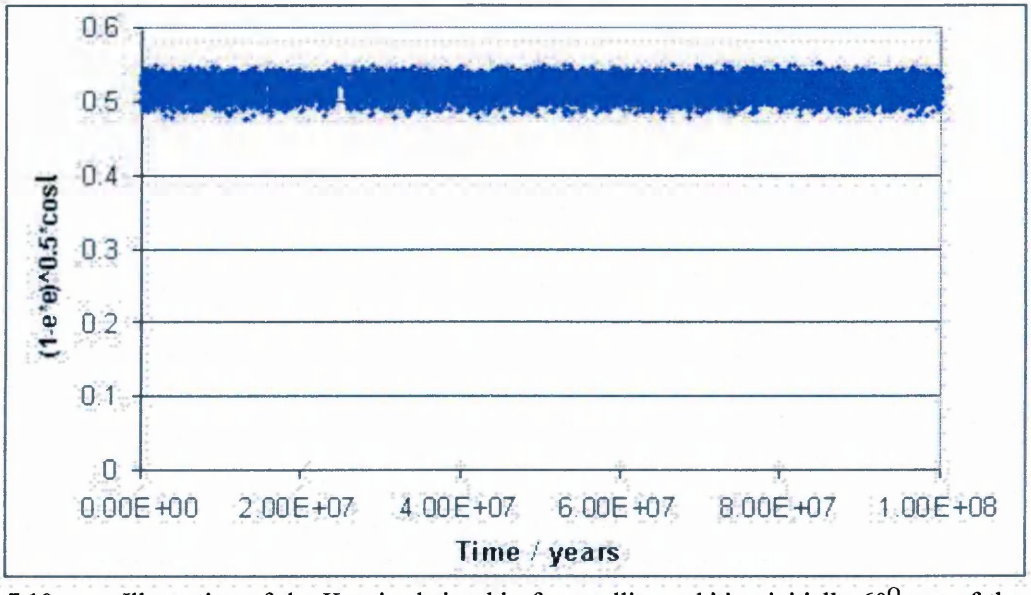

Figure 7.10 Illustration of the Kozai relationship for satellites orbiting initially 60^{O} out of the orbital plane of the giant, as in Type 1.

Plots of eccentricity against inclination for both types of satellite inclination are shown in figures 7.8 and 7.9. Figure 7.8 clearly shows that there is some relation between eccentricity and orbital inclination for satellites orbiting outside the giant's orbital plane, whereas figure 7.9 shows no such relation for satellites orbiting in the plane of the giant's rotation with the star's orbit inclined. When equation 7.1 is applied to the data in figure 7.8 a constant value is obtained with time, as shown in figure 7.10, confirming the Kozai relationship in this case.

The decreasing stability of the satellite orbits with increasing orbital inclination could be due to the high eccentricity of the orbits induced by high inclinations according to the Kozai relationship. With highest eccentricities during their periods of highest inclination during their runs, satellites may be able to gather sufficient energy from the giant in the form of gravitational assists during their very close periplanet passes to enable them to escape the giant and have a close encounter with the star. Consequently when a satellite is launched at a higher orbital inclination it must be closer to the planet to remain sufficiently within the giants gravity well in order not to escape or destabilise via gravitational assists.

The differences in results between the two types of inclination, where the better results are for type 1 inclinations, must be due to the small body being inclined rather than the large body of the star as in type 2 inclinations. Clearly the integrator is not designed to accurately represent such unusual configurations as in type 2; hence it gives wildly varying results for these runs, and no evidence for the Kozai relation.

7.4 Outcome of the HD 28185 Integrations – with the J_2 Effect

A more realistic approach to studying satellite orbits around HD 28185b is to incorporate the J_2 effect from the giant, introducing planetary oblateness. As the J_2 value is not known, the value accepted for that of Jupiter is incorporated into the integrations, where J_2 = 0.014736. Note that the gravitational field contribution corresponding to the J_2 value decreases with distance from the giant by the inverse square (Murray & Dermott, 1999, page 151). Table 7.7 is less exhaustive than table 7.5 as comparisons are sought, with and without the J_2 value, between stable orbit and unstable orbit boundaries around the giant. Since this study was meant to reflect real satellite systems, only type 2 inclinations were studied, hence the planet's rotation axis was tilted relative to the star, or from the integrator's view, the "star's orbit" is inclined, giving the perspective that the satellites orbit in the plane of the giant planet's rotation, as in most satellite systems within the Solar System (see Figure 7.7).

The outcomes of all the integration runs incorporating the J_2 effect are shown in table 7.7. For the type 2 orbits, the distances where they destabilise are identical to those in the absence of the J_2 effect, even with an island of stability at 0.055AU to 0.057AU for satellites launched at coincident periplanet with the star. Integrations inclined at 180^O to the giant's orbital plane, i.e with retrograde orbits, are also stable at 0.050AU. The results in table 7.8 are similar to those in table 7.6 for low angle inclination orbits, however the destabilising of orbits inclined at 60^O occurs a little nearer to the planet. For orbits inclined at 75^O, there appears to be no stability possible. When no J_2 term is present, these orbits are stable to 0.04AU; however its presence clearly has an increasing destabilisation effect on orbits when launched closer to the giant and at high inclinations. Indeed it appears that the destabilising effect of the J_2 term close to the planet for highly inclined orbits, coupled with gravitational assists caused by their induced high eccentricity by a **possible** Kozai relationship not shown here, could be sufficient to generate a "no go" area for such satellites. If orbits inclined at 75^O or more are not stable at any distance, how do the satellites of Uranus remain where they are? The answer is undoubtedly due to its low J_2 value of 0.003343 (Murray & Dermott, 1999, page 531) compared to the 0.014736 value used here.

On analysis of eccentricity and inclination with time, there **appears** to be no evidence for the Kozai relationship, as was observed for similarly inclined orbits with no J_2 term (see Figure 7.9), although it would be necessary to explain the "no go" region for highly inclined orbits. The inclination again varies wildly from 0^O to almost twice the star's initial inclination angle. The only instance of a stable inclination angle was for the two runs of type 1, when the satellite was initially inclined at 30^O, giving similar results to the corresponding run with no J_2 effect. These results only reinforce that the integrator is not designed to accurately represent such unusual configurations as in type 2; hence it gives wildly varying results for these runs.

Table 7.7 Orbital runs for an Earth-Moon satellite orbiting the minimum mass giant HD 28185b in the habitable zone of its star, including J_2 effects.

Starting Parameters			Parameter variation during a run				t/years	O
E-M a / AU	p / °	i / °	Earth-Moon e	Earth-Moon a / AU	$\Delta\varpi$ / °	ΔI / °		
0.01	0	75s*	10^{-5}	0.01	-	-	581	PC
0.01	180	75s*	10^{-5}	0.01	-	-	1695	PC
0.015	0	75s*	10^{-5} – 0.382011	0.01499 ± 0.00001	0 - 360	0 - 30	1.329×10^4	PC
0.015	180	75s*	10^{-5}	0.01	-	-	1079	PC
0.02	0	75s*	10^{-5} – 0.917460	0.01988 ± 0.00012	0 - 360	0 - 143	2.160×10^5	PC
0.02	180	75s*	10^{-5} – 0.278916	0.01998 ± 0.00002	0 - 360	0 - 88	1.570×10^4	PC
0.025	0	75s*	10^{-5} – 0.960493	0.02482 ± 0.00018	0 - 360	0 - 146	2.134×10^5	PC
0.025	180	75s*	10^{-5} – 0.921550	0.02480 ± 0.00196	0 - 360	0 - 149	5.299×10^5	PC
0.03	0	75s*	10^{-5} – 0.958547	0.02969 ± 0.00031	0 - 360	0 - 147	2.442×10^5	PC
0.03	180	75s*	10^{-5} – 0.960249	0.02958 ± 0.00046	0 - 360	0 - 149	1.273×10^6	PC
0.035	0	75s*	10^{-5} – 0.931963	0.03470 ± 0.00196	0 - 360	0 - 148	1.593×10^5	PC
0.035	180	75s*	10^{-5} – 0.304826	0.03468 ± 0.00032	0 - 360	0 - 60	1.479×10^4	PC
0.039	0	75s*	10^{-5} – 0.906034	0.03857 ± 0.00115	0 - 360	0 - 147	2.655×10^5	PC
0.039	180	75s*	10^{-5} – 0.922875	0.03847 ± 0.00089	0 - 360	0 - 93	7.053×10^4	PC
0.04	0	60s*	10^{-5} – 0.924859	0.03921 ± 0.00143	0 - 360	0 - 131	$>10^8$	-
0.04	180	60s*	10^{-5} – 0.715523	0.03929 ± 0.00177	0 - 360	0 - 119	$>10^8$	-
0.04	0	75s*	10^{-5} – 0.965091	0.03906 ± 0.00094	0 - 360	0 - 131	1.755×10^5	PC
0.04	180	75s*	10^{-5} – 0.853920	0.03948 ± 0.00052	0 - 360	0 - 132	5.056×10^4	PC
0.041	0	60s*	10^{-5} – 0.769299	0.04007 ± 0.00145	0 - 360	0 - 121	$>10^8$	-
0.041	180	60s*	10^{-5} – 0.950609	0.03970 ± 0.00199	0 - 360	0 - 132	8.040×10^7	PC
0.042	0	60s*	10^{-5} – 0.920106	0.04115 ± 0.00166	0 - 360	0 - 128	6.406×10^7	PC
0.042	180	60s*	10^{-5} – 0.766175	0.04114 ± 0.00163	0 - 360	0 - 120	$>10^8$	-
0.045	0	0	10^{-5} – 0.102444	0.04354 ± 0.00146	0 - 360	0	$>10^8$	-
0.045	180	0	10^{-5} – 0.117081	0.04373 ± 0.00152	0 - 360	0	$>10^8$	-
0.045	0	30	10^{-5} – 0.111294	0.04356 ± 0.00144	0 - 360	27 - 30	$>10^8$	-
0.045	180	30	10^{-5} – 0.109340	0.04372 ± 0.00146	0 - 360	27 - 30	$>10^8$	-
0.045	0	60s*	10^{-5} – 0.865016	0.04470 ± 0.00261	0 - 360	0 - 118	1.798×10^6	PC
0.045	180	60s*	10^{-5} – 0.861896	0.04355 ± 0.00166	0 - 360	0 - 120	2.419×10^6	PC
0.045	0	90s*	10^{-5}	0.045	-	-	3	PC
0.045	180	90s*	10^{-5}	0.045	-	-	3	PC
0.05	0	0	10^{-5} – 0.145227	0.04778 ± 0.00222	0 - 360	0	$>10^8$	-
0.05	180	0	10^{-5} – 0.174090	0.04814 ± 0.00238	0 - 360	0	$>10^8$	-
0.05	0	30s*	10^{-5} – 0.152647	0.04778 ± 0.00222	0 - 360	0 - 60	$>10^8$	-
0.05	180	30s*	10^{-5} – 0.154690	0.04807 ± 0.00225	0 - 360	0 - 60	$>10^8$	-
0.05	0	60s*	10^{-5}	0.05	-	-	9661	ce
0.05	180	60s*	10^{-5} – 0.611746	0.04876 ± 0.00124	0 - 360	0 - 117	3.126×10^5	ce
0.05	0	180s*	10^{-5} – 0.149081	0.04837 ± 0.00163	0 - 360	180	$>10^8$	-
0.05	180	180s*	10^{-5} – 0.102216	0.04854 ± 0.00158	0 - 360	180	$>10^8$	-
0.051	0	0	10^{-5} – 0.381616	0.04917 ± 0.00362	0 - 360	0	$>10^8$	-
0.051	180	0	10^{-5} – 0.419545	0.04923 ± 0.00305	0 - 360	0	3.223×10^5	ce
0.052	0	0	10^{-5}	0.052	-	-	1184	ce
0.052	180	0	10^{-5}	0.052	-	-	136	ce
0.053	0	0	10^{-5}	0.053	-	-	153	ce
0.053	180	0	10^{-5}	0.053	-	-	306	ce
0.054	0	0	10^{-5}	0.054	-	-	17	ce
0.054	180	0	10^{-5}	0.054	-	-	26	ce
0.055	0	0	10^{-5} – 0.267928	0.05167 ± 0.00333	0 - 360	0	$>10^8$	-
0.055	180	0	10^{-5}	0.055	-	-	8	ce
0.056	0	0	10^{-5} – 0.249269	0.05260 ± 0.00371	0 - 360	0	$>10^8$	-
0.056	180	0	10^{-5}	0.056	-	-	16	ce
0.057	0	0	10^{-5} – 0.235232	0.05324 ± 0.00378	0 - 360	0	$>10^8$	-
0.057	180	0	10^{-5}	0.057	-	-	15	ce
0.058	0	0	10^{-5}	0.058	-	-	74	ce
0.058	180	0	10^{-5}	0.058	-	-	10	ce
0.059	0	0	10^{-5}	0.059	-	-	5	ce
0.059	180	0	10^{-5}	0.059	-	-	5	ce
0.06	0	0	10^{-5}	0.060	-	-	15	PC
0.06	180	0	10^{-5}	0.060	-	-	4	ce
0.065	0	0	10^{-5}	0.065	-	-	2	ce
0.065	180	0	10^{-5}	0.065	-	-	4	ce
0.07	0	0	10^{-5}	0.070	-	-	248	E
0.07	180	0	10^{-5}	0.070	-	-	30	ce

* Measurements taken after the first 10^7 years to allow for orbital stabilisation.
s* Star is inclined to the equator of the giant planet.
a Satellite was launched at apoplanet
ce Close encounter to within $0.1R_H$ of the star.

PC Earth-Moon satellite collides with its parent planet.
E Earth-Moon is ejected from the system.

Table 7.8 Distances of satellite orbits out to which stable orbits are maintained for inclinations in the giant's rotation plane but out of the plane of its orbit.

Launch Longitude / ^{O} →	**0**	**180**
Orbital Inclination / ^{O}	**Distance from the giant to which satellite orbits are stable / AU**	
0	0.051	0.050
30	0.050	0.050
60	0.041	0.040
75	0	0
90	0	0
180	0.050	0.050

7.5 Varying the Mass of the Satellite.

This investigation was only undertaken for satellites orbiting within the plane of the giant's orbit and rotation in both the absence and presence of the J_2 term. The distance of orbital destabilisation in the giant's orbital plane has now been determined as 0.051AU for Earth-Moon mass satellites with an initial periplanet launch longitude of 0^{O} with respect to periastron and 0.050AU for satellites with an initial periplanet launch longitude of 180^{O} with respect to periastron. Hence integrations were run with different planet masses only around this region. Tables 7.9 and 7.10 show that orbital stability or instability are the same with or without the J_2 term (i.e. beyond its influence), for each run. The only differences for unstable runs are in the length of time before a close encounter with the star occurs.

Table 7.9 Orbital runs for Earth-Moon satellites of different mass orbiting the minimum mass giant HD 28185b in the habitable zone of its star, excluding J_2 effects.

Starting Parameters			**Parameter variation during a run**			***t* / years**	***O***
E-M *mass* / $M_{\oplus}$	**E-M *a* / AU**	***p* / °**	**Earth-Moon *e***	**Earth-Moon *a* / AU**	**$\Delta\varpi$ / °**		
0.1	0.05	0	10^{-5} – 0.145098	0.04777 ± 0.00223	0 - 360	$>10^{8}$	-
0.1	0.05	180	10^{-5} – 0.172407	0.04814 ± 0.00239	0 - 360	$>10^{8}$	-
0.1	0.051	0	10^{-5} – 0.388253	0.04916 ± 0.00362	0 - 360	$>10^{8}$	-
0.1	0.051	180	10^{-5} – 0.303855	0.05097 ± 0.00003	0 - 360	1.379×10^{4}	ce
0.3	0.051	0	10^{-5} – 0.380263	0.04918 ± 0.00365	0 - 360	$>10^{8}$	-
0.3	0.051	180	10^{-5} – 0.068166	0.05075 ± 0.00025	0 - 360	1.552×10^{4}	ce
1	0.05	0	10^{-5} – 0.145817	0.04775 ± 0.00225	0 - 360	$>10^{8}$	-
1	0.05	180	10^{-5} – 0.218670	0.04826 ± 0.00263	0 - 360	$>10^{8}$	-
1	0.051	0	10^{-5} – 0.383854	0.04920 ± 0.00366	0 - 360	$>10^{8}$	-
1	0.051	180	10^{-5} – 0.295583	0.04953 ± 0.00270	0 - 360	1.118×10^{5}	ce
1	0.052	0	10^{-5}	0.052	-	779	ce
1	0.052	180	10^{-5}	0.052	-	679	ce
3	0.051	0	10^{-5} – 0.391620	0.04931 ± 0.00378	0 - 360	$>10^{8}$	-
3	0.051	180	10^{-5} – 0.238944	0.04865 ± 0.00235	0 - 360	5.736×10^{4}	ce
10	0.05	0	10^{-5} – 0.144185	0.04779 ± 0.00222	0 - 360	$>10^{8}$	-
10	0.05	180	10^{-5} – 0.170129	0.04813 ± 0.00236	0 - 360	$>10^{8}$	-
10	0.051	0	10^{-5} – 0.398435	0.04928 ± 0.00373	0 - 360	$>10^{8}$	-
10	0.051	180	10^{-5} – 0.405572	0.04962 ± 0.00391	0 - 360	$>10^{8}$	-
10	0.052	0	10^{-5}	0.052	0 - 360	8896	ce
10	0.052	180	10^{-5}	0.052	0 - 360	306	ce

ce Close encounter to within $0.1R_H$ of the star.
$M_{\oplus}$ Earth-Moon mass

The planet masses covered were from $0.1M_{\oplus}$ to $10M_{\oplus}$, the range where planets could support life, as discussed in chapter 3, section 1. The only difference observed in the trend of increasing satellite mass, is that runs are unstable when launched at 0.051AU with

a periplanet launch longitude of 180^{O} for satellite masses to $3M_{\oplus}$. The same launch conditions give a stable orbit, however, for a $10M_{\oplus}$ satellite. This is due to the mutual attraction between the two bodies, according to Newton's Law of Gravitation, being just great enough for a stable satellite orbit to exist. For a satellite with a mass less than $10M_{\oplus}$, this is not so and orbits destabilise. Overall, increasing the satellite mass would not have a great effect on satellite orbits in HD 28185 or in any other system with a sizeable giant. The effect on the size of the giant on satellite orbital stability is for possible future investigation.

Table 7.10 Orbital runs for Earth-Moon satellites of different mass orbiting the minimum mass giant HD 28185b in the habitable zone of its star, including J_2 effects.

Starting Parameters			Parameter variation during a run			t / years	O
E-M *mass* / $M_{\oplus}$	E-M a / AU	p / °	Earth-Moon e	Earth-Moon a / AU	$\Delta\varpi$ / °		
0.1	0.045	0	10^{-5} – 0.145098	0.04354 ± 0.00146	0 - 360	$>10^{8}$	-
0.1	0.045	180	10^{-5} – 0.116897	0.04373 ± 0.00152	0 - 360	$>10^{8}$	-
0.1	0.050	0	10^{-5} – 0.144414	0.04777 ± 0.00223	0 - 360	$>10^{8}$	-
0.1	0.050	180	10^{-5} – 0.174667	0.04815 ± 0.00240	0 - 360	$>10^{8}$	-
0.1	0.051	0	10^{-5} – 0.385071	0.04915 ± 0.00360	0 - 360	$>10^{8}$	-
0.1	0.051	180	10^{-5} – 0.401347	0.04894 ± 0.00206	0 - 360	2.792×10^{4}	ce
0.1	0.052	0	10^{-5}	0.052	-	1584	ce
0.1	0.052	180	10^{-5}	0.052	-	964	ce
0.3	0.051	0	10^{-5} – 0.382246	0.04919 ± 0.00363	0 - 360	$>10^{8}$	-
0.3	0.051	180	10^{-5} – 0.357561	0.04972 ± 0.00284	0 - 360	1.276×10^{5}	ce
1	0.045	0	10^{-5} – 0.102444	0.04354 ± 0.00146	0 - 360	$>10^{8}$	-
1	0.045	180	10^{-5} – 0.117081	0.04373 ± 0.00152	0 - 360	$>10^{8}$	-
1	0.050	0	10^{-5} – 0.145227	0.04778 ± 0.00222	0 - 360	$>10^{8}$	-
1	0.050	180	10^{-5} – 0.174090	0.04814 ± 0.00238	0 - 360	$>10^{8}$	-
1	0.051	0	10^{-5} – 0.381616	0.04917 ± 0.00362	0 - 360	$>10^{8}$	-
1	0.051	180	10^{-5} – 0.419545	0.04923 ± 0.00305	0 - 360	3.223×10^{5}	ce
1	0.052	0	10^{-5}	0.052	-	1184	ce
1	0.052	180	10^{-5}	0.052	-	136	ce
3	0.051	0	10^{-5} – 0.383097	0.04926 ± 0.00369	0 - 360	$>10^{8}$	-
3	0.051	180	10^{-5} – 0.141056	0.04904 ± 0.00196	0 - 360	3.679×10^{4}	ce
10	0.045	0	10^{-5} – 0.101533	0.04354 ± 0.00146	0 - 360	$>10^{8}$	-
10	0.045	180	10^{-5} – 0.114470	0.04373 ± 0.00151	0 - 360	$>10^{8}$	-
10	0.050	0	10^{-5} – 0.143241	0.04778 ± 0.00222	0 - 360	$>10^{8}$	-
10	0.050	180	10^{-5} – 0.170861	0.04814 ± 0.00238	0 - 360	$>10^{8}$	-
10	0.051	0	10^{-5} – 0.397796	0.04927 ± 0.00372	0 - 360	$>10^{8}$	-
10	0.051	180	10^{-5} – 0.412805	0.04966 ± 0.00391	0 - 360	$>10^{8}$	-
10	0.052	0	10^{-5}	0.052	-	3114	ce
10	0.052	180	10^{-5}	0.052	-	1266	ce

ce Close encounter to within $0.1R_{H}$ of the star.
$M_{\oplus}$ Earth-Moon mass

7.6 Conclusion and Discussion

For both HD 23079 and HD 28185, there are many unstable integration runs which result in the satellite having gained enough energy from the planet in the form of gravitational assists to either have a close encounter with the star or escape from the system. Restricted three-body problem theory suggests all unstable satellite orbits should result in a satellite-giant collision. The general orbital trends for stable satellite orbits in each system were the same. Satellites launched at quadrature periplanet longitudes with respect to the star's periplanet longitude (periastron) were destabilised at closer distances than those launched at $\Delta\varpi = 0^{O}$ or 180^{O}.

Summarising the HD 23079 integration runs:

- Satellite orbits launched at quadrature destabilised at 0.054AU.
- Satellite orbits launched at $\Delta\varpi = 0^O$ or 180^O destabilised at 0.061AU
- Two further stable orbits were present among satellite orbits launched at $\Delta\varpi = 0^O$ at 0.068AU and 0.070AU.

Summarising the HD 28185 integration runs:

- Satellite orbits launched at quadrature destabilised at 0.046AU.
- Satellite orbits launched at $\Delta\varpi = 0^O$ or 180^O destabilised at 0.051AU and 0.050AU respectively.
- An island of stable orbits were present among satellite orbits launched at $\Delta\varpi = 0^O$ between 0.055AU and 0.057AU.
- Including the J_2 term appeared to have only a significant difference on the properties of highly inclined satellite orbits, although for satellites in close orbits to the giant with zero inclination, it preserves initial satellite orbital eccentricity.
- There was little or no difference between Type 1 or Type 2 inclined satellite orbital properties in the absence of the J_2 term. Satellite orbits were stable to lesser distances from the giant as inclination increased.
- Type 2 highly inclined satellite orbits were severely affected by the J_2 term so as to create a "no go" area between inclinations of 60^O and 90^O.
- Increasing the satellite mass had little effect on their orbital stability with no perceptible differences in the presence or absence of the J_2 term. The only trend found was by increasing the satellite mass from $3M_\oplus$ to $10M_\oplus$ (Earth-masses). This stabilised the orbit of the heavier satellite at 0.051AU launched with zero inclination and at a periplanet longitude of 180^O.

The giants in both HD 23079 and HD 28185 have been orbiting within each star's habitable zone in excess of the 2Gyr required for life to have made any atmospheric changes. In contrast to a planet, the differences for such a satellite are that it would be tidally locked to the giant, hence days would be long. If, in such a case, the orbit were greatly inclined, the seasonal variation would then be considerable. The satellite would need to be distant enough from the giant to be free from tidal distortions within it, if either in an eccentric orbit or where other large satellites were present. This would also be so if the giant had a powerful magnetic field, so life would only be possible on satellites in stable orbits far enough away. So if requirements are met, both HD23079 and HD 28185 are systems in which their known giant planets could support habitable satellites.

8. Conclusions and Future Research

8.1 Orbital Integrations

The orbital integration studies of the three single-giant planetary systems revealed that Earth-mass planets could exist in stable orbits confined to the habitable zones for two of the three systems. The best candidate is HD 52265 where the giant planet, at 0.49AU, is in a much larger orbit than the "Warm Jupiter" of ρ Coronae Borealis, the similar system previously examined (Jones et al., 2001). The giant planet appears to have no influence on terrestrial planets in confined orbits across the entire habitable zone, even when its mass is raised up to 8 times its minimum mass. The HD 196050 system could house a possible Earth-mass planet but only close to the inner edge of the habitable zone, similar to the previously studied system of 47 Ursae Majoris (Jones & Sleep, 2002) and only if the giant planet was of minimum mass. The giant planet's orbital parameters in the τ^1 Gruis system have recently changed and the new parameters have the habitable zone completely engulfed by the planet's influence. The system is at the end of its main sequence lifetime and the integrations using the previous parameters implied that life could have survived on a putative planet in the past. Unfortunately this is no longer so, however the study here could be useful for systems similar to the original form of τ^1 Gruis, which have yet to be discovered. Future investigations could examine the nature of orbital resonance regions, as touched on in the τ^1 Gruis integrations, to possibly explain why bodies launched at varying distances near to a resonance distance tend to converge towards it. The nature of secular resonances, also broached in this study could also be examined in more detail.

The integration studies on the (then) three-giant system of 55 Cancri indicates that the system alone can only exist with stable orbits provided the masses of the giants are less than 1.2 times minimum mass. This implies that the system must be inclined at an angle greater than 56^{O} 27' to the plane of the sky, contrary to findings of previous work involving the studies of a dust disk within the system. Trilling et al., 2000, implied an inclination angle of 27^{O} determined from the apparent ellipticity of the dust ring, assuming it is circular. The distances of the giants either side of the habitable zone, two inferior and one superior, are far enough to not destabilise any Earth-mass planets in orbits confined to the HZ. Initially this would appear to be a good candidate to possibly house a habitable terrestrial planet. However, the giants within the system appear to be in a fine gravitational balance between order and chaos, making putative 'Earth' orbits chaotic and possibly unstable where stability would be normally expected.

The fourth giant planet of 55 Cancri, which resulted in modified parameters after 11/04/2005, does not appear to allow the system to be stable, according to runs performed using the Mercury Orbital Integrator. Future work will be required to verify the stability of this configuration. This may be helped by the introduction of a relativistic term into the Mercury Orbital Integrator program, which would allow a more accurate representation of the orbits of the innermost giants, b, c and e.

The integrations for the satellite systems of HD 23079 and HD 28185 required the use of the RADAU integrator in the Mercury Program. This proved to be successful despite the unusual configuration required where the giant planet was placed at the centre of the (Ptolomaic-like) system. Stable orbits for Earth-mass satellites were found to exist within 0.42 Hill Radii of the giant planet in each system, implying the possible existence of habitable satellites around the giants orbiting within the stars' habitable zones. This agrees with previous results in theoretical systems by Barnes & O'Brien, 2002. Future work here would be a further study into orbits of satellites which appear to gain sufficient energy to destabilise what should be stable orbits, and to ascertain maximum limits on the energy

gains. An investigation into inclined satellite orbits may also prove useful, with particular regard to the Kozai relationship.

8.2 Stellar Models and Habitable Zones

The construction of the stellar matrix from the stellar evolution model has allowed an estimation of the limits of the habitable zones for 150 of the 178 stars with known exoplanetary systems for all of their main sequence lifetimes. The positions of the giant planet(s) in these systems and their gravitational reach have been mapped onto these zones, enabling regions within systems to be rapidly identified as to where a putative terrestrial planet could exist, in a stable orbit confined to the habitable zone.

The use of the 3× Hill radius boundary around giant planets appears to be an initially sound decision for the limits of planet gravitational reach, but only when the giant orbits beyond a putative terrestrial planet. Investigations by Jones et al. (2005) indicate that the gravitational influence of inferior giants extends outwards much further than the 3× Hill radius when the orbital eccentricity of the giant planet exceeds zero, the results of which are used here to determine which systems can house possible life supporting planets with stable orbits confined to the habitable zone.

If such an orbit were confined to the habitable zone, for a minimum of order 1Gyr, then any life would have had the time necessary to make the atmospheric changes, which spectroscopes may detect from Earth. Currently 85 or more of the 178 systems (as at 10th October, 2006) could possibly have detectable life on a terrestrial planet within a confined orbit, and 113 or more could do so at some time during their main sequence lifetime. These estimates are more optimistic than the findings of Turnbull & Tarter, 2003, due to their more stringent requirements for intelligent extraterrestrial life. Menou & Tabachnik, 2003 conclude that only ¼ of their 85 investigated systems could be habitable, although among their criteria was the habitable planets' orbits must always lie within the HZ, not the orbital semimajor axis as required here.

One shortcoming of the optimistic estimations that more than one half of known exosystems could have life-bearing planets is that one third of the known systems have "Hot Jupiter" or "Warm Jupiter" giant planets. Here a giant planet migrated to its present close-in orbit at very early stages of the exosystems evolution. This process may have cleared the regions of debris, where terrestrial planets within habitable zones could have formed. One aim for future work would be to simulate these processes, using the Mercury Orbital Integrator, to see if the optimism for a possible abundance of terrestrial planets is justified. Fogg & Nelson, 2005 and Mandell & Sigurdsson, 2003 have already pursued investigations in this area with positive results. The Integrator may also be used to investigate another hitch, where no regard is given to a giant planet's ability to gravitationally prevent planets from forming inside its orbit, such as Jupiter has with any planet formation within the asteroid belt. This may affect the possibility of planets existing within the habitable zone when a giant orbits close to its outer boundary, as in HD 196050 and 47 Ursae Majoris. Finally, but not exhaustively, orbital integrations could be used to examine giant planet shielding during the early formation period of exoplanetary systems, where a giant planet would act as an attraction for cometary bodies, protecting smaller terrestrial-sized bodies from such intense bombardment.

Any Earth-sized satellites of giants within the habitable zone may have to suffer tidal distortions, induced by the giant planet and the star. Such stresses may make the surface of a world uninhabitable due to excessive volcanic activity and plate tectonics. So although the opportunities initially look promising, much investigative research is necessary before the current optimism can be born out.

8.3 An Abundance of Earths in the Near Future?

Despite the uncertainty of whether terrestrial planets can survive the stresses of their everyday life, or even form under certain circumstances, the mechanisms are now in place to categorise quickly exosystems discovered in the future, with regard to the possibility that they may house extraterrestrial life. The quick application of these techniques is particularly important, as the rate of exosystem discovery is increasing and the floodgates are soon expected to open with, in the next few years, new ground-based surveys with improved instruments such as OWL (www.eso.org/projects/owl) the Overwhelmingly Large Telescope, plus the impending launches of satellites made specifically for exoplanetary searches such as The James Webb Space Telescope (www.jwst.nasa.gov) and Darwin (http://ast.star.rl.ac.uk/darwin). It is hoped this categorisation of data will be of assistance in searches for extraterrestrial life, guiding instruments towards the most likely exoplanetary system candidates. From indications so far, there is every reason for optimism that one of the armada of satellites due for launch within the next 15 years, could detect the signs of life on another planet, outside of our Solar System, before 2020.

Appendices

Appendix 1 Derivation of the Hill Radius Formula used in the Mercury Orbital Integrator

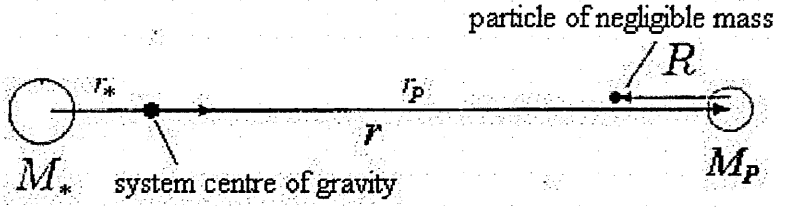

Figure A1.1 Required parameters for the Hill radius derivation

Let a planet of mass, M_p, be at a distance, r, from a star of mass, M_*. Let a particle of negligible mass, with respect to the other masses in the system, be on the radius vector between the star and planet at distance, R, from the planet (Figure A1.1). By Newton's Law of gravity, the gravitational acceleration, f_g, exerted on the particle by the star and planet towards the star is:

$$f_g = \frac{GM_*}{(r-R)^2} - \frac{GM_p}{R^2} \qquad \text{A1.1.}$$

Let R_H be the distance from the planet along its radius vector from the star, where the gravitational forces exerted on a particle by the star and planet balance, so subsequently let $R = R_H$. For this special case, both planet and particle revolve around the system centre of gravity with angular velocity, ω. So for the star and planet at distances r_* and r_P from the centre of gravity respectively, and where $r_* + r_P = r$, then by Newton's third law:

$$M_* r_* \omega^2 = M_P r_P \omega^2 \Rightarrow M_* r_* = M_P r_P \qquad \text{A1.2.}$$

Now $M_* >> M_P$, so from (A1.2) $r_P >> r_*$ and hence $r_P \approx r$. So by Newton's Gravitational Law, for the planet:

$$\frac{GM_* M_P}{r^2} = M_P r_P \omega^2 \approx M_P r \omega^2 \qquad \text{A1.3,}$$

hence:

$$\omega = \left(\frac{GM_*}{r^3}\right)^{1/2} \qquad \text{A1.4.}$$

The centripetal acceleration, $\dot{v}$, of the particle towards the star is given by:

$$\dot{v} = (r - R_H)\omega^2 = \frac{GM_*(r-R_H)}{r^3} \qquad \text{A1.5.}$$

For the particle to remain at this position, $\dot{v} = f_g$, so in (A1.1):

$$\frac{GM_*(r-R_H)}{r^3} = \frac{GM_*}{(r-R_H)^2} - \frac{GM_p}{R_H^2} \qquad \text{A1.6.}$$

For a planet orbiting a star, $R_H \ll$ r, so by the binomial expansion theory:

$$\frac{1}{(r-R_H)^2} = \frac{1}{r^2}\left(1-\frac{R_H}{r}\right)^{-2} = \frac{1}{r^2}\left(1+\frac{2R_H}{r}+O\left(\frac{R_H}{r}\right)^2\right) \approx \frac{1}{r^2}+\frac{2R_H}{r^3} \qquad \text{A1.7.}$$

Substituting from (A1.7) into (A1.6) gives:

$$\frac{GM_*(r-R_H)}{r^3} = \frac{GM_*}{r^2} + \frac{2GM_* R_H}{r^3} - \frac{GM_p}{R_H^2} \qquad \text{A1.8,}$$

so:

$$\frac{3M_* R_H}{r^3} = \frac{M_p}{R_H^2} \qquad \text{A1.9,}$$

and hence:

$$R_H = r\left(\frac{M_p}{3M_*}\right)^{1/3} \qquad \text{A1.10.}$$

Over the course of an eccentric planet orbit, r will vary between $a(1 + e)$ at apastron and $a(1 - e)$ at periastron, where a is the orbital semimajor axis and e is its eccentricity, so the Hill radius will vary accordingly. The Mercury program circumvents this variation by letting the Hill radius be dependent on **only** the semimajor axis, a, throughout the orbit. This does have its shortcomings; however, as in reality the Hill radius of a planet will be larger at apastron than at periastron. Despite this, the Hill radius formula within the Mercury Orbital integrator then becomes,

$$R_H = a\left(\frac{M_p}{3M_*}\right)^{1/3} \qquad \text{A1.11}$$

Appendix 2 Derivation of Zero-Velocity Curves from Restricted Three-Body Problem Theory

Zero-velocity curves are imaginary lines around a binary system, such as a star and planet, where the purely pseudo-potential energy of a much smaller particle having zero-velocity in the rotating frame, is the same. Zero-velocity curves of different values can be represented as a three-dimensional zero-velocity surface for any binary system. It should be noted that the shape of zero-velocity curves and surfaces are not dependent on absolute masses and distances but on relative masses and distances. The system mass is defined as $G(M + m) = 1$, where G is the universal gravitational constant, M is the mass of the primary and m is the mass of the secondary. The distance between the primary and secondary bodies is always unity, and the angular velocity, ω, of these bodies about their centre of mass is unity. If these parameters had a value of anything other than unity, the determination of these curves would incorporate the use of many constants and would be considerably (and unnecessarily) more complicated. The derivation of zero-velocity curves here are simplifications of those by Murray and Dermott, 1999.

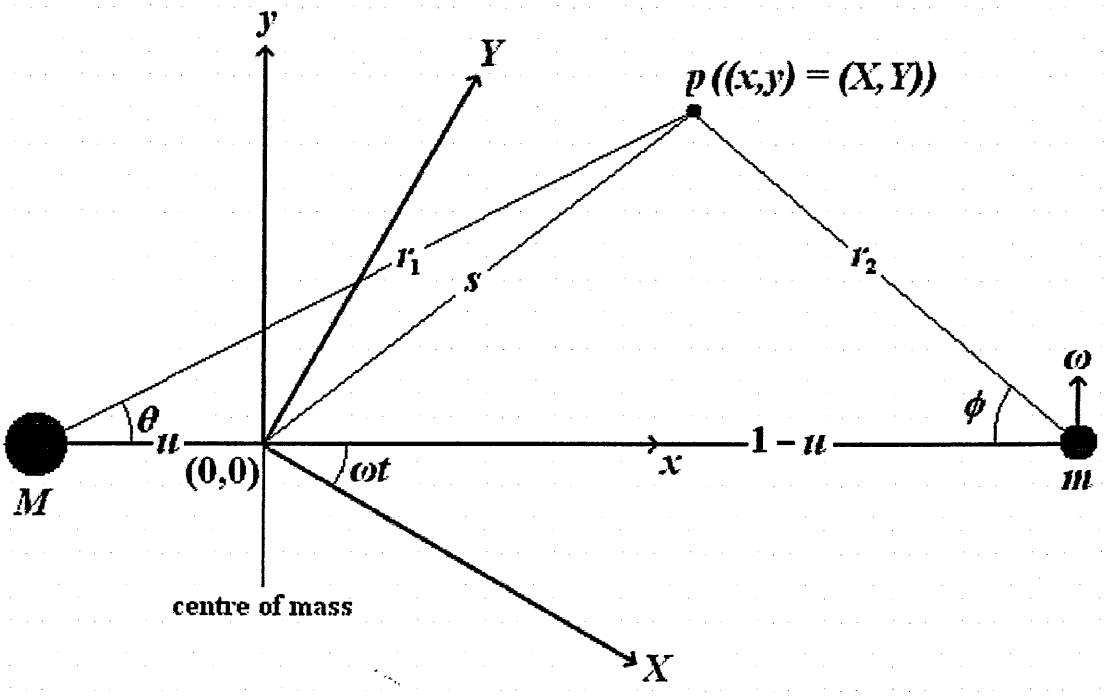

Figure A2.1 The configuration for determining pseudo-gravitational potentials.

Figure A2.1 shows two masses, M and m, $0 < m \leq M$, which are unit distance apart and orbiting their centre of mass, (0,0), with angular velocity, ω. Although ω has already been defined as 1, for now it will be incorporated into equations for clarity of derivations. A third particle, p, is of negligible mass and lies at arbitrary co-ordinates (x,y) in the x-y coordinate system, r_1 from mass M, r_2 from mass m, and s from the centre of gravity. Masses M and m always lie on the x-axis of a reference frame that also rotates with angular velocity, ω. Since the third body, p, is of negligible mass then the mass fraction of the system, u, of the second body, m, is,

$$\frac{m}{M+m} = u \qquad \text{A2.1.}$$

Hence, since $G(M + m) = 1$ by definition, then $Gm = u$, $GM = 1 - u$ and $0 < u < 1$. If the distance of M from the centre of gravity is χ, then the distance of m from the centre of gravity is $1\text{-}\chi$, then by Newton's third law of motion,

$$m(1 - \chi)\omega^2 = M\chi\omega^2 \quad \Rightarrow \quad m(1 - \chi) = M\chi \qquad \text{A2.2.}$$

From equation A2.1, $M/m + 1 = 1/u = (1 - \chi)/\chi + 1$, hence $\chi = u$. Bodies M, m and particle p move in the x-y plane, so any z-components for all three masses are zero, i.e., $z = \dot{z} = \ddot{z} = 0$, where $\dot{z}$ is any velocity component and $\ddot{z}$ is any acceleration component in the z-direction.

Let us commence by considering what the forces would be acting on particle, p, in a non-rotating frame of reference, given by the X-Y coordinates in figure A2.1. Let the x-y coordinate system rotate about the centre of mass, at (0,0), with angular velocity ω and be coincident with the X-Y coordinate system at time $t = 0$, so that after time, t, it has rotated through an angle ωt with respect to the X-Y system. Let θ be the angle between p, M and m and let ϕ be the angle between p, m and M. Since $GM = 1 - u$ and $Gm = u$, then in the X-direction,

$$-\ddot{X} = \frac{(1-u)\cos(\theta+\omega t)}{r_1^2} + \frac{u\cos(\phi-\omega t)}{r_2^2} \qquad \text{A2.3,}$$

and in the Y-direction,

$$-\ddot{Y} = \frac{(1-u)\sin(\theta+\omega t)}{r_1^2} + \frac{u\sin(\phi-\omega t)}{r_2^2} \qquad \text{A2.4.}$$

Note that the acceleration terms are negative. They are positive in the direction *towards* the centre of mass, i.e. in the opposite direction of X and Y. Now $\cos(\theta + \omega t) = (X + u\cos(\omega t))/r_1$, $\sin(\theta + \omega t) = (Y + u\sin(\omega t))/r_1$, $\cos(\phi - \omega t) = (X - (1 - u)\cos(\omega t))/r_2$ and $\sin(\phi - \omega t) = (Y - (1 - u)\sin(\omega t))/r_2$. Hence,

$$-\ddot{X} = \frac{(1-u)(X+u\cos(\omega t))}{r_1^3} + \frac{u(X-(1-u)\cos(\omega t))}{r_2^3} \qquad \text{A2.5,}$$

and,

$$-\ddot{Y} = \frac{(1-u)(Y+u\sin(\omega t))}{r_1^3} + \frac{u(Y-(1-u)\sin(\omega t))}{r_2^3} \qquad \text{A2.6.}$$

From simple geometry, $X = x\cos(\omega t) - y\sin(\omega t)$ and $Y = x\sin(\omega t) + y\cos(\omega t)$. Differentiating with respect to time to find velocities, then,

$$\dot{X} = \cos(\omega t)(\dot{x} - \omega y) - \sin(\omega t)(\dot{y} + \omega x) \qquad \text{A2.7}$$

$$\dot{Y} = \cos(\omega t)(\dot{y} + \omega x) + \sin(\omega t)(\dot{x} - \omega y) \qquad \text{A2.8.}$$

Differentiating again with respect to time to find accelerations,

$$\ddot{X} = \cos(\omega t)(\ddot{x} - 2\omega\dot{y} - \omega^2 x) - \sin(\omega t)(\ddot{y} + 2\omega\dot{x} - \omega^2 y) \qquad \text{A2.9}$$

and,

$$\ddot{Y} = \cos(\omega t)(\ddot{y} + 2\omega\dot{x} - \omega^2 y) + \sin(\omega t)(\ddot{x} - 2\omega\dot{y} - \omega^2 x) \qquad \text{A2.10.}$$

Hence substituting for X and Y in equations A2.5 and A2.6, gives A2.11 and A2.12, where,

$$\cos(\omega t)(\ddot{x} - 2\omega\dot{y} - \omega^2 x) - \sin(\omega t)(\ddot{y} + 2\omega\dot{x} - \omega^2 y) =$$

$$-\frac{(1-u)(x\cos(\omega t) - y\sin(\omega t) + u\cos(\omega t))}{r_1^3} - \frac{u(x\cos(\omega t) - y\sin(\omega t) - (1-u)\cos(\omega t))}{r_2^3} \qquad \text{A2.11}$$

$$\cos(\omega t)(\ddot{y} + 2\omega\dot{x} - \omega^2 y) + \sin(\omega t)(\ddot{x} - 2\omega\dot{y} - \omega^2 x) =$$

$$-\frac{(1-u)(x\sin(\omega t) + y\cos(\omega t) + u\sin(\omega t))}{r_1^3} - \frac{u(x\sin(\omega t) + y\cos(\omega t) - (1-u)\sin(\omega t))}{r_2^3} \qquad \text{A2.12}$$

Multiplying equation A2.11 by $\sin(\omega t)$ and equation A2.12 by $\cos(\omega t)$ and subtracting A2.11 from A2.12 gives,

$$\ddot{y} + 2\omega\dot{x} - \omega^2 y = -\frac{(1-u)y}{r_1^3} - \frac{uy}{r_2^3} \qquad \text{A2.13,}$$

Multiplying equation A2.11 by $\cos(\omega t)$ and equation A2.12 by $\sin(\omega t)$ and adding gives,

$$\ddot{x} - 2\omega\dot{y} - \omega^2 x = -\frac{(1-u)(x+u)}{r_1^3} - \frac{u(x-1+u)}{r_2^3} \qquad \text{A2.14.}$$

The two "ω^2" terms in equations A2.13 and A2.14 are the accelerations due to the centrifugal force on particle, p, whether it is stationary or moving with respect to the rotating frame. The two "ω" terms are Corioli's forces, which act only on a moving particle with respect to a rotating frame. Here, the angular velocity of the rotating reference frame is, by definition, unity so $\omega = 1$. Now from Pythagoras theorem,

$$r_1 = \sqrt{(x+u)^2 + y^2} \qquad \text{A2.15,}$$

and $$r_2 = \sqrt{(x-1+u)^2 + y^2} \qquad \text{A2.16.}$$

Hence substituting from equations A2.15 and A2.16 into equations A2.13 and A2.14,

$$\ddot{y} + 2\dot{x} - y = -\frac{(1-u)y}{((x+u)^2 + y^2)^{3/2}} - \frac{uy}{((x-1+u)^2 + y^2)^{3/2}} \qquad \text{A2.17,}$$

and $$\ddot{x} - 2\dot{y} - x = -\frac{(1-u)(x+u)}{((x+u)^2 + y^2)^{3/2}} - \frac{u(x-1+u)}{((x-1+u)^2 + y^2)^{3/2}} \qquad \text{A2.18.}$$

Now $$\frac{\partial}{\partial x}\left(\frac{1}{r_1}\right) = \frac{\partial}{\partial x}\left(\frac{1}{((x+u)^2 + y^2)^{1/2}}\right) = -\frac{x+u}{((x+u)^2 + y^2)^{3/2}} \qquad \text{A2.19,}$$

$$\frac{\partial}{\partial x}\left(\frac{1}{r_2}\right) = \frac{\partial}{\partial x}\left(\frac{1}{((x-1+u)^2 + y^2)^{1/2}}\right) = -\frac{x-1+u}{((x-1+u)^2 + y^2)^{3/2}} \qquad \text{A2.20,}$$

$$\frac{\partial}{\partial y}\left(\frac{1}{r_1}\right) = \frac{\partial}{\partial y}\left(\frac{1}{((x+u)^2 + y^2)^{1/2}}\right) = -\frac{y}{((x+u)^2 + y^2)^{3/2}} \qquad \text{A2.21,}$$

and $$\frac{\partial}{\partial y}\left(\frac{1}{r_2}\right) = \frac{\partial}{\partial y}\left(\frac{1}{((x-1+u)^2 + y^2)^{1/2}}\right) = -\frac{y}{((x-1+u)^2 + y^2)^{3/2}} \qquad \text{A2.22.}$$

Substituting equations A2.19 and A2.20 into equation A2.18 gives,

$$\ddot{x} - 2\dot{y} = x + (1-u)\frac{\partial}{\partial x}\left(\frac{1}{r_1}\right) + u\frac{\partial}{\partial x}\left(\frac{1}{r_2}\right) \qquad \text{A2.23,}$$

and substituting equations A2.21 and A2.22 into equation A2.17 gives,

$$\ddot{y} + 2\dot{x} = y + (1-u)\frac{\partial}{\partial y}\left(\frac{1}{r_1}\right) + u\frac{\partial}{\partial y}\left(\frac{1}{r_2}\right) \qquad \text{A2.24.}$$

The potential term, U, is now introduced, where,

$$\frac{\partial U}{\partial x} = \ddot{x} - 2\dot{y} \qquad \text{A2.25,}$$

and $$\frac{\partial U}{\partial y} = \ddot{y} + 2\dot{x} \qquad \text{A2.26,}$$

Hence $$U = \frac{x^2}{2} + \frac{y^2}{2} + \frac{(1-u)}{r_1} + \frac{u}{r_2} + k \qquad \text{A2.27,}$$

where k is a constant of integration. Multiplying equation A2.25 by $\dot{x}$, multiplying equation A2.26 by $\dot{y}$ and adding the two new equations gives,

$$\frac{\partial U}{\partial x}\dot{x} + \frac{\partial U}{\partial y}\dot{y} = \ddot{x}\dot{x} + \ddot{y}\dot{y} = \frac{dU}{dt} \qquad \text{A2.28.}$$

This equation can be integrated with respect to time giving,

$$U = \frac{\dot{x}^2}{2} + \frac{\dot{y}^2}{2} + \frac{C_J}{2} \qquad \text{A2.29,}$$

where C_J is another constant of integration, which incorporates k, and is referred to as the Jacobian constant. As there is no motion in the z-direction, $\dot{x}^2 + \dot{y}^2 = v^2$, then equation A2.29 becomes,

$$v^2 = 2U - C_J \qquad \text{A2.30,}$$

or from equations A2.15, A2.16 and A2.27,

$$C_J = x^2 + y^2 + 2\frac{(1-u)}{\sqrt{(x+u)^2 + y^2}} + 2\frac{u}{\sqrt{(x-1+u)^2 + y^2}} - v^2 \qquad \text{A2.31.}$$

The Jacobian constant, C_J, is an energy term consisting of a kinetic component given by v^2 (or $\dot{x}^2 + \dot{y}^2$) and a potential component given by the other four terms. If a particle has no velocity in the rotating frame at a series of distances from masses M and m, then the Jacobian constant will give its potential energy at "zero-velocity". These pseudo-potentials (since the reference frame is rotating) will trace out distinctive curves around M and m, for different values of C_J, known as zero-velocity curves, of which the shape of each can be determined by,

$$C_J = x^2 + y^2 + 2\frac{(1-u)}{\sqrt{(x+u)^2 + y^2}} + 2\frac{u}{\sqrt{(x-1+u)^2 + y^2}} \qquad \text{A2.32.}$$

On inspection, if $C_J = 0$, the equation is insoluble for real roots only, both in x for any given value of y and in y for any given value of x. Hence C_J can never be zero for real values of x and y, and since x^2 and y^2 are always positive, then C_J is always positive. When $y = 0$ and $x = -u$, i.e. at the position of the primary body, or $y = 0$ and $x = 1 - u$, i.e. at the position of the secondary body, then C_J will have an infinite value. Also as x and/or y approach infinity, C_J will approach infinity.

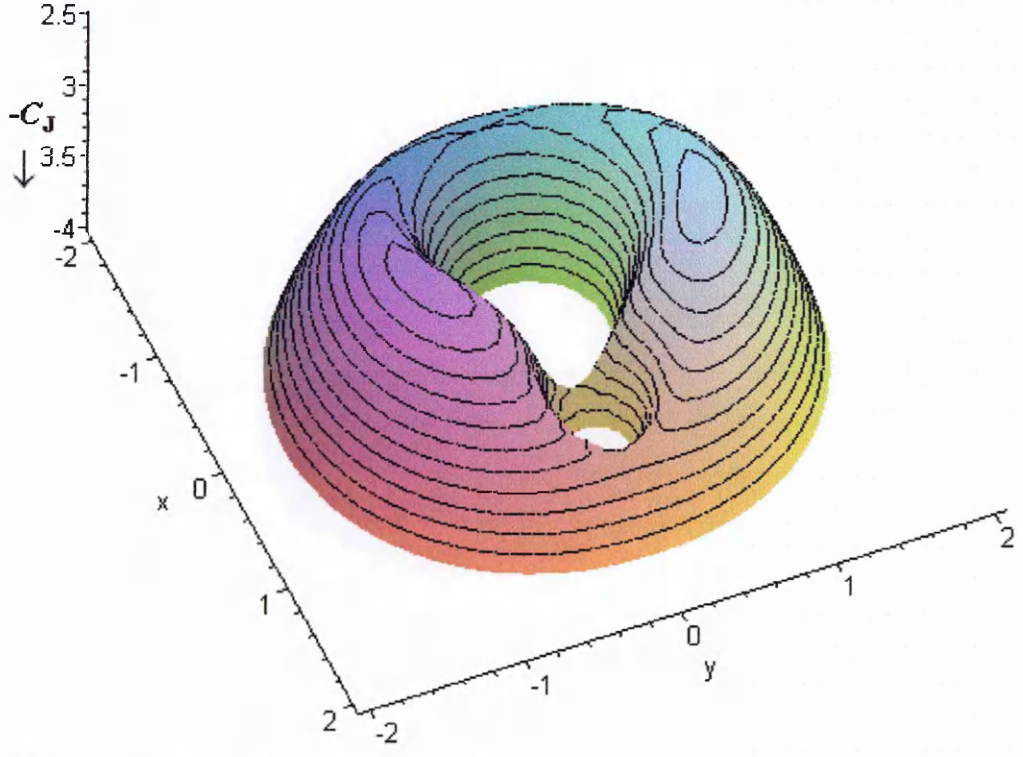

Figure A2.2 Zero-velocity surface for a binary system where $u = 0.2$.

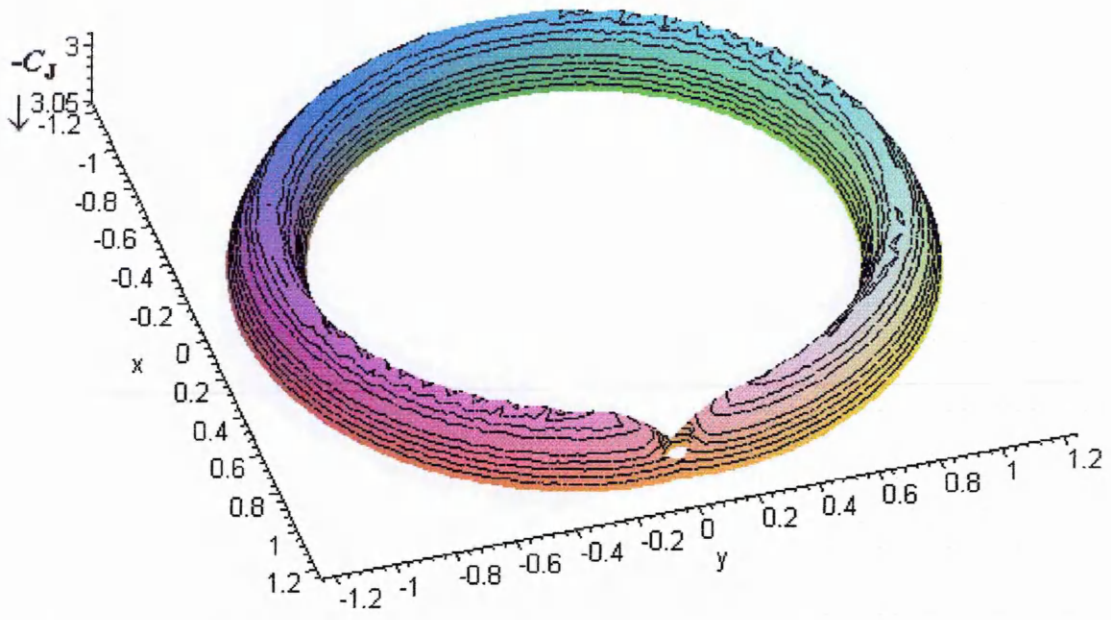

Figure A2.3 Zero-velocity surface for a binary system where $u = 0.001$.

Equation A2.32 can be used to generate a series of zero-velocity curves with different C_J values, known as a zero-velocity surface. This was initially achieved using the program Maple V Release 5 (Waterloo Maple Inc. November 27th 1997). Figures A2.2 and A2.3 show two zero-velocity surfaces, where Figure A2.2 would more likely represent a binary star. The larger hole is the potential "well" of the primary, the smaller hole that of the secondary. Figure A2.3 would more likely represent a star-planet system and the potential well of the planet is much smaller than that of the central star. Note that the z-axis depicts "$-C_J$" in both of these representations, as this gives better depictions of gravity "wells"; otherwise they would appear upside down. By taking slices through different values of the Jacobian constant for this system in figure A2.3, a series of zero-velocity curves can be plotted, shown in figure A2.4. This again shows the large potential well of the star centred on x,y co-ordinates (-0.001,0) and the much smaller well of the planet at (0.999,0). For particles with zero-velocities within the smallest circle surrounding the planet, then these bodies would be bound to orbit the planet only and could never orbit the star, provided there was no energy exchange with the star or planet. A zero-velocity curve of particular interest is that which has a Jacobian constant between the values of the L_1 point and the L_2 point. This is enlarged in figure A2.5 to show its shape around the planet. Zero-velocity curves within the "mouth" of this curve would circle the planet, whilst zero-velocity curves outside the "mouth" but bounded be the two lines would form a "horseshoe" shaped curve, which goes around the other side of the star, one of which is shown in figure A2.6. The thin lines within the horseshoe curve in figure A2.4 are zero-velocity curves very close to the L_4 and L_5 points (see Figure A2.7).

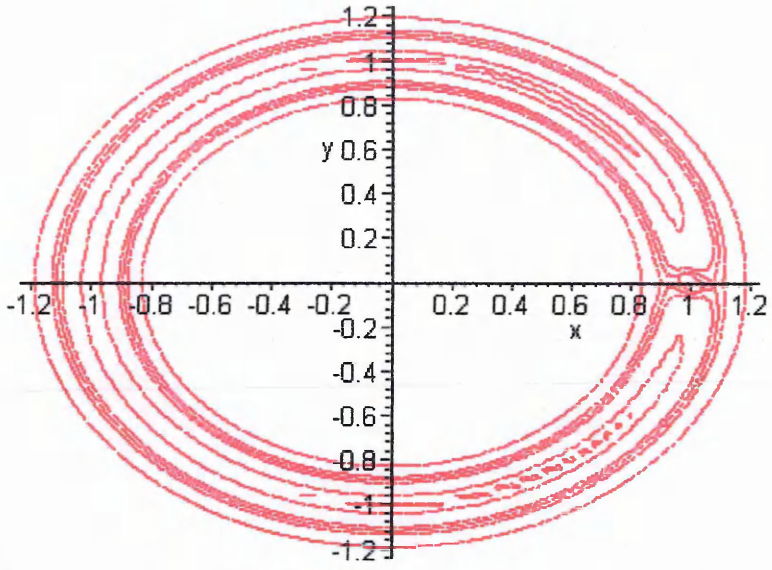

Figure A2.4 Zero-velocity curves for different Jacobian constants where $u = 0.001$.

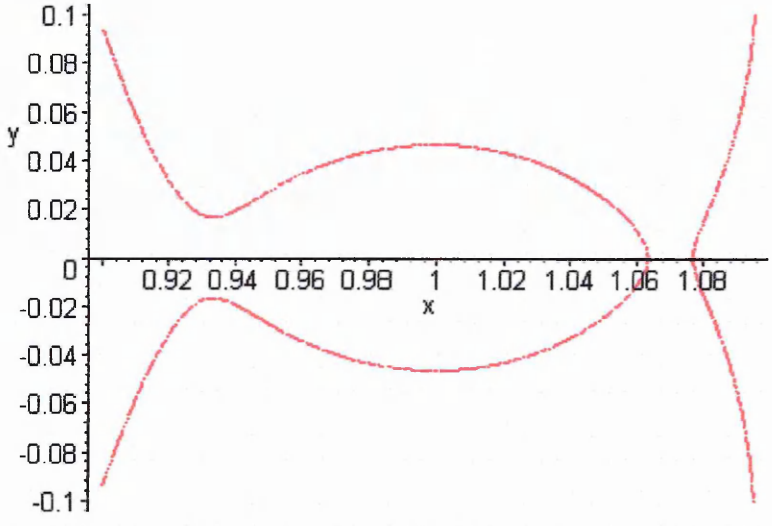

Figure A2.5 Magnified view of the zero-velocity curve of $C_J = 3.039$,

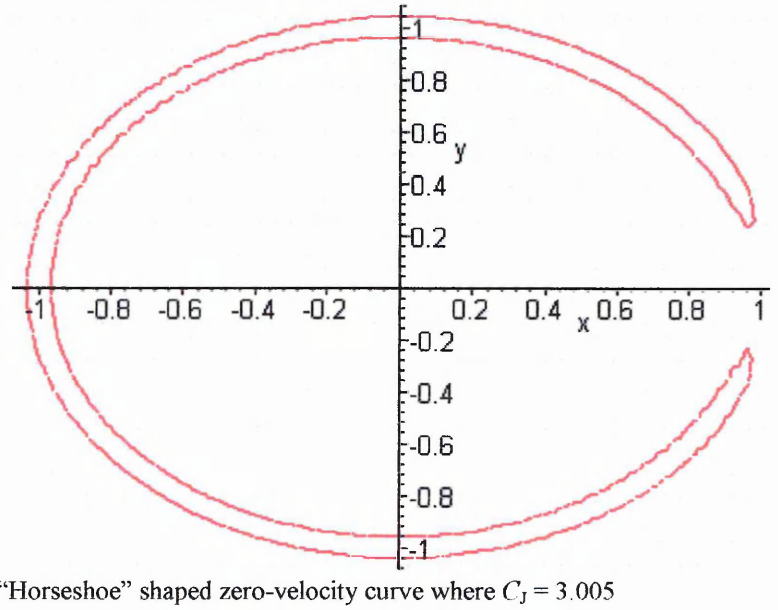

Figure A2.6 "Horseshoe" shaped zero-velocity curve where $C_J = 3.005$

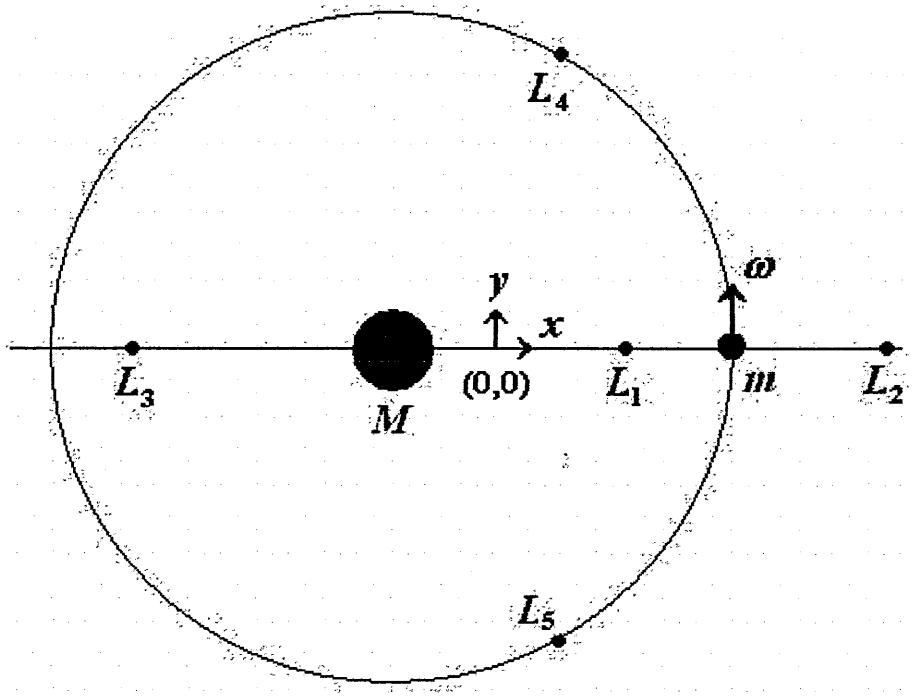

Figure A2.7 Locations of the Lagrangian equilibrium points.

The horizontal sections of zero-velocity surfaces show the shapes of zero-velocity curves for differing values of the Jacobian constant, C_J. Also of interest are vertical sections of zero-velocity surfaces, particularly the vertical section where $y = 0$, i.e. along the x-axis, which passes through the two major bodies and the Lagrangian points L_1, L_2 and L_3, the positions of which are shown in figure A2.7, along with the L_4 and L_5 points. The Lagrangian points within a system are where particles at these locations will be in a 1:1 resonance with the two major bodies as they orbit the centre of mass. The L_1, L_2 and L_3 positions are all unstable, the L_4 and L_5 positions are unstable but become stable when $u \leq \frac{9-\sqrt{69}}{18} \approx 0.03852$ (Murray and Dermott, 1999, page 93).

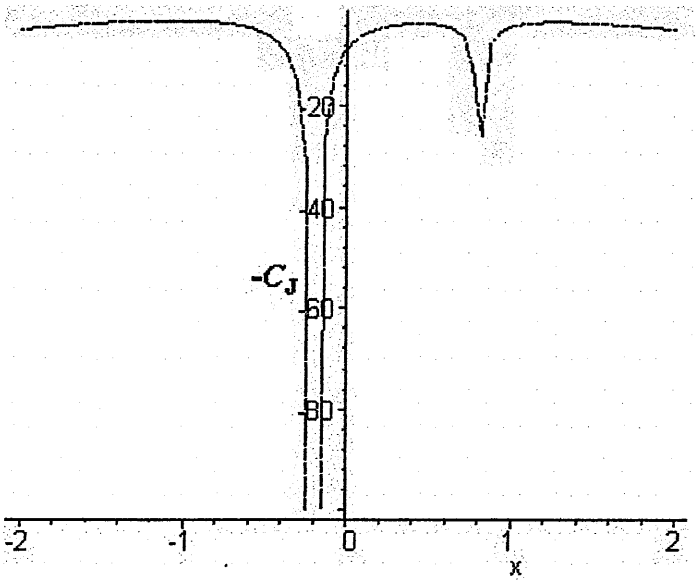

Figure A2.8 Profile of Jacobian constants through the x-axis for $u = 0.2$.

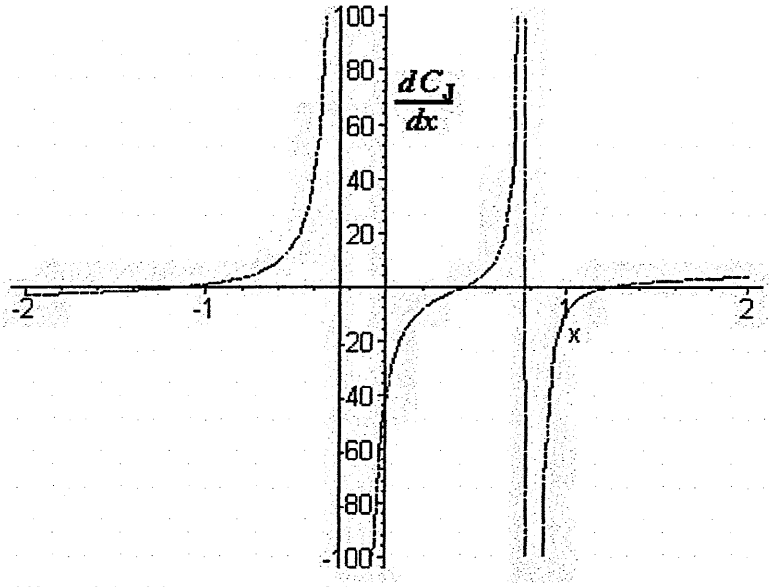

Figure A2.9 Differential with respect to x of the figure A2.8 profile.

A profile of Jacobian constants along the x-axis is seen in figure A2.8, again obtained using Maple V Release 5 (Waterloo Maple Inc. November 27th 1997). This profile shows the variation of $-C_J$ with x for $u = 0.2$, again $-C_J$ is used to better depict gravitational potential wells. The profile clearly shows the positions of the two major masses at $x = -0.2$ and $x = 0.8$. The positions along the x-axis where $dC_J/dx = 0$ are the locations of the Lagrangian points, seen most easily by plotting dC_J/dx against x, as in figure A2.9. The solutions for the positions of the Lagrangian points along the x-axis when $u = 0.2$, according to the Maple V program, are $L_1 = 0.438$, $L_2 = 1.271$ and $L_3 = -1.083$. These x-coordinates give Jacobian constants at these positions of 3.805, 3.552 and 3.197 for L_1, L_2 and L_3 respectively, which agree with those values for the exact same example in Murray and Dermott (1999). Also the slope of dC_J/dx versus x (or d^2C_J/dx^2) is positive at all three Lagrangian points revealing that they are all unstable. In theory the depths of each potential well in figure A2.8 should be infinite, the reason the secondary body peaks at approximately $C_J = 27$ is due to the plot resolution being too coarse. However, extensive computing power would be required to increase the resolution, which is not required here as the diagram already serves its purpose by showing the nature of the profile.

The profile in figure A2.8 is easily obtained by substituting y = 0 into equation A2.32 and determining C_J for varying x. When this is so, the profile equation becomes,

$$C_J = x^2 \pm \frac{2(1-u)}{(x-u)} \pm \frac{2u}{(x-1+u)} \qquad \text{A2.33.}$$

The two quotient terms can be positive or negative as they are the square roots of squared terms (simplified here). The differential with respect to x of equation A2.33 is given by,

$$\frac{dC_J}{dx} = 2x \mp \frac{2(1-u)}{(x-u)^2} \mp \frac{2u}{(x-1+u)^2} \qquad \text{A2.34.}$$

The Maple V program automatically assigns the correct symbol to the ± terms by the use of the "csgn" function, where,

$$\text{csgn}(x) = 1 \text{ if } \text{Re}(x) > 0 \text{ or } \text{Re}(x) = 0 \text{ and } \text{Im}(x) > 0 \qquad \text{A2.35a}$$

$$\text{csgn}(x) = -1 \text{ if } \text{Re}(x) < 0 \text{ or } \text{Re}(x) = 0 \text{ and } \text{Im}(x) < 0 \qquad \text{A2.35b}$$

The appropriate value of csgn((1-u)/(x-u)) and csgn(u/(x-1+u)) needs to be found in order to proceed with calculating correct values of C_J. The four figures, A2.10a to A2.10d, show each of the possible profiles for the different combinations of csgn() values assigned to equation A2.33. Unfortunately, none of the four profiles match that in Figure A2.9. To analyse these four curves further, they need to be differentiated, the graphic representations of which are shown in figures A2.11a to A2.11d.

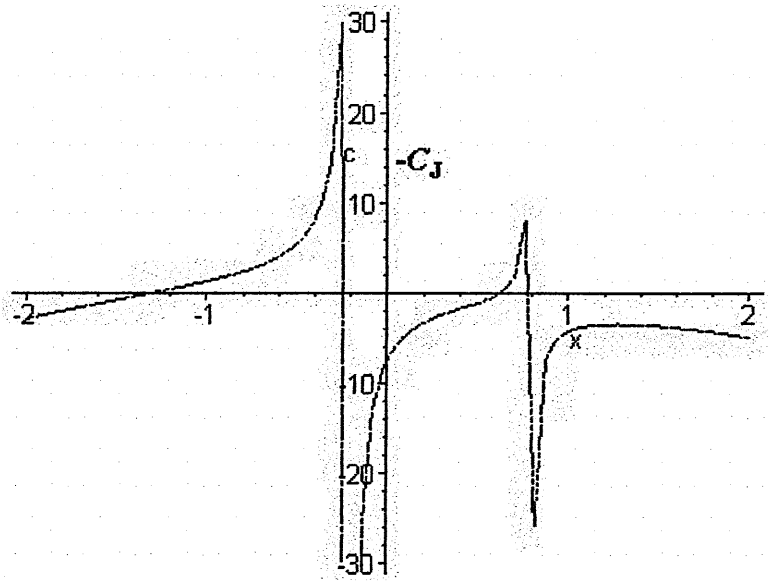

Figure A2.10a Profile of the Jacobian constant along the x-axis where csgn((1-u)/(x-u) = 1 and csgn(u/(x-1+u)) = 1.

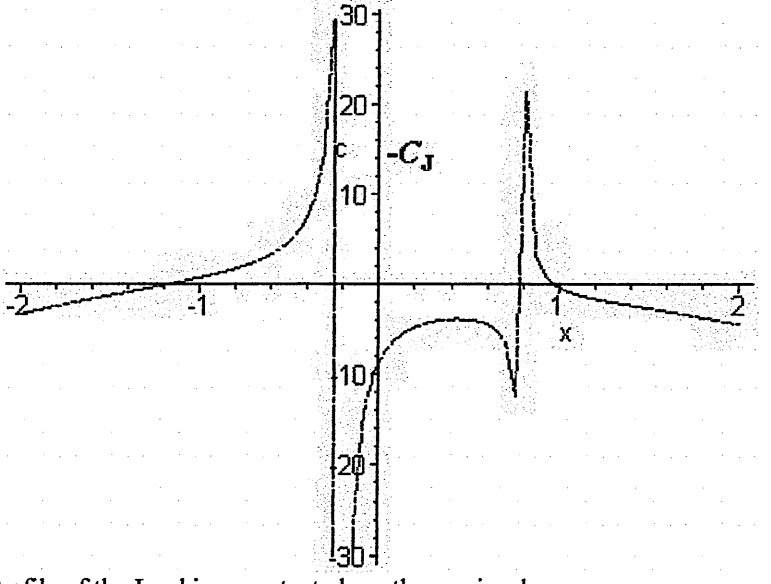

Figure A2.10b Profile of the Jacobian constant along the x-axis where csgn((1-u)/(x-u) = 1 and csgn(u/(x-1+u)) = -1.

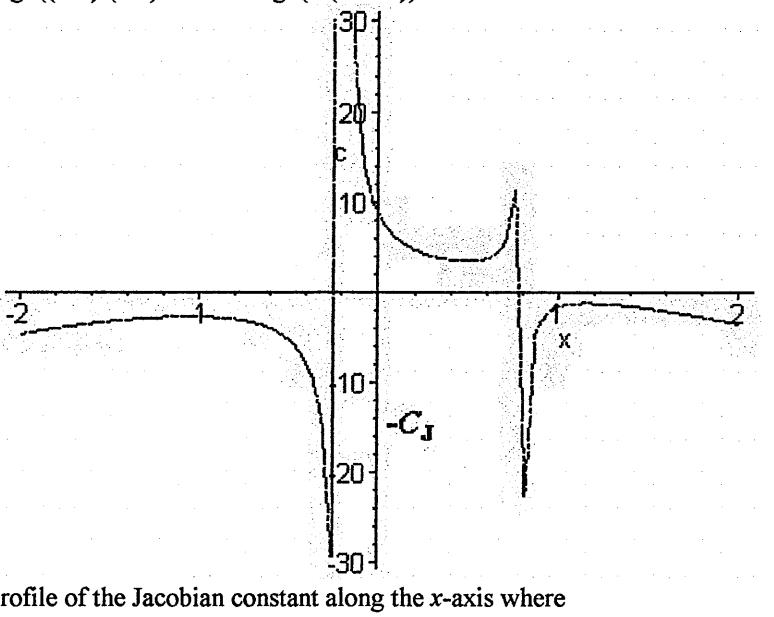

Figure A2.10c Profile of the Jacobian constant along the x-axis where csgn((1-u)/(x-u) = -1 and csgn(u/(x-1+u)) = 1.

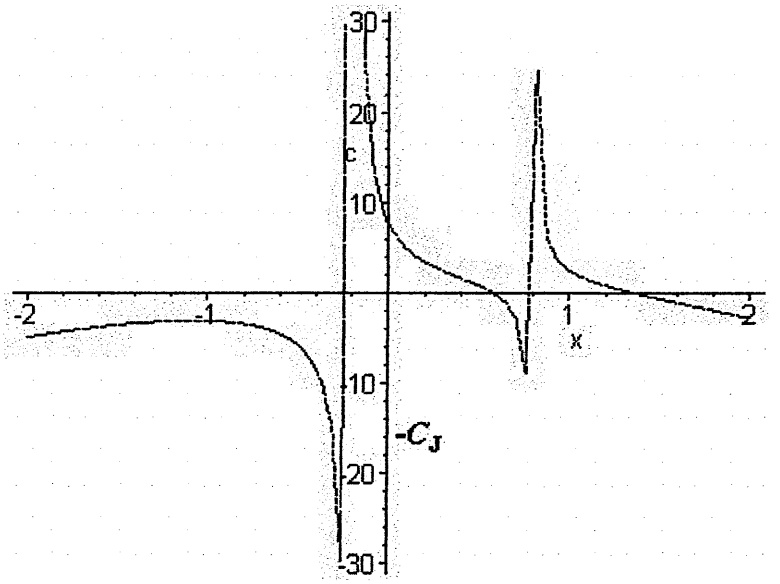

Figure A2.10d Profile of the Jacobian constant along the x-axis where csgn((1-u)/(x-u) = -1 and csgn(u/(x-1+u)) = -1.

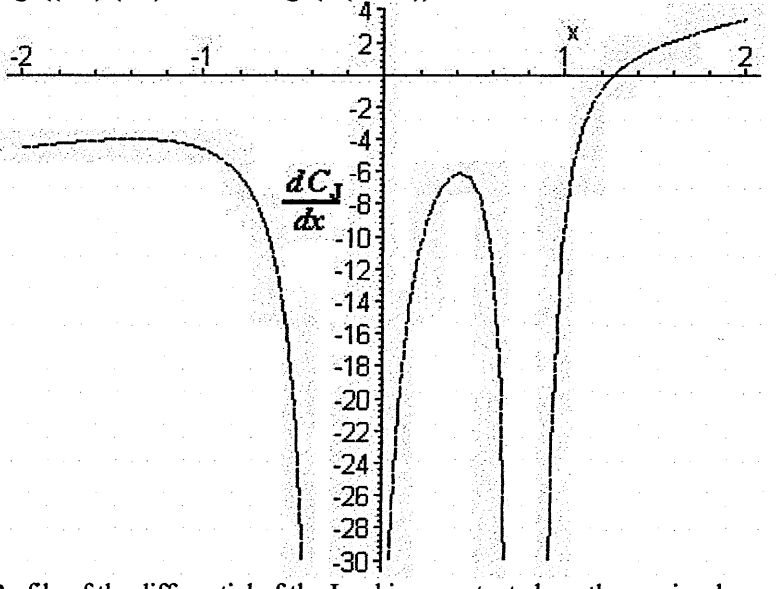

Figure A211a Profile of the differential of the Jacobian constant along the x-axis where csgn((1-u)/(x-u)^2) = -1 and csgn(u/(x-1+u)^2) = -1.

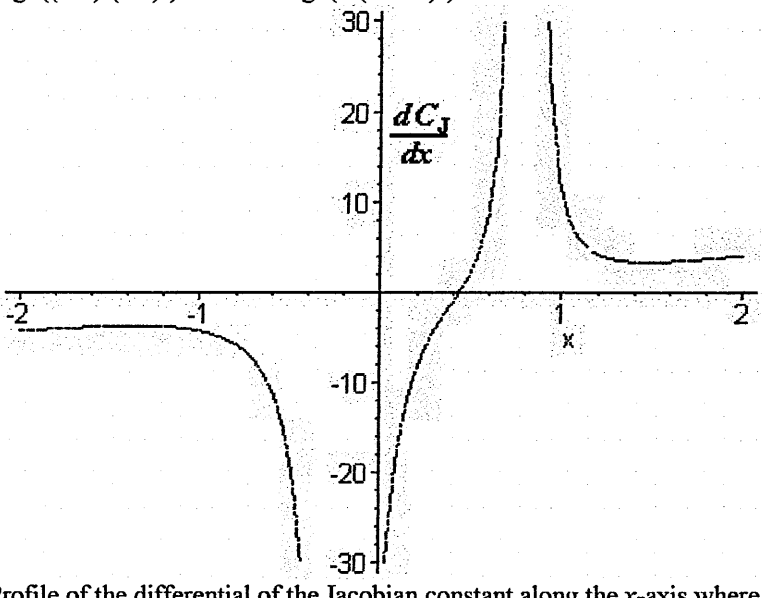

Figure A2.11b Profile of the differential of the Jacobian constant along the x-axis where csgn((1-u)/(x-u)^2) = -1 and csgn(u/(x-1+u)^2) = 1.

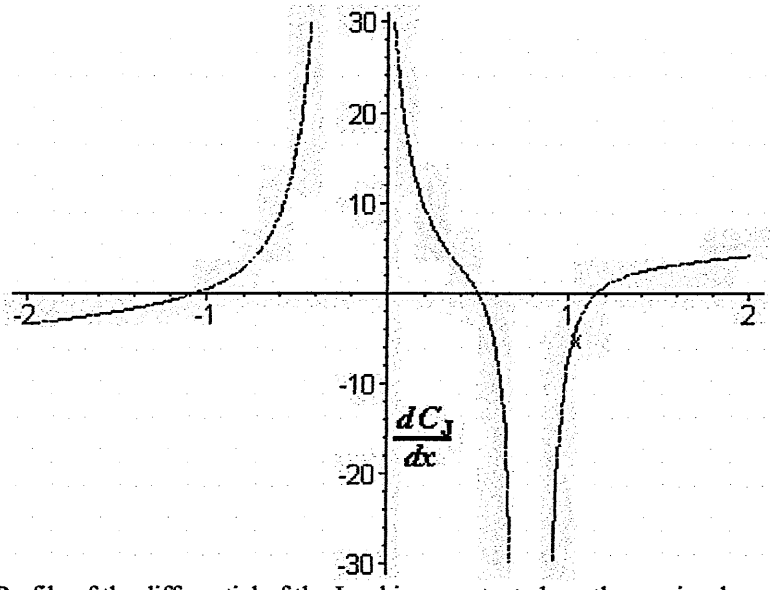

Figure A2.11c Profile of the differential of the Jacobian constant along the x-axis where $\text{csgn}((1-u)/(x-u)^2) = 1$ and $\text{csgn}(u/(x-1+u)^2) = -1$.

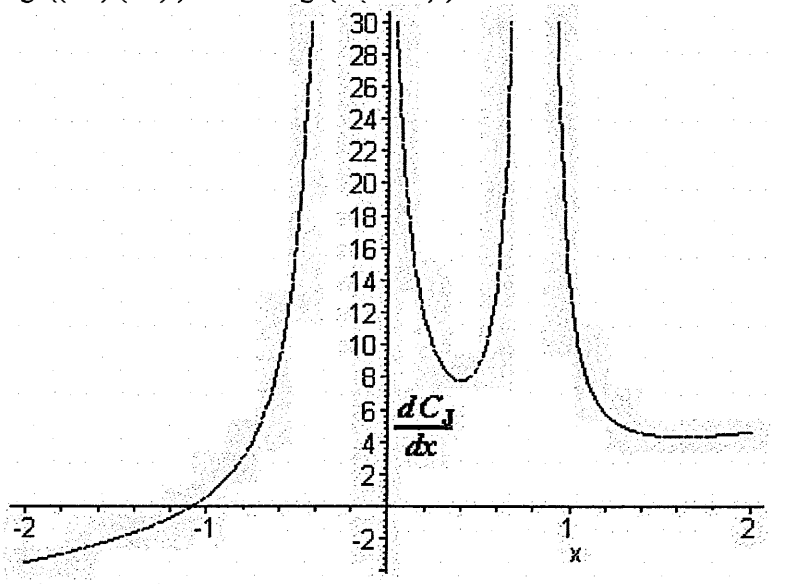

Figure A2.11d Profile of the differential of the Jacobian constant along the x-axis where $\text{csgn}((1-u)/(x-u)^2) = 1$ and $\text{csgn}(u/(x-1+u)^2) = 1$.

Notice that in figures A2.11a to A2.11d, the csgn() values are opposite to the values in the corresponding curves in figures A2.10a to A2.10d due to the differentiation of a reciprocal term. According to the Maple V program, when $dC_J/dx = 0$ in equation A2.34, the four combinations of csgn() values give real solutions of x in each case. These can be seen where the dC_J/dx versus x curve crosses the x-axis once each in figures A2.11a, A2.11b and A2.11d, where the positive slope of each of these curves, or d^2C_J/dx^2, indicates that they are unstable. The points on the x-axis where $dC_J/dx = 0$ in figures A2.11a, A2.11b and A2.11d correspond to the L_2, L_1 and L_3 points respectively in figures A2.8 and A2.9. So the appropriate value of csgn(), or the correct use of sign, in equation A2.34, will lead to the correct positions of L_1, L_2 and L_3. The csgn() values used in figures A2.10c and A2.11c give three real values where $dC_J/dx = 0$. However one value of d^2C_J/dx^2 indicates a stable "L_1" point, which is incorrect. Hence these results are discarded.

Appendix 3 Derivation of a Second Hill Radius Formula

A second Hill radius formula can be derived from equation A2.18, which occurs during the derivation of equation 6.3 in Appendix 2,

$$\ddot{x}-2\dot{y}-x=-\frac{(1-u)(x+u)}{((x+u)^2+y^2)^{3/2}}-\frac{u(x-1+u)}{((x-1+u)^2+y^2)^{3/2}} \qquad \text{A3.1.}$$

If u is assumed to be small with respect to unity, then,

$$\ddot{x}-2\dot{y}-x=-\frac{x}{(x^2+y^2)^{3/2}}-\frac{u(x-1)}{((x-1)^2+y^2)^{3/2}} \qquad \text{A3.2,}$$

The x-axis is now transformed to $x + 1$, with no changes in the y-axis, so that,

$$\ddot{x}-2\dot{y}-x-1=-\frac{x+1}{((x+1)^2+y^2)^{3/2}}-\frac{ux}{(x^2+y^2)^{3/2}} \qquad \text{A3.3,}$$

The coordinate system has now been re-centred closer to the secondary body, so we assume x and y are small, hence, using a binomial expansion in equation A3.4,

$$\ddot{x}-2\dot{y}=1-\frac{1}{(1+2x)^{3/2}}-\frac{ux}{(x^2+y^2)^{3/2}}\approx 3x-\frac{ux}{(x^2+y^2)^{3/2}} \qquad \text{A3.4.}$$

Letting equation A3.4 equal a modified potential U_H and for $\sqrt{x^2+y^2}=R_H$, the Hill radius around the smaller body, then

$$\frac{\partial U_H}{\partial x}=\left(3-\frac{u}{R_H^3}\right) \qquad \text{A3.5.}$$

Hence when the gradient of this potential, U_H, is zero, i.e. when the attracting forces of the primary and secondary masses are equal, then,

$$R_H=\left(\frac{u}{3}\right)^{1/3} \qquad \text{A3.6.}$$

Remember that here the distance between the two bodies is unity, so if the real distance, a, is known, then R_H will scale with this so that finally,

$$R_H=a\left(\frac{u}{3}\right)^{1/3} \qquad \text{A3.7.}$$

Appendix 4 Computer Programs written in 'C' to determine Zero-Velocity Surfaces and Zero-Velocity Curves

Program A4.1 – The Determination of Zero-Velocity Surfaces.

zvcurves.c

```
#include <stdio.h>
#include <stdlib.h>
#include <math.h>

#define pi 3.14159265358979323846264338327950288419716939937510
#define ITSTEP 100

/* xx = abscissa */
/* y = ordinate */
/* c = Jacobian constant */
/* u = second body's mass fraction of the system */
/* p = second body's mass (in Jupiters) */
/* m = primary body's mass (in solar masses) */
/* a = distance between the bodies (in AU) */
/* dx = resolution of 3-D plot */

int main()
{
  double x[ITSTEP], w[ITSTEP], v[ITSTEP];
  float p, m, a, u, dx, xx, y, c, d, e, f, L1, L2, L3, LP;
  int i, j, k, l, n;
  FILE *fh;

  /* Primary body's mass (in solar masses), m. */
  printf("Enter the primary body's mass (in solar masses): ");
  scanf("%f", &m);
  if ( m <= 0 ) {
    printf("The primary's mass must be greater than zero.\n");
    exit(EXIT_FAILURE);
  }

  /* Second body's mass (in Jupiters), p. */
  printf("Enter the second body's mass (in Jupiters): ");
  scanf("%f", &p);
  if ( ( p <= 0 ) || ( p > 1047.672 * m ) ) {
    printf("The secondary's mass must be greater than zero and less than
half the system's.\n");
    exit(EXIT_FAILURE);
  }

  /* Distance between the two bodies (in AU), a. */
  printf("Enter the distance between the two bodies (in AU): ");
  scanf("%f", &a);
  if ( a <= 0 ) {
    printf("The distance must be greater than zero.\n");
    exit(EXIT_FAILURE);
  }

  /* Calculate the secondary's mass fraction of the system. */
  u = p * ( 1.8986 / 1989.11 ) / ( m + p * 1.8986 / 1989.11 );
  printf("The mass fraction of the secondary, u, of the system is %e\n",
u);

  /* Determine the distance of L1, L2 and L3 from the system's centre of
mass. */
  LP = a*(powf((u/3),0.3333333333));
```

```
  L1 = a*(1-u)-LP;
  L2 = a*(1-u)+LP;
  L3 = -a*(u+1);
  printf("The distance of the Hill radius from the planet is %f AU.\n",
LP);
  printf("The planet's inner Hill radius from the system's centre of mass
is %f AU.\n", L1);
  printf("The planet's outer Hill radius from the system's centre of mass
is %f AU.\n", L2);
  printf("The planet's opposition point from the system's centre of mass
is %f AU.\n", L3);
  printf("These distances start the iterations to find the L1, L2 and L3
x-coordinates.\n");

  /* Perform Iteration to find L1, L2 and L3 */
  k=0;
  x[0]=1-u-(LP/a);
  while ( k < ITSTEP ) {
    x[k+1]=x[k]-(x[k]-(1-u)/((x[k]+u)*(x[k]+u))+u/((x[k]-1+u)*(x[k]-
1+u)))/(1+2*(1-u)/powf((x[k]+u),3)-2*u/powf((x[k]-1+u),3));
    k = k + 1;
  }
  printf("The distance of the L1 point from the system's centre of mass
is %f AU.\n", a*x[ITSTEP]);
  d=-(2*(1-u)/(x[ITSTEP]+u)-2*u/(x[ITSTEP]-1+u)+(x[ITSTEP]*x[ITSTEP]));
  l=0;
  w[0]=1-u+(LP/a);
  while ( l < ITSTEP ) {
    w[l+1]=w[l]-(w[l]-(1-u)/((w[l]+u)*(w[l]+u))-u/((w[l]-1+u)*(w[l]-
1+u)))/(1+2*(1-u)/powf((w[l]+u),3)+2*u/powf((w[l]-1+u),3));
    l = l + 1;
  }
  printf("The distance of the L2 point from the system's centre of mass
is %f AU.\n", a*w[ITSTEP]);
  e=-(2*(1-u)/(w[ITSTEP]+u)+2*u/(w[ITSTEP]-1+u)+(w[ITSTEP]*w[ITSTEP]));
  n=0;
  v[0]=-1-u;
  while ( n < ITSTEP ) {
    v[n+1]=v[n]-(v[n]+(1-u)/((v[n]+u)*(v[n]+u))+u/((v[n]-1+u)*(v[n]-
1+u)))/(1-2*(1-u)/powf((v[n]+u),3)-2*u/powf((v[n]-1+u),3));
    n = n + 1;
  }
  printf("The distance of the L3 point from the system's centre of mass
is %f AU.\n", a*v[ITSTEP]);
  f=-(-2*(1-u)/(v[ITSTEP]+u)-2*u/(v[ITSTEP]-1+u)+(v[ITSTEP]*v[ITSTEP]));
  printf("The Jacobian Constants are %f at L1, %f at L2 and %f at L3.\n",
-d, -e, -f);

  /* Determine the plot resolution. */
  printf("Enter the number of plotted points between the two bodies (10
to 100)\n");
  printf("(This will fit on an Excel plot only if the number is 15 or
less): ");
  scanf("%f", &dx);
  if ( ( dx < 10 ) || ( dx > 100 ) ) {
    printf("The x-axis intervals must be between the stated options
inclusively.\n");
    exit(EXIT_FAILURE);
  }

  /* Open the data file. */
  fh = fopen("zvcurves.dat", "w");
  if ( fh == NULL ) {
    printf("Cannot open the signal data file.\n");
    exit(EXIT_FAILURE);
```

```
  }

  /* Make headers for output file. */
  fprintf(fh, "  x-value\t");
  fprintf(fh, "  y-value\t");
  fprintf(fh, "Jacobian Constant\n");
  fprintf(fh, "\n");

  /* Calculate the zero velocity curves. */
  for ( i = 0 ; i < 1 + 4*dx ; i = i + 1 ) {
    xx = -2+i/dx;
    for ( j = 0 ; j < 1 + 4*dx ; j = j + 1 ) {
      y = -2+j/dx;
      c=-((2*(1-u)/(sqrt((xx+u)*(xx+u)+y*y)))+(2*u/(sqrt((xx-1+u)*(xx-
1+u)+y*y)))+(xx*xx)+(y*y));
      fprintf(fh, "%f\t", a*xx);
      fprintf(fh, "%f\t", a*y);
      fprintf(fh, "%f\n", c);
    }
  }

  /* Close the file and program. */
  fclose(fh);
  printf("The program completed successfully.\n");
  printf("The output is stored in the file 'zvcurves.dat'.\n");
  printf("Now please change the name of 'zvcurves.dat' or it will be
overwritten.\n");
  printf("To find zero-velocity curves for particular Jacobian Constants,
type '2dcurves'.\n");
}
```

Program A4.2 – The Determination of Zero-Velocity Curves

2dcurves.c

```
#include <stdio.h>
#include <stdlib.h>
#include <math.h>

#define pi 3.14159265358979323846264338327950288419716939937751
#define ITSTEP 100

/* xx = abscissa */
/* y = ordinate */
/* c and cc = Jacobian constant */
/* u = second body's mass fraction of the system */
/* p = second body's mass (in Jupiters) */
/* m = primary body's mass (in solar masses) */
/* a = distance between the bodies (in AU) */
/* dx = resolution of 2-D plot */

int main()
{
  double x[ITSTEP], w[ITSTEP], v[ITSTEP], b;
  float p, m, a, u, dx, xx, y, c, cc, d, e, f, L1, L2, L3, LP;
  int i, j, k, l, n, s;
  FILE *fh;

  /* Primary body's mass (in solar masses), m. */
  printf("Enter the primary body's mass (in solar masses): ");
  scanf("%f", &m);
  if ( m <= 0 ) {
    printf("The primary's mass must be greater than zero.\n");
```

```
    exit(EXIT_FAILURE);
  }

  /* Second body's mass (in Jupiters), p. */
  printf("Enter the second body's mass (in Jupiters): ");
  scanf("%f", &p);
  if ( ( p <= 0 ) || ( p > 1047.672 * m ) ) {
    printf("The secondary's mass must be greater than zero and less than
half the system's.\n");
    exit(EXIT_FAILURE);
  }

  /* Distance between the two bodies (in AU), a. */
  printf("Enter the distance between the two bodies (in AU): ");
  scanf("%f", &a);
  if ( a <= 0 ) {
    printf("The distance must be greater than zero.\n");
    exit(EXIT_FAILURE);
  }

  /* Jacobian constant value, c. */
  printf("Enter the value of the Jacobian constant: ");
  scanf("%f", &c);
  if ( c < 3 ) {
    printf("This value will give an empty data-set.\n");
    exit(EXIT_FAILURE);
  }

  /* Calculate the secondary's mass fraction of the system. */
  u = p * ( 1.8986 / 1989.11 ) / ( m + p * 1.8986 / 1989.11 );
  printf("The mass fraction of the secondary, u, of the system is %e\n",
u);

  /* Determine the distance of L1, L2 and L3 from the system's centre of
mass. */
  LP = a*(powf((u/3),0.3333333333));
  L1 = a*(1-u)-LP;
  L2 = a*(1-u)+LP;
  L3 = -a*(u+1);
  printf("The distance of the Hill radius from the planet is %f AU.\n",
LP);
  printf("The planet's inner Hill radius from the system's centre of mass
is %f AU.\n", L1);
  printf("The planet's outer Hill radius from the system's centre of mass
is %f AU.\n", L2);
  printf("The planet's opposition point from the system's centre of mass
is %f AU.\n", L3);
  printf("These distances start the iterations to find the L1, L2 and L3
x-coordinates.\n");

  /* Perform Iteration to find L1, L2 and L3 */
  k=0;
  x[0]=1-u-(LP/a);
  while ( k < ITSTEP ) {
    x[k+1]=x[k]-(x[k]-(1-u)/((x[k]+u)*(x[k]+u))+u/((x[k]-1+u)*(x[k]-
1+u)))/(1+2*(1-u)/powf((x[k]+u),3)-2*u/powf((x[k]-1+u),3));
    k = k + 1;
  }
  printf("The distance of the L1 point from the system's centre of mass
is %f AU.\n", a*x[ITSTEP]);
  d=-(2*(1-u)/(x[ITSTEP]+u)-2*u/(x[ITSTEP]-1+u)+(x[ITSTEP]*x[ITSTEP]));
  l=0;
  w[0]=1-u+(LP/a);
  while ( l < ITSTEP ) {
```

```
    w[l+1]=w[l]-(w[l]-(1-u)/((w[l]+u)*(w[l]+u))-u/((w[l]-1+u)*(w[l]-
1+u)))/(1+2*(1-u)/powf((w[l]+u),3)+2*u/powf((w[l]-1+u),3));
    l = l + 1;
  }
  printf("The distance of the L2 point from the system's centre of mass
is %f AU.\n", a*w[ITSTEP]);
  e=-(2*(1-u)/(w[ITSTEP]+u)+2*u/(w[ITSTEP]-1+u)+(w[ITSTEP]*w[ITSTEP]));
  n=0;
  v[0]=-1-u;
  while ( n < ITSTEP ) {
    v[n+1]=v[n]-(v[n]+(1-u)/((v[n]+u)*(v[n]+u))+u/((v[n]-1+u)*(v[n]-
1+u)))/(1-2*(1-u)/powf((v[n]+u),3)-2*u/powf((v[n]-1+u),3));
    n = n + 1;
  }
  printf("The distance of the L3 point from the system's centre of mass
is %f AU.\n", a*v[ITSTEP]);
  f=-(-2*(1-u)/(v[ITSTEP]+u)-2*u/(v[ITSTEP]-1+u)+(v[ITSTEP]*v[ITSTEP]));
  printf("The Jacobian Constants are %f at L1, %f at L2 and %f at L3.\n",
-d, -e, -f);

  /* Determine the plot resolution. */
  printf("Enter the number of plotted points between the two bodies (1000
to 5000): ");
  scanf("%f", &dx);
  if ( ( dx < 1000 ) || ( dx > 5000 ) ) {
    printf("The x-axis intervals must be between the stated options
inclusively.\n");
    exit(EXIT_FAILURE);
  }

  /* Open the data file. */
  fh = fopen("2dcurves.dat", "w");
  if ( fh == NULL ) {
    printf("Cannot open the signal data file.\n");
    exit(EXIT_FAILURE);
  }

  /* Make headers for output file. */
  fprintf(fh, "Jacobian constant is %f\n", c);
  fprintf(fh, "\n");
  fprintf(fh, "  x-value\t");
  fprintf(fh, "  y-value\n");
  fprintf(fh, "\n");

  /* Calculate the zero velocity curves. */
  fprintf(fh, "%f\t", -u*a);
  fprintf(fh, "%f\n", 0);
  fprintf(fh, "%f\t", (1-u)*a);
  fprintf(fh, "%f\n", 0);
  s=0;
  for ( i = 0 ; i < 1 + 4*dx ; i = i + 1 ) {
    xx = -2+i/dx;
    for ( j = 0 ; j < 1 + 4*dx ; j = j + 1 ) {
      y = -2+j/dx;
      cc=((2*(1-u)/(sqrt((xx+u)*(xx+u)+y*y)))+(2*u/(sqrt((xx-1+u)*(xx-
1+u)+y*y)))+(xx*xx)+(y*y));
      b = cc - c;
      if ( fabs(b) < 0.0001 ) {
        fprintf(fh, "%f\t", a*xx);
        fprintf(fh, "%f\n", a*y);
        s=s+1;
      }
    }
  }
```

```
  printf("There are %u points to plot, if using Excel there must be less
than 32,000.\n\n", s);

  /* Close the file and program. */
  fclose(fh);
  printf("The program completed successfully.\n");
  printf("The output is stored in the file '2dcurves.dat' in this
program's folder.\n");
  printf("Now please change the name of '2dcurves.dat' or it will be
overwritten.\n");
  printf("To find zero-velocity curves for all Jacobian Constants, type
'zvcurves'.\n");
}
```

Program A4.3 – The Determination of the Zero-Velocity Curve around the Minor Body of a Binary, which passes through the L_1 Point.

l1curve.c

```
#include <stdio.h>
#include <stdlib.h>
#include <math.h>

#define pi 3.14159265358979323846264338327950288419716939937510
#define ITSTEP 100

/* xx = abscissa */
/* y = ordinate */
/* c and d = Jacobian constant */
/* u = second body's mass fraction of the system */
/* p = second body's mass (in Jupiters) */
/* m = primary body's mass (in solar masses) */
/* a = distance between the bodies (in AU) */
/* dx = resolution of 2-D plot */

int main()
{
  printf("For full use of this program, please read the screen output
carefully.\n\n");
  double x[ITSTEP], b, c, d;
  float p, m, a, u, dx, xx, y, LP;
  int i, j, k, l, n, s;
  FILE *fh;

  /* Primary body's mass (in solar masses), m. */
  printf("Enter the primary body's mass (in solar masses): ");
  scanf("%f", &m);
  if ( m < 0.0799999 ) {
    printf("The primary's mass must be greater than 0.08 solar
masses.\n");
    exit(EXIT_FAILURE);
  }

  /* Second body's mass (in Jupiters), p. */
  printf("Enter the second body's mass (in Jupiters): ");
  scanf("%f", &p);
  if ( ( p <= 0 ) || ( p > 15 ) ) {
    printf("The secondary's mass must be greater than zero and up to 15
Jupiters.\n");
    exit(EXIT_FAILURE);
  }
```

```
  /* Distance between the two bodies (in AU), a. */
  printf("Enter the distance between the two bodies (in AU): ");
  scanf("%f", &a);
  if ( a <= 0 ) {
    printf("The distance must be greater than zero.\n");
    exit(EXIT_FAILURE);
  }

  /* Calculate the secondary's mass fraction of the system. */
  u = p * ( 1.8986 / 1989.11 ) / ( m + p * 1.8986 / 1989.11 );
  printf("The mass fraction of the secondary, u, of the system is %e\n",
u);

  /* Determine the distance of L1 from the system's centre of mass. */
  LP = a*(powf((u/3),0.3333333333));
  printf("The distance of the Hill radius from the planet is %f AU.\n",
LP);

  /* Perform Iteration to find L1 */
  k=0;
  x[0]=1-u-(LP/a);
  while ( k < ITSTEP ) {
    x[k+1]=x[k]-(x[k]-(1-u)/((x[k]+u)*(x[k]+u))+u/((x[k]-1+u)*(x[k]-
1+u)))/(1+2*(1-u)/powf((x[k]+u),3)-2*u/powf((x[k]-1+u),3));
    k = k + 1;
  }
  d=2*(1-u)/(x[ITSTEP]+u)-2*u/(x[ITSTEP]-1+u)+(x[ITSTEP]*x[ITSTEP]);
  printf("The Jacobian Constant at L1 is %f.\n", d);

  /* Determine the plot resolution. */
  printf("Enter the number of points between the planet and star (10000
to 50000): ");
  scanf("%f", &dx);
  if ( ( dx < 10000 ) || ( dx > 50000 ) ) {
    printf("The x-axis intervals must be between the stated options
inclusively.\n");
    exit(EXIT_FAILURE);
  }

  /* Open the data file. */
  fh = fopen("L1curve.dat", "w");
  if ( fh == NULL ) {
    printf("Cannot open the signal data file.\n");
    exit(EXIT_FAILURE);
  }

  /* Make headers for output file. */
  fprintf(fh, "Jacobian constant is %f\n", d);
  fprintf(fh, "\n");
  fprintf(fh, "  x-value\t");
  fprintf(fh, "  y-value\n");
  fprintf(fh, "\n");

  /* Calculate the L1 zero velocity curve. */
  fprintf(fh, "%f\t", a*(1-u));
  fprintf(fh, "%f\n", 0);
  printf("The distance of the L1 point from the planet is %f AU.\n",
a*(1-u-x[ITSTEP]));
  s=1;
  n=0;
  for ( i = 0 ; i < 1 + 2*LP*dx/a ; i = i + 1 ) {
    xx = (1-u-LP/a)+i/dx;
    for ( j = 0 ; j < 1 + 2*LP*dx/a ; j = j + 1 ) {
      y = -LP/a+j/dx;
```

```
      c=((2*(1-u)/(sqrt((xx+u)*(xx+u)+y*y)))+(2*u/(sqrt((xx-1+u)*(xx-
1+u)+y*y)))+(xx*xx)+(y*y));
      b = c - d;
      if ( fabs(b) < 0.00001 ) {
        fprintf(fh, "%f\t", a*xx);
        fprintf(fh, "%f\n", a*y);
        s=s+1;
        if ( ( xx > 1 - u ) && ( ( fabs(y) < 0.0001 ) ) && ( n == 0 ) ) {
          printf("The distance of the L1 curve opposite the planet from
the star is %f AU.\n", a*(xx-1+u));
          n = n + 1;
        }
      }
    }
  }
  for ( l = 0 ; l < 1 + 0.5*LP*dx/a ; l = l + 1 ) {
    y = 0.5*LP/a+l/dx;
    c=2*(1-u)/(sqrt(1+y*y))+2*u/y+(1-u)*(1-u)+y*y;
    b = c - d;
    if ( fabs(b) < 0.0001 ) {
      printf("The distance of the L1 curve at quadrature from the planet
is %f AU.\n", a*y);
      l=1+0.5*LP*dx/a;
    }
  }

  /* Close the file and program. */
  fclose(fh);
  printf("There are %u points to plot, if using Excel there must be less
than 32,000.\n", s);
  printf("Note that these L1 planet distances are only accurate to three
decimal places.\n");
  printf("If less than three of these are shown, increase the point
resolution.\n\n");
  printf("The program completed successfully.\n");
  printf("The output is stored in the file 'L1curve.dat' in this
program's folder.\n");
  printf("Now please change the name of 'L1curve.dat' or it will be
overwritten.\n");
}
```

Program A4.4 – The Determination of the Zero-Velocity Curve around the Minor Body of a Binary, which passes through the L_2 Point.

l2curve.c

```
#include <stdio.h>
#include <stdlib.h>
#include <math.h>

#define pi 3.14159265358979323846264338327950288419716939937510
#define ITSTEP 100

/* xx = abscissa */
/* y = ordinate */
/* c and d = Jacobian constant */
/* u = second body's mass fraction of the system */
/* p = second body's mass (in Jupiters) */
/* m = primary body's mass (in solar masses) */
/* a = distance between the bodies (in AU) */
/* dx = resolution of 2-D plot */

int main()
```

```
{
  printf("For full use of this program, please read the screen output
carefully.\n\n");
  double x[ITSTEP], b, c, d;
  float p, m, a, u, dx, xx, y, LP;
  int i, j, k, l, n, s;
  FILE *fh;

  /* Primary body's mass (in solar masses), m. */
  printf("Enter the primary body's mass (in solar masses): ");
  scanf("%f", &m);
  if ( m < 0.0799999 ) {
    printf("The primary's mass must be greater than 0.08 solar
masses.\n");
    exit(EXIT_FAILURE);
  }

  /* Second body's mass (in Jupiters), p. */
  printf("Enter the second body's mass (in Jupiters): ");
  scanf("%f", &p);
  if ( ( p <= 0 ) || ( p > 15 ) ) {
    printf("The secondary's mass must be greater than zero and up to 15
Jupiters.\n");
    exit(EXIT_FAILURE);
  }

  /* Distance between the two bodies (in AU), a. */
  printf("Enter the distance between the two bodies (in AU): ");
  scanf("%f", &a);
  if ( a <= 0 ) {
    printf("The distance must be greater than zero.\n");
    exit(EXIT_FAILURE);
  }

  /* Calculate the secondary's mass fraction of the system. */
  u = p * ( 1.8986 / 1989.11 ) / ( m + p * 1.8986 / 1989.11 );
  printf("The mass fraction of the secondary, u, of the system is %e\n",
u);

  /* Determine the distance of L2 from the system's centre of mass. */
  LP = a*(powf((u/3),0.3333333333));
  printf("The distance of the Hill radius from the planet is %f AU.\n",
LP);

  /* Perform Iteration to find L2 */
  k=0;
  x[0]=1-u+(LP/a);
  while ( k < ITSTEP ) {
    x[k+1]=x[k]-(x[k]-(1-u)/((x[k]+u)*(x[k]+u))-u/((x[k]-1+u)*(x[k]-
1+u)))/(1+2*(1-u)/powf((x[k]+u),3)+2*u/powf((x[k]-1+u),3));
    k = k + 1;
  }
  d=2*(1-u)/(x[ITSTEP]+u)+2*u/(x[ITSTEP]-1+u)+(x[ITSTEP]*x[ITSTEP]);
  printf("The Jacobian Constant at L2 is %f.\n", d);

  /* Determine the plot resolution. */
  printf("Enter the number of points between the planet and star (10000
to 50000): ");
  scanf("%f", &dx);
  if ( ( dx < 10000 ) || ( dx > 50000 ) ) {
    printf("The x-axis intervals must be between the stated options
inclusively.\n");
    exit(EXIT_FAILURE);
  }
```

```
  /* Open the data file. */
  fh = fopen("L2curve.dat", "w");
  if ( fh == NULL ) {
    printf("Cannot open the signal data file.\n");
    exit(EXIT_FAILURE);
  }

  /* Make headers for output file. */
  fprintf(fh, "Jacobian constant is %f\n", d);
  fprintf(fh, "\n");
  fprintf(fh, "  x-value\t");
  fprintf(fh, "  y-value\n");
  fprintf(fh, "\n");

  /* Calculate the L2 zero velocity curve. */
  fprintf(fh, "%f\t", a*(1-u));
  fprintf(fh, "%f\n", 0);
  /* printf("The distance of the L2 point from the planet is %f AU.\n",
a*(1-u-x[ITSTEP])); */
  s=1;
  n=0;
  for ( i = 0 ; i < 1 + 5*LP*dx/(2*a) ; i = i + 1 ) {
    xx = (1-u-LP/a)+i/dx;
    for ( j = 0 ; j < 1 + 2*LP*dx/a ; j = j + 1 ) {
      y = -LP/a+j/dx;
      c=((2*(1-u)/(sqrt((xx+u)*(xx+u)+y*y)))+(2*u/(sqrt((xx-1+u)*(xx-
1+u)+y*y)))+(xx*xx)+(y*y));
      b = c - d;
      if ( fabs(b) < 0.00001 ) {
        fprintf(fh, "%f\t", a*xx);
        fprintf(fh, "%f\n", a*y);
        s=s+1;
        if ( ( xx > 1 - u ) && ( ( fabs(y) < 0.0001 ) ) && ( n == 0 ) ) {
          printf("The distance of the L2 point from the planet is %f
AU.\n", a*(xx-1+u));
          n = n + 1;
        }
      }
    }
  }
  for ( l = 0 ; l < 1 + 0.5*LP*dx/a ; l = l + 1 ) {
    y = 0.5*LP/a+l/dx;
    c=2*(1-u)/(sqrt(1+y*y))+2*u/y+(1-u)*(1-u)+y*y;
    b = c - d;
    if ( fabs(b) < 0.0001 ) {
      printf("The distance of the L2 curve at quadrature from the planet
is %f AU.\n", a*y);
      l=1+0.5*LP*dx/a;
    }
  }

  /* Close the file and program. */
  fclose(fh);
  printf("There are %u points to plot, if using Excel there must be less
than 32,000.\n", s);
  printf("Note that these L2 planet distances are only accurate to three
decimal places.\n");
  printf("If less than two of these are shown, increase the point
resolution.\n\n");
  printf("The program completed successfully.\n");
  printf("The output is stored in the file 'L2curve.dat' in this
program's folder.\n");
  printf("Now please change the name of 'L2curve.dat' or it will be
overwritten.\n");
}
```

References

Alcock C. (2000). "Binary microlensing events from the MACHO project." Astrophysical Journal **541**: 270.

Asghari N., Broeg C., et al. (2004). "Stability of terrestrial planets in the habitable zone of Gl 777A, HD 72659, Gl 614, 47 UMa and HD 4208." Astronomy and Astrophysics **426**: 353-365.

Bahcall J.C., Serenelli A.M., et al. (2005). "New solar opacities, abundances, helioseismology, and neutrino fluxes." Astrophysical Journal **621**: L85-L88.

Bakos G., Pal A., et al. (2006). "A Stellar Companion in the HD 189733 System with a Known Transiting Extrasolar Planet." Astrophysical Journal Letters **641**: L57-L60.

Baliunas S.L., Henry G.W., et al. (1997). "Properties of sun-like stars with planets. II Rho-1 Cancri, Tau Bootis and Upsilon Andromedae." Astrophysical Journal **474**: L119-L122.

Baraffe I., Chabrier G., et al. (2005). "Hot-Jupiters and hot-Neptunes: a common origin." Astronomy and Astrophysics **436**: L47-L51.

Barnes J.W. and O'Brien D.P. (2002). "Stability of satellites around close-in extrasolar giant planets." Astrophysical Journal **575**: 1087-1093.

Barker J. and Kolb U. (2003). "The minimum period problem in cataclysmic variables." Monthly Notices of the Royal Astronomical Society **340**: 623-631.

Basri G. (2004). "Extrasolar Planets: Too Close for Comfort." Nature **430**: 24.

Beatty J.K., Peterson C.C., et al. (1999). The New Solar System, Cambridge University Press.

Beauge C., Ferraz-Mello S., et al. (2003). "Extrasolar planets in mean-motion resonance: Apses alignment and asymmetric stationary solutions." Astrophysical Journal **593**: 1124-1133.

Benedict G.F., McArthur B.E., et al. (2002). "A mass for the extrasolar planet Gl 876b determined from Hubble Space Telescope fine guidance sensor 3 astrometry and high-precision radial velocities." Astrophysical Journal **581**: L115.

Bennett D.P. and Rhie S.H. (2002). "Simulation of a space-based microlensing survey for terrestrial extrasolar planets." Astrophysical Journal **574**: 985-1003.

Bodenheimer P., Laughlin G., et al. (2003). "On the radii of extrasolar giant planets." Astrophysical Journal **592**: 555-563.

Bonfils X., Forveille T., et al. (2005). "The HARPS search for southern extra solar planets - VI: A Neptune mass planet around the nearby M dwarf Gl 581." Astronomy and Astrophysics **443**: L15.

Britt R.R. (2006). Definition of 'Planet' Expected in September, 2006 http://www.space.com/scienceastronomy/060608_planet_definition.html, accessed 02/07/2006.

Burke C.J., DePoy D.L., et al. (2004). "Survey for Transiting Extrasolar Planets in Stellar Systems (STEPSS): I. Fundamental Parameters of the Open Cluster NGC 1245." Astronomical Journal **127**: 2382-2397.

Butler R.P., Vogt S.S., et al. (2004). "A Neptune-mass planet orbiting the nearby M-dwarf GJ 436." Astrophysical Journal **617**: 580-588.

Butler R.P., Marcy G.W., et al. (2003). "Seven new Keck planets orbiting G and K dwarfs." Astrophysical Journal **582**: 455-466.

Butler R.P., Marcy G.W., et al. (2002). "On the double planet system around HD 83443." Astrophysical Journal **578**: 565-572.

Butler R.P., Tinney C.G., et al. (2001). "Two new planets from the Anglo-Australian planet search." Astrophysical Journal **555**: 410-417.

Butler R.P., Vogt S.S., et al. (2000). "Planetary companions to the metal-rich stars BD -10°3166 and HD 52265." The Astrophysical Journal **545**: 504-511.

Butler R.P., Marcy G.W., et al. (1999). "Evidence for multiple companions to Upsilon Andromedae." Astrophysical Journal **526**: 916-927.

Carroll B.W. and Ostlie D.A.. (1996). An Introduction to Modern Astrophysics, Addison Wesley.

Carter B.D., Butler R.P., et al. (2003). "A planet in a circular orbit with a 6 year period." Astrophysical Journal **593**: L43-L46.

Chambers J.E., (2006). John Chambers Home Page, star.arm.ac.uk/~jec/home.html, accessed 22/02/2006.

Chambers J.E., (2004). Personal communication at the Second Darwin/TPF Conference (26/7/04 to 29/7/04), San Diego, California, 27/07/2004.

Chambers J.E. (1999). "A hybrid symplectic integrator that permits close encounters between massive bodies." Monthly Notices of the Royal Astronomical Society **304**: 793-799.

Chambers J.E. and Migliorini F. (1997). "A new software package for orbital integrations." Bulletin of the American Astronomical Society **29**: 1024.

Chaplin M. (2004). The phase diagram of water, London South Bank University. **2004,** http://www.lsbu.ac.uk/water/ accessed 23/3/05

Charbonneau D., Brown T.M., et al. (2002). "Detection of an extrasolar planet atmosphere." Astrophysical Journal **568**: 377-384.

Charbonneau D., Brown T.M., et al. (2000). "Detection of planetary transits across a Sun-like star." Astrophysical Journal **529**: L45-L48.

Cody A.-M. and Sasselov D. (2002). "HD 209458: Physical parameters of the parent star and the transiting planet." Astrophysical Journal **569**: 451-458.

Cox A.N. (2000). Allen's Astrophysical Quantities, Springer-Verlag.

Cuk M. and Burns J.A. (2004). "On the secular behaviour of irregular satellites." Astronomical Journal **128**: 2518-2541.

Cullerne J.P. and Illingworth V. (2000). The Penguin Dictionary of Physics, Penguin.

D'Antona F.D. and Mazzitelli. I. (1985). "Evolution of very low mass stars and brown dwarfs. I. The minimum main-sequence mass and luminosity." Astrophysical Journal **296**: 502-513.

David E.-M., Quintana E.V., et al. (2003). "Dynamical stability of Earth-like planetary orbits in binary systems." Publications of the Astronomical Society of the Pacific **115**: 825-836.

Decin G., Dominik C., et al. (2000). "The Vega phenomenon around G dwarfs." Astronomical Astrophysics **357**: 533-542.

Els S.G., Sterzik M.F., et al. (2001). "A second substellar companion in the Gliese 86 system: A brown dwarf in an extrasolar planetary system." Astronomy and Astrophysics **370**: L1-L4.

Everhart E. (2002). Integrator RADAU, http://data.astronomycamp.org/2002/Advanced Teen/raw/mlof3/orbit_determine/src/prelim/mistery/ra15.f, accessed 16/02/2007.

Everhart E. (1974). "Implicit Single Sequence Methods for Integrating Orbits." Celestial Mechanics **10**: 35-55.

Fernandez J. and Santos N.C. (2004). "Detailed theoretical models for extra-solar planet-host stars: The "red stragglers" HD 37124 and HD 46375." Astronomy and Astrophysics **427**: 607-612.

Fischer D.A., Marcy G.W., et al. (2003). "A planetary companion to HD 40979 and additional planets orbiting HD 12661 and HD 38529." Astrophysical Journal **586**: 1394-1408.

Fischer D.A., Marcy G.W., et al. (1999). "Planetary companions around two solar-type stars: HD 195019 and HD 217107." Publications of the Astronomical Society of the Pacific **111**: 50-56.

Fogg M.J. and Nelson R.F. (2005). "Oligarchic and giant impact growth of terrestrial planets in the presence of gas giant planet migration." Astronomy and Astrophysics **441**: 791-807.

Ford E.B. and Tremaine S. (2003). "Planet finding prospects for the Space Interferometry Mission." Publications of the Astronomical Society of the Pacific **115**: 1171-1186.

Ford E.B., Rasio F.A., et al. (1999). "Structure and evolution of nearby stars with planets. I. Short-period systems." Astrophysical Journal **514**: 411-429.

Forget F. and Pierrehumbert R.T. (1997). "Warming early Mars with carbon dioxide clouds that scatter infrared radiation." Science **278** (5341): 1273-1276.

Galland F., Lagrange A.M., et al. (2005). "Extrasolar planets and brown dwarfs around F-type stars. II. A planet found with ELODIE around the F6V star HD 33564." Astronomy and Astrophysics **444**: L21.

Gaudi B.S. (2000). Microlensing and the Search for Extrasolar Planets. Doctorate Thesis Department of Astronomy, Ohio State University.

Ge J., Mahadevan S., et al. (2006). "A First Extrasolar Planet Discovered with a New Generation High Throughput Doppler Instrument." Bulletin of the American Astronomical Society **37**(4): 191-202.

Ge J. (2002). "Fixed delay interferometry for Doppler extrasolar planet detection." Astrophysical Journal **571**: L165-L168.

Gilliland R.L. (1989). "Solar evolution." Global Planet Change **1**: 35-55.

Girardi L., Bressau A., et al. (2000). "Evolutionary tracks and isochrones for low- and intermediate-mass stars: From 0.15 to 7 solar masses, and from Z = 0.0004 to 0.03." Astronomy and Astrophysics Supplement Series **141**(371-383).

Goldstein H. (1980). Classical Mechanics, Addison-Wesley.

Gonzalez G. and Laws C. (2000). "Parent Stars of Extrasolar Planets V. HD 75289." Astronomical Journal **119**: 390-396.

Gonzalez G. (1999). "Are stars with planets anomalous." Monthly Notices of the Royal Astronomical Society **308**: 447-458.

Gough D.O. (1981). "Solar interior structure and luminosity variations." Solar Physics **74**: 21-34.

Greaves J., Holland W., et al. (1998). "A dust ring around Epsilon Eridani: analogue to the young solar system." Astrophysical Journal **506**: L133.

Guyon O. and Roddier F. (2002). "A nulling wide field imager for exoplanet detection and general astrophysics." Astronomy and Astrophysics **391**: 379 - 395.

Hadjifotinou K.G. (2000). "Numerical integration of satellite orbits around an oblate planet." Astronomy and Astrophysics **354**: 328-333.

Hadjifotinou K.G. and Harper D. (1995). "Numerical integration of orbits of planetary satellites." Astronomy and Astrophysics **303**: 940-944.

Hamilton C.J. (2005). Views of the solar system. **2005**, http://www.solarviews.com/eng/data2.htm (19/1/05)

Hart M.H. (1979). "Habitable zones about main sequence stars." Icarus **37**: 351-357.

Hatzes A.P., Cochran W.D., et al. (2003). "A planetary companion to Gamma Cephei A." Astrophysical Journal **599**: 1383-1394.

Henry G.W., Donahue R.A., et al. (2002). "A false planet around HD 192263." Astrophysical Journal **577**: L111-L114.

Henry G.W., Baliunas S.L., et al. (1997). "Properties of Sun-like stars with planets: 51 Pegasi, 47 Ursae Majoris, 70 Virginis, and HD 114762." Astrophysical Journal **474**: 503-510.

Holman M. J. and Wiegert P.A. (1999). "Long-term stability of planets in binary systems." Astronomical Journal **117**: 621-628.

Iben I. (1967). "Stellar evolution. VI. Evolution from the main sequence to the red-giant branch for stars of mass 1M(sol), 1.25M(sol and 1.5M(sol)." Astrophysical Journal **147**: 624-649.

Ichtiaroglou S. and Voyatzis G. (1990). "On the effect of the eccentricity of a planetary orbit on the stability of satellite orbits." Journal of Astrophysical Astronomy **11**: 11-22.

Illingworth V. (1985). MacMillan Dictionary of Astronomy, MacMillan.

Jacobsen R.A. (2005). Planetary satellite mean orbital parameters, NASA. **2005**, http://ssd.jpl.nasa.gov/sat_props.html (19/1/05)

Ji J., Kinoshita H., et al. (2003). "Could the 55 Cancri planetary system really be in the 3:1 mean motion resonance." Astrophysical Journal **585**: L139-L142.

Jones B.W., Sleep P.N., et al. (2006). "Habitability of Known Exoplanetary Systems Based on Measured Stellar Properties." Astrophysical Journal **649**: 1010-1019.

Jones B.W., Underwood D.R., et al. (2005). "Prospect for habitable "Earths" in known exoplanetary systems." Astrophysical Journal **622**: 1091-1101.

Jones B.W. (2004). Life in the Solar System and Beyond, Springer Praxis.

Jones B.W. (2003). How to find exoplanets. Exoplanets - Four Graduate Lectures. Open University, Milton Keynes: 13.

Jones B.W. and Sleep P.N. (2003). "The orbits of terrestrial planets in the habitable zones of known exoplanetary systems." Scientific Frontiers in Research on Extrasolar Planets ASP Conference Series. **298**, 225-230

Jones B.W. and Sleep P.N. (2002). "The stability of the orbits of Earth-mass planets in the habitable zone of 47 Ursae Majoris." Astronomy and Astrophysics **393**: 1015-1026.

Jones B.W., Sleep P.N., et al. (2001). "The stability of the orbits of terrestrial planets in the habitable zones of known exoplanetary systems." Astronomy and Astrophysics **366**: 254-262.

Jones B.W. (1999). Discovering the Solar System, John Wiley & Sons.

Jones H.R.A., Butler R.P., et al. (2006). "High-eccentricity planets from the Anglo-Australian Planet Search." Monthly Notices of the Royal Astronomical Society **369** (1): 249-256.

Jones H.R.A., Butler R.P., et al. (2003). "An exoplanet in orbit around Tau-1 Gruis." Monthly Notices of the Royal Astronomical Society **341**: 948-952.

Jones H.R.A., Butler R.P., et al. (2002). "Extrasolar planets around HD 196050, HD 216437 and HD 160691." Monthly Notices of the Royal Astronomical Society **337**: 1170-1178.

Kaisler D., Zuckerman B., et al. (2003). "A Keck adaptive optics search for young extrasolar planets." Astronomical Society of the Pacific **294**: 91-94.

Kasting J.F., Whitmire D.P., et al. (1993). "Habitable zones around main sequence stars." Icarus **101**: 108-128.

Kitchin C.R. (1998). Astrophysical Techniques, Institute of Physics, London.

Kolb U. (2003), Personal Communication, 18/02/2003.

Kolb U., Davies M.B., et al. (2000). "The violent past of Cygnus X-2." Monthly Notices of the Royal Astronomical Society **317**: 438-446.

Kolb U. and Ritter H. (1992). "Advantages and limitations of the biopolytrope model for computing the secular evolution of cataclysmic variables." Astronomy and Astrophysics **254**: 213-223.

Konacki M. (2005). "An extrasolar giant planet in a close triple-star system." Nature **436**: 230-233.

Konacki M., Torres G., et al. (2003). "An extrasolar planet that transits the disk of its parent star." Nature **421**: 507-509.

Korzennik S.G., Brown T.M., et al. (2000). "A high-eccentricity low-mass companion to HD 89744." Astrophysical Journal **533**: L147-L150.

Kozai Y. (1962). "Secular perturbations of asteroids with high inclination and eccentricity." Astronomical Journal **67**(9): 591-598.

Kudryavtsev S.M. (1995). "The fifth-order analytical solution of the equations of motion of a satellite in orbit around a non-spherical planet." Celestial Mechanics and Dynamical Astronomy **61**: 207-215.

Lagrange A.M. (2003). Direct imaging of extrasloar planets. Extrasolar Planets, Today and Tomorrow, IAP, Paris.

Laughlin G. and Chambers J.E. (2002). "Extrasolar Trojans: The viability and detectability of planets in the 1:1 resonance." Astronomical Journal **124**: 592-600.

Laws C., Gonzalez G., et al. (2003). "Parent stars of extrasolar planets. VII. New abundance analyses of 30 systems." Astronomical Journal **125**: 2664-2677.

Laws C. and Gonzalez G. (2001). "A differential spectroscopic analysis of 16 Cygni A and B." Astrophysical Journal **553**: 405-409.

Leger A., Selsis F., et al. (2003). "A new family of planets? 'Ocean planets'." Icarus **169**: 499-504.

Lequeux J., Peimbert M., et al. (1979). "Chemical composition and evolution of irregular and blue compact galaxies." Astronomical Astrophysics **80**: 155-166.

Lissauer J.J. (2002). "Extrasolar Planets." Nature **419**: 355-358.

Lissauer J.J. and Rivera E.J. (2001). "Stability analysis of the planetary system orbiting Upsilon Andromedae. II. Simulations using new Lick Observatory fits." Astrophysical Journal **554**: 1141 - 1150.

Mallen-Ornelas G., Seager S., et al. (2003). "The EXPLORE Project 1: A deep search for transiting extrasolar planets." Astrophysical Journal **582** (10th January): 1123 - 1140.

Marcy G.W., Butler R.P., et al. (2005). "Five new extrasolar planets." Astrophysical Journal **619**: 570-584.

Marcy G.W., Butler R.P., et al. (2002). "A planet at 5 AU around 55 Cancri." Astrophysical Journal **581**: 1375-1388.

Marcy G.W., Butler R.P., et al. (1999). "Two new candidate planets in eccentric orbits." Astrophysical Journal **520**: 239-247.

Marcy G.W. and Butler R.P. (1996). "A planetary companion to 70 Virginis." Astrophysical Journal **464**: L147-L151.

Mandell A.M. and Sigurdsson S. (2003). "Survival of terrestrial planets in the presence of giant planet migration." Astrophysical Journal **599**: L111-L114.

Mayor M., Udry S., et al. (2004). "The CORALIE survey for southern extra-solar planets XII. Orbital solutions for 16 extra-solar planets discovered with CORALIE." Astronomy and Astrophysics **415**: 391-402.

Mayor M. and Queloz D. (1995). "A Jupiter-mass companion to a solar-type star." Nature **378**: 355-359.

Mazzitelli I. (1989). "The core mass at the helium flash - influence of numerical and physical inputs." Astrophysical Journal **340**: 249-255.

McArthur B., Endl M., et al. (2004). "Detection of a Neptune-mass planet in the Rho-1 Cancri system using the Hobby-Eberly telescope." Astrophysical Journal **614**: L81-L84.

McCarthy C., Butler R.P., et al. (2004). "Multiple companions to HD 154857 and HD 160691." Astrophysical Journal **617**: 575-579.

Menou K. and Tabachnik S (2003). "Dynamical habitability of known extrasolar planetary systems." Astrophysical Journal **583**: 473-488.

Mikkola S. (1999). "Efficient symplectic integration of satellite orbits." Celestial Mechanics and Dynamical Astronomy **74**: 275-285.

Mischna M.A., Kasting J.F., et al. (2000). "Influence of carbon dioxide clouds on the early Martian climate." Icarus **145**: 546-554.

Montalban J., Antona F.D., et al. (2000). "Structure and evolution of low-mass population II stars." Astronomy and Astrophysics **360**: 935-951.

Moutou C., Mayor M., et al. (2005). "The HARPS search for southern extra-solar planets IV. Three close-in planets around HD 2638, HD 27894 and HD 63454." Astronomy and Astrophysics **439**: 367-373.

Murray C.D. and Dermott S.F. (1999). Solar System Dynamics, Cambridge University Press.

Naef D., Mayor M., et al. (2003). "The ELODIE survey for northern extra-solar planets II. A Jovian planet on a long-period orbit around GJ777A." Astronomy and Astrophysics **410**: 1051-1054.

Naef D., Latham D.W., et al. (2001). "HD 80606b, a planet on an extremely elongated orbit." Astronomy & Astrophysics **375**: L27-L30.

Naef D., Mayor M., et al. (2001). "The CORALIE survey for southern extrasolar planets V. 3 new extrasolar planets." Astronomy & Astrophysics **375**: 205 - 218.

Newman M.J. and Rood R.D. (1977). "Implications of solar evolution for the Earth's early atmosphere." Science **198**: 1035-1037.

Noble M., Musielak Z.E., et al. (2002). "Orbital stability of terrestrial planets inside the habitable zones of extrasolar planetary systems." Astrophysical Journal **572**: 1024-1030.

Ollivier M. (2003). Search for life: Darwin/TPF. Extrasolar Planets, Today and Tomorrow, IAP, Paris.

Pagel B.E.J., Simonson E.A., et al. (1992). "The primordial helium abundance from observations of extragalactic HII regions." Monthly Notices of the Royal Astronomical Society **255**: 325-345.

Pepe F., Mayor M., et al. (2004). "The HARPS search for southern extra-solar planets I. HD 330075b: A new "Hot Jupiter"." Astronomy and Astrophysics **423**: 385-389.

Pepe F., Mayor M., et al. (2002). "The CORALIE survey for southern extra-solar planets VII. Two short-period Saturnian companions to HD 108147 and HD 168746." Astronomy and Astrophysics **388**: 632-638.

Perrier C., Sivan J.-P., et al. (2004). "The ELODIE survey for northern extra-solar planets I. 6 new extra-solar planet candidates." Astronomical Astrophysics **410**: 1039-1051.

Phillips A.C. (1994). The Physics of Stars, Wiley.

Reddy B.E., Lambert D.L., et al. (2002). "A search for ^{6}Li in stars with planets." Monthly Notices of the Royal Astronomical Society **335**: 1005-1016.

Rivera E.J., Lissauer J.J., et al. (2005). "A ~7.5 Earth-Mass Planet Orbiting the Nearby Star, GJ876." Astrophysical Journal **634**: 625-640.

Ryan S.G. (2000). "The host stars of extrasolar planets have normal lithium abundances." Monthly Notices of the Royal Astronomical Society **316**: L35-L39.

Sadakane K., Ohnishi T., et al. (2005). "Metallicities in four planet-harbouring K-type giants: HD 47536, HD 59686, HD 137759, and HD 219449." Publications of the Astronomical Society of Japan **57**: 127-133.

Saffe C., Gomez M., et al. (2005). "On the ages of exoplanet host stars." Astronomy and Astrophysics **443**: 609-626.

Santos N.C., Mayor M., et al. (2002). "The CORALIE survey for southern extra-solar planets IX. A 1.3-day period brown dwarf disguised as a planet." Astronomy and Astrophysics **392**: 215-229.

Sasselov D. (2003). "The New Transiting Planet OGLE-TR-56b: Orbit and Atmosphere." Astrophysical Journal **596**: 1327-1331.

Schneider J. (2006). Interactive Extra-Solar Planets Catalog, exoplanet.eu/catalog.php, accessed 05/07/2006.

Segura A., Scalo J., et al. (2006). "Effects of Stellar Flares on the Atmospheres of Oxygen-Rich Habitable Planets." American Astronomical Society, DPS Meeting #38.

Setiawan J., Rodmann J., et al. (2005). "A substellar companion around the intermediate-mass giant star HD 11977." Astronomy and Astrophysics **437**: L31-L34.

Shkolnik S., Gaidos E., et al. (2006). "No Detectable H_3^+ Emission from the Atmospheres of Hot Jupiters." Astronomical Journal **132**: 1267-1274.

Sleep P.N. (2005). Earths in known exoplanetary systems. Doctorate Thesis, Physics and Astronomy Department. Milton Keynes, Open University.

Solomon S.C. and Head J.W. (1991). "Fundamental issues in the geology and geophysics of Venus." Science **252**: 252-260.

Sozzetti A., Udry S., et al. (2006). "A Massive Planet to the Young Disc Star HD 81040." Astronomy and Astrophysics **449**: 417.

Sozzetti A., Casertano S., et al. (2003). "The GAIA astrometric survey of the solar neighbourhood and its contribution to the target database for Darwin/TPF". Towards Other Earths, Darwin/TPF and the Search for Extrasolar Terrestrial Planets, Heidelberg, European Space Agency, 22-25, April, 2003.

Stehle R., Kolb U., et al. (1994). "Evolutionary aspects of population II cataclysmic variables." Memorie della Societa Astronomia Italiana **65**: 415-416.

Tinney C.G., Butler R.P., et al. (2005). "Three low-mass planets from the Anglo-Australian planet search." Astrophysical Journal **623**: 1171-1179.

Tinney C.G., Butler R.P., et al. (2003). "Four new planets orbiting metal-enriched stars." Astrophysical Journal **587**: 423-428.

Trilling D.E., Brown R.H., et al. (2000). "Circumstellar dust disks around stars with known planetary companions." Astrophysical Journal **529**: 499 - 505.

Tsangarides S., (2003), Personal Communication, 11/3/03

Turnbull M.C. and Tarter J.C. (2003). "Target selection for SETI. I. A catalog of nearby habitable stellar systems." Astrophysical Journal Supplement Series **145**: 181-198.

Udry S., Mayor M., et al. (2003). "The CORALIE survey for southern extra-solar planets X. A Hot Jupiter orbiting HD 73256." Astronomy and Astrophysics **407**: 679-684.

Udry S., Mayor M., et al. (2002). "The CORALIE survey for southern extra-solar planets VIII. The very low-mass companions of HD 141937, 162020, HD 168443 and HD 202206: Brown dwarfs or "superplanets"?" Astronomy and Astrophysics **390**: 267-279.

Udry S., Mayor M., et al. (2000). "The CORALIE survey for southern extra-solar planets II. The short-period planetary companions to HD 75289 and HD 130322." Astronomy and Astrophysics **356**: 590-598.

Underwood D.R., Jones B.W., et al. (2003). "The evolution of habitable zones during stellar lifetimes and its implications on the search for extraterrestrial life." International Journal of Astrobiology **2** (4): 289-299.

Valenti J.A. and Fischer D.A. (2005). "Spectroscopic properties of cool stars (SPOCS). I. 1040 F, G, and K dwarfs from Keck, Lick, and AAT planet search programs." Astrophysical Journal Supplement Series **159**(141-146).

Vidal-Madjar A., Lecaveller des Etangs A., et al. (2003). "An extended upper atmosphere around the extrasolar planet HD 209458 b." Nature **422**: 143-146.

Vogt S.S., Butler R.P., et al. (2005). "Five new multicomponent planetary systems." Astrophysical Journal **632**: 638-658.

Vogt S.S., Butler R.P., et al. (2002). "Ten low-mass companions from the Keck precision velocity survey." Astrophysical Journal **568**: 352-362.

Ward P.D. and Brownlee D. (2000). Rare Earth. New York, Copernicus, Springer-Verlag.

Weiss J.W. and Stewart G.R. (2002). "Evolution of the orbits of extrasolar planet moons during planet migration." Bulletin of the American Astronomical Society **34**: 893.

Weldrake D.T.F., Sackett P.D., et al. (2005). "An Absence of Hot Jupiter Planets in 47 Tucanae: Results of a Wide Field Transit Search." Astrophysical Journal **620**: 1043-1051.

Williams D.M and Kasting J.F. (1997). "Habitable planets with high obliquities." Icarus **129**: 254-268.

Williams D.M, Kasting J.F., et al. (1997). "Habitable moons around extrasolar planets." Nature **385**: 234-236.

Williams D.M and Pollard D. (2002). "Earth-like worlds on eccentric orbits: excursions beyond the habitable zone." International Journal of Astrobiology **1**(1): 61-69.

Wisdom J. (1996). "Symplectic Correctors." Fields Institute Communications. **10**: 217.

Wolszczan A. and Frail D.A. (1992). "A planetary system around the millisecond pulsar PSR1257+12." Nature **355**: 145-147.

Wu Y. and Murray N. (2003). "Planet migration and binary companions: the case of HD 80606b." Astrophysical Journal **589**: 605-614.

Young H.D. and Freedman R.A. (2000). University Physics, Addison Wesley Longman, Inc.

Young P., Mamajek E., et al. (2001). "Observational tests and predictive stellar evolution." Astrophysical Journal **556**: 230-244.

Zeilik M. and Gregory S.A. (1998). Astronomy and Astrophysics, Saunders College Publishing.

Zhou L.-Y., Lehto H.J., et al. (2004). "Apsidal corotation in mean motion resonance: the 55 Cancri system as an example." Monthly Notices of the Royal Astronomical Society **350**: 1495-1502.